32nd Annual Meeting of the

German Crystallographic Society (DGK) e. V.

Abstract book

Table of content

Oral presentations

Poster presentations

Plenary lectures

PL-1

Structural biology post-AlphaFold

R. J. Read (Cambridge/UK)

AlphaFold and other new machine-learning structure prediction algorithms have dramatically changed the way structural biology in general, and protein crystallography in particular, is carried out. This new technology influences everything from how you define your scientific question, how you design an expression construct, how you determine and refine your protein structure, and how you compare it to related proteins.

AlphaFold models can be remarkably accurate and are incredibly useful, but they are not perfect and they do not replace the need for experimental structural biology. To make the best use of these models, it is essential to be aware of their strengths and their weaknesses. Fortunately, AlphaFold is also very good at assessing the accuracy of the models, both through the per-residue pLDDT quality scores and the estimates of precision of longer-distance relationships in the PAE matrix.

The success of machine-learning methods in structure prediction is inspiring a whole new set of approaches to addresses issues where AlphaFold is weak: how do ligands and ions bind, what is the effect of disease-associated mutations to medically-relevant proteins, and how does conformational change contribute to function?

PL-2

High-pressure synthesis and crystal chemistry: current state and perspectives

M. Bykov (Frankfurt am Main/DE)

Pressure is an important thermodynamic variable that allows for the alteration of chemical paradigms and the creation of compounds with extraordinary properties, stoichiometries, and bonding types. Applying extreme conditions in chemical synthesis enables novel routes to metastable and kinetically hindered compounds, which were previously unthinkable at ambient conditions and open entirely new horizons. Developments in multigrain single-crystal X-ray diffraction methods using laser-heated diamond anvil cells, high-brilliance microfocus synchrotron, and in-house X-ray sources, along with the focused ion beam technique for the analysis of recovered samples, now enable systematic studies of chemical reactions at ultrahigh pressures and the study of recovered materials. As a result of these recent developments, high-pressure chemistry—especially at pressures above 50 GPa—is experiencing a phase of very rapid knowledge accumulation. In this talk, I will review the current status of methodological breakthroughs in high-pressure crystallography and demonstrate how these methods are applied to study the chemistry of binary and ternary nitrides and polynitrides under extreme conditions.

PL-3

Order-disorder transitions in intercalation type batteries

D. B. Ravnsbæk (Aarhus C/DK)

The functionality of rechargeable ion batteries is largely governed by the ability of the electrodes to store and transport electrons and active ions, such as Li-ions in Li-ion batteries. The efficiency and reversibility of these processes depend on the nature of the structural transformations accompanying charge and discharge. It is pertinent to probe these processes under dynamic conditions resembling those of the real operating battery, i.e. using operando techniques.

In the quest to understand the structural changes in battery electrodes, the focus has mainly been on elucidating structures of the crystalline parts of the electrode materials, e.g. by diffraction methods. However, as evidenced in a growing number of studies,1 ion-intercalation can induce structural disorder ranging from defect formation to complete amorphization. Furthermore, recent attention to the phenomena has revealed that the order-disorder transition can occur in both reversible and irreversible manners. Interestingly, this is not necessarily linked to the reversibility of the ion-storage process.

This talk will demonstrate how we combine operando synchrotron X-ray diffraction and total scattering with pair distribution function (PDF) analysis to elucidate the structural evolution in a series of battery electrode materials, which undergo various degrees of disordering during charge or discharge. The talk will demonstrate the approaches through interesting findings in e.g. nano LixMO2 and layered NaxMO2 (M = transition metal) electrodes for Li- and Na-ion batteries, respectively.2-4 Furthermore, we will look into new findings regarding beam damage during operando synchrotron studies of batteries5 and see how the use of structure mining and non-negative-matrix factorization,6,7 have become game-changers for approaching the often complex operando PDF analysis.

References

(1) C. K. Christensen, D. B. Ravnsbæk, Understanding disorder in oxide-based electrode materials for rechargeable batteries, IOP Journal of Physics: Energy 3, 031002 (2021.

(2) C. K. Christensen, M. A. Hasen Mamakhel, B. B. Iversen, A. R. Balakrishna, Y.-M. Chiang, D. B. Ravnsbæk, "Order-disorder transition in nano-rutile TiO2 anodes: A high capacity low-volume change Li-ion battery material" Nanoscale 11, 12347-12357 (2019).

(3) C. L. Jakobsen, M. Brighi, B. P. Andersen, G. Ducrest, R. Cerny, D. B. Ravnsbæk, Expanded solid-solution behavior and charge-discharge asymmetry in NaxCrO2 Na-ion battery electrodes, J. Power Sources, in press (2022)

(4) Andreas Østergaard Drejer, Mickey Sejerup Pedersen, Morten Johansen, and Dorthe Bomholdt Ravnsbæk, "Local and global structures in the phase evolution of P2-NaxFeyMn1-yO2 electrodes for Na-ion batteries", ACS Applied Energy Materials 2023, 6, 4909–4921.

(5) Christian Kolle Christensen, Martin Aaskov Karlsen, Andreas Østergaard Drejer, Bettina Pilgaard Andersen, Christian Lund Jakobsen, Morten Johansen, Daniel Risskov Sørensen, Innokenty Kantor, Mads Ry Vogel Jørgensen, Dorthe Bomholdt Ravnsbæk, "Beam damage in operando X-ray diffraction studies of Li-ion batteries", J. Synchrotron Rad. 2023, DOI: 10.1107/S160057752300142X.

(6) L. Yang, E. A. Culbertson, H. T. Vuong, N. K. Thomas, E. T. S. Kjear, K. M. Ø. Jensen, M. G. Tucker, S. J. L. Billinge, A cloud platform for atomic pair distribution function analysis: PDFitc. Acta Crystallogr. A. 77, 2-6.

(7) Z. Thatcher, C.-H. Liu, L. Yang, B. C. McBride, G. T. Tran, A. Wustrow, M. A. Karlsen, J. R. Neilson, D. B. Ravnsbæk, S. J. L. Billinge, arXiv:2112.13300 (2022).

PL-4

Aperiodic crystals: atomic structure and phason modes

M. de Boissieu (Grenoble/FR)

For more than a century the understanding of the structure, physical and chemical properties of solids has been based on the notion of periodicity in a crystal, associated to long-range order. Aperiodic crystals are solids with long-range order yet without lattice translation at least in one dimension [1]. Aperiodic crystals are generally classified in three groups: incommensurately modulated phases, incommensurate composites and quasicrystals. They have been found in a very wide range of compounds, from single element under pression, organic compounds, intermetallic, ferrolectrics and even proteins. The lack of periodicity, yet with long range order, opened a completely new field of research where the understanding of the atomic structure and associated physical and chemical properties had to be reconsidered with new perspectives.

The structure of aperiodic crystals is now very well understood, thanks to the development of the superspace crystallography, associated softwares and 2D detectors data acquisition. I will review some of the recent results, obtained in particular for quasicrystals where the crystal-chemistry is well explained.

Understanding the physical properties of aperiodic crystals is still a challenging task. There is however one property related to the peculiar dynamics of aperiodic crystals and named phason modes. I will illustrate this fascinating dynamics with a few recently studied compounds either incommensurately modulated structure or quasicrystals. Phason modes can be nicely evidenced using diffuse scattering measurements and inelastic x-ray or neutron scattering depending on the associated time scale. I will finally discuss their possible influence on the stability of aperiodic crystals.

References

(1) T. Janssen, G. Chapuis, and M. de Boissieu, Aperiodic Crystals. From modulated phases to quasicrystals (second edition) (Oxford University Press, Oxford, 2018), Vol. 20, IUCr Monographs on Crystallography, 532 pages.

MS 1: Structural biology I: New structures – enzymes

OP-001

Insights into the Three-dimensional and Electronic Structure of [FeFe] Hydrogenases

I. Span (Erlangen/DE)

[FeFe] hydrogenases are highly efficient metalloenyzmes for hydrogen conversion. Their active site cofactor (the H-cluster) is composed of a canonical [4Fe-4S] cluster linked to a unique organometallic di-iron subcluster, [2Fe]. [FeFe] hydrogenases have a high activity and are biased towards generating molecular hydrogen. However, their active site is rapidly degraded when exposed to oxygen. The enzyme from *Desulfovibrio desulfuricans* has evolved a unique mechanism to protect the [2Fe] from oxygen. The mechanism of biological hydrogen generation remains a topic of debate. Our goal is to understand how these enzymes function.

We combine X-ray crystallography with single-crystal spectroscopy and computational methods to obtain insights into the three-dimensional and electronic structure of the enzyme. We are also investigating the architecture of the gas channel in [FeFe] hydrogenases.

Based on our experimental data, including atomic resolution crystal structures, we proposed a mechanism for the reversible formation of the oxygen-resistant state Hinact and the reactivation of this state. In addition, we mapped the gas channel and obtained important insights on the role of amino acid residues inside the channel.

These insights contribute to unraveling the reaction mechanism of [FeFe] hydrogenases. Our findings are of great interest for biotechnological applications for green hydrogen production and will inspire the development of novel molecular catalysts.

Fig. 1

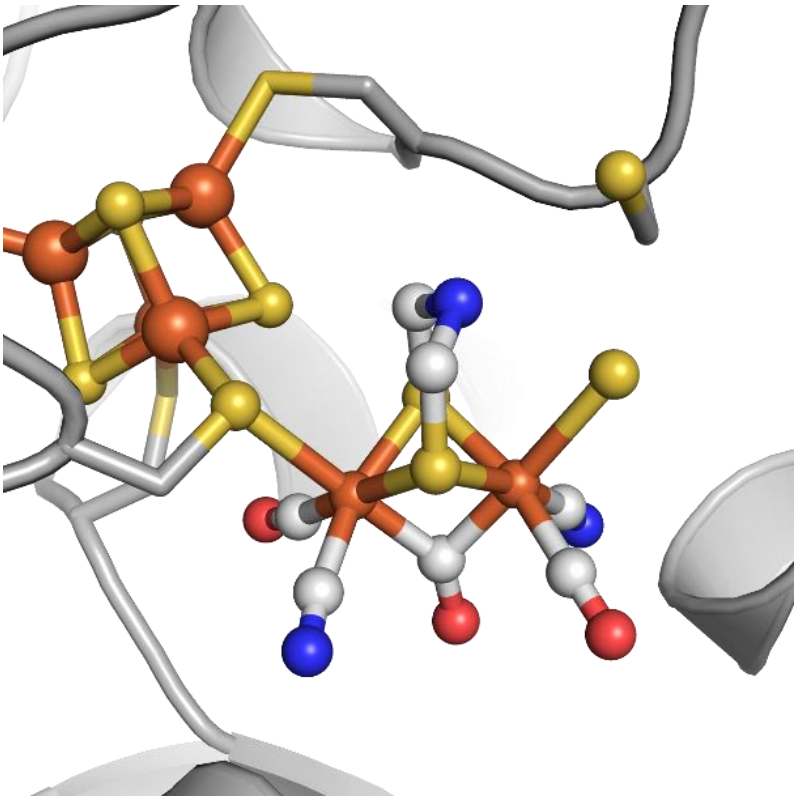

OP-002

Structural analysis of PLD3 reveals insights into the mechanism of lysosomal 5' exonuclease-mediated nucleic acid degradation

Y. Roske (Berlin/DE), C. Cappel (Kiel/DE), O. Daumke (Berlin/DE), M. Damme (Kiel/DE)

The phospholipase D (PLD) family is comprised of enzymes bearing phospholipase activity towards lipids or endo- and exonuclease activity towards nucleic acids. PLD3 is synthesized as a type II transmembrane protein and proteolytically cleaved in lysosomes, yielding a soluble active form. The deficiency of PLD3 leads to the slowed degradation of nucleic acids in lysosomes and chronic activation of nucleic acid-specific intracellular toll-like receptors. While the mechanism of PLD phospholipase activity has been extensively characterized, not much is known about how PLDs bind and hydrolyze nucleic acids. Here, we determined the high-resolution crystal structure of the luminal N-glycosylated domain of human PLD3 in its apo- and single-stranded DNA-bound forms. PLD3 has a typical phospholipase fold and forms homodimers with two independent catalytic centers via a newly identified dimerization interface. The structure of PLD3 in complex with an ssDNA-derived thymidine product in the catalytic center provides insights into the substrate binding mode of nucleic acids in the PLD family. Our structural data suggest a mechanism for substrate binding and nuclease activity in the PLD family and provide the structural basis to design immunomodulatory drugs targeting PLD3.

Fig. 1

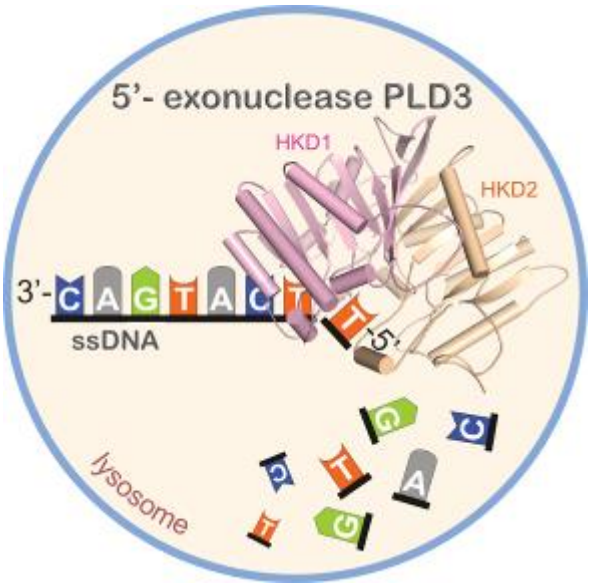

OP-003

Structural and functional insights into tRNA recognition by human tRNA guanine transglycosylase

P. Neumann (Göttingen/DE), K. Sievers (Göttingen/DE), L. Sušac (Frankfurt a. M./DE), S. Da Vela (Hamburg/DE), M. Graewert (Hamburg/DE), S. Trowitzsch (Frankfurt a. M./DE), D. Svergun (Hamburg/DE), R. Tampé (Frankfurt a. M./DE), R. Ficner (Göttingen/DE)

Eukaryotic tRNA guanine transglycosylase (TGT) is an RNA modifying enzyme catalyzing the base exchange of guanine 34 of $tRNAs^{Asp,Asn,His,Tyr}$ for queuine, a hypermodified 7-deazaguanine derivative. Q-modification is important for regulation of decoding efficiency and translation. Atypical levels of Q-modifications are linked to cancer and to neurological and metabolic disorder. Furthermore, Q-modification is a requirement for virulence in *Shigella flexneri*, a causative agent of diarrhea in humans.

Eukaryotic TGT is a heterodimer comprising a catalytic (QTRT1) and a non-catalytic (QTRT2) subunit. The recently solved crystal structure of a human tRNA anticodon loop bound to the active site in QTRT1 revealed structural details of TGT substrate recognition. However, the contribution of the non-catalytic subunit to tRNA binding remained enigmatic. Here, we report a cryo-EM structure of the human TGT in complex with a complete tRNA. It reveals virtually identical interactions between QTRT1 and the tRNA anticodon stem loop as observed in the crystal structure. The additional contacts between tRNA and QTRT2 appear to be made possible by some conformational changes of both TGT and tRNA. In particular, the TGT has a larger diameter (97 Å) than what was previously observed for the crystal structures of free or stem loop-bound protein (92 Å). We collected SAXS data of both free and tRNA bound TGT in solution and found that the "extended" cryo-EM structure best fits the experimental SAXS data. This suggests that the solution state of apo TGT is more extended than previously assumed based on the crystal structure.

Taken together, we deciphered the functional significance of the additional tRNA binding sites on a non-catalytic subunit QTRT2, analyzed the solution state conformation using SAXS and examined the overall flexibility of the complex. The obtained structural results could be used for the development of novel antibacterial agents against resistant *S. flexneri* strains.

Fig. 1

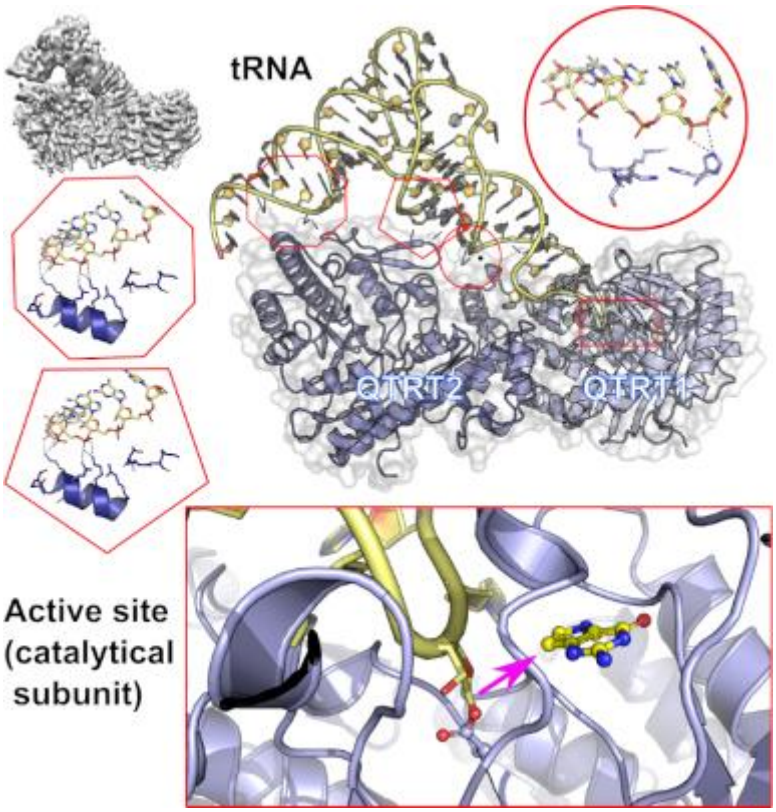

OP-004

Tapinella atrotomentosa: Solving a molecular structure from the wild

A. Thorn (Hamburg/DE)

Fungi are generally under-researched compared to humans, plants and animals, yet they have a huge impact on every aspect of life. They are also, biochemically speaking, able to achieve many functions other organisms cannot, such as the non-ribosomal synthesis of peptides with uncommon amino acids, breaking down plastic or creating energy equivalents from uncommon energy sources.

Using a traditional biochemical approach, we purified proteins directly from *Tapinella atrotomentosa* fruit bodies collected in the wild, and crystallized them, thereby retaining post-translational modifications. We were able to solve a structure of one of the more prevalent macromolecules. In this talk, I will present our rather exploratory crystallographic approach to the fungal kingdom, how we phased a structure not knowing its sequence or function and what we learned from this project.

OP-005

Structural and functional investigations into Glycocin-Glycosyltransferases

C. Roth (Berlin/DE), M. Krummhaar (Berlin/DE), A. Langhans (Berlin/DE), B. Koksch (Berlin/DE)

Glycocins are a family of short ribosomally synthesized and post-translationally modified peptides (RiPPs) that often show high potency, and low toxicity. Glycocins require a glycosylation to exhibit antimicrobial activity and thus have been termed glycoactive bacteriocins [1]. The carbohydrate moiety of glycocins is installed by a specific subfamily of glycosyltransferases the glycocin-glycosyltransferases (GGTs). Despite being in the same family, these GGTs show a remarkable diversity in terms of donor specificity, peptide specificity, acceptor selectivity and number of glycosylations that are carried out. We characterised several GGTs to shed light on the structural characteristics that contribute to this remarkable diversity and determine general principles governing the glycosyl transfer onto the peptidogenic substrate. Understanding the key elements of the catalytic site and the mechanism may allow to use the transferases as valuable tools to synthesise glycocins, glycopeptides and neo-glycopeptides in general. We identified several putative glycocins and their cognate GGTs using bioinformatics. The recombinant production and purification of several GGTs was established. These GGTs were characterised in regard of the metal ion dependency and the carbonucleotide specificity. Using SPPS, we synthesised the aglycone peptide and proved their selective glycosylation by the cognate GGT. To investigate the molecular determinants for the observed differences in specificity in terms of preferred sugars and their *acceptor* selectivity, we obtained structures for four GGTs with noticeably different specificities, For one GGT we were able to obtain snapshots along the reaction pathway, providing inside into the glycosylation pathway and peptide specificity.

References:

(1) Norris, G. E.; Patchett, M. L., The glycocins: in a class of their own. Current Opinion in Structural Biology 2016, 40, 112-119.

MS 2: Experimental methods I: Extreme conditions

OP-006

New opportunities for high-pressure crystallography and crystal chemistry at the Extremely Brilliant Source of the ESRF

A. Rosa (Grenoble/DE), G. Garbarino (Grenoble/DE), O. Mathon (Grenoble/DE)

The new Extremely Brilliant Source of the ESRF (EBS), which operates since 2021, offers exceptional opportunities for high-pressure crystallography and crystal chemistry. This very intense and coherent X-ray source makes it possible to approach subjects of a very high complexity such as, the emergence of superconductivity, the effect of electronic transitions on mineral physical properties, the synthesis and characterization of new super-hard materials, and the determination of phase relations in chemically complex samples at extreme P/T conditions. In this presentation, I will show through selected examples, the potential impact of two ESRF-EBS beamlines on this field: the high-brilliance spectroscopy beamline ID24-DCM and the high-pressure diffraction beamline ID15b. I will put a special emphasis on the added value of combining XRD and XAS measurements to obtain unprecedented structural and vibrational information of materials under extreme *P-T* conditions.

OP-007

Single-crystal elastic properties from high-pressure experiments: a comparison of inversion strategies

J. Buchen (Bayreuth/DE), A. Kurnosov (Bayreuth/DE), G. Criniti (Bayreuth/DE, Washington, DC/US), H. Marquardt (Oxford/GB), T. Boffa Ballaran (Bayreuth/DE)

The elastic properties of crystals contain information on interatomic forces and the shape of the interatomic potential. The evolution of elastic properties with increasing pressure is of particular interest since compression changes the interatomic distances. In geophysics, the elastic properties of rock-forming minerals determine the propagation of seismic waves through Earth's deep interior and, if known, can be used to extract information about the structure and composition of the Earth's interior. As a consequence, experimental techniques have been developed to determine the elastic properties of crystals at high pressures. Most of these techniques, however, sample the elastic properties indirectly in the form of related properties such as sound wave velocities and unit cell parameters. The resulting experimental datasets then need to be inverted for the elastic properties, which in some cases may raise problems if datasets are incomplete or under-determined due to experimental limitations.

Here we compare different strategies to extract elastic properties from experimental datasets collected at high pressures. In particular, we compare the traditional approach to invert datasets at individual pressures with an alternative approach that simultaneously inverts datasets collected at different pressures. By connecting the components of the elasticity tensors at different pressures through a finite-strain formalism, this new approach may help to extract information even from partial datasets that may otherwise not constrain all components of the elasticity tensor. Different inversion strategies are assessed in terms of the accuracy and precision with which they reproduce the original elastic properties.

The results of our analysis may help improve the information yield of expensive and time-consuming high-pressure experiments and guide the design of experimental studies on the elastic properties of crystals at high pressures.

OP-008

Advances in Neutron Diffraction at High Pressure and Temperature

C. Bull (Didcot/GB), C. Ridley (Didcot/GB), N. Funnell (Didcot/GB)

The PEARL instrument at ISIS has been designed for, and dedicated to, in situ studies of materials at high pressure, using the Paris–Edinburgh press. In recent years, upgrades to the instrument have led to improvements in data quality and the range of achievable pressures and temperatures; currently 0.5–28 GPa and 80–1400 K. This contribution describes the technical characteristics of the instrument, its current and new capabilities

The advantages of neutron radiation in diffraction, compared to those of X-rays, have been well documented as has the role of high pressure in neutron diffraction experiments. Neutrons have a high penetration depth in comparison to X-rays and so sample environments such as metal pressure cells can be accommodated. Lastly, as a result of their intrinsic spin, neutrons are sensitive to magnetic order within materials, allowing determination of their magnetic structure.

Taking examples from experiments performed on the Pearl instrument, we will present recent scientific highlights where the experiments have made use of new anvil materials, low and high temperature setups and the new instrument capabilities itself. We will also show developments which are currently in progress. Future envisaged high pressure developments will also be presented.

OP-009

A self-consistent approach to describe unit-cell parameter and volume variations with pressure and temperature

R. J. Angel (Padova/IT), M. Mazzucchelli (Lausanne/CH), J. Gonzalez-Platas (La Laguna/ES), M. Alvaro (Pavia/IT)

The changes in the unit-cell parameters and volumes of crystals with temperature and hydrostatic pressure provide fundamental information about the nature and anisotropy of the bonding in crystals. Variations of individual unit-cell parameters with P and T are commonly described by "axial eos" in which the cell parameters are cubed and then fitted using EoS for volumes. In most cases the axial eos provide an accurate description of the variation of the individual unit-cell parameters with P and/or T and yield linear compressibilities and moduli that agree with those determined by direct measurements of the elastic tensors.

Because the volume and the unit-cell parameters of a crystal are not independent of one another, the use of independent equations for the variation of the unit-cell parameters and the volume introduces additional false degrees of freedom into the description of the behaviour of the crystal. Further, we will show that the specific constraints required by symmetry between the bulk modulus of a crystal and the axial moduli cannot be maintained at all pressures when axial and volume EoS are used together. This physical inconsistency arises from the anisotropy of the pressure derivatives of the axial compressibilities and therefore applies to all crystal systems except cubic. Discrepancies are greatest for highly anisotropic soft materials such as some metal–organic frameworks and molecular crystals.

We will describe one possible method for the self-consistent description of the large variations of unit-cell parameters of crystals with pressure and temperature, which has been implemented in the CrysFML Fortran subroutine library. The unit-cell parameters and the compressibility and thermal expansion tensors of crystals can be calculated from axial and volume eos in an internally consistent manner in a new utility in the EosFit7c program, which is available as freeware at www.rossangel.net.

MS 3: Theoretical methods I: Theoretical methods and crystallographic software

OP-010

Digital Chemistry in Action: Insights from Merck's Crystal Prediction

J. G. Brandenburg (Darmstadt/DE)

Digital chemistry has the potential to significantly accelerate discovery and formulation in our industry. This talk will delve into our crystal structure prediction endeavors, from pharmaceutical formulation to OLED material production. Using a blend of cheminformatics and advanced computational techniques like dispersion-corrected DFT, we efficiently identify polymorphs and solvate forms. While speed often trumps precision in industrial settings, understanding and conveying prediction errors remains important. With substantial value generated in the past years and significant integration of digital insights into our workflows, our experiences provide a unique academic-industrial interface worth exploring.

OP-011

How to determine the crystallinity of nanoparticles from HRTEM images: A neural network training pipeline based on simulated HRTEM images

N. Gumbiowski (Essen/DE), J. Barthel (Jülich/DE), K. Loza (Essen/DE), M. Heggen (Jülich/DE), M. Epple (Essen/DE)

High-resolution transmission electron microscopy (HRTEM) images can visualize size, shape and crystal structure of nanoparticles. However, accessing these data is not always straightforward and often a time consuming and tedious manual process. Assessment of the internal crystallinity is usually only performed for a few individual particles with clearly visible lattice planes. We have developed a tool (ANTEMA) to detect nanoparticles and to analyze them for shape and size.[1] For a comprehensive assessment, it is important to elucidate the crystallinity of the particles well, e.g. single-crystalline, twinned, or amorphous. To automatically analyze particles for their crystallinity, a neural network training pipeline was developed and trained to distinguish between monocrystalline, polycrystalline and amorphous particles.

A major obstacle for a crystallographic classifier is the generation of the training data. Creating a dataset of classified TEM data for training is very time-consuming and prone to error by manual analysis. Therefore, we endeavored to create HRTEM images of nanoparticles with different crystallinity on a thin amorphous support by simulations using the Dr. Probe software.[2] The simulations produced adequate data with tens of thousands of simulated particles including a variation of imaging conditions to train neural network classifiers for assessment of the crystallinity. A dataset of manually labelled real TEM images was then used to validate the performance of the trained network. The network showed an excellent performance on these real data, i.e. to recognize the internal crystallinity of nanoparticles.

References:

(1) N. Gumbiowski, K. Loza, M. Heggen, M. Epple, *Nanoscale Adv.* **2023**, *5*, 2318–2326.
(2) J. Barthel, *Ultramicroscopy* **2018**, *193*, 1–11.

OP-012

Ray-tracing Simulations of Microabsorption Effects in Reflection Geometry on Samples with arbitrary Microstructure

J. Dallmann (Erlangen/DE), J. Graetz (Erlangen/DE), R. Hock (Erlangen/DE)

Microabsorption denotes the influence of the local microstructure of a sample on the intensities measured in an XRD or XRF experiment. Microstructure, such as surface roughness or bulk porosity, leads to a change of the path lengths and consequently the attenuation of individual x-rays traversing the sample. Due to the microstructure, the x-ray paths in and out of the sample may become correlated, ultimately leading to microabsorption effects [1]. When significant, correction of these effects is important for precise data analysis.

To obtain a precise microabsorption correction, every individual x-ray beam path needs to be considered. This requires either simplified sample models [2] or statistical approaches [3]. The presented ray-tracing simulation enables the user to calculate precise microabsorption corrections for arbitrary sample models in reflection geometry, provided the microstructure of the sample is modelled on a sufficiently fine voxel grid.

Modelling pseudo-random surfaces based on Perlin-noise allows for direct control of the lateral and vertical scales on which the height along the surface varies. The numerically calculated microabsorption corrections for these models provide insight about the importance of specific surface features such as short range roughness and long range waviness.

Fig.1:
Illustration of surfaces modelled based on Perlin noise (a) and their corresponding microabsorption corrections (b) for a simulated, symmetric measurement. Surface waviness (bottom) leads to a significant increase of the microabsorption correction at small angles, while surface roughness (top) results in a largely angular independent and small correction. The combined surface (middle) shows features of both.

References:
1) R. J. Harrison, A. Paskin (1964). *Acta Cryst.*, **17**(4), 325-331
2) B. Borie (1981). *J. of Appl. Cryst.*, **14**(4), 219-222
3) H. Hermann, M. Ermrich (1987). *Acta Cryst. A*, **43**(3), 401-405

Fig. 1

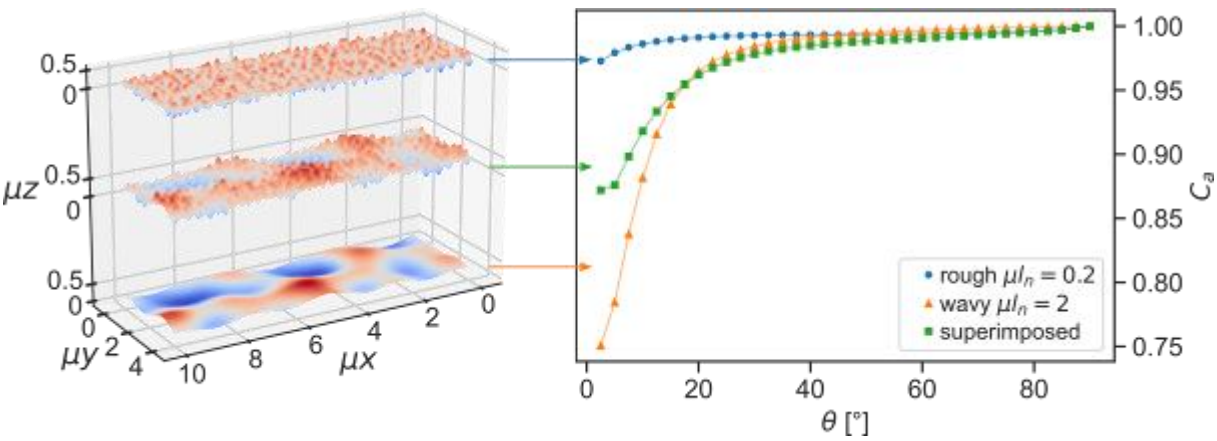

OP-013

Beamstop Outliers Rejection Based On Modern Robust Clustering in AUSPEX

Y. Gao (Hamburg/DE), A. Thorn (Hamburg/DE)

In macromolecular X-ray crystallography, extensive tools are available to find the proper high resolution cutoff for a dataset, i.e. CC(1/2) (1). However, low resolution data inclusion is rarely addressed as the statistics in low resolution bins usually look decent. Low resolution reflections are, however, crucial for phasing and contain important information about peak height, center of mass in the unit cell and solvent. Nevertheless, if such outliers do not "annoy" the data reduction pipeline, they tend to be retained in the dataset throughout further processing.

There are two types of outliers related to beamstops: observations 1) that overlap with the beamstop shadow and 2) that are close to or under the unmasked physical obstruction. The former ones are usually strong and hence can be detected with Wilson statistics. The rejection of rogue data arising from potential beamstop shadow has been implemented in many data reduction programs (2). The latter outliers present as small and negative reads with or without redundancy. During an inspection on the to-date PDB entries with available raw images in AUSPEX (3), we often can observe peculiar clusters of weak signals at the lowest resolution. Though it is not always clear whether the depositors masked the beamstop properly, the re-integration of these data sets shows that the low-resolution weak signals indeed come from insufficient beamstop modelling - and most importantly, that they were retained throughout data processing.

We demonstrate a new tool called NEMO based on modern robust clustering to find and omit these outliers in AUSPEX, and will discuss in how far this can improve structure solution and quality.

References:

(1) Karplus PA, Diederichs K (2012) Science 336,1030.
(2) Evans PR, Murshudov GN (2013) Acta Cryst. D69,1204.
(3) Thorn A, Parkhurst J, Emsley P, Nicholls RA, Vollmar M, Evans G, Murshudov GN (2017) Acta Cryst. D73:729.

MS 4: Materials science crystallography I: Total scattering techniques and local structure analysis

OP-014

Functional disorder in crystals

N. Roth (Aarhus/DK)

Disorder in crystals is often far from random, and in some cases the local correlations of disorder can be controlled. Here it is demonstrated how crystals with identical stoichiometries and average crystals structures can have different local orderings. Through single-crystal diffuse scattering experiments and three-dimensional difference pair distribution function analysis, their local structures are identified. It is further shown how different types of correlated disorder can give rise to different electronic and vibrational states. By changing the type of disorder from random to correlated, it is possible to open band gaps and tune the delocalization of modes, allowing for drastic changes to electronic properties. The three-dimensional difference pair distribution function is further extended for analysis of diffuse magnetic neutron scattering data, allowing for spin-spin correlations to be identified in crystals with magnetic disorder. Control over correlated disorder allows a new handle for tuning materials properties.

OP-015

Characterization of single-atom catalysts with X-ray total scattering and pair distribution function analysis

I. Kappel (Muhlheim an der Ruhr/DE), M. W. Terban (Stuttgart/DE), M. Vennewald (Aachen/DE), N. Sackers (Aachen/DE), J. Baums (Aachen/DE), M. Etter (Hamburg/DE), R. Palkovits (Aachen/DE), C. Weidenthaler (Muhlheim an der Ruhr/DE)

For more sustainable chemical processes, the development of efficient catalysts plays a major role. In this context, single-atom catalysts (SACs) have a huge potential as they can bridge the gap between homogeneous and heterogeneous catalysis due to unique performance, better catalyst separation, and maximum metal utilization [1]. Many questions arise when working with SACs such as confirming the presence of SAs, their coordination and how this relates to their catalytic performance. A comprehensive structural understanding, ideally under reaction conditions, is a base for knowledge-driven catalyst design. Typical characterization techniques leave questions open, so additional complementary methods need to be evaluated for the ability to obtain local structure information about such challenging systems. Here, we focus on synchrotron-based X-ray total scattering (TS) and pair distribution function (PDF) analysis for the characterization of 0.5 wt.% Pd immobilized on exfoliated graphitic carbon nitride (ECN) [2]. The difference PDF analysis of SAC samples with different amounts of Pd are shown in *fig 1*. A pair correlation at ~ 2.04 Å grows with increased loading. In combination with DFT calculations, this peak can be assigned to Pd-N/O. The absence of Pd-Pd distances in all the SAC samples confirms a high dispersion of the metal centers. X-ray TS and atomic dPDF analysis have the potential to contribute to the understanding of SACs on polymeric support with very low metal loading.

We acknowledge funding by the Cluster of Excellence Fuel Science Center (EXC 2186, ID: 390919832) by the Excellence Initiative by the German federal and state governments to promote science and research at German universities.

References:

(1) Soorholtz, M., et al. *ACS Catalysis 6.4*. **2016**, 2332.
(2) Vennewald, M., et al. *J. Catal.* **2023**, 421, 134.

Fig.1) dPDF analysis of SACs with different Pd loading and a sample containing Pd nanoparticles (NP)

Fig. 1

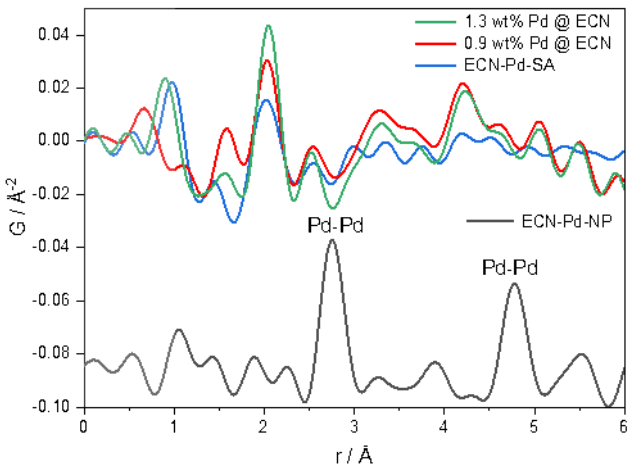

OP-016

Multi-phase PDF analysis of the near ambient condition phase transitions of quantum-crystalline brookite

O. Thueringer (Bremen/DE), A. Wollbrink (Bremen/DE), K. Kraemer (Bremen/DE), M. Bäumer (Bremen/DE), L. Robben (Bremen/DE), T. M. Gesing (Bremen/DE)

Titania (TiO_2) is widely used as photocatalytic material for wastewater treatment [1]. Of the known polymorphs, rutile ($P4_2/mnm$), anatase ($I4_1/amd$) and brookite (Pbca), rutile is the high-temperature and thermodynamic stable modification. Anatase and brookite are metastable modifications. Anatase can directly be converted into rutile, whereas brookite could either form anatase or rutile [2]. The phase-transition temperatures (PTT) of the anatase-rutile conversion is at ~1020 K, those of the brookite-anatase polymorphic change at ~720 K. While starting the latter one from quantum crystalline brookite, the phase-transition temperature is strongly correlated with the average crystallite size (ACS) [3,4]. With increasing ACS, the phase transition is shifted to higher temperatures. Therefore, systematic studies of the short- and long-range ordering during the phase transition are important to understand the ACS dependency to the PTT. Therefore, brookite, as quantum crystalline phase, is the synthesized phase using a sol-gel method. Its phase-transition kinetic is studied at different temperatures by means of XRPD Rietveld and multi-phase PDF analysis, as well as UV/Vis- and FTIR-spectroscopy. The results reveal a time-resolved phase-transition rate from brookite to anatase of about 0.7 wt-%/day at ambient conditions. After about 9 weeks under these conditions, the transformation stagnates at an equilibrium of about 60 wt-% brookite and 40 wt-% anatase. This seems to be the thermodynamic equilibrium at the given temperature. This is supported by the observation, that higher temperatures shift the equilibrium to higher anatase contents.

We acknowledge support by DFG under grant number GE1981/13-1.

References:

(1) H.-J. Oh et al. Appl. Catal. B, 84 (2008) 142-147.
(2) Q. Xu,et al. Chem. Asian J. 5 (2010) 2158-2161.
(3) A. Gribbet et al. Am. Mineral. 82 (1997) 717-728.
(4) N. Allen et al. Polym. Degrad. Stab. 150 (2018) 31-36.

OP-017

Exploring the effects of the photochromic response and crystallization on the non-crystalline niobium oxide

E. Onur (Muhlheim an der Ruhr/DE), J. Lee (Muhlheim an der Ruhr/DE), R. Aymerich-Armengol (Dusseldorf/DE), H. Tüysüz (Muhlheim an der Ruhr/DE), C. Scheu (Dusseldorf/DE), C. Weidenthaler (Muhlheim an der Ruhr/DE)

Niobium oxide (Nb_2O_5) is a versatile semiconductor material with photochromic properties and applications in capacitors, electrochromic devices, and sensors. They are also of great interest in heterogeneous catalysis as catalysts or as cocatalysts. In catalysis research, the focus often lies on studying faulted, disordered, or non-crystalline materials. Understanding the structural relationships in catalysis is crucial for connecting structure with catalytic performance. This study investigates the local structure of short-range-ordered (SRO) niobium oxide synthesized via a sol-gel method from $Nb(OEt)_5$ precursor. X-ray total scattering (TS) experiments, along with subsequent atomic pair distribution function (PDF) analysis, unveil the structural arrangements within the SRO material. The heat-induced crystallization process was also tracked using *in situ* TS and X-ray diffraction (XRD) techniques, revealing the transformation of ordered structural units mainly into the TT-type Nb_2O_5 crystalline structure after heat treatment at 550 °C. In addition, the effect of photocatalytic conditions on the material"s structure was examined by subjecting the SRO and crystalline samples to ultraviolet (UV) light exposure, resulting in a reversible photochromic color change from white to dark brown or blue. *In situ* TS and PDF analysis indicates the reversible elongation of nearest neighbor Nb-O bonds within an octahedral configuration during the color change of the SRO material. Optical band gap calculations based on the UV-visible spectra collected for the SRO and crystallized materials indicate that the band gaps reduced with the darkened colors go back to the initial values after bleaching. Furthermore, electron energy loss spectroscopy reveals the reduction of Nb centers as a residual effect. This comprehensive investigation establishes a correlation between the band gap and the structure of niobium oxide, shedding light on its atomic-level structure-performance relationship.

MS 5: Structural biology II: New structures – cellular signaling

OP-018

Allosteric Inhibition of Sialic Acid TRAP Transporter SBPs by VHH Antibodies

N. Schneberger (Bonn/DE), P. Hendricks (Bonn/DE), S. C. Binder (Bonn/DE), M. F. Peter (Bonn/DE), P. A. Koenig (Bonn/DE), S. Menzel (Bonn/DE), M. Geyer (Bonn/DE), G. H. Thomas (York/GB), G. Hagelueken (Bonn/DE)

Some pathogenic bacteria rely on the import of sialic acid by tripartite ATP-independent periplasmic (TRAP) transporters to survive in the host environment. In *Vibrio cholerae* the availability of this sugar enhances pathogenicity, whereas *Haemophilus influenzae* uses it to modify its lipopolysaccharide shell and thereby to actively evade the immune response of the host. A better understanding of the TRAP transporter mediated sialic acid transport mechanism may help to combat these pathogens more efficiently.

TRAP transporters employ dedicated substrate binding proteins (SBPs) that contribute to a selective and efficient transport process by binding the substrate and delivering it to the transporter. It is known that camelid derived VHH antibodies are able to inhibit SBPs of ABC transporters and can serve as tools to investigate their mechanistic and structural details. We identified a set of 11 VHH antibodies that specifically target the sialic acid TRAP transporter SBPs (also called P-domains) from *H. influenzae* and *V. cholerae*, two of which potently inhibit substrate binding.

A thorough structural and biophysical characterization of the VHH/SBP complexes revealed an allosteric mechanism that does not only inhibit the high-affinity binding of Neu5Ac but also ejects an already bound sugar molecule from the binding pocket. Furthermore, structure-guided mutagenesis highlighted a hydrophobic surface cavity containing residue W73 as a key element in the conformational rearrangement upon sialic acid binding. Our results shed new light on the structural mechanism of the substrate-induced closure of TRAP transporter SBPs.

This analysis of SBP-VHH antibody complexes helps to gain further insight into the mechanism of TRAP transporters and reveals interesting starting points for drug development efforts against the severe diseases caused by *H. influenzae* and *V. cholerae*.

OP-019

GAP together! Structural and biochemical analysis of the RalGAP complexes

R. Rasche (Münster/DE), L. H. Apken (Münster/DE), B. U. Klink (Münster/DE), E. Michalke (Münster/DE), C. Gatsogiannis (Münster/DE), A. Oeckinghaus (Münster/DE), D. Kümmel (Münster/DE)

The small Ras-like GTPases RalA and RalB are involved in control of proliferation, regulation of autophagy, endocytosis and exocytosis and are related to Ras signalling [1]. Thus, they play a crucial role in the progression of cancers like pancreatic ductal adenocarcinoma. Hence, the heterodimeric RalGAP complexes, which deactivate Ral by catalysing GTP hydrolysis, are potent tumour suppressors [2]. Furthermore, the atypical Ras-like protein κB-Ras, which is also involved in NFκB inflammatory processes, interacts constitutively with RalGAP. So far, no (sub)structures of these complexes have been reported and the molecular and biological mechanism of Ral regulation by RalGAP remains puzzling. Bioinformatical and biochemical analysis leads to the conclusion that RalGAP harbours an asparagine-thumb GAP domain. As a unique feature, RalGAP needs both of its subunits for GAP activity on Ral, assuming that the catalytic mechanism differs from other GAPs of this family. Furthermore, it was shown that κB-Ras is required for RalGAP activity *in vivo* and κB-Ras deficiency is related to Ral driven tumour progression [3]. To understand the GAP mechanism and elucidate the role of κB-Ras, we combine biochemical and structural (X-ray crystallography, cryo EM, computational modelling) approaches. We recently determined the crystal structure of κB-Ras bound to the interaction domain of RalGAP. The structure reveals the molecular basis for the uncommonly weak G-nucleotide binding behaviour of κB-Ras and a G-nucleotide independent binding mode of the κB-Ras:RalGAP interaction. Our data also suggest a non-canonical GTP hydrolysis mechanism of κB-Ras that does not require a catalytic residue. This adds a piece to a more complete understanding of Ral signalling regulation and related disease development.

References:

(1) Apken, L.H. *et al*. *Int. Rev. Cell Mol. Biol.* **2021**, *361*, 21-105.
(2) Shirakawa, R. *et al. JBC* **2009**, *285* (32), 21580-21588.
(3) Oeckinghaus, A. *et al. Cell Rep.* **2014**, *8*, 1793–1807.

Fig. 1

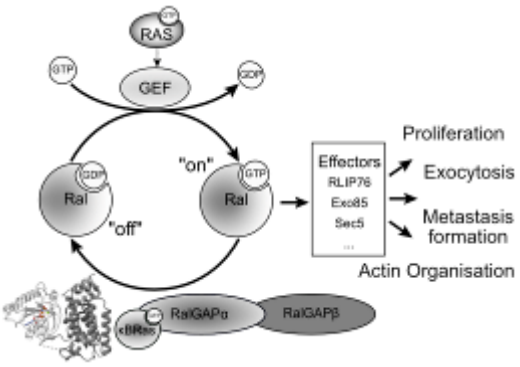

OP-020

DARPins as biological tools to reactivate wild-type and mutant p53 in cancer cells

D. I. Balourdas (Frankfurt a. M./DE), P. Münick (Frankfurt a. M./DE), B. Yüksel (Frankfurt a. M./DE), A. Strubel (Frankfurt a. M./DE), B. Schäfer (Zurich/CH), J. Schaefer (Zurich/CH), A. Plückthun (Zurich/CH), S. Knapp (Frankfurt a. M./DE), A. C. Joerger (Frankfurt a. M./DE), V. Dötsch (Frankfurt a. M./DE)

The transcription factor p53, also known as the guardian of the genome, is inactivated in virtually every tumor, either by mutation in the *TP53* gene or by dysregulation of its regulatory pathways. Most of the p53 cancer mutations are missense mutations in the DNA-binding domain (DBD), and many of them reduce the conformational stability of the protein, resulting in rapid unfolding, followed by aggregation. Therapeutic efforts to restore p53 conformational stability and transcriptional activity involve diverse strategies that aim to either protect p53 from its negative regulators or restore the functionality of mutant p53 proteins. Here we propose Designed Ankyrin Repeat Proteins (DARPins) as a potential novel therapeutic strategy to reactivate both wild-type and mutant p53 DBD.

Through ribosome display, we identified DARPin C10 that selectively binds to the p53 DBD with an affinity of 250 nM. Our structural and transactivation assay data demonstrate that C10 stabilizes and restores the transcriptional activity of wild-type p53 in papilloma virus infected HeLa cells by blocking the HPV-E6 mediated degradation of p53 (Fig. 1). Analysis of the p53-C10 interface suggested that DARPin C10 may also be used as molecular chaperone to stabilize and reactivate conformationally unstable mutants. In a proof-of-concept study, we therefore performed systematic dose-response thermal stability and transactivation assays with a series of cancer hotspot mutants, complemented by high-resolution co-crystal structures of the mutant p53 DBD-C10 complexes, showing that C10 can stabilize and potentially reactivate conformationally unstable p53 mutants in cancer cells (Fig. 2). Future studies will focus on further improving the binding affinity of DARPin C10 for the p53 DBD, screening the p53 cancer mutome to identify and classify targetable mutants, and the development of cellular delivery systems for therapeutic exploitation of our generic p53-stabilizing DARPins.

Fig. 1

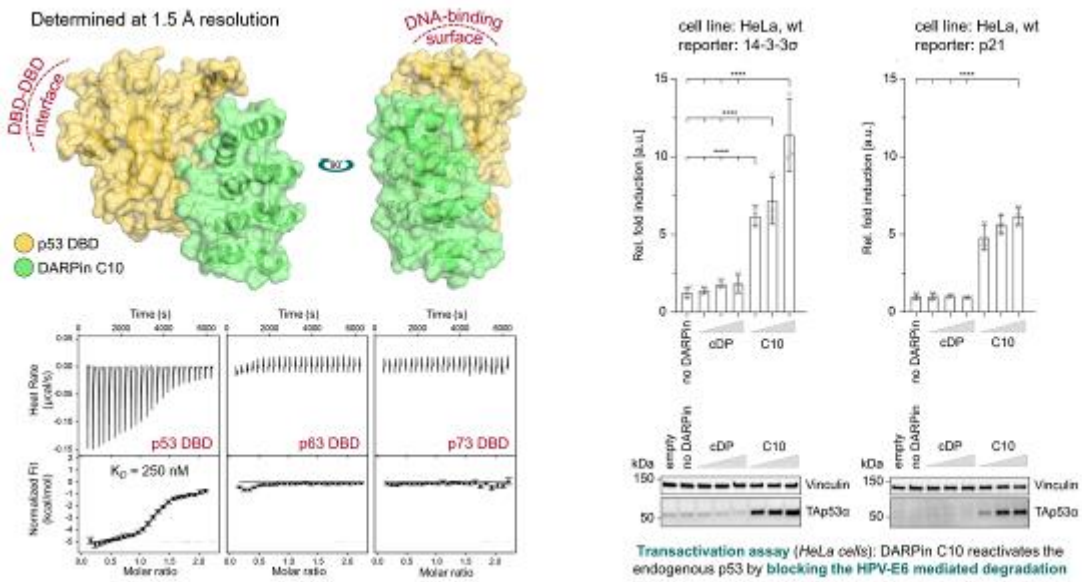

Fig. 2

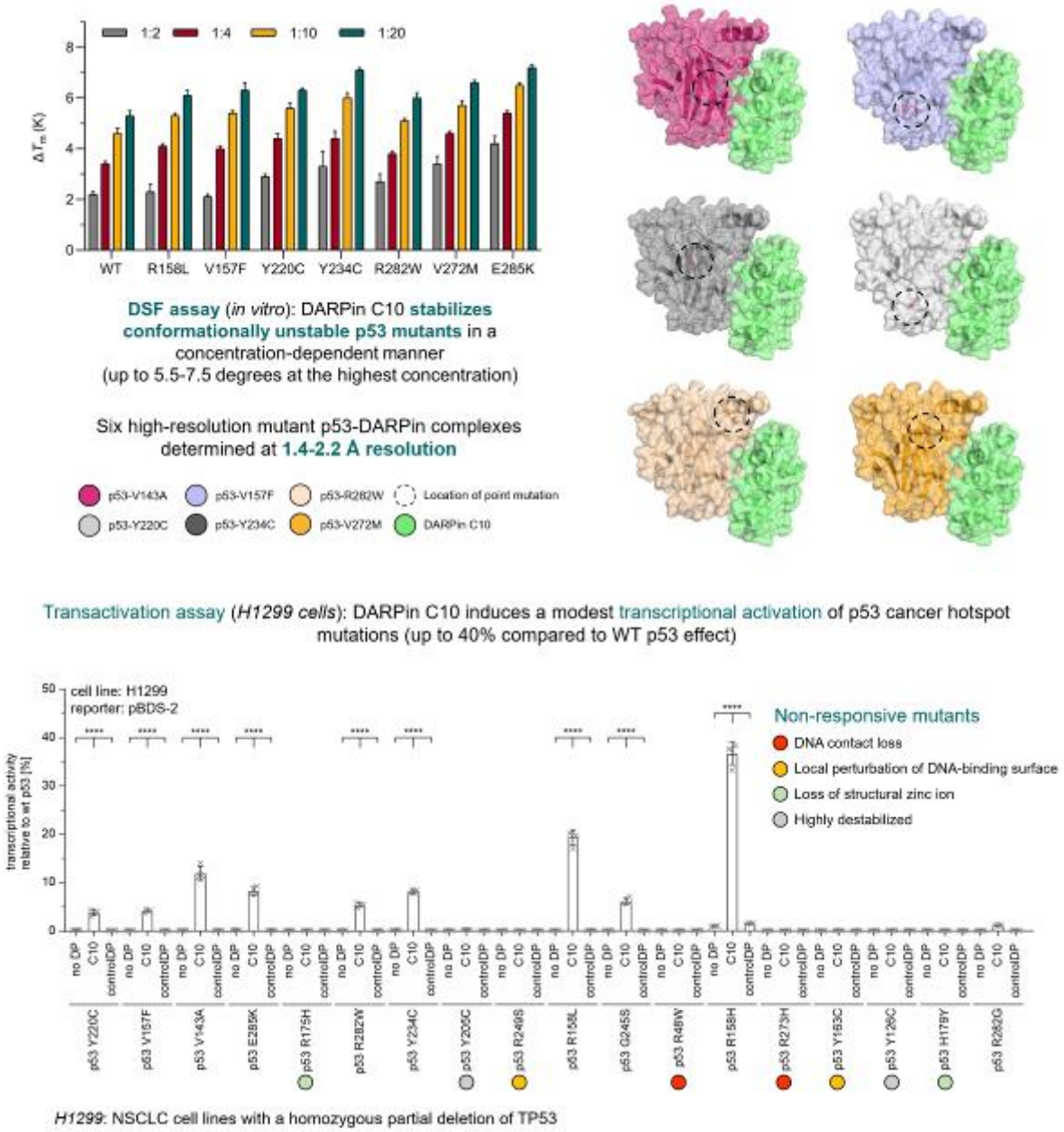
1:2
1:4
1:10
1:20
ΔTm (K)
WT
R158L
V157F
Y220C
Y234C
R282W
V272M
E285K
DSF assay (in vitro): DARPin C10 stabilizes conformationally unstable p53 mutants in a concentration-dependent manner
(up to 5.5-7.5 degrees at the highest concentration)
Six high-resolution mutant p53-DARPin complexes determined at 1.4-2.2 Å resolution
p53-V143A
p53-V157F
p53-R282W
Location of point mutation
p53-Y220C
p53-Y234C
p53-V272M
DARPin C10
Transactivation assay (H1299 cells): DARPin C10 induces a modest transcriptional activation of p53 cancer hotspot mutations (up to 40% compared to WT p53 effect)
cell line: H1299
reporter: pBDS-2
transcriptional activity relative to wt p53 [%]
Non-responsive mutants
DNA contact loss
Local perturbation of DNA-binding surface
Loss of structural zinc ion
Highly destabilized
H1299: NSCLC cell lines with a homozygous partial deletion of TP53

OP-021

New insights into the structural biology of Cytotoxic Necrotizing Factors

S. Dong (Braunschweig/DE), P. Lukat (Braunschweig/DE), S. zur Lage (Braunschweig/DE), A. Steffen (Braunschweig/DE), T. E. B. Stradal (Braunschweig/DE), W. Blankenfeldt (Braunschweig/DE)

Cytotoxic Necrotizing Factors (CNFs) are single-chain protein toxins of pathogenic bacteria such as uropathogenic Escherichia coli or Yersinia pseudotuberculosis. They consist of a cell-binding and translocation apparatus within the first half of the sequence, followed by a toxic fragment that constitutively activates RhoGTPases once it has reached the cytosol of the targeted eukaryotic cell, leading to cell death and tissue necrosis. Our previous work showed that the structure of Y. pseudotuberculosis CNFY consists of five domains within its 1014 amino acids in a relatively compact way. While this structure may serve as a paradigm for other CNFs, it does not explain differences to other homologs, such as e.g. an additional receptor binding site for Lu/BCAM in the C-terminal region of E. coli CNF1. To characterize CNF1 and its interaction with the Lu/BCAM receptor, full-length CNF1 and Lu/BCAM as well as fragments of both proteins were produced recombinantly. The structure of full-length CNF1 was determined at 3.75 Å resolution. The asymmetric unit contained two independent copies of the protein in a similar conformation, revealing that CNF1 adopts a much less compact structure than CNFY despite consisting of similar domains and having 65% sequence identity. The structure of a complex of the catalytic domain of CNF1 and a fragment of Lu/BCAM at 2.0 Å resolution shows that both proteins interact with 1:1 stoichiometry. Surprisingly, the binding interface involves different residues than were reported previously. This region differs from CNFY, explaining why the latter cannot use Lu/BCAM as a receptor. Our new data shine the first light on the interaction of CNF1 with its co-receptor Lu/BCAM. In addition, the significant differences between the structures of full-length CNF1 and CNFY may indicate that the CNFs possess high internal flexibility that may be required to orchestrate the various steps that these toxins need to perform to intoxicate host cells.

OP-022

The crystal structure of the Legionella effector Lem3 in a stabilized complex with the human GTPase Rab1 sheds light on substrate-recognition and de-phosphocholination mechanisms

V. Pogenberg (Hamburg/DE), M. Kaspers (Hamburg/DE), C. Pett (Umeå/SE), S. Ernst (Munich/DE), F. Ecker (Munich/DE), P. Ochtrop (Umeå/SE), M. Groll (Munich/DE), C. Hedberg (Umeå/SE), A. Itzen (Hamburg/DE)

Many pathogenic bacteria use post-translational modifications (PTMs) to manipulate host cell functions and signaling pathways. For example, *Legionella pneumophila,* the causative agent of Legionnaires disease, secretes a plethora of effectors into the host, including some enzymes that can perform PTMs and others that are able to reverse them. It is often challenging to elucidate the structural mechanisms by which these enzymes recognize and modify their protein targets. Indeed, structural studies, including those performed using new artificial intelligence tools, often fail due to the transient nature of the enzyme-substrate interactions.

We recently developed a new approach to stabilize enzyme-substrate complexes making use of thiol-reactive co-substrates. The modifying enzymes are strategically mutated to place a cysteine in their active sites, coupling them to the co-substrate to create reactive binary probes for covalent substrate capture. This method allowed us to obtain a number of highly stable enzyme:PTM:substrate complexes and determine their crystal structures.

One of these enzymes, *Legionella* AnkX, uses cytidine diphosphate-choline to add a phosphocholine moiety to the human small G-protein Rab1 at a single specific position. Later in the infection, the *legionella* enzyme Lem3 removes the phosphocholine group. With the help of the above-mentioned capture approach, we were able to solve the crystal structure of the Lem3:Rab1b complex. This structure reveals that Lem3 acts on Rab1 by locally unfolding it, providing a rationale for how Lem3 is able to recognize and de-phosphocholinate modified Rab1. Since Lem3 shares striking structural homology with metal-dependent protein phosphatases, our findings also have important implications for the field of de-phosphorylation.

MS 6: Extreme conditions I: Oxides and complex materials

OP-023

Recent Developments in the High-Pressure/High-Temperature Chemistry of Oxonitridoborates

H. Huppertz (Innsbruck/AT), I. Widmann (Innsbruck/AT), B. Fuchs (Innsbruck/AT)

Recently, we were able to synthesize the first high-pressure chromium oxonitridoborate with the composition CrB_4O_6N.[1]The compound crystallizes in the non-centrosymmetric space group $P6_3mc$ (no. 186) with the lattice parameters a = 5.1036(1), c = 8.3519(3) Å, and a volume of 188.40(1) Å^3. It was synthesized in a high-pressure/high-temperature experiment at 7 GPa and 1673 K. The structure of CrB_4O_6N, as shown in Figure 1, is built up of starlike-shaped entities of four BO_3N tetrahedra, linked via one common nitrogen atom that resembles the fourfold-coordinated nitrogen atoms in the homeotypic nitridosilicates $MYbSi_4N_7$ (M = Eu, Sr, Ba).[2] Building up a network with channels that contain the Cr^{3+}ions, CrB_4O_6N contains for the first time a tetrahedral building unit in contrast to the trigonal planar $B(O/N)_3$ entities in all other known oxonitridoborates. The structural relations of this compound as well as the results of spectroscopic measurements, calculations and ongoing attempts to realize highly interesting substitution variants of this compound will be presented.

Fig. 1: Crystal structure of CrB_4O_6N.

References:

(1) B. Fuchs, D. Johrendt, L. Bayarjargal, H. Huppertz, *Angew. Chem. Int. Ed.* **2021**, *60*, 21801-21806.
(2) H. Huppertz, W. Schnick, *Angew. Chem. Int. Ed.* **1996**, *35*, 1983-1984.

Fig. 1

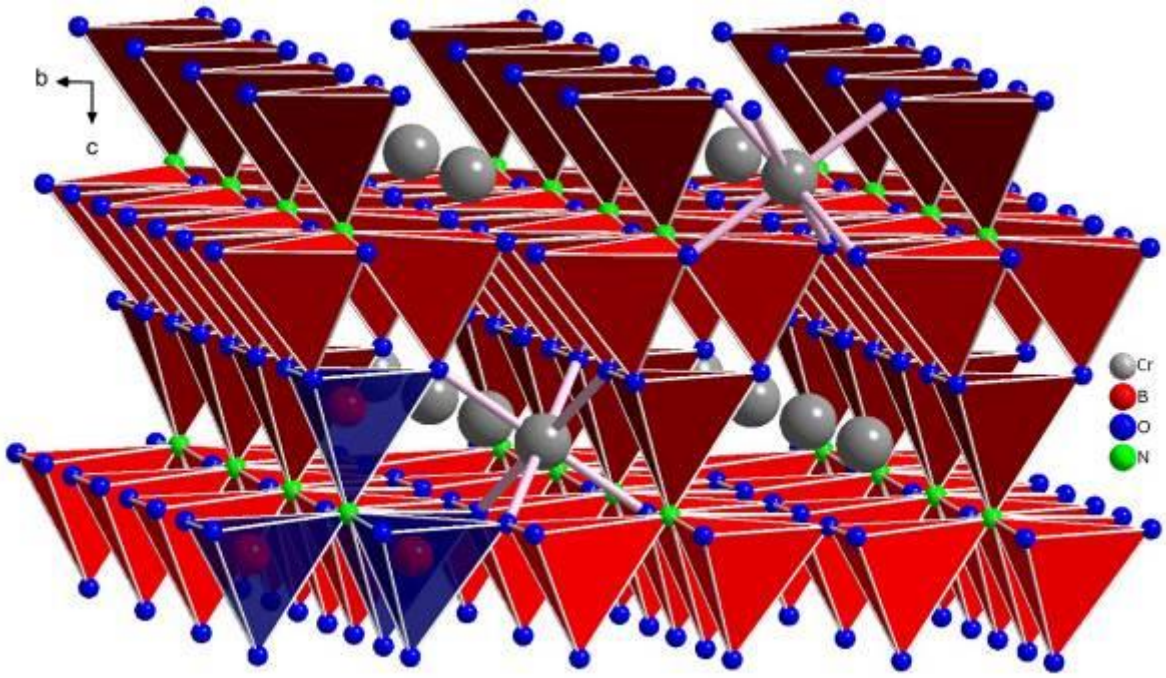

OP-024

Pressure assisted synthesis of highly crystalline Li_xMoS_2 and related compounds

S. Schwarzmüller (Innsbruck/AT), H. Huppertz (Innsbruck/AT)

Li_xMoS_2 is not only discussed as lithium battery material, but is also an important precursor for the synthesis of MoS_2 nanomaterials.[1,2] Current syntheses of MoS^2 like in n-butyllithium / $LiBH^4$ or electrochemically are not satisfying in terms of defined stoichiometry and crystallinity.[3] Since this compound is notoriously difficult to prepare in good quality, an accurate experimental crystal structure determination of this important and widely used material is longingly awaited. Applying a high-pressure/high-temperature synthesis, highly crystalline 1*T*''''-Li_xMoS_2 (x = 1, 1.333) was obtained. 1*T*''''-$LiMoS_2$ crystallizes in the space group *P*-1 with a = 6.2482(3) Å, b = 6.6336(3) Å, c = 6.7480(3) Å, α = 119.321(2)°, β = 90.010(2)° and γ = 90.077(2)°.[4] The arrangement of Mo atoms within the *b*-*c*-plane confirm a predicted Peierls distortion.[5] A similar atom distribution pattern as for Mo is also observed for the lithium atoms. Calculation of bond valence site energies gave an activation barrier of 1.244 eV for 2D lithium-ion migration. For x = 1.333, a phase pure synthesis was achieved. A similar synthesis technique can also be applied for the other alkali metal molybdenum / tungsten sulfides.

References:

(1) Z. Li, I Sami, J. Yang, J. Li, r. V. Kumar, M. Chhowalla, *Nat. Energy* **2023**, *8*, 84-93.
(2) M. Chhowalla, H. S. Shin, G. Eda, L.-J. Li, K. P. Loh, H. Zhang, *Nat. Chem.* **2013**, *5*, 263-275.
(3) X. Rocquefelte, I Bouessay, F. Boucher, P. Gressier, G. Ouvrard, *J. Solid State Chem.* **2003**, *175*, 380-383.
(4) S. Schwarzmüller, K. Wurst, G. Heymann, H. Huppertz, *Chem. Eur. J.* **2023**, e202302565.
(5) M. Song, Q. Shi, D. Kan, S. Wie, F. Xu, W. Huo, K. Chen, *Appl. Surf. Sci.* **2023**, *612*, 155761.

Figure 1: Left: Crystal structure of $LiMoS_2$ along the *b* direction. Right: Mo-Mo connectivity within the *b*-*c* plane at a≈0 (black) with indicated atomic distances in Å. Li-Li connectivity within the *b*-*c* plane at a≈0.5 (grey) with indicated atomic distances in Å.

Fig. 1

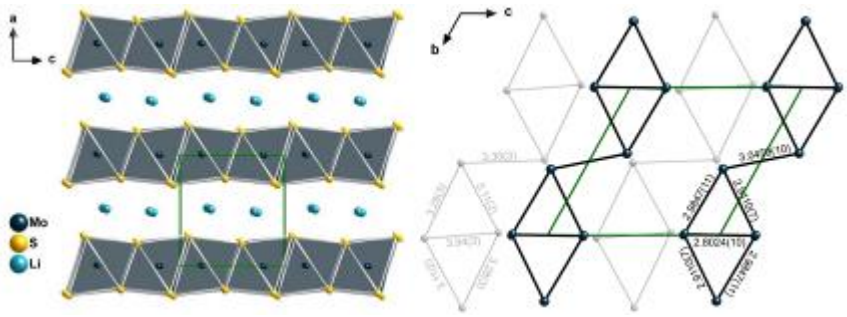

OP-025

High-Pressure Synthesis of Spinels in the Element System Ge-Ga-Cr-O-N

M. Schwarz (Freiberg/DE), F. Sieg (Freiberg/DE), T. Boyko (Saskatchewan/CA), E. Kroke (Freiberg/DE)

As reasearcher of TU Bergakademie Freiberg it is particularly appealing to do exciting science that deals with at least one of the chemical elements which have been discovered at this University more than one century ago: Germanium (Ge), or Indium (In). For example, spinel-type γ-Ge_3N_4 is a highly interesting high-pressure-derived nitride semiconductor material, first synthesized at the end of the 1990ies (outside Freiberg) in close temporal proximity with the two other IV-III spinel nitrides γ-Si_3N_4 and γ-Sn_3N_4. Here we show that charge-neutral exchange of Ge-N pairs in γ-Ge_3N_4 with trivalent metal Ions Cr^{3+} and Ga^{3+} together with oxygen, gives rise to a new and unexplored phase field of spinel-type solid solutions in the quinternary element system Ge-Ga-Cr-O-N. With a compositionally tunable band gap in the visible and UV, the GeCrON, GaCrON and GeGaCrON spinels are potential candidates for overall water-splitting by sunlight, occurrence of magnetic frustration and, possibly, antiferromagnetic spintronics. They can be made by a solvothermal route from suitable precursors, employing high-pressure high temperature synthesis, e.g. in a multianvil press.

Fig. 2

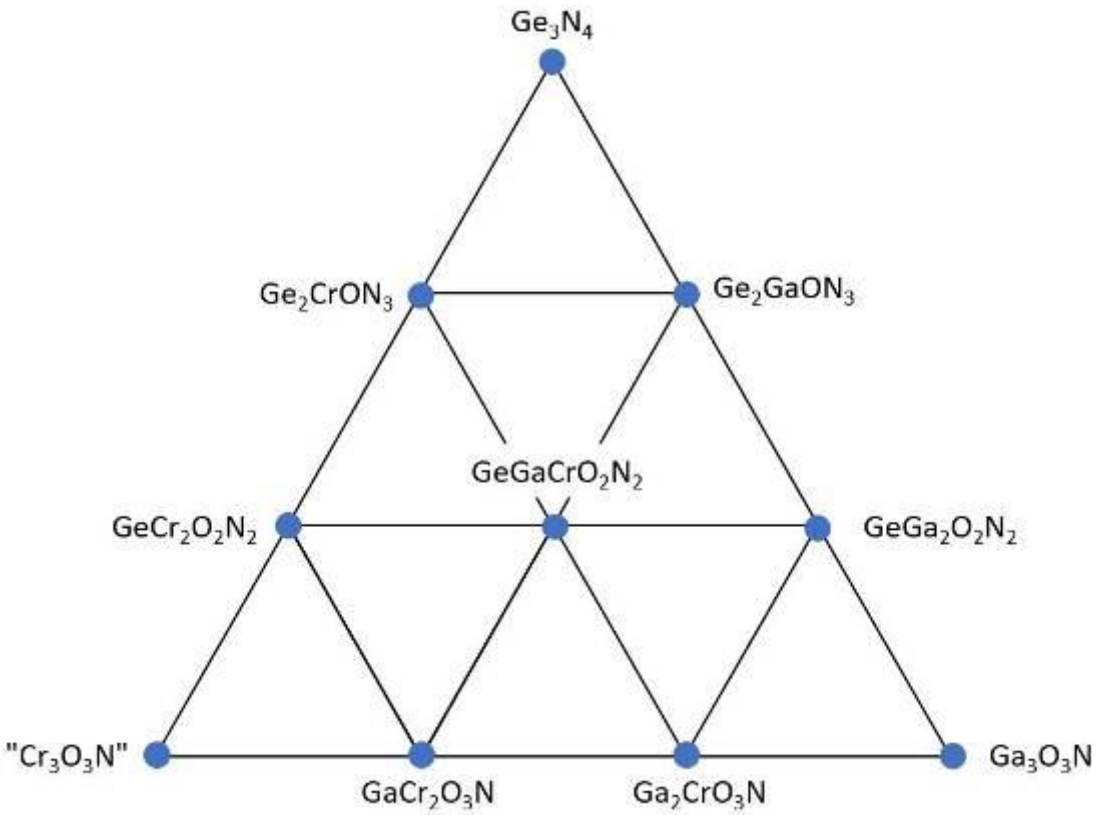

OP-026

A piezo-driven dynamic diamond anvil cell for measurements of pressure-dependent second harmonic generation

T. H. Reuter (Frankfurt a. M./DE), L. Bayarjargal (Frankfurt a. M./DE), B. Winkler (Frankfurt a. M./DE)

For detailed investigation of pressure-dependent phase transitions, it is desirable to be able to vary the pressure in small steps. One option to achieve this is to employ piezo-driven diamond anvil cells (DACs), where a piezo actuator expands when voltage is applied, increasing pressure in the DAC[1]. This setup also allows for investigations with high compression rates[1].

We integrated a piezo-driven DAC into our second harmonic generation (SHG) measurement setup[2]. This enables quasi-continuous pressure-dependent SHG measurements. An initial fluorescence measurement is carried out for pressure determination, followed by a series of SHG measurements, which are averaged, concluded by pressure determination for every data point. Fig. 1 shows the relation between the voltage applied to the piezo actuator and resulting pressure in a DAC. A quasi-continuous pressure increase can be achieved and enables detailed characterizations of pressure-dependent phenomena. Fig. 2 shows the pressure-dependent SHG signal of $BaTiO_3$, where we compare data obtained by manually increasing the pressure using a gearbox to data obtained using the quasi-continuous piezo setup presented here. The trend of the averaged data of quasi-continuous measurements is in good agreement with the data of stepwise pressure increase. Causes of deviation of individual data from the average require further investigation.

Financial support by the DFG (project BA4020/4-1) is gratefully acknowledged.

Fig. 1 Voltage applied to the piezo actuator and resulting pressure increase in a DAC.

Fig. 2 Pressure-dependent SHG signal of $BaTiO_3$. Circles and dashed line represent stepwise measurements, where pressure was increased via a gearbox. Diamonds represent data and the continuous line represents the moving average of SHG signals obtained by quasi-continuous pressure increase using the piezo-driven DAC.

References:

(1) [1]Jenei et al. *REV SCI INSTRUM* **2019** 90, 6, 65114.
(2) [2]Bayarjargal et al. *Z KRIST-CRYST MATER* **2014** 229, 2.

Fig. 1

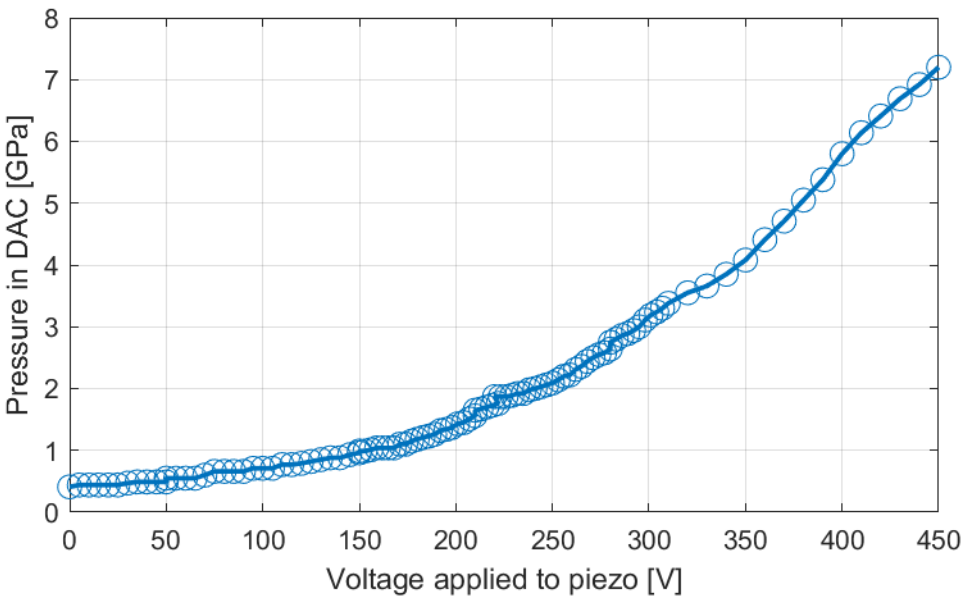

Fig. 2

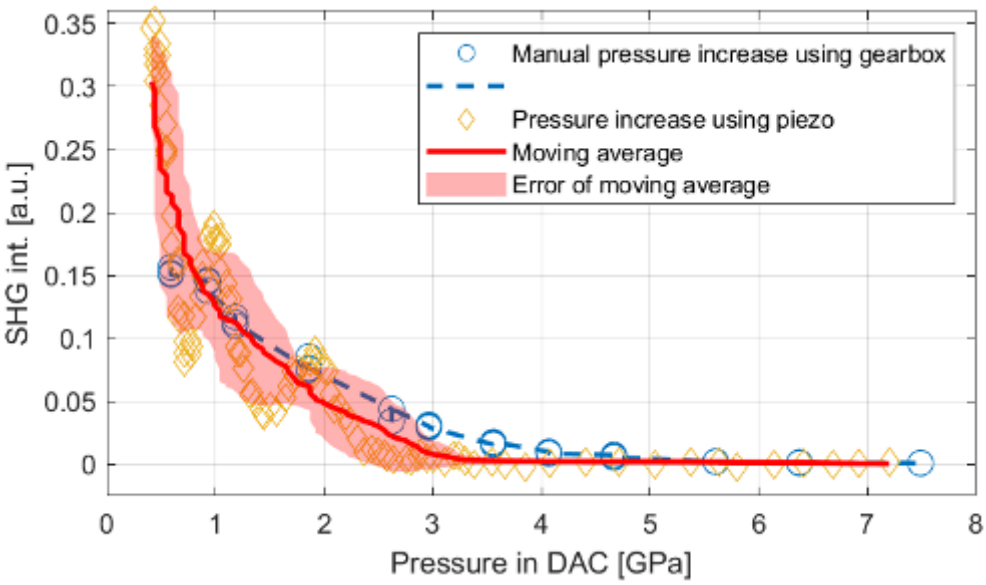
Manual pressure increase using gearbox
Pressure increase using piezo
Moving average
Error of moving average
SHG int. [a.u.]
Pressure in DAC [GPa]
0.35
0.3
0.25
0.2
0.15
0.1
0.05
0
0
1
2
3
4
5
6
7
8

MS 7: Chemical crystallography I: Solid state compounds

OP-027

Electron Diffraction Tomography on Two-Phase Nano-Lamellae of Topochemically Synthesized $Cu(Sb_2S_3)Cl$

W. Carrillo-Cabrera (Dresden/DE), O. Dreimann (Dresden/DE), A. Krasheninnikov (Dresden/DE), M. Ruck (Dresden/DE)

Question

Can we use heterogeneous topochemical transformation under soft conditions to synthesize potentially metastable compounds that are otherwise inaccessible? How can we characterize them structurally?

Methods

High temperature synthesis of the precursor. Aqueous leaching of the precursor. EDX analysis. Transmission electron microscopy. Selected-area electron diffraction. Selected-area precession electron-diffraction tomography. UV-vis spectroscopy. DFT calculations.

Results and Conclusion

The dark red semiconductor $Cu(Sb_2S_3)Cl$ was obtained by leaching the layered precursor $Cu(Sb_2S_3)[AlCl_4]$ in 0.1 molar HCl. The extraction of $AlCl_3$ yielded a mica-like lamellar product of poor crystallinity. Misalignment of lamellae down to the nanoscale prevented structure determination by conventional single-crystal X-ray diffraction, but a combination of transmission electron microscopy, selected area electron diffraction, and manual selected area electron precession diffraction tomography on a nanoscale spot with largely ordered crystalline lamellae facilitated the determination of the crystal structures of two intergrown modifications. Orthorhombic o-$Cu(Sb_2S_3)Cl$ and monoclinic m-$Cu(Sb_2S_3)Cl$ have similar layers as the precursor. These consist of uncharged Sb_2S_3 strands whose sulfide ions, together with chloride ions, coordinate the copper(I) cations. Only one chloride ion remained from the $[AlCl_4]^-$ group. DFT calculations confirm the structure solution for the orthorhombic form and suggest that the monoclinic structure is metastable against a transformation to o-$Cu(Sb_2S_3)Cl$. Since attempts to synthesize $Cu(Sb_2S_3)Cl$ directly from CuCl and Sb_2S_3 have not been successful, the use of the structurally close precursor and the moderate conditions of the topochemical reaction seem to be indispensable.

Figure 1: Crystal structures of the precursor $Cu(Sb_2S_3)[AlCl_4]$ and the leaching product o-$Cu(Sb_2S_3)Cl$.

Fig. 1

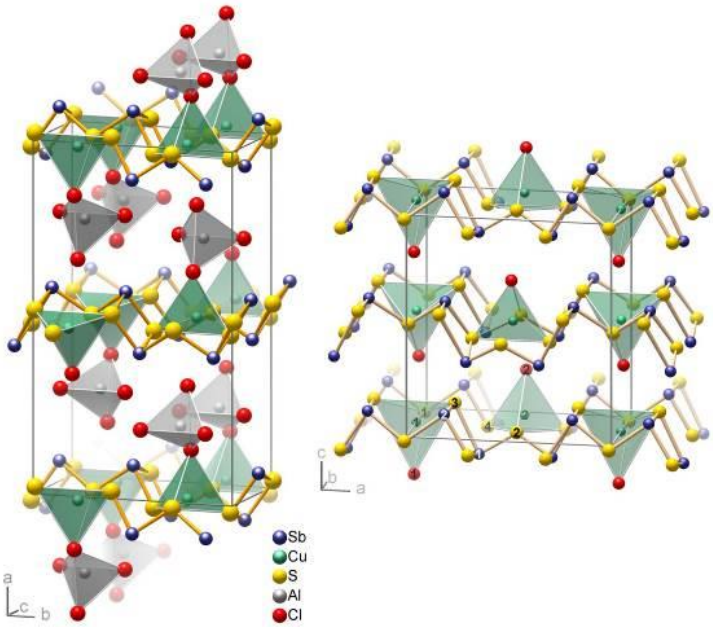
Sb
Cu
S
Al
Cl
a
c
b

OP-028

Topochemical modifications of perovskite materials by fluoride doping

S. Kunz (Stuttgart/DE), L. Sahoo (Stuttgart/DE), O. Clemens (Stuttgart/DE)

Perovskite compounds ABO_3 exhibit structural and compositional flexibility at both cation A and B sites, as well as on the anion sublattice site [1]. The introduction of anions in the host lattice modifies the chemical properties by influencing the transition metal-oxygen bond, as well as the oxidation states of the B cations [2]. Typical application fields for mixed anion perovskite structure types are for example magnetoelectrics and catalysts [3]. However, mixed anion compounds often lack thermal or thermodynamic stability. To address such challenges well adapted synthesis conditions are highly important.

In the present study, we systematically investigate the structural changes of Ba-rich transition metal oxides $BaFe_{1-x}Co_xO_{3-d}F_y$, $BaFe_{1-x}Ti_xO_{3-d}F_y$, $BaCo_{1-x}Ti_xO_{3-d}F_y$ with increasing amount of fluorine (y = 0; 0.34; 0.5; 0.75; 1). The parent oxide structure of newly synthesized oxyfluorides is tunable by the given ratio of transition metals. The fluorination of Ba-rich transition metal oxides has been achieved via low-temperature topochemical reaction route by using PVDF as fluorinating agent [4]. Upon fluorination, the structural changes induced as function of the degree of fluorine content combined with a different ratio of B site cations reveal a complex competition between anion ordering, structural rearrangements, and the thermodynamic stability.

References:

(1) Y. Kobayashi et al, *Annu. Rev. Mater. Res.* **2018**, 48, 303.
(2) O. Clemens et al, *Rev. Inorg. Chem.* **2018**, 33, 2-3, 105.
(3) A. Hossain et al, *Ceram. Int.* **2018**, 45, 4152.
(4) S. Perween et al, *Inorg. Chem.* **2023**, 62, 40, 16329.

Acknowledgment: DFG Fund within FLAIR CRC 1548

OP-029

New Pt-Ge-As and Pt-Ge-Sb compounds exhibit ternary variants of the $CaCl_2$ structure type

K. Witthaut (Munich/DE), D. Johrendt (Munich/DE)

We present the first compounds within the ternary systems of Pt-Ge-As and Pt-Ge-Sb. The primary compound discovered was $Pt_3Ge_3As_3$. It exhibits the known FeAsS structure type[1] in the space group *P*21/*c* (no. 14), which can be derived from the CaCl2 structure[2] by distortion of the Cl layers. The structure can be described as edge-sharing chains of $Fe(As_3S_3)$ octahedra with alternating Fe – Fe distances (fig. 1a). Further research revealed $Pt_3Ge_2As_4$, and $Pt_3Ge_4As_2$ both in the same space group *P*21/*c* (no. 14) inhabiting variants of this structure, leading to a change of the Pt – Pt distances. The low X-ray contrast of Ge and As made a crystallographic analysis in regard to the Ge/As occupation difficult. Energy dispersive X-ray spectroscopy (EDX) measurements together with density functional theory calculations performed with the "Vienna Ab Initio Simulation Package" (VASP)[3] were used to identify a likely distribution for Ge and As (fig. 1b-d).

To support the structure models for the Pt-Ge-As compounds a substitution of As by Sb was tried, which indeed lead to the compounds $Pt_3Ge_3Sb_3$ (*P*21/*c*, no. 14) and $Pt_3Ge_2Sb_4$ (*P*21/*c*, no. 14) exhibiting the postulated $Pt_3Ge_3As_3$ structure and $Pt_3Ge_2As_4$ structure, respectively. In the process two additional Pt-Ge-Sb compounds were discovered. PtGeSb exhibits the CoPSe structure type[4] in the space group *Pbca* (no. 61). Pt_2GeSb_3 crystallizes in its own structure type in the space group *Pbca* (no. 61) with a = 6.4286(3) Å, b = 6.4286(3) Å and c = 24.2446(13) Å. Figure 2 shows view on the *b*-*c* plane of both compounds illustrating the orientation of the edge-sharing $Pt(Ge_3As_3)$ octahedra pairs (blue and grey, edge-sharing on the Ge side) and the corner-sharing $PtSb_6$ octahedra (beige). In contrast the Pt-Ge-As compounds consist of only edge-sharing $Pt(Ge,As)_6$ octahedra.

References:

(1) L. Bindi, Y. Moelo, P. Leone, M. Suchaud, *Can. Mineral.,* **2012**, 50, 471–479.
(2) A. K. van Bever, W. Nieuwenkamp, *Z. Kristallogr.,* **1935**, 90, 374–376.
(3) G. Kresse, J. Hafner, *Phys. Rev. B,* **1993**, 47.
(4) H. Nahigian, J. Steger, H. L. McKinzie, R. J. Arnott, A. Wold, *Inorg. Chem.,* **1974**, 13, 1498–1503.

Fig. 1

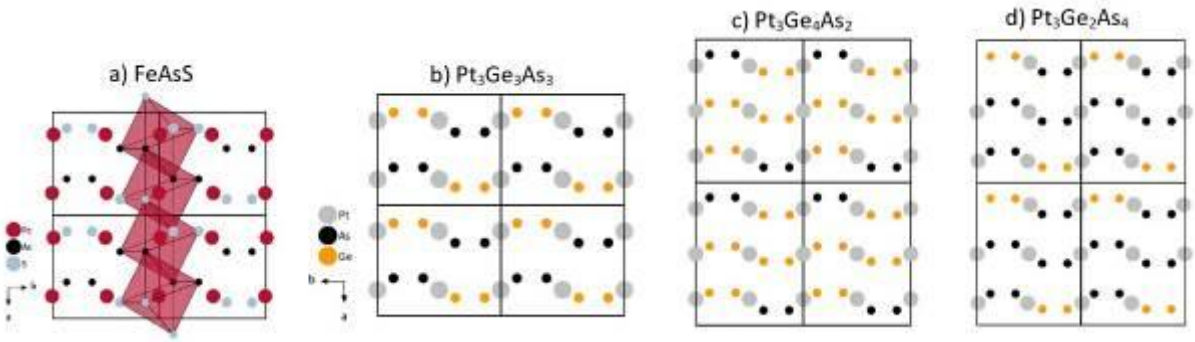

Fig. 2

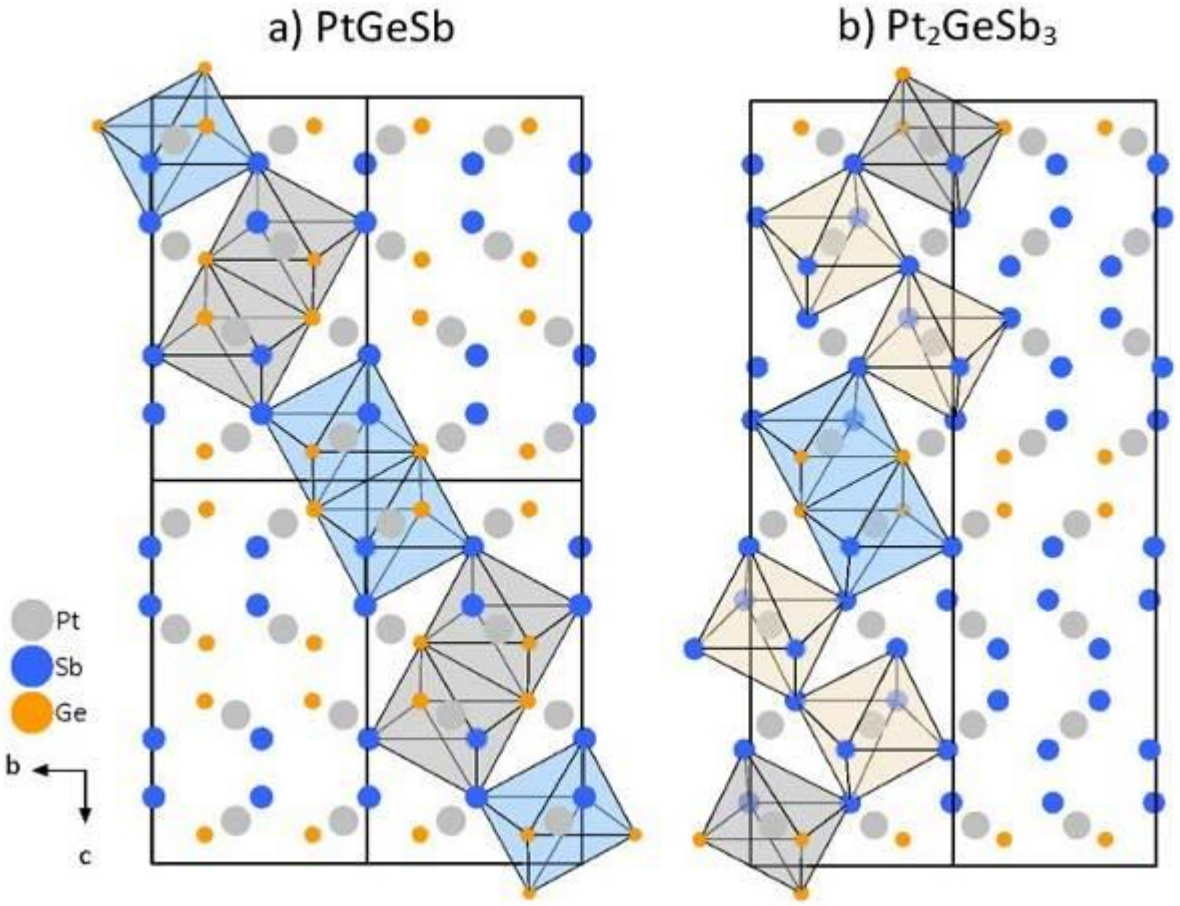

OP-030

A novel Chromate(II)

G. Thiele (Berlin/DE), A. Ghazanfari (Berlin/DE)

An unprecedented sulfido chromate(II) salt is presented. Pecularities arising from the single crystal diffraction results are discussed based on energy dispersive X-ray spectroscopy and X-ray absorption spectrocopy. In combination with magnetic analyses a Jahn-Teller distorted structure with a verified d4 configuration is proposed.

MS 8: Experimental methods II: Imaging, spectroscopy, diffraction

OP-031

Accessibility, Quality and Scalability: The future of X-ray Powder Diffraction is Brilliant

B. Hinrichsen (Mannheim/DE), M. W. Terban (Mannheim/DE)

X-ray scattering and total scattering pair distribution function analysis have become ever more powerful tools to characterise the structure of materials. The crystal structure, local structure, disorder and microstructure can in many cases be routinely determined. Modern synchrotron facilities offer brilliant radiation enabling extremely short data collection times. This positive development comes with challenges for the facilities. Shorter experiments lead to higher visiting scientist turnover and an added load to the reviewing process. We will be presenting an alternative method for synchrotron access using an X-ray powder diffraction and total scattering experiment that we have devised. It will be able to provide a huge number of researchers with excellent data and data analysis tools. We will show how the experimental design ensures high data quality and how the process developed for access and analysis guarantees every researcher equitable opportunity. The short turnaround times, an often neglected quality which is especially important for shortening research cycles can be ensured with this process. Data analysis enhanced by AL/ML is of growing importance and will become more viable from the high number and quality of data that this system can provide. We see this as a paradigm shift for powder diffraction, but even more a huge opportunity for the advancement of the total scattering and pair distribution function method.

Fig. 1

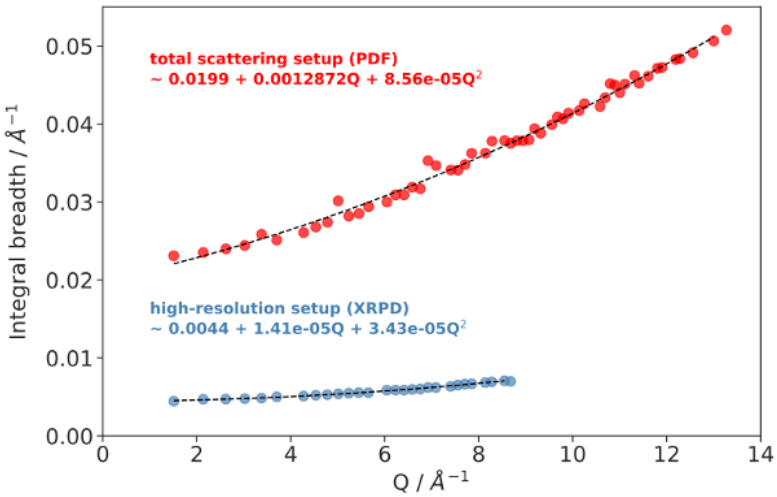

Fig. 2

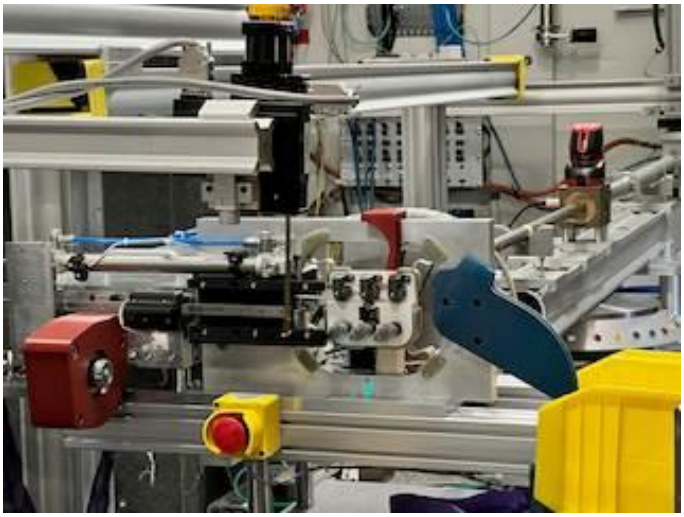

OP-032

Millisecond cryo-trapping by the spitrobot crystal plunger simplifies time-resolved crystallography

P. Mehrabi (Hamburg/DE), S. Sung (Hamburg/DE), D. von Stetten (Hamburg/DE), A. Prester (Hamburg/DE), C. E. Hatton (Hamburg/DE), S. Kleine-Döpke (Hamburg/DE), A. Berkes (Hamburg/DE), G. Gore (Hamburg/DE), J. P. Leimkohl (Hamburg/DE), H. Schikora (Hamburg/DE), M. Kollewe (Hamburg/DE), H. Rohde (Hamburg/DE), M. Wilmanns (Hamburg/DE), F. Tellkamp (Hamburg/DE), E. C. Schulz (Hamburg/DE)

Uniquely, time-resolved crystallography (TRX) enables the determination of structural intermediates of enzymes during catalysis. Although very powerful this method is fairly complex and often beyond the scope of non-specialized groups. To simplify TRX and make it more accessible to the large MX user base, we have developed the *SPITROBOT*, a protein crystal plunger, enabling reaction quenching via cryo-trapping with millisecond time-resolution [1].

SPINE standard MicroMesh mounted protein crystals are placed on an electropneumatic piston in a humidity (<99%) and temperature-controlled (4°C – 40°C) environment. Reactions are initiated by a burst of picoliter-sized droplets of substrate solution shot onto the crystals via our established LAMA technology [2] and quenched after a defined delay time (min. 50 ms) by plunging the sample into a liquid nitrogen submerged storage puck.

The SPINE standard directly connects TRX to existing high-throughput MX data-collection and processing workflows. To benchmark the *SPITROBOT* we show binding of multiple ligands in beta-lactamase CTX-M-14 and xylose isomerase over a range of time-scales, and demonstrate trapping of reaction intermediates and conformational changes during tryptophan synthase catalysis.

The practical advantages and its versatility (crystal size, data-collection routines, time-delays, environmental control) put the *SPITROBOT* into an ideal position for the transition from static structure determination to time-resolved crystallography projects at ambient temperatures. The simplicity of the *SPITROBOT* now makes TRX accessible to most MX laboratories. Here we introduce the next generation of the device: *SPITROBOT-II.*

References:

(1) Mehrabi, P. *et al.* Millisecond cryo-trapping by the spitrobot crystal plunger simplifies time-resolved crystallography. *Nat Commun* **14**, 2365 (2023).
(2) Mehrabi, P. *et al.* Liquid application method for time-resolved analyses by serial synchrotron crystallography. *Nat Methods* **16**, 979–982 (2019).

Fig. 1

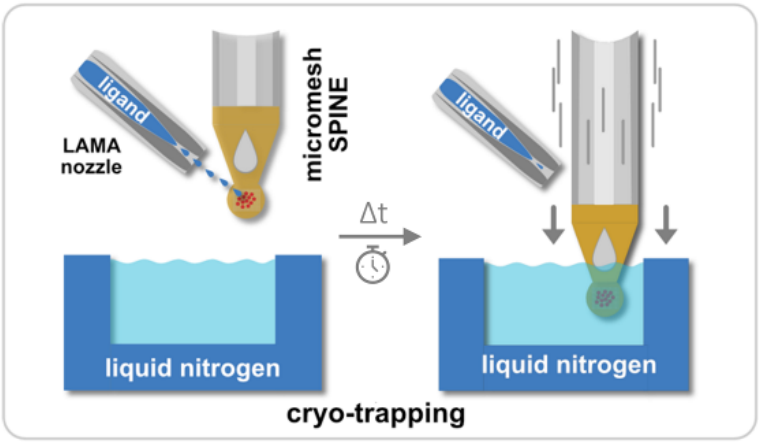

Figure: Working principle of the spitrobot

Fig. 2

OP-033

Probing the chemical environment of uranium in NaUF-materials using single-crystal X-ray diffraction anomalous dispersion refinement (SC-XRD-ADR)

F. Meurer (Regensburg/DE, Grenoble/FR), M. Bodensteiner (Regensburg/DE), G. Morrison (Columbia, SC/US), V. Svitlyk (Grenoble/FR), H. C. zur Loye (Columbia, SC/US), C. Hennig (Grenoble/FR)

The immobilization of uranium in chemically inert, crystalline materials is one possible pathway to resolve the nuclear waste disposal problem. While doped Zirconia already proved as a viable route for a secure nuclear waste storage [1], NaUF compounds promise a higher mass efficiency of stored roadiactive material. For actinide compounds, the oxidation state of the metal is highly influential to the overall stability of the chemical composition. However, especially for crystalline materials with different metal positions, the investigation of this oxidation state can be challenging even with sophisticated spectroscopic methods. Here, we want to test, if the refinement of anomalous dispersion parameters is able to help [2].

Using single-crystal X-ray diffraction data at multiple wavelengths around the L_3 absorption edge as "diffraction spectroscopy" to investigate the inelastic behavior of interaction to gather clues about oxidation states. Similar to X-ray absorption near edge spectroscopy (XANES), we expect a blue-shift of the absorption edge with higher nuclear charge. While multiple diffraction experiments of course yield a much more coarse "spectrum", each data point is supported by the reflections in the diffraction experiment and different atomic sites can be spatially differentiated. In this study, we investigate this behavior for different uranium compounds.

As preleminary results show (Fig. 1), the refinement of anomalous dispersion parameters yields values which are in good agreement with the recorded X-ray absorption spectrum. In contrast, calculated values from the Brennan & Cowan method [3] differ strongly. The remaining examples will give insight intothe sensitivity of this method for different uranium environments.

Figure 1: X-ray absorption spectra and calculated f' (black lines) with refined f'' (top, red) and f' (bottom, red) values.

[1] https://doi.org/10.1111/jace.18735

[2] https://doi.org/10.1107/S2052252522006844

[3] https://doi.org/10.1063/1.1142625

Fig. 1

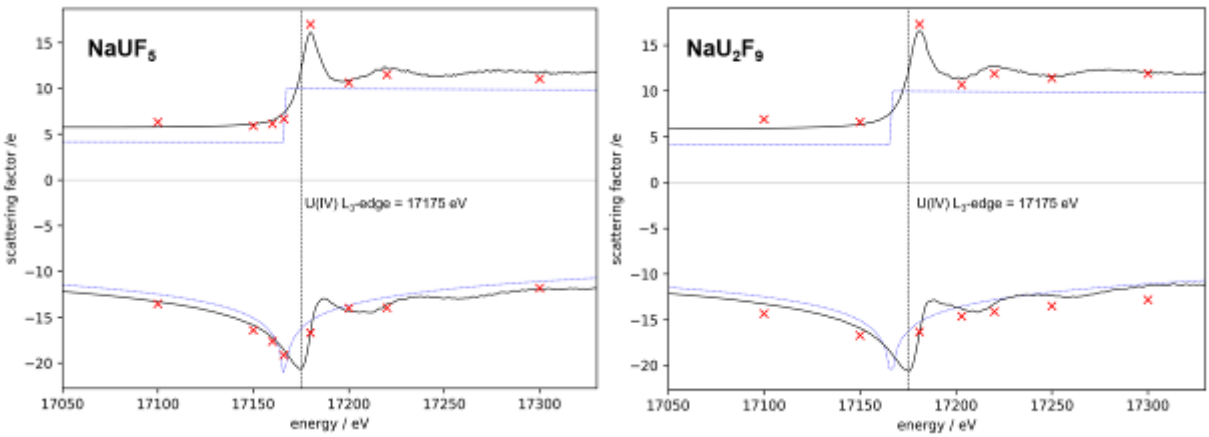

OP-034

Examining the different placement possibilities of the collimating mirror for the future quick-EXAFS beamline AppAnaXAFS at PETRA IV

M. Nentwich (Hamburg/DE), E. Welter (Hamburg/DE), D. Novikov (Hamburg/DE)

PETRA III stands as a premier storage ring X-ray radiation source, offering exceptional possiblities for scientific research. The forthcoming PETRA IV upgrade will further extend the capabilities, empowering researchers to analyze *in-situ* and *operando* processes occurring within catalysts, batteries, and microchips. The *Applied and Analytical quick X-ray Absorption Spectroscopy beamline* (AppAnaXAFS), will be one of the first operating beamlines within the second phase of the upgrade, which focuses on the construction and commissioning of the new west hall. The scientific scope of this beamline lies on spectroscopic *in-situ* and *operando* analysis of various catalytic processes for efficient conversion with special focus on high time resolution.

Especially for the quick-EXAFS measurements a source with a broad and continuous spectrum is favorable, which is why the use of a 3-pole Wiggler is intended. However, this Wiggler comes at the cost of high divergence and an imminent loss of intensity at various "obstacles" along the beamline, e.g. photon shutters and monochromator. To reduce this loss as much as possible, the use of a collimating mirror before the monochromator is desired. Generally, optical elements like mirrors are placed outside the tunnels to ensure easy maintenance. For PETRA IV, the placement closest to the source, but outside the tunnel would be at 42 m. Discussions with the responsible vacuum group revealed a possible position of collimating mirrors at 22 m within the tunnel.

In order to evaluate the advantages and disadvantages of the different mirror positions, an extensive x-ray tracing study was performed, consideringnot only the mirror position, but also different geometries (parabolic, toroidal, bent), lengths, coatings, and two different Wiggler settings.

MS 9: Teaching and Lightning talks of young crystallographers

OP-LT 1

'Escape our Lab' - a materials science/crystallography escape room

C. Schimpf (Freiberg/DE), J. Lachmann (Freiberg/DE), M. Wetzel (Freiberg/DE), P. Fischer (Freiberg/DE), A. Leineweber (Freiberg/DE), D. Rafaja (Freiberg/DE)

In order to counteract the present trend of decreasing enrolments in the study courses related to science, technology, engineering and mathematics (STEM fields), we transformed one of our laboratories into an 'escape room'. With inviting pupils into this laboratory, from which they should escape through solving different puzzles, we hope to raise the interest of pupils in the fields of materials science and crystallography. The game concept addresses the following central issues: (i) How can the work of crystallographers and/or materials scientists be made more accessible to pupils?; (ii) How can scientific tasks from crystallography or materials science be condensed into simple and easily comprehensible experiments?; and (iii) Can these experiments be used to trigger the interest of the players for the field of science?

Our concept is characterised by a high flexibility of the game play and variability with respect to the level of difficulty addressing player groups with different knowledge bias. In this contribution, the design and setup of the whole game as well as the background of individual puzzles will be presented. Some details of the realisation will be shown that should motivate interested listeners to put effort in similar projects with the aim of rising interest for crystallography and materials science among the youngsters. Finally, our experience in performing the game with different groups of players, from pupils to teachers will be reported.

OP-LT 2

Crystal Structures in High School Chemistry Classes

E. Irmer (Göttingen/DE)

Training in X-ray structural analysis often starts for students only in the Master's program or even during their doctorate. Undergraduates or teacher students come into contact with the method only very rarely or cursorily.

However, even in high school chemistry classes, the results of single crystal X-ray structure analyses can be used in a variety of ways to illustrate and reinforce important structural chemical concepts. To do so, the complex theoretical principles of the method must be didactically reduced and examples of application relevant to school must be identified. Therefore, we present two approaches how high school students can work with crystal structures.

Firstly, experiences from school lessons and at the student laboratory with students working with crystal structures from the Cambridge Structural Database [1] are presented. In this project, the students examine molecules for aromaticity, check the validity of the VSEPR model on structures and identify hydrogen bonds.

We also present materials which enable even high school and undergraduate students to use professional programs for structure solution and refinement of crystal structures in order to perform simple structure determinations largely independently after a short instruction. The user interfaces ShelXle [2] and Olex2 [3] were used, and these are compared in terms of their use with students.

References:

(1) Battle, G.M.; Ferrence, G.M.; Allen, F.H. (2010): Applications of the Cambridge Structural Database in chemical education. J. Appl. Cryst., 43 (Pt 5), 1208–1223.
(2) Hübschle, C.B., Sheldrick, G.M., Dittrich, B. (2011): ShelXle: a Qt graphical user interface for SHELXL. J. Appl. Cryst., 44, 1281-1284.
(3) Dolomanov, O.V.; Bourhis, L.J.; Gildea, R.J.; Howard, J.A.K.; Puschmann, H. (2009): OLEX2: A complete structure solution, refinement and analysis program. J. Appl. Cryst., 42, 339-341.

LT-03

Controlled Assemblies of Supramolecular Organometallic Complexes in the Solid-State

J. Zuber (Garching/DE), A. Heidecker (Garching/DE), A. Pöthig (Garching/DE)

In the intricate web of life on our planet, complex biological mechanisms stand as indispensable prerequisites, utterly reliant on the presence of supramolecular interactions, which are held together by the delicate threads of non-covalent bonds. Various structures, ranging in size and complexity, self-assemble from a myriad of small building blocks. This remarkable correlation of nature's craftsmanship serves as the inspiration for the captivating and dynamic scientific discipline known as "chemistry beyond the molecule," where scientists strive to unravel and mimick these essential processes.[1]

A subclass of such supramolecular organometallic complexes (SOCs)[2] is depicted by pillarplexes $M_8L_2(X)_4$ (M = Ag, Au), which are octanuclear NHC complexes forming metallocavitand structures. Apart from the properties of pillarplexes, such as hosting linear molecules in their tubular cavity, intrinsic luminescence or tunable solubilty,[3] modification of the counterion or the rim of the macrocyclic ligand entails several structural allignments and self-recognition properties. Small inorganic anions like tetrafluoroborate lead to the formation of tubular pillarplex channels in the solid-state (Figure 1). By functionalization of the rim the intermolecular properties can be tuned and hence, a controllable sequence of $Ag_8L_2(BF_4)_4$ and $Au_8L_2(BF_4)_4$ in the solid-state could be engineerd while maintaining the dense tubular assembly.

The successful formation of $Ag_8L_2(BF_4)_4$ and $Au_8L_2(BF_4)_4$, respectively, is validated by NMR spectroscopy, elemental analysis and HRESI-MS. The solid-state structures and assemblies are solved by single crystal X-Ray diffraction and electron diffraction.

References:

(1) J. M. Lehn, *Science* **1993**, 1762.
(2) A. Pöthig, A. Casini, *Theranostics,* 2019, **9**, 3150.
(3) P. J. Altmann, A. Pöthig, *J. Am. Chem, Soc.,* **2016**, 138, 13171.

Fig. 1

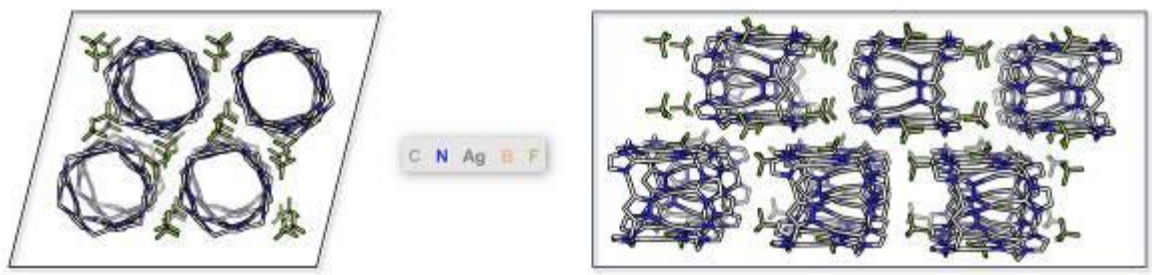

LT-04

XDSGUI: a graphical user interface for XDS, SHELX and ARCIMBOLDO

W. Brehm (Hamburg/DE), J. Triviño (Barcelona/ES), J. M. Krahn (Durham, NC/US), I. Usón (Barcelona/ES), K. Diederichs (Konstanz/DE)

XDSGUI is a lightweight graphical user interface (GUI) for the ***XDS***, ***SHELX*** and ***ARCIMBOLDO*** program packages that serves both novice and experienced users in obtaining optimal processing and phasing results for X-ray, neutron and electron diffraction data. The design of the program enables data processing and phasing without command line usage, and supports advanced command flows in a simple user-modifiable and user-extensible way. The GUI supplies graphical information based on the tabular log output of the programs, which is more intuitive, comprehensible and efficient than text output can be.

XDSGUI may be used for graphical analysis of any existing files and subdirectories written by ***XDS***, ***SHELX*** and ***ARCIMBOLDO***, or creates input files and runs the programs.

The main function of the program is to mediate between command-line-driven computational programs, reading and writing ASCII output files, and a user who expects easy configuration of the computational programs and meaningful information about processing results.

User interaction occurs through buttons labeled *e.g.* `Run XDS' or `Run SHELXC' or labeled buttons that run a script. These scripts are shown as one line of editable text below the respective buttons, and consist of shell commands that are separated by semicolons. The scripts are usually short, but in principle they may be arbitrarily long, and can invoke programs or other scripts. This allows a productivity enhancement through leveraging of external programs that are not part of the computational program packages. Default scripts are provided, and can be edited by changing or deleting existing commands and/or inserting new commands. This constitutes a simple way of customizing and extending ***XDSGUI***.

The presentation will also demonstrate the latest developments: annotated predictions superimposed with the diffraction image (Fig. 1), and support for segmented detectors (Fig. 2).

References:

(1) Brehm et al. (2023) *J. Appl. Cryst.* **56**, 1585-1594

Fig. 1

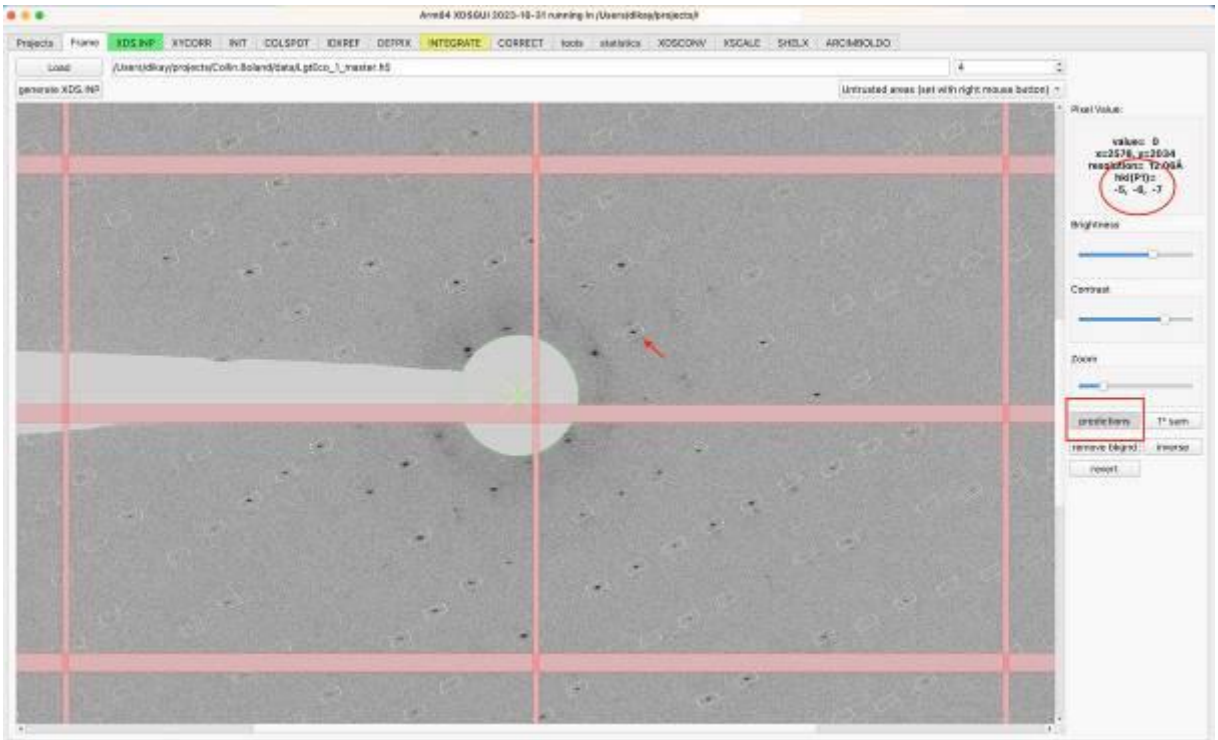

Fig. 2

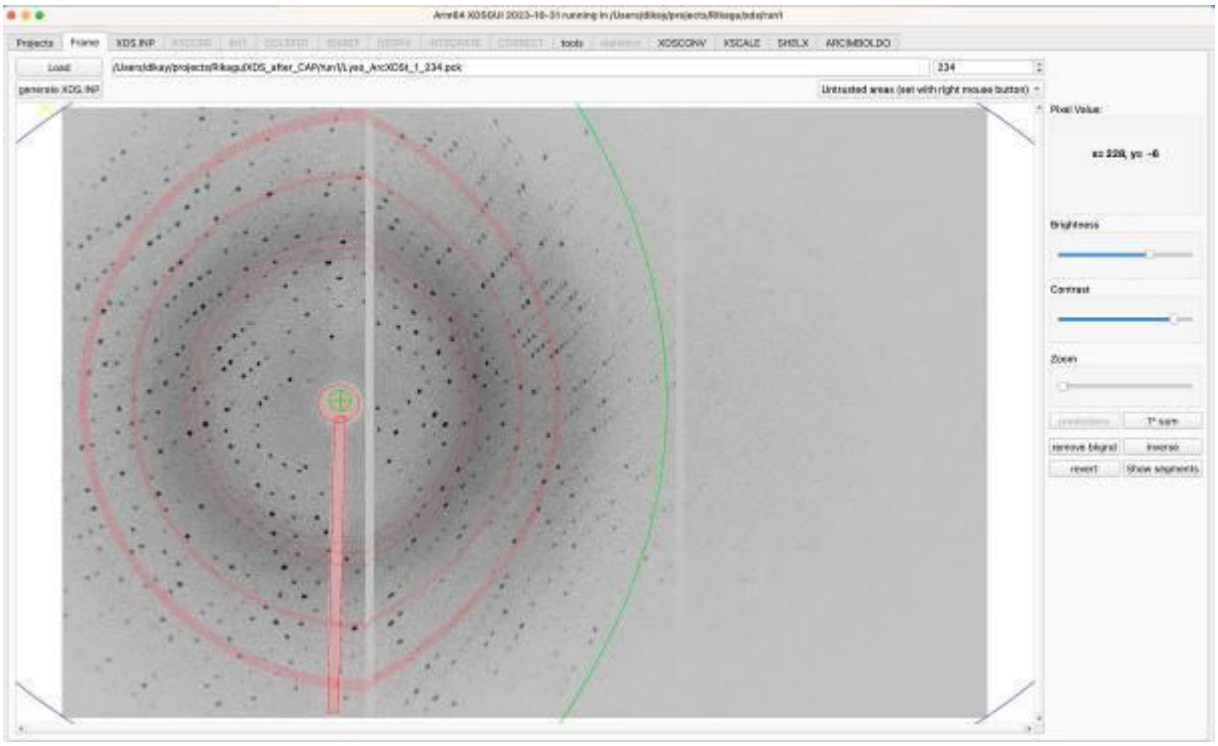
Projects
Frame
XDS.INP
tools
XDSCONV
XSCALE
SHELX
ARCIMBOLDO
Load
generate XDS.INP
234
Untrusted areas (set with right mouse button)
Pixel Value:
Brightness
Contrast
Zoom
remove blgrnd
inverse
revert
Show segments

LT-05

A DFT-based study for optimizing clinoptilolite models and their cation distributions for environmental remediation.

L. Saeed Abdelrazik Aly (Bremen/DE), M. Fischer (Bremen/DE)

Conventional wastewater treatment facilities are insufficient to effectively remove environmentally harmful pharmaceuticals and personal care products (PPCPs), one of the largest and most persistent groups of emerging contaminants. The ability of the low-cost natural zeolite, clinoptilolite, for ion exchange, for example, due to the movable extra-framework cations can make it a suitable adsorbent for wastewater treatment. In the present study, hundreds of clinoptilolite models were generated for which the distribution of Al and its effect on the extra-framework cations such as Na+ were investigated using density functional theory and were found to be in very good agreement with experiments. It turns out that Na+ prefers coordinating with framework oxygen surrounding the T2 and T3 sites to compensate the negative framework charge due to the substitution of Si with Al whereas it repels the rest of the Al in any other tetrahedral site. While these trends can be observed in all the optimized configurations with all the tested functionals, only B97-D3 functional was able to reproduce the experimental bond lengths very well.

The presence of those extra-framework cations can limit the adsorption capacity of this natural zeolite; hence, the adsorption of the harmful compounds "might" happen at the surface level. To this end, surface models with different Miller indices, particularly the lower Miller indices, from the lowest energy bulk configurations were created. Moreover, additional surface models with different cations are investigated with extra emphasis on the (010) surface being the perfect cleavage plane for clinoptilolites. Those surface models are polar, thereupon DFT simulations with polar corrections will be carried out, and asymmetric because of the atomically different terminations exposed following cleavage. The ones suitable will be utilized for further studying the adsorption of PPCPs employing both DFT and force-field simulations.

LT-06

Systematic multi-temperature comparison of β-lactamase ligand complexes

G. Gore (Hamburg/DE), A. Prester (Hamburg/DE), D. von Stetten (Hamburg/DE), E. C. Schulz (Hamburg/DE)

Biomolecular structures are dominated by data collection at cryogenic temperatures, mostly in order to mitigate the effects of radiation damage. While the detrimental effects of radiation damage can largely be circumvented by serial data-collection approaches, higher temperatures might hold information about the protein"s conformational flexibility close to physiological conditions. Hence, multi-temperature serial synchrotron crystallography (SSX) can not only eliminate flash-cooling induced structural artefacts but can also provide access to a trove of information about the protein energy landscape and conformational dynamics. Our environmental control system[1] enables multi-dimensional SSX by precisely controlling the temperature and humidity for the existing LAMA[2] and HARE[3] technology.

Here, we focus on the systematic multi-temperature (-80ºC, 20ºC, 37ºC) comparison of the medically relevant extended spectrum β-lactamase CTX-M-14; causative agent of a prevalent bacterial antibiotic resistance mechanism in nosocomial infections.

To address temperature-dependent differences in ligand binding, the-wild type enzyme and its activity impaired mutant E166-A in complex with 4 different inhibitors and 9 different antibiotics respectively, were analyzed. The systematic comparison of these 45 structures, an analysis of water networks, B-factors and prominent structural differences will provide us with a more complete picture of the protein in response to changing external stimuli such as ligand binding events and temperature.

References:

(1) Mehrabi, P. *et al*. An environmental control box for serial crystallography enables multi-dimensional experiments, bioRxiv 2021.11.07.467596
(2) Mehrabi, P. *et al.* Liquid application method for time-resolved analyses by serial synchrotron crystallography, *Nat.Methods* **16**, 979–982 (2019)
(3) Schulz, E. C. *et al.* The hit-and-return system enables efficient time-resolved serial synchrotron crystallography, *Nat. Methods* **15**, 901–904 (2018)

LT-07

Methylated nucleobases crystal structures and new insights on cocrystals synthesis

R. Cameli Manzo (Stuttgart/DE, Hamburg/DE), M. Etter (Hamburg/DE)

Methylated nucleobases are of great importance for their application in studies concerning DNA-specific pairing in nucleobases cocrystals [1,2]. Furthermore, these compounds are seeing a growing interest for their pharmacological applications [3, 4]. Nonetheless, crystallographic studies on many methylated and alkylated nucleobases are still missing.

Here we have solved the crystal structures of methylated nucleobases missing in crystallographic databases using powder X-ray diffraction. Noteworthy, 3-Methyladenine crystal structure solution revealed the presence of structural water, which is bonded to the glycosidic nitrogen molecular site. In-situ heating experiments of this compound revealed that after complete water removal and before the melting point, the crystalline powder undergo a phase transition at high-temperature.

Understanding conditions leading to polymorphs is an important topic for crystallographers, especially in the cases where it could affect pharmaceutical performance. Furthermore, our findings suggest that the presence of a methyl group located at site N3 of the methylated nucleobases could prevent the molecules to form strong hydrogen bonds interfering with co-crystallization of nucleobases pairs. Ongoing solid-state milling and in solution studies on pairing of modified nucleobases represent important experimental evidence of the assembly observed in DNA.

References:

(1) K. Hoogsteen. Acta Cryst, 16 (1963), p. 907
(2) T. Stolar, S. Lukin, M. Rajic ☐Linaric ☐, M. Etter, K. Uzˇarevic ☐, E. Mesˇtrovic ☐, I. Halasz, Chem. Commun. 2020,56, 13524–13527.
(3) Kirsanov K., Fetisov T., Antoshina E., Trukhanova L., Gor"kova T., Vlasova O., Khitrovo I., Lesovaya E., Kulbachevskaya N., Shcherbakova T., Belitsky G., Yakubovskaya M., Švedas V. and Nilov D. (2022).
(4) Front. Pharmacol. 13:842316.
(5) Heckmann BL, Yang X, Zhang X, Liu J. Br J Pharmacol. 2013 Jan;168(1):163-71.

LT-08

Understanding crystallization process to improve quality and resolution of crystal diffraction

A. Ghosh (Berlin/DE), J. H. Jeoung (Berlin/DE), P. Liebers (Berlin/DE), H. Dobbek (Berlin/DE)

Introduction:

Probing the intricacies of protein crystallization, we present a novel enzyme, Dodecameric Tyrosine-Coordinated Heme Protein (DTHP), derived from *Oligotropha carboxydovorans*.The barrel-shaped DTHP enzyme, displaying ring-like C6 symmetry akin to its hexameric counterpart, hexameric tyrosine-coordinated heme protein (HTHP) found in *Silicibacter pomeroyi*, comprises monomers with three α helices forming a solvent-exposed Fe-PPIX cofactor binding pocket. The central Fe ion coordinates with Tyrosine 46's phenolic oxygen, presenting an intriguing structural arrangement. Dodecamer (dimer of hexamer) forms only after harbouring Fe-PPIX.

Methods:

Despite sharing structural similarities with HTHP, DTHP exhibits a distinctive dodecameric assembly in both solution and crystal structures, which we confirmed using analytical size exclusion chromatography and high-resolution (dmin = 0.94 Å) crystallography. Crystallization with oxidized Fe-PPIX under similar crystallization conditions revealed four distinctive space groups with varying morphologies, with most crystals diffracting to atomic resolutions.

Results and Questions:

In the realm of protein crystallization with oxidized Fe-PPIX, our study reveals a fascinating diversity with at least four distinctive space groups with different morphology under similar chemical compositions: - *I412*, *P222*, *P622*, and *C222*. Our goal was to understand how small adjustments in the crystallization conditions could lead to obtain various space groups and improve resolution.

Conclusion:

This investigation delves into the underlying mechanisms of crystal formation and unravels dynamic aspects of proteins within these crystals.This contributes to the broader understanding of crystal formation mechanisms in proteins.

References:

(1) Jae-Hun Jeoung, Diana A. Pippig, Berta M. Martins, Nadine Wagener, Holger Dobbek, HTHP: A Novel Class of Hexameric, Tyrosine-coordinated Heme Proteins, Journal of Molecular Biology, 2007

LT-09

***In situ* gas sorption study of CALF-20 by X-ray powder diffraction**

A. Sleptsova (Stuttgart/DE), S. Bette (Stuttgart/DE), F. Adams (Stuttgart/DE), R. E. Dinnebier (Stuttgart/DE)

In the last two decades, metal organic frameworks (MOFs) have gained significant attention as adsorbents and membrane materials for gas separations [1]. One of the already known and industrially produced MOF is zinc-based Calgary Framework 20 (CALF-20) that consists of 1,2,4-triazolate and oxalate ions [2]. CALF-20 shows an effective physical sorption of CO_2 even in humid environment up to and beyond 40%. However, the ability of this MOF to sorption of other gases, has not yet been investigated.

Thus, in this work we studied the ability of CALF-20 to absorb various noble gases and C_2H_2, C_2H_4, C_2H_6. For each gas loading, we conducted an *in situ* variable temperature powder X-ray diffraction experiment (VT-PXRD) in temperature range from 130°C to -100°C. Utilizing fully weighted Rietveld refinement, the lattice parameters upon gas loading as well as gas occupancies and its approximate positions in the pores were determined.

Experiments with hydrocarbons show an increase in lattice volume of up to 3% compared to vacuum experiment at -70°C. The gas content in this series increases during cooling from 130°C to room temperature, and then reaches a plateau and does not change up to -70°C. Moreover, the curves of the gas occupancies for all hydrocarbon gases have the same tendency and reach about 0.5 mol/mol Zn.

In case of noble gases occupancies of the guest atoms during cooling remain relatively low till 50°C and then monotonically increase up to -100°C never reaching a plateau. Such behavior correlates well with lattice volume changes (Fig. 1).

In conclusion, CALF-20 showed a good reversibility of the crystal structure upon loading and release as well as impressive stability due to its physical mechanism of sorption.

References:

(1) Daglar, S. Keskin, *Coordination Chemistry Reviews*, **2020**, *422*, 213470.
(2) Lin et al., *Science*, **2021**, *374*, 1464–1469.

Fig. 1

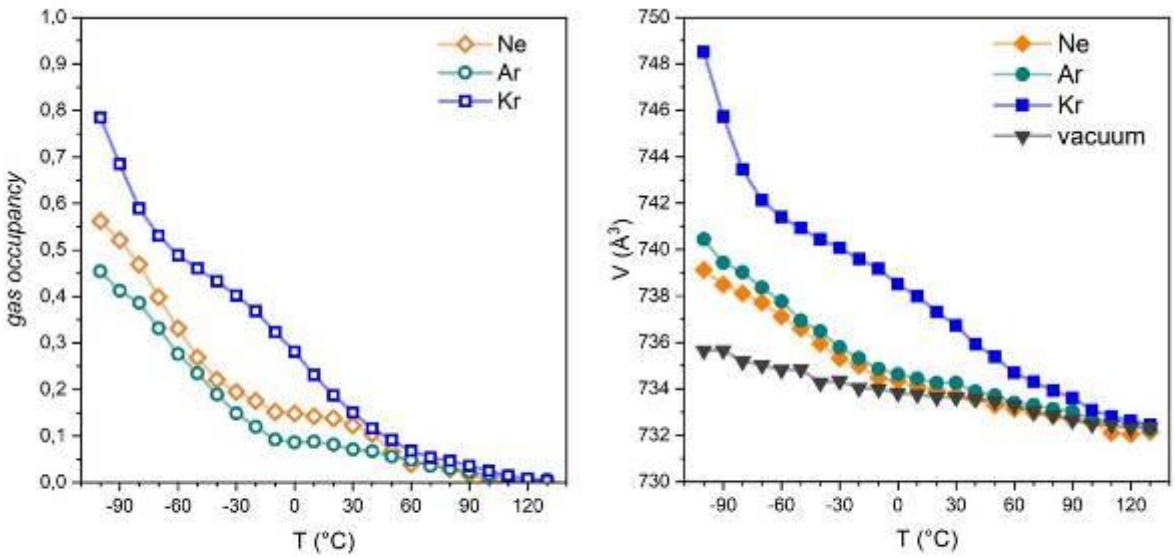

Figure 1. Gas occupancy and lattice volume against temperature

LT-10

$(CN_5H_3)_2[B_{12}H_{12}] \cdot 2\ H_2O$: A Low-Carbon High-Energy Compound Based on 5–Aminotetrazolium and Dodecahydro-*closo*-Dodecaborate Ions

R. Aghaei Hakkak (Stuttgart/DE), T. M. Klapötke (Munich/DE), T. Schleid (Stuttgart/DE)

In the realm of high energetic materials, 5-aminotetrazole is a well-established chemical [1]. In contrast, dodecahydro-*closo*-dodecaborates are renowned for their exceptional stability within the hydroborate family, owing to their quasi-aromatic high-symmetry structure. Simple salts of $[B_{12}H_{12}]^{2-}$ with alkali and alkaline-earth metals exhibit thermal stability up to around 700 °C. However, when the icosahedral $[B_{12}H_{12}]^{2-}$ anion is combined with energetic cations, these salts become less stable and decompose at far lower temperatures (200–300 °C), having the capability to release large amounts of energy upon their structural collapse [2,3]. For instance $(N_2H_5)_2[B_{12}H_{12}] \cdot 2\ N_2H_4$ sets free 435 kJ/mol of energy under inert-gas conditions.

Figure 1. View at the crystal structure of $(CN_5H_3)_2[B_{12}H_{12}] \cdot 2\ H_2O$ along [001].

The reaction between 5-aminotetrazole and the aqueous acid $(H_3O)_2[B_{12}H_{12}]$ in a molar ratio of 1 : 2 leads to the formation of bis-5-aminotetrazolium dodecahydro-*closo*-dodecaborate dihydrate $(CN_5H_3)_2[B_{12}H_{12}] \cdot 2\ H_2O$ (Figure 1). This compound crystallizes monoclinically in the space group $P2_1/c$ with lattice parameters of a = 726.23(4) pm, b = 1772.06(9) pm, c = 707.35(4) pm and β = 101.534(3)° for Z = 2. Its thermal decomposition under a nitrogen-gas atmosphere results in the release of 452 kJ/mol (Figure 2).

Figure 2. Thermal decomposition of $(CN_5H_3)_2[B_{12}H_{12}] \cdot 2\ H_2O$ as screened by TG and DSC.

References:

(1) H. Delalu, K. Karaghiosoff, T. M. Klapötke, C. Miró Sabaté, *Cent. Eur. J. Energ. Mater*. **7** (2010) 197.
(2) L. W. Zimmermann, R. Aghaei Hakkak, M. Ranjbar, Th. Schleid, *Int. J. Hydrog. Energy*. (2024) in press.
(3) R. Aghaei Hakkak, Th. Schleid, *J. Solid State Chem*. **329** (2024) 124416.

Fig. 1

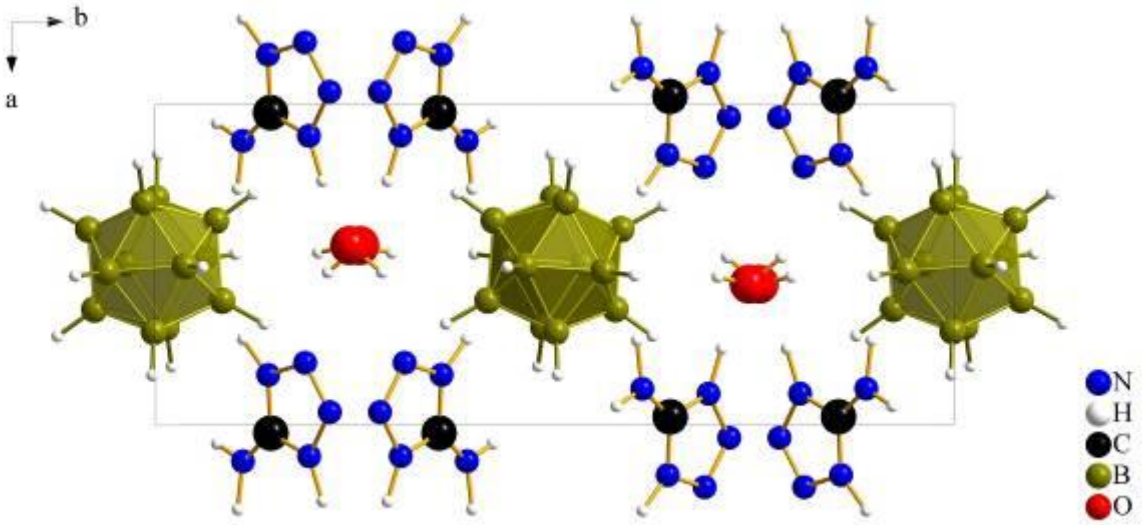

Fig. 2

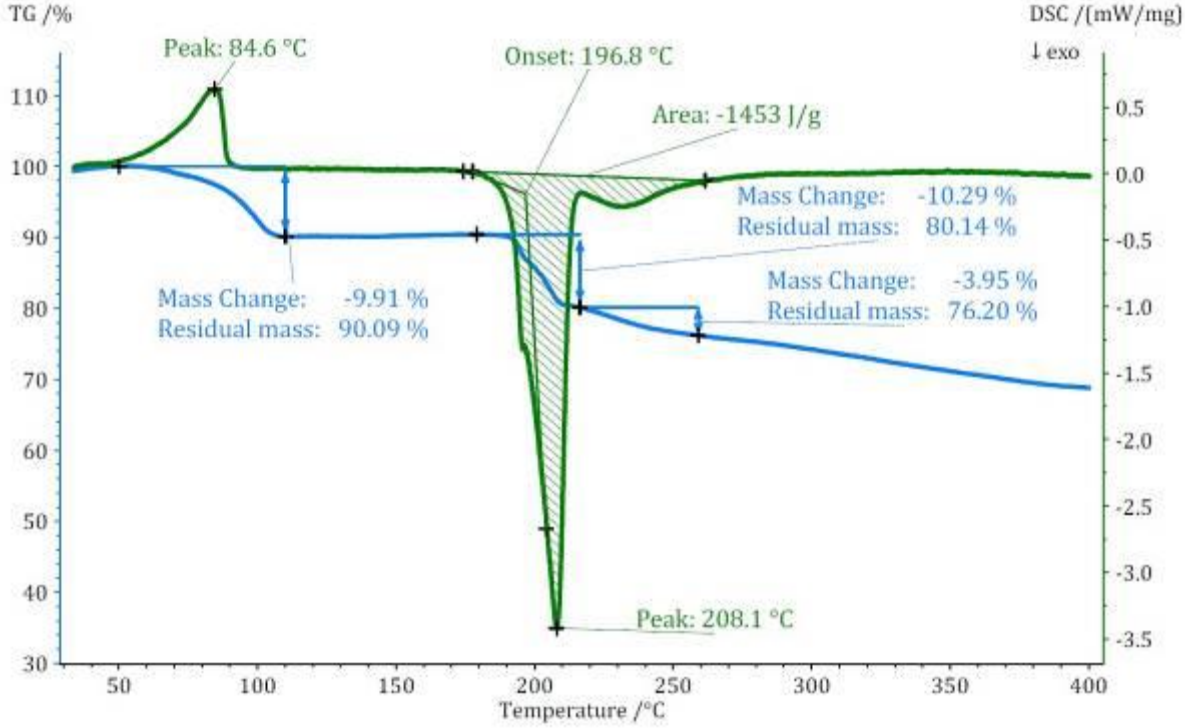
TG /%
DSC /[mW/mg]
↓ exo
Peak: 84.6 °C
Onset: 196.8 °C
Area: -1453 J/g
Mass Change: -10.29 %
Residual mass: 80.14 %
Mass Change: -9.91 %
Residual mass: 90.09 %
Mass Change: -3.95 %
Residual mass: 76.20 %
Peak: 208.1 °C
Temperature /°C

LT-11

Hydroflux synthesis – A novel approach to oxide materials of rare-earth elements

Y. Li (Dresden/DE), M. Ruck (Dresden/DE)

Due to their special electronic structure, rare earth elements have excellent properties, which are widely used in the field of magnetic and optical materials as well as catalysis.[1] Most of the materials are prepared at high temperature, and expensive reaction equipment is needed. We are currently exploring the potential of ultra-alkaline aqueous media, known as hydroflux,[2] for the facile and resource-efficient synthesis of functional inorganic materials and, in particular, are testing the applicability of the method for the preparation of rare-earth compounds. The hydroflux method distinguishes itself from hydrothermal conditions due to the very low water content and activity, allowing for nearly pressure-free syntheses at approximately 200 °C and the formation of moisture sensitive products. Hydroflux syntheses proceed within a few hours and require only a PTFE-lined autoclave that is inert to the alkaline medium and ensures that no water is lost during the reaction. We obtained hydroxo-metalates such as $Sr_3[RE(OH)_6]_2$ (*RE* = Sc, Y, Ho – Lu), $Ba_3[RE(OH)_6]_2$ (*RE* = Sc, Y, Ho – Lu) and $Ba[RE(OH)_5]$ (*RE* = Dy, Tb, Ho),[3] but also more complex compounds, e.g. the selenide $Na_4[Sc(OH)_6]Se{\cdot}H_2O$, the borates $Na_2[RE(BO_3)(OH)_2]$ (*RE* = Y, Gd – Er) and the bihalogenide $Na_{12}[Sc(OH)_6]_3ClF_2$.

Figure 1. (a) Crystal structure and (b) photograph of Ba[Dy(OH)5]. (c) Crystal structure and (d) photograph of Na2[Ho(BO3)(OH)2].

References:

(1) R. Zhang, Z. Wang, X. Xu, X. Mao, J. Xiong, Y. Yang, K. Han, *Adv. Opt. Mater.* **2021**, *9*, 2100689
(2) W. M. Chance, D. E. Bugaris, A. S. Sefat, H.-C. zur Loye, *Inorg. Chem.* **2013**, *52*, 11723–11733
(3) Y. Li, R. Albrecht, M. Ruck, *Z. Anorg. Allg. Chem*. **2022**, *648*, e202200314

Fig. 1

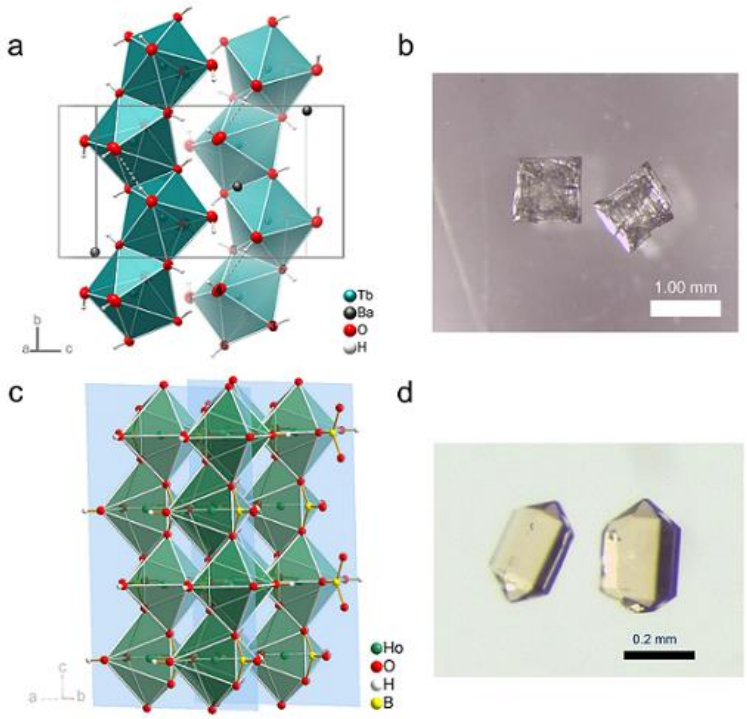

LT-12

An Insight into Halide Perovskites Solutions: Precursors Arrangement Before Crystallisation

A. Palacios Saura (Berlin/DE), J. Breternitz (Berlin/DE, Steinfurt/DE), A. Hoell (Berlin/DE), S. Schorr (Berlin/DE)

Halide perovskites (HPs) as an absorber material for solar cells has drawn the attention of the scientific community due to it outstanding increase in efficiency up to 26.1%[1] as well as low-cost solution-based processing methods.

Despite the popularity of HPs, it is not yet fully understood how anions, cations and the solvent influence the early stages of crystallisation. For this reason, we used small angle X-ray scattering (SAXS) to investigate the precursor solution of (Rb,K,Na)PbI_3 in γ-butyrolactone (GBL), dimethylformamide (DMF) and mixtures. This follows a previous study where we investigated the precursor solution of (FA,MA)Pb(I,Br)$_3$ in the aforementioned solvents.[2] We performed SAXS experiments at BESSYII, at PTB's four-crystal monochromator beamline[3] using the ASAXS endstation.[4]

Previously[2], we developed a core-shell model with [PbX_6] (X=I,Br) octahedra surrounded by solvent molecules to explain the distance between adjacent scattering objects (d_{exp}). The core can be arranged as a single octahedron or as corner-sharing octahedra, depending on the anion and the solvent. It was shown that a molecular A-cation (MA, FA) does not affect the precursors arrangement. In this study, we demonstrate that alkali metals as A-cation influence d_{exp} due to higher charge density than molecular cations. Thus, we extended the core-shell model assuming that the A-cation and the solvent molecules compete to surround the core. The [PbX_6] octahedra are surrounded by a solvent shell with randomly oriented molecules or by an A-cation shell. The SAXS data analysis (using SASfit[5]) shows higher polydispersity as the previous model, which indicates an increase in the heterogeneity of the solution, this agrees with the proposed extended model.

References:

(1) www.nrel.gov/pv/cell-efficiency.html
(2) Palacios Saura et al., in preparation
(3) Krumrey et al., Nucl. Instrum.Methods Phys.Res.Sect. A,2001,467,1175
(4) Hoell et al., DE102006029449,2007
(5) Breßler et al., J.Appl.Cryst.,2015,48,1587

LT-13

Unveiling the Twin Challenge: New Teaching Tools in Modern Single Crystal Diffraction Software

C. Lenczyk (Karlsruhe/DE), T. Stürzer (Karlsruhe/DE), J. Lübben (Karlsruhe/DE), C. Hübschle (Karlsruhe/DE)

Twinned crystals are characterized by the simultaneous presence of multiple crystal domains. This usually results in an increased complexity of data interpretation and structure solution. Especially students and novices face difficulties in recognizing and dealing with various aspects of crystal twinning, from identification to processing, which may result in incorrect crystal structures. In such a scenario, SC-XRD software packages should not only offer a wide variety of tools, but also a user-friendly interface and comprehensive functionalities to address the challenge and simplify data processing.

The APEX5 software suite offers a robust solution to guide all users, from students to experts, through the potential pitfalls associated with processing twinned crystal data.

Using carefully selected examples, we will discuss the challenges of crystal twinning in single crystal diffraction and show how users can overcome these issues using the latest improvements in our software.

Special attention will be given to manual twin indexing using intuitive indexing tools. We will also demonstrate the power of fully automated solutions based on powerful algorithms.

Finally, we will show how advanced visualization plug-ins and seamlessly integrated data reduction tools enable accurate model refinement and mitigate the challenges typically associated with twinning.

MS 10: Extreme conditions II: Polyanion compounds

OP-035

Applying methods of high-pressure crystallography in studies of high pressure chemistry of metal borides

E. Bykova (Frankfurt a. M./DE)

The materials with high hardness and low compressibility traditionally attract a great interest for industry as cutting and abrasive tools and components of protective coatings. A common approach to design such materials is to consider compounds that combine metals with high valence electron density and light elements (such as B, C, N) that form strong covalent bonds. Boron-rich transition metal borides with metal boron ratio ≥ 2 are often proposed as potential candidates for superconductive, hard and incompressible materials [1]. For example, hardness of rhenium diboride, ReB2, and tungsten tetraboride (WB4 or its derivatives WB4-*x*, WB4+*x*) according some estimates [2,3] could exceed 40 GPa, that brings them to a class of superhard materials. Rhenium borides with boron content higher than in ReB2 have never been obtained experimentally, but theoretical studies suggest them to have similar mechanical properties with ReB2. Crystal structure of the stoichiometric WB4 phase still remains debatable to date.

Applying extreme conditions, such as high pressures and high temperatures and/or huge temperature gradients, opens novel routes to metastable and kinetically hindered compounds. Here we have applied methods of single-crystal X-ray diffraction in laser-heating diamond anvil cells (DACs) in order to synthesize novel boron-rich borides of transition metals (ex. ReB3, ReB4, stoichiometric WB4, etc); characterize their crystal structure and compression behavior. We discuss their structural, mechanical and electronic properties derived from theoretical and experimental methods and compare them with the literature data.

References:

(1) Akopov, G., Yeung, M.T. & Kaner, R.B. (2017). *Adv. Mater.* **29**, 1604506.
(2) Chung, H.-Y. Y., Weinberger, M. B., Levine, J. B., Kavner, A., Yang, J.-M. M., Tolbert, S. H. & Kaner, R. B. (2007). *Science.* **316**, 436–439.
(3) Gu, Q., Krauss, G. G. & Steurer, W. (2008). *Adv. Mater.* **20**, 3620–3626

OP-036

High-pressure reactions between the pnictogens: the rediscovery of BiN

K. Glazyrin (Hamburg/DE), A. Aslandukov (Bayreuth/DE), A. Aslandukova (Bayreuth/DE), T. Fedotenko (Hamburg/DE), S. Khandarkhaeva (Bayreuth/DE), D. Laniel (Edinburgh/GB), M. Bykov (Cologne/DE), L. Dubrovinsky (Bayreuth/DE)

Understanding chemical reactions between Bi and N, elements representing the first and the last stable elements of the nitrogen group is important, and it is far from being complete if we consider their structure, physical and chemical properties of their compounds under ambient and extreme conditions. We report our findings with respect to the BiN compound, including high-pressure high-temperature synthesis of orthorhombic Pbcn BiN (S.G. #60) from Bi and N 2 precursors at pressures above 40 GPa. Using synchrotron single crystal X-ray diffraction on the polycrystalline sample, we characterized the compound"s structure and studied its behavior and compressibility on decompression to ambient pressure. We confirm the stability of Pbcn BiN to pressures as low as 12.5(4) GPa. Below that pressure value, we observed a group-subgroup phase transformation resulting in the formation of a non-centrosymmetric BiN with space group Pca2 1 (S.G. #29). We use ab-initio calculations to characterize the polymorphs of BiN and their evolution with compression in greater detail. Our calculations provide additional insight to our experimental observations, in particular those corresponding to peculiar Bi-N bond evolution under pressure and resulting in a change of the coordination number of Bi and N within the explored stability field of BiN.

OP-037

Structural evolution of Fe-bearing langasite at high-pressure and low-temperature conditions

K. Skrzyńska (Sosnowiec/PL), A. Pakhomova (Grenoble/FR), I. Galuskina (Sosnowiec/PL)

Question Langasite family includes compounds with general formula $^{VIII}A_3{}^{VI}B^{IV}C_3{}^{IV}D_2O_{14}$, where *A* = La, Ga, *etc*; *B* = Ga, Ta, *etc*; *C* = Si, Ga, *etc*; *D* = Fe, Al, *etc*. Recently, Fe-bearing langasites have attracted great interest as a new type of multiferroics. In recent high-pressure (HP) low-temperature (LT) experiments using synchrotron Mösbauer source (SMS), the series of the magnetic and electronic transitions were observed in $Ba_3NbFe_3Si_2O_{14}$ [1] and in $Ba_3TaFe_3Si_2O_{14}$ [2]. Insightful crystallographic studies are still missing despite the envisage of symmetry lowering based on SMS data. The current study aimed to study the HP-LT structural evolution of Fe–bearing langasites to elaborate on nature of earlier observed phase transitions.

Methods The *in situ* HP-LT single-crystal X-ray diffraction experiments on natural langasites, $Ca_3Ti(Fe^{3+},Al,Si)_3Si_2O_{14}$, were carried out on beamlines ID27 and ID15B at the European Synchrotron Radiation Facility. The HP measurements were performed up to 47 GPa, whereas LT experiments were conducted in the 10-230 K range.

Results Upon compression at ambient temperature, the Fe-bearing langasite preserved *P*321 symmetry up to 19 GPa. However, an increase of Fe coordination number from IV to VI takes place at about 12 GPa as well a progressive increase of atomic displacement parameters of oxygens is observed (Fig. 1). Above 19 GPa, some oxygen sites split that is accompanied by symmetry lowering to *P*3. The abrupt change in the evolution of unit cell parameters (UCPs) above 35 GPa indicates a phase transition. Compression at 130 K revealed similar features. LT experiments revealed an anomalous increase of UCPs below 150 K. Details of HP-LT structural evolution and possible correlation of structural and magnetic properties will be discussed.

References:

(1) Lyubutin et al. (2018) *Appl. Phys. Lett.*, 112, 242405.
(2) Lyubutin et al. (2017) *JETP Letters*, 1-8

Fig. 1 Part of langasite-type structure at 18.7 GPa along [101] (A); along [001] (B)

Fig. 1

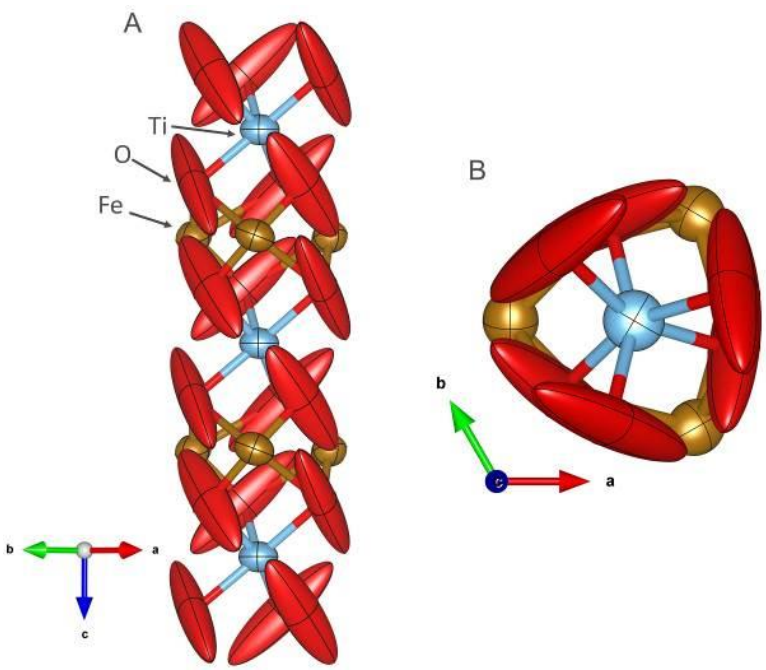

OP-038

Aluminium carbonates and isostructural compounds

L. Bayarjargal (Frankfurt a. M./DE), D. Spahr (Frankfurt a. M./DE), V. Milman (Cambridge/GB), J. Marquardt (Frankfurt a. M./DE), N. Giordano (Hamburg/DE), B. Winkler (Frankfurt a. M./DE)

Carbonates are the major reservoir of carbon on the Earth's surface and play an important role in the deep carbon cycle. Therefore, phase stabilities and properties of the most common Mg, Ca and Fe carbonates have been extensively investigated at high (p,T) conditions [1]. Al-oxide is the fourth most abundant component in the Earth's mantle after Mg-, Fe- and Si-oxides. Therefore, the question arises if Al-oxide reacts with carbon and forms an Al-carbonate at mantle conditions. Until now, the formation of Al carbonates was conjectured based on IR measurements [2] from the surface reaction between Al_2O_3 and CO_2 at low pressures. Also, a theoretical study predicted Al-carbonates [3], but the existence of such phases have not been experimentally confirmed.

Here we synthesized the Al-carbonates $Al_2[C_2O_5][CO_3]_2$ and $Al_2[CO_3]_3$ by reacting Al_2O_3 with CO_2 at high (p, T) conditions and characterised them by Raman spectroscopy [4]. Their structures were solved by X-ray diffraction. $Al_2[CO_3]_3$ forms at around 24-28 GPa, while $Al_2[C_2O_5][CO_3]_2$ forms above 38 GPa. The distinguishing feature of the new $Al_2[C_2O_5][CO_3]_2$-structure type is the presence of pyrocarbonate $[C_2O_5]^{2-}$-groups, $[CO_3]^{2-}$-groups and octahedrally coordinated trivalent cations. $Al_2[CO_3]_3$ has isolated $[CO_3]$-groups. Both Al-carbonates can be recovered to ambient conditions. DFT calculations predict that CO_2 will react with Fe_2O_3, Ti_2O_3, Ga_2O_3, In_2O_3, and $MgSiO_3$ at high pressures to form compounds which are isostructural to $Al_2[C_2O_5][CO_3]_2$. $Mg[C_2O_5][CO_3]_2$ is predicted to be stable at pressures relative to abundant mantle minerals in the presence of CO_2.

We acknowledge funding from the DFG (BA4020, WI1232) and DESY for beam time. B.W. is grateful for support by the BIOVIA Science Ambassador program.

References:

(1) Litasov, et al., Carbon in Earth's Interior 2020, 137-165
(2) Parkyns, J Phys Chem. 1971, 75, 526-531
(3) Nelson, et al., Phys. Rev. Materials 2021, 5, 123801
(4) Bayarjargal, et al., Inorg. Chem., 2023, 62, 13910

Fig. 1

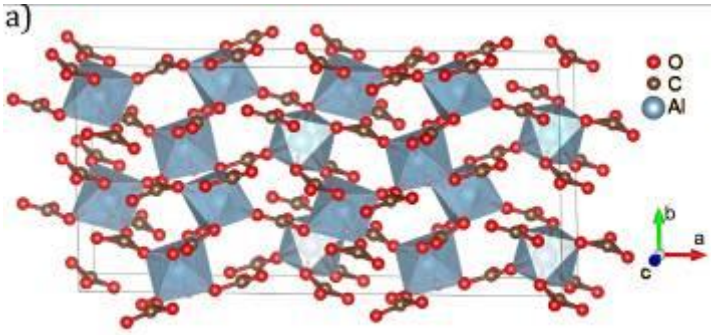

Structure of $Al_2[CO_3]_3$ at 0 GPa

Fig. 2

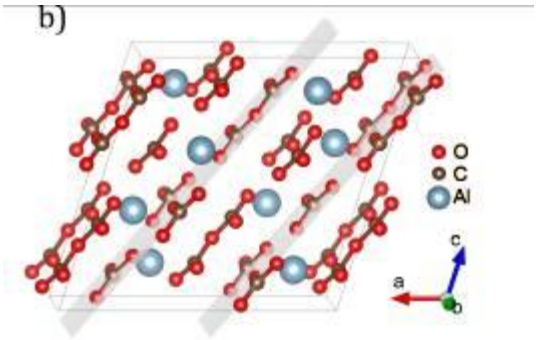

Structure of $Al_2[C_2O_5][CO_3]_2$ at 45(3) GPa

MS 11 Chemical crystallography II: Molecular structures

OP-039

A secret of constructing hollow nano-sized supramolecule

E. Peresypkina (Regensburg/DE), A. Virovets (Frankfurt a. M./DE)

In the world of giant molecular (or discrete) aggregates [1], be they clusters or polynuclear complexes, they principally have either compact cores or hollow shells. Many metal clusters and polynuclear complexes are compact and represent finite fragments either of close packing or of unique (e.g. icosahedral) structure. Here, the initially formed seed pre-determines the rest of the core; the growth stops if controlled by e.g. blocking ligands.

In contrast, a hollow shell grows by filling not a volume, but a curved surface with no visible support (unless it is templated). Its formation requires the directed self-assembly of hundreds of building units in many independent steps. Nevertheless, the hollow supramolecules occur in many classes of chemically completely different compounds [1]. The principles of the formation of closed shells are considered to be governed by specific geometric characteristics of the "secondary building units" (SBUs) [3]. The linked SBUs become "nodes" comprising a metal-organic polyhedron (MOP). However, the formation of coordination polymers is explained similarly.

Our own 20-year experience with Cp^RFeP_5 as building blocks [2] shows that they form hollow supramolecules with M = Cu^+ or Ag^+, sometimes with different organic spacers. However, in many cases, coordination polymers are formed. Moreover, even when Cp^RFeP_5 SBUs, M^+ and spacers form a giant molecule or an ion, they are not necessarily hollow [4]. We are going to discuss the applicability of the concepts of "building blocks" and "node and spacer", their usefulness in planning the synthesis, as well as positive and negative examples.

References:

(1) A. V. Virovets, E. Peresypkina, M. Scheer (2021) *Chem. Rev.*, ***121***, 14485.
(2) E. Peresypkina, A. V. Virovets, M. Scheer (2021) *Coord. Chem. Rev.*, **446**:*213995.*
(3) D. J. Tranchemontagne, Z. Ni, M. O"Keeffe, O. M. Yaghi. (2008) *Angew. Chem. Int. Ed.*, **47**, 5136.
(4) S. Heinl, E. Peresypkina, W. Kremer, M. Scheer. (2023) *Chem. Commun.*, **59**, 10263.

Fig. 1

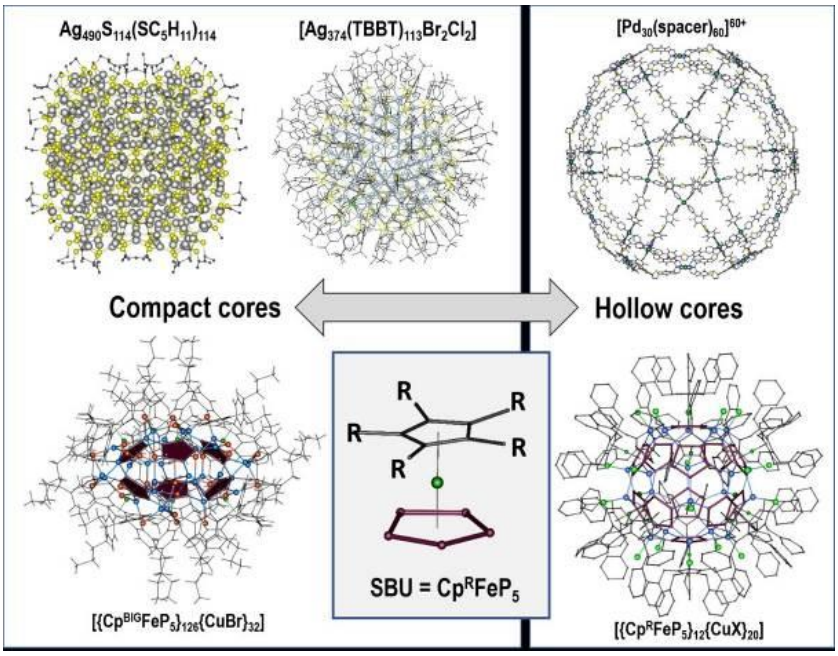

OP-040

A New Polymorph of White Phosphorus at Ambient Conditions[1]

R. Herbst-Irmer (Göttingen/DE)

Phosphorus exists in several different allotropes: white, red, violet, and black. So far, three polymorphs of white phosphorus, all consisting of P_4 tetrahedra, have been described. Among these, β-P_4 crystallizes in space group *P-1* and γ-P_4 in space group *C2/m*.[2] α-P4 forms soft plastic crystals with a proposed structure in the cubic space group *I-43m* with lattice constant *a* = 18.51(3) Å, consisting of 58 rotationally disordered tetrahedra and thus similar to the structure of α-Mn.[2-4] Here we present a new polymorph, δ-P_4. It crystallizes as a six-fold twin with cell dimensions *a* = 18.302(2), *b* = 18.302(2), *c* = 36.441(3) Å in space group $P2_12_12_1$ with 29 P_4 tetrahedra in the asymmetric unit. Their arrangement resembles the structure of α-Mn, but δ-P4 differs from α-P4. DFT calculations show δ-P_4 to be metastable at a similar energy level to that of γ-P_4.

Figure 1: Packing of α-Mn compared to δ-P_4**:** left: α-Mn looking along the *a* axis, which is identical to the *b* and *c* axes caused by the cubic symmetry. Centre: centroids of the P_4 tetrahedra along the *a* axis (top), the *b* axis (middle) and the *c* axis (bottom). Right: full tetrahedra of the new δ-P_4 polymorph along the *a* axis (top), the *b* axis (middle) and the *c* axis (bottom).

References:

(1) Herbst-Irmer, R., Wang, X., Haberstock, L., Köhne, I., Oswald, R., Behler, J. & Stalke, D. (2023). *IUCrJ* **11**, 766–771.
(2) Simon, A., Borrmann, H. & Horakh, J. (1997). *Chem. Ber.* **130**, 1235–1240.
(3) Schnering, H. G. von (1981). *Angew. Chem. Int. Ed.* **20**, 33–51.
(4) Oberteuffer, J. A. & Ibers, J. A. (1970). *Acta Cryst.* **B26**, 1499–1504.

Fig. 1

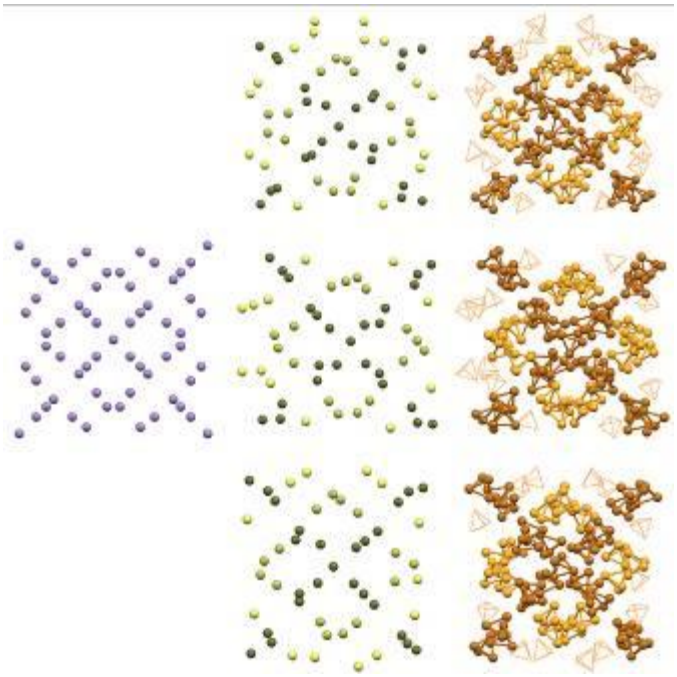

OP-041

Structural Characterisation of Copper Clusters as Decomposition Products of Copper(I) Boryl Complexes

W. Drescher (Braunschweig/DE), C. Borner (Braunschweig/DE), C. Kleeberg (Braunschweig/DE)

Introduction

During our studies on copper(I) borly complexes as reactive intermediates in copper catalysed borylation reactions[1] with diboranes(4) we observed repeatedly various low-valent copper clusters (Figure 1) as decomposition products.[2-4] Besides the still unclear role of these clusters in the borylation catalysis, these clusters are a structurally fascinating group of compounds and provide some crystallographic challenges.

Methods

All clusters were obtained in small or minute amounts (<1-10%) as small single crystals with a black metallic appearance. As a result the clusters could so far essentially only be characterised by single-crystal X-ray diffraction.[2-4]

Results & Conclusions

Figure 1: Selected views of the molecular structures of the discussed clusters.

Some of the clusters, $[(IDipp)_6Cu_{55}]$, $[(IDipp)_{12}Cu_{179}]$ and $[(Me_2IiPr)_{10}Cu_{23}(PMe_3)_2]$ exhibit a centred copper icosahedron as a common feature (Figure 1). These clusters – containing only NHC/phosphine ligands – may be considered as Cu^0 clusters. However, the presence of hydrides cannot be excluded on the basis of the single-crystal X-ray diffraction data. The boryl containing clusters $[Cu_5(Me_2IiPr)_3(Bdmab)_3]$ and $[(iPr_2P)_2Cu_8(BiPrEn)_3(OtBu)_3]$ are structurally quite different from the afore mentioned clusters but may also be considered as low-valent copper clusters (Figure 1). The fascinating and to some extend unprecedented structures of the copper clusters and their challenging single-crystal X-ray diffraction studies will be discussed in detail.

References:

(1) D. Hemming, R. Fritzemeier, S. A. Westcott, W. Santos, P. G. Steel, *Chem. Soc. Rev.* **2018**, *47*, 7477.
(2) C. Borner, L. Anders, K. Brandhorst, C. Kleeberg, *Organometallics,* **2017**, *36*, 4687
(3) C. Kleeberg, C. Borner, *Organometallics* **2018**, *37*, 4136.
(4) W. Drescher, C. Borner, C. Kleeberg, *N. J. Chem.* **2020**, *45,* 14957.

Fig. 1

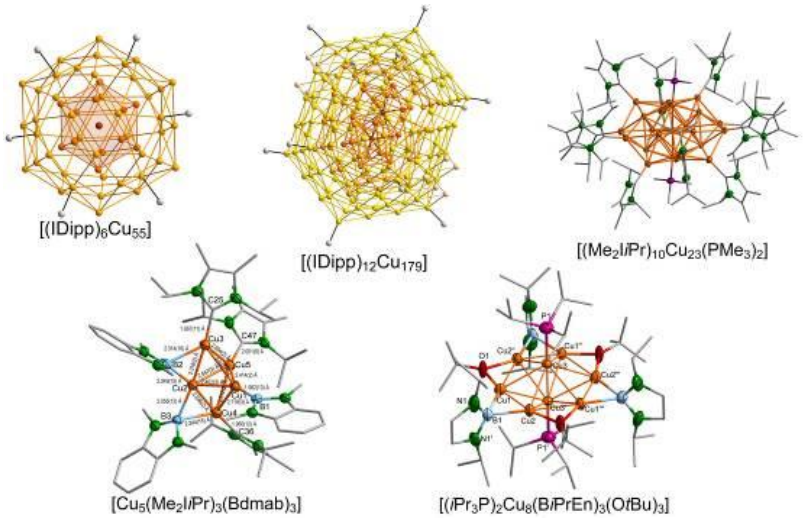

OP-042

Direct micro crystallization on TEM grids, using < 100 mug of material, for 3D Electron Diffraction experiments

G. Santiso-Quinones (Allschwil/CH), D. Stamm (Allschwil/CH), J. Merkelbach (Allschwil/CH)

3D ED has been rapidly evolving as a complementary technique for SCXRD experiments.[1] Continuous rotation ED experiments work in the same manner as SCXRD experiments, though the size of the crystals to study must be in the nanometer range. Therefore, ED can be of great help for those cases where single crystals of suitable size for XRD experiments are not achieved. Dedicated electron diffractometers[2] make the technique accessible to almost everyone. Moreover, recently many publications have appeared where these commercial electron diffractometers have been used.[3]

Though as in any diffraction experiment, the material studied must be crystalline. The degree of crystallinity can make the difference between a successful experiment or failure to obtain anything. Not to mention that if the quality of the diffraction obtained is poor (low resolution or intensity, lack of completeness), it is almost impossible to solve or refine a structure.

Recently we have been able to crystallize various natural products having less than 1 mg of sample.[4] By using a dedicated approach, we have been able to crystallize these natural products using less than 100 mug of material. The crystallization was performed directly on a 3 mm Ø TEM grid, for ED experiments. Structural information was obtained from those nano crystals grown. We will highlight the direct nano-crystallization using < 100 mug of material and show some case studies and the interesting results found using ED experiments.

References:

(1) T. Gruene, E. Mugnaioli. *Chem. Rev*. **2021**, *121*, 11823-11834.
(2) Two commercial companies have develop and sell electron diffractometers: Eldico Scientific AG (www.eldico-scientific.com); Rigaku (www.rigaku.com).
(3) Personal selection of a growing list of publications. A) J. F. Woods, et. al., *Nature Communications*, **2023**, *14*, 4725. B) E. M. Schmidt, et. al., *Nature Communications*, **2023**, *14*, 6512.
(4) Commercial samples, though will show some of the side products / impurities obtained.

MS 12: Theoretical methods II: Quantum crystallography and charge density studies

OP-043

Systematic Benchmark of Levels of Theory in NoSpherA2-HAR

F. Kleemiss (Aachen/DE), D. Brüx (Aachen/DE)

There have been various studies probing different aspects of the accuracy of refinement results using Hirshfeld Atom Refinement (HAR) [1] on different levels of theory, ranging from initial general studies [2] over various aspects of metal-organic and metal-hydride systems [3,4] towards post-Hartree-Fock (HF) and tailor-made hybrid functionals for the refinement of hydrogen-bonded molecules. [5,6]

While previous studies focus on selected combinations of basis sets and methods, no previous study provides an extensive overview of the available options. In this work we present a systematic study of various families of methods covering HF, LDA-, GGA-, hybrid-GGA, meta-GGA and meta-hybrid-GGAs and new possibilities of non-local dispersion correction of the electron density.

To address this lack of comparisons and formulate a recommendation on settings a series of high-quality datasets were measured and refined to obtain a systematic study of the effects of different choices of the level of theory inside NoSpherA2, the HAR engine inside Olex2. [7–9]

Results indicate that well established functionals are easily outperformed by modern and faster choices and that a bigger basis set is not necessarily beneficial for the refinement.

References:

(1) S. C. Capelli, et al., *IUCrJ* **2014**, *1*, 361–379.
(2) M. Fugel, et al., *IUCrJ* **2018**, *5*, 32–44.
(3) S. Pawlędzio, et al., *IUCrJ* **2021**, *8*, 608–620.
(4) M. Woińska, et al., *J. Phys. Chem. A* **2023**, *127*, 3020–3035.
(5) E. K. Wieduwilt, et al., *J. Mol. Struct.* **2020**, *1209*, 127934.
(6) B. Landeros-Rivera, et al., *Phys. Chem. Chem. Phys.* **2023**, *25*, 12702–12711.
(7) F. Kleemiss, et al., *Chem. Sci.* **2021**, *12*, 1675–1692.
(8) O. V. Dolomanov, et al., *J. Appl. Cryst.* **2009**, *42*, 339–341.
(9) L. J. Bourhis, et al., *Acta Cryst. A* **2015**, *71*, 59–75.

OP-044

ReCrystal: An Advanced Quantum Crystallography Method for Studying Charge Density using the full Periodic Wavefunction

M. Patzer (Muhlheim an der Ruhr/DE), C. W. Lehmann (Muhlheim an der Ruhr/DE)

A Python-based code has been developed to perform quantum crystallographic (QCr) single crystal structure refinements with aspherical form factors obtained from a solid-state single point calculation using the program code CRYSTAL17. ReCrystal uses the Fourier transform of the theoretical periodic static electron density to derive theoretical multipole parameters. In contrast, the well-established "Hirshfeld atom refinement" method translates the theoretical static electron density directly into aspherical form factors via Hirshfeld partitioning. ReCrystal is an iterative extension of the transferable multipole approach. A particular advantage of ReCrystal is that it is not tied to specific databases. Whether periodic boundary conditions actually lead to a better result in a QCr refinement remains to be clarified. To this end, a number of crystal structures with different intermolecular bonding motifs, such as hydrogen bonding networks, were refined. The influence of the basis set and the functional group was intensively studied. It is found that there is a strong dependence of the refinement result on the basis set, but not on the DFT functional. Furthermore, small basis sets such as MINIX or STO-3G are not suitable due to the poor description of the inner core electron distribution. The advantage of the periodic charge density model has been demonstrated in some cases, but the improvement in the fit largely depends on the quality of the original diffraction data. Finally, the theoretical multipole parameters obtained can be used as a starting point for multipole refinement if this is thought desirable.

Fig. 1

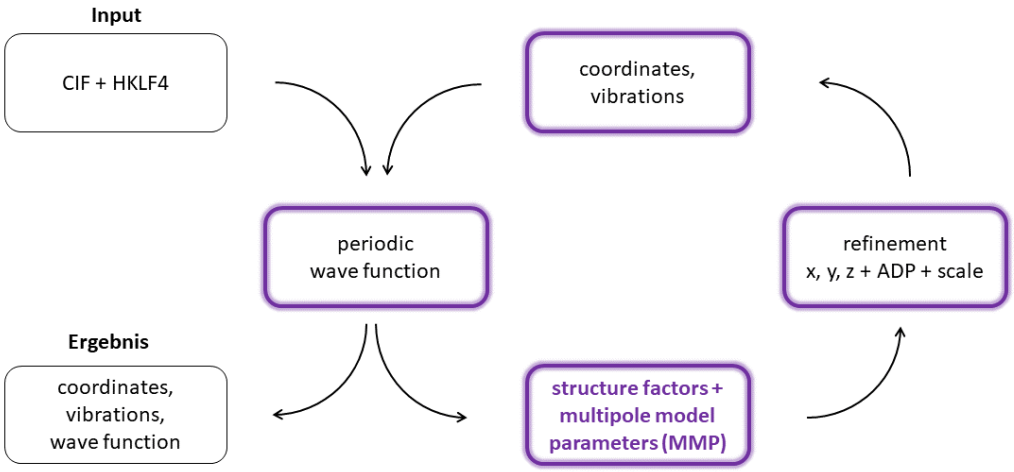

OP-045

Data Quality Evaluation in Diffraction Experiments

J. Henn (Bayreuth/DE)

It is dicussed and shown that the overwhelming majority of all published single crystal diffraction data sets is contaminated by sometimes severe systematic errors with unknown effects on the model parameters and model parameter errors. It is suggested to incorporate the existence and signs of systematic errors by standard into crystallographic data reports in order to overcome this problem. Suggestions for helpul metrics are made and some misconceptions for the quantification of systematic errors are discussed as well why so many errors go unnoticed.

OP-046

XtaLAB Synergy and CrysAlisPro – Hardware and Software in Harmony

M. Meyer (Wrocław/PL), D. Kucharcyzk (Wrocław/PL), J. Blaszczak (Wrocław/PL), C. Göb (Neu-Isenburg/DE), C. Schürmann (Neu-Isenburg/DE), K. N. Truong (Neu-Isenburg/DE), J. Wojciechowski (Neu-Isenburg/DE), J. Ferrara (The Woodlands, TX/US), F. White (Neu-Isenburg/DE)

Modern diffractometers are comprised of multiple components each of which is developed to be the best it can be. Using those components effectively can be a daunting prospect. Different hardware combinations, scientific applications, techniques and experimental requirements can make it difficult for a user to know the best approaches for all configurations and outcomes.

Rigaku"s CrysAlisPro software began development nearly two and a half decades ago with one goal in mind. To make using X-ray diffractometers and getting high-quality structures easier. CrysAlisPro has long offered automated structure solution, and now, new hardware automation has recently opened a wider range of possibilities. The introduction of fully motorized optics, our iOptiX system, has made achieving maximum source performance a push-button operation. Our new IGH has been improved to enable X-ray centering under software control, automatically and intelligently.

In this presentation, we will discuss best practices for data collection to maximize data quality and how automation can assist with obtaining better data.

MS 13: Materials science crystallography II: Combination of characterization methods

OP-047

Combining IR spectroscopy and density functional theory calculations to investigate the interaction of functional organic molecules with zeolites

M. Fischer (Bremen/DE), L. Mino (Turin/IT), R. Fantini (Modena/IT), J. Brauer (Bremen/DE), R. Arletti (Modena/IT)

Introduction

The adsorption of functional organic molecules, such as pharmaceuticals or personal care products (*e.g.*, fragrances, UV filters, disinfectants) in zeolites is of interest for different potential applications. On the one hand, zeolites can be employed for the removal of emerging organic contaminants from wastewaters. On the other hand, they can also be used as host materials, *e.g.*, in drug delivery or for the encapsulation of organic UV filters. Although diffraction experiments can elucidate the location of adsorbed organic molecules in favorable cases (Confalonieri *et al.* 2022), guest molecule disorder often limits the insights that can be obtained. In this contribution, it will be demonstrated how a combination of IR spectroscopy and density functional theory (DFT) calculations can be used to analyze the interactions between zeolites and functional organics, focusing on UV filters.

Results

A combined IR spectroscopic and DFT study of a composite of octinoxate (OMC), an organic UV filter, and zeolite NaX (FAU topology) revealed that adsorbed OMC is dominantly present in the *trans* form. Since this isomer is a more efficient UV absorber than the *cis* counterpart, this finding is in line with the good UV absorption properties of OMC@NaX composites (Fantini *et al.* 2021). While an interpretation based on DFT adsorption energies alone indicates a (slight) preference for the *cis* isomer, a combination of steric and diffusion considerations, informed by further calculations, explains why OMC remains mostly in the *trans* form in the adsorbed state. For avobenzone (AVO), an analogous combination of experiments and DFT calculations is used to resolve whether the adsorbed AVO is present as keto or enol tautomer.

References

(1) Confalonieri, G., et al (2022). *Microporous Mesoporous Mater.* **344**, 112212.
(2) Fantini, R., et al (2021). *Microporous Mesoporous Mater.* **328**, 111478.
(3) Financial support through DFG projects 455871835 and 492604837 is gratefully acknowledged.

OP-048

Investigation of monazite as a waste form for long-term disposal of radionuclides: structural flexibility and effects of radiation damage

T. Lender (Aachen/DE), L. B. F. dos Santos (Dresden/DE), S. Gilson (Dresden/DE), N. Huittinen (Dresden/DE), G. Murphy (Jülich/DE), M. Henkes (Jülich/DE), A. Bukaemskiy (Jülich/DE), M. Klinkenberg (Jülich/DE), J. Marquardt (Frankfurt a. M./DE), E. Bazarkina (Dresden/DE, Grenoble/FR), K. Kvashnina (Dresden/DE, Grenoble/FR), V. Svitlyk (Dresden/DE, Grenoble/FR), C. Hennig (Dresden/DE, Grenoble/FR), J. Nießen (Aachen/DE), L. Peters (Aachen/DE)

Monazite (*Ln*PO4, *Ln*=La-Gd) is being considered one of the most promising crystalline host materials for long-term storage of actinides due to its chemical flexibility, excellent aqueous durability and remarkable recrystallization properties [1]. Monazites can accommodate large amounts of trivalent actinides within their crystal structure [2] but aliovalent substitution has proven challenging, even though natural monazite often contains significant amounts of Th and U [3].

To facilitate assessments with respect to the chemical flexibility and aqueous durability, efforts are made to identify inactive surrogate models. The use of cerium as a surrogate for tetravalent actinides will be discussed for monazite-type phases based on the solid solution La1-*x*Ca*x*/2Ce*x*/2PO4, which was extensively studied using powder and single crystal XRD, EPMA, Raman spectroscopy and synchrotron based techniques such as in-situ HERFD-XANES experiments.

To study the impact of disorder introduced in solid solutions on the effects of radiation on the monazite structure various compositions of the La1-*x*Ce*x*PO4 solid solution were irradiated with 14 MeV Au ions to simulate the recoil of daughter products from α-decay and analyzed with SEM and grazing incidence XRD to investigate their radiation stability and recrystallization properties. While amorphization occured at intermediate fluences the short-range order is preserved and restored at higher fluences *via* simultaneous annealing.

These findings underscore the chemical flexibility of monazite and its exceptional ability for recrystallization.

References:

(1) Schlenz, H. et al. (2013) *Z. Kristallogr*. **228**:113-123.
(2) Dacheux, N., et al. (2013) *Am. Mineral*. **98**:833-847.
(3) Ewing, R. C., Wang, L. (2002*) Rev. Mineral. Geochem.* **48:**673-699.

Diffraction images of a CePO4 pellet (a) pristine, (b) irradiated with 1014 ions/cm2 resulting in amorphization while preserving local order, (c) irradiated with 1015 ions/cm2 showing a high degree of recrystallization.

Fig. 1

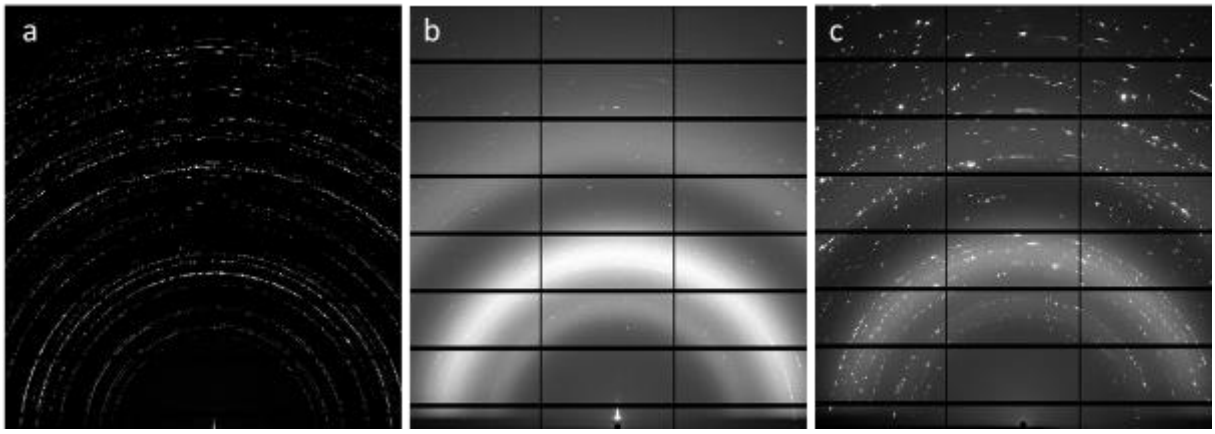

OP-049

Exploring the Transition Mechanisms in the Spin Crossover Compound [Fe(Pm-BiA)$_2$(NCS)$_2$]: A Lattice Dynamical Approach

P. Prakash (Jülich/DE), A. Grzechnik (Jülich/DE, Aachen/DE), J. Qi (Jülich/DE), H. Shahed (Jülich/DE), B. Gasharova (Karlsruhe/DE), Y. L. Mathis (Karlsruhe/DE), D. Chernyshov (Grenoble/FR), J. Voigt (Jülich/DE), M. Angst (Jülich/DE), J. Perßon (Jülich/DE), K. Friese (Jülich/DE, Aachen/DE)

A substitute for conventional vapor compression technology is the solid-state refrigeration, which utilizes the barocaloric effect to induce a temperature change in response to external hydrostatic pressure [1]. The spin crossover compounds are promising candidates for barocaloric applications due to their substantial isothermal entropy and adiabatic temperature changes, along with the reversible nature of the spin phase transition with different external stimuli e.g., temperature, pressure, light irradiation [2].

The origin of the driving force that governs the SCO phenomenon is directly associated with the entropy increase upon low spin→high spin (LS→HS) transition and is primarily dominated by the vibrational entropy change [3]. In this study, we examine lattice dynamics in [Fe(Pm-BiA)$_2$(NCS)$_2$], where Pm-BiA = (N-(2'-pyridylmethylene)-4-amino-bi-pheynyl). The compound crystallizes in two polymorphs with distinct mechanisms of spin transition: monoclinic ($P2_1/c$) with a gradual transition and orthorhombic (*Pccn*) with an abrupt transition [4].

In this work, we aim to address the underlying dynamical features that govern the different nature of transitions in the two polymorphs using temperature dependent infrared and Raman spectroscopy. We highlight the main differences in the phonon modes of the two polymorphs, across the spin-crossover transition. We further correlate our results with synchrotron single-crystal diffraction measurements [4] to understand the role of cooperativity. We also investigate the temperature dependence of vibrational entropy and its evolution across the SCO transitions. The results of this study are complemented with first principles calculations.

References:

(1) Zhao Zhang et al., *Mater. Horiz*. **10**, 977 (2023)
(2) P.J. von Ranke et al., *Solid State Commun.* **336**, 114427 (2021)
(3) A. Bousseksou et al., *Chem. Phys. Lett.* **318**, 409-416 (2000)
(4) H. Shahed et al., *Acta Cryst.* B**79**, (2023)

OP-050

Crystallographic characterization of ultrasmall elemental nanoparticles of 4d transition metal

N. Kost (Essen/DE), K. Loza (Essen/DE), N. Gumbiowski (Essen/DE), O. Prymak (Essen/DE), M. Epple (Essen/DE)

Background: Ultrasmall elemental metal particles as small as 3 nm are of interest because of their large specific surface area, as they are chemically stable under many reaction conditions. Especially the 4d transition metal nanoparticles are interesting for catalysis. Typical wet chemical syntheses are based on the reduction of the corresponding metal cations, followed by colloidal stabilization by a suitable ligand. Palladium, rhodium, and ruthenium nanoparticles tend to be spontaneously oxidized. However, for catalysis, M0 nanoparticles are required.

Objective: The intention of this work is to establish a reproducible synthesis of ultrasmall elemental nanoparticles of palladium, rhodium and ruthenium with glutathione or amines as a ligand, followed by their in-depth crystallographic characterization.

Methods: The particles are reduced starting from metal salts, isolated by centrifugation, and then comprehensively characterized by NMR spectroscopy, X-ray powder diffraction, transmission electron microscopy, disc centrifugation and small angle X-ray scattering.

Results: For the 4d transition metal nanoparticles, a correlation between the ligand and the oxidation state of the nanoparticle was observed. For example, an oxidized particle was observed for sulfur-containing ligands and a metallic nanoparticle was observed for amine-containing ligands. A similar trend was expected for rhodium and ruthenium.

Conclusion: It is possible to produce ultrasmall metallic nanoparticles from palladium, rhodium or ruthenium. The selection of the ligand has a considerable effect on the oxidation state of the particle. By using amine ligands, it was possible to obtain non-oxidized nanoparticles that are of particular interest for application in catalysis.

MS 14: Extreme conditions III: Organic and other materials

OP-051

Single-crystal X-ray diffraction and Raman spectroscopy on high-pressure ethane up to 150 GPa

L. Toraille (Bruyères-le-Châtel/FR), G. Weck (Bruyères-le-Châtel/FR), G. Garbarino (Grenoble/FR), G. Geneste (Bruyères-le-Châtel/FR), P. Loubeyre (Bruyères-le-Châtel/FR)

The characterization of the physico-chemical properties of the C-H system under high-pressure and high-temperature is of great importance in many fields such as organic, bio and petroleum chemistry as well as in planetary science.

Surprisingly little is known about high-pressure ethane (C2H6), with only a few studies mainly based on X-ray diffraction [1,2] (XRD) and Raman spectroscopy [1,3], often with contradictory conclusions. Various phase transitions reportedly witnessed with Raman spectroscopy have not been observed through XRD. The goal of this study was to resolve these contradictions.

We coupled single-crystal XRD with Raman spectroscopy, infrared absorption and ab initio calculations up to 150~GPa. We did multiple experiments with both pure ethane and ethane in helium to improve the hydrostaticity of the compression.

We determined precisely the structure, stability regions and vibration modes of two phases of solid C2H6. The Raman spectroscopy in particular reveals interesting phenomena. We obtained the equation of state of ethane giving a relation for the evolution of the volume of ethane with pressure.

These new updated results improve the general knowledge on high-pressure ethane.

References:

(1) E. Stavrou, *et al.*, *The Journal of Chemical Physics* **155**, 184503 (2021).
(2) M. Podsiadlo *et al.*, *Cryst. Growth Des.* **17**, 228-232 (2017).
(3) L.Q. Read *et al.*, *J Raman Spectrosc.* **51**, 2311– 2317 (2020).

OP-052

High-pressure behavior of pyrene studied up to 35 GPa using single-crystal X-ray diffraction in a diamond anvil cell

W. Zhou (Bayreuth/DE), Y. Yin (Bayreuth/DE), A. Aslandukov (Bayreuth/DE), L. Dubrovinsky (Bayreuth/DE), N. Dubrovinskaia (Bayreuth/DE)

Exploring the behavior of pyrene under high pressure provides insights into the structural transitions and intermolecular interactions of polycyclic aromatic hydrocarbons (PAHs). Here, we report the results of investigations of pyrene up to ~35 GPa by a combination of *in situ* single-crystal synchrotron X-ray diffraction (SCXRD) in a diamond anvil cell (DAC) and *ab initio* calculations. Experimental SCXRD measurements at room temperature in DACs with helium as a pressure-transmitting medium reveal a series of pressure-induced phase transitions: from pyrene-I at ambient conditions to pyrene-II (at 0.7 GPa), pyrene-IV (at 2.7 GPa), and pyrene-V (at 7.3 GPa). Pyrene-IV and pyrene-V have not been reported before. The latter is preserved up to 35 GPa. The analysis of the structures and the chemical bonding reveals that pyrene-I, pyrene-II and pyrene-IV have similar sandwich-herringbone molecular packing, which becomes more compact due to a general shortening of intermolecular distances and decrease of interplanar angles, as well as due to a mutual shift of the molecules in sandwiches under pressure. Further compaction leads to the collapse of the sandwich structure in pyrene-V, which possesses herringbone packing of considerably curved molecules. *Ab initio* calculations suggest that the phases we found are thermodynamically metastable.

OP-053

High-pressure enhancement of metal-free luminescence of anthracene-based materials

A. Krawczuk (Göttingen/DE), A. Olejniczak (Poznan/PL), R. Crespo-Otero (London/GB)

Solid-state luminescent materials based on pure fluorescent organic molecules have received considerable attention because of potential applications in the field of optics, optoelectronics and bioimaging. However, their rational design is challenging because the photoluminescence properties, which strongly depend on molecular conformation and non-covalent interactions (NCI) in the solid state, are hardly predictable. In various cases, although a molecule exhibits strong photoluminescence in a solution, upon aggregation, the effect is quenched (aggregation-caused-quenching), whereas in other cases modes of aggregation actually enhance the luminescent properties (aggregation-induced-emission).[1,2] One of the efficient ways to alter the response of crystalline material is to subject it to high pressure.

Here we present pressure-induced emission enhancement (PIEE) of sulfur-oxidized anthracene, [1-(S)PPh_2-($C_{14}H_9$)], crystallizing in monoclinic $P2_1/c$ space group.[1] Application of pressure up to 2.9 GPa decreases the distance between the anthracene rings by almost 10%, which suggests the reduction of the energy gap between ground and excited states and promotion of excimer formation which would be expressed in bathochromic shift of the emission maxima. As expected, application of high-pressure redshifts the emission band from 550 nm to 570, already at low pressure, *i.e.* 0.3GPa, however further increase of the pressure does not affect further bathochromic shift, except for the band broadening. What one observes instead, is the decrease of emission intensity upon applied pressure by 55% but also enhancement of the lifetime from 30 ns at ambient conditions to 40 ns at 2.72 GPa is observed. To explain the phenomenon extensive quantum crystallography tools are employed and possible mechanism is revealed.

References:

(1) A. Krawczuk, M. A. Sidat, A. Olejniczak, A. Katrusiak, R. Crespo-Otero (2023), in preparation

OP-054

High-pressure synthesis and crystal structure of Mg_5Bi_3

T. Neziraj (Dresden/DE), L. Akselrud (Lviv/UA), Y. Grin (Dresden/DE), U. Schwarz (Dresden/DE)

Introduction

The only binary intermetallic compound in the magnesium-bismuth system known to date Mg_3Bi_2 [1] was discovered more than one century ago by Zintl, and it remained the only example of a structurally characterized alkaline-earth bismuth compound for several decades. The effect of high pressures has been shown to be crucial for the formation of new binary bismuth phases, such as $CoBi_3$, $Cu_{11}Bi_7$, and CuBi [2-4].

Objectives

Here, we performed a study of the system magnesium-bismuth under extreme conditions. As a result, we report on the formation of the new binary phase of Mg_5Bi_3, and its crystal structure.

Materials and Methods

The new compound of Mg_5Bi_3 is synthesized by high-pressure high-temperature synthesis using a hydraulic press with a Walker-type module. It is characterized using powder X-ray diffraction, energy and wavelength dispersive X-ray spectroscopy, and differential scanning calorimetry.

Results

High-pressure high-temperature synthesis of Mg_5Bi_3 is performed at a pressure of 4-5 GPa at a temperature range of 773-1072 K for several hours before quenching under load. The analysis of the X-ray powder diffraction patterns and EDXS measurements confirmed the formation of the Mg_5Bi_3 compound. Refinements using powder data reveal β-Yb_5Sb_3-type crystal structure, space group *Pnma*, a = 11.5400(2), b = 8.9503(2), c = 7.8678(2)Å, V = 813.57(5)Å^3. At ambient pressure, the compound decomposes into Mg_3Bi_2 and Bi upon heating at approximately 516 (10) K, as evidenced by thermal analysis.

Conclusion

The new binary phase of Mg_5Bi_3 is synthesized by high-pressure synthesis. This compound adopts the crystal structure of β-Yb_5Sb_3-type and is a metastable phase at ambient pressure.

References:

(1) E. Zintl, E. Husemann, *Z. Phys. Chem.*, **1933**, *21B, 138-155*.
(2) U. Schwarz, et al. *Angew. Chem. Int. Ed.*, **2013**, *52, 37, 9853-9857*.
(3) S. M. Clarke, et al. *Angew. Chem. Int. Ed.*, **2016**, *55, 43, 13446-13449*.
(4) K. Guo, et al. *Angew. Chem. Int. Ed.*, **2017**, *56, 20, 5620-5624*.

MS 15: Oral posters

OPo-1

Using indium *K*a radiation from a MetalJet X-ray source for a charge-density analysis of the YLID

N. Graw (Göttingen/DE), P. N. Ruth (Durham/GB), T. Ernemann (Göttingen/DE), R. Herbst-Irmer (Göttingen/DE), D. Stalke (Göttingen/DE)

With the MetalJet X-ray source a high-brilliance X-ray source for in-home diffraction experiments using indium *K*a radiation is available.[1] Since indium *K*a radiation has an even shorter wavelength than silver *K*a radiation, it allows for a higher theoretical resolution and should result in less absorption. Paired with the high intensity of the MetalJet source, this should yield ideal conditions to collect high resolution data for experimental charge density analyses.

The setup in this study consisted of a D2 MetalJet X-ray source from Excillum combined with Incoatec multilayer optics optimised for In *K*a radiation and a Dectris Eiger2 CdTe 1M detector all integrated in a Bruker D8 Venture diffractometer. The source used ExAlloy I3 (75% Ga, 25% In) as anode material. Diffraction experiments were performed on a crystal of C11H10O2S. A multipole model according to the Hansen-Coppens formalism[2] was refined and the obtained electron density was analysed according to Baders´s QTAIM.[3]

The results of this investigation allow for a detailed discussion of the bonding situation in the YLID compound. Furthermore, they indicate the capability of the diffraction setup used to collect high quality data demonstrating that In *K*a radiation can be used for experimental charge-density investigations.[4]

References:

(1) D. H. Larsson, P. A. C. Takman, U. Lundström, A. Burvall, H. M. Hertz, *Rev. Sci. Instrum*. **2011**, *82*, 123701.
(2) N. K. Hansen, P. Coppens, *Acta Cryst. A* **1978**, *34*, 909.
(3) R. F. W. Bader, *Atoms in Molecules*. *A Quantum Theory*, Clarendon Press, Oxford, New York, **1990**.
(4) a) N. Graw, P. N. Ruth, T. Ernemann, R. Herbst-Irmer, D. Stalke, *J. Appl. Cryst.* **2023**, *56*, 1315.
b) P. N. Ruth, N. Graw, T. Ernemann, R. Herbst-Irmer, D. Stalke, *J. Appl. Cryst.* **2023**, *56*, 1322.

OPo-2

Investigations of accelerated CO_2 sequestration of artificial lime-sand bricks

C. H. Rüscher (Hannover/DE), N. Och (Hannover/DE), C. Rozanski (Hannover/DE), Z. Istanbuly (Hannover/DE), W. Eden (Hannover/DE)

The production of 7.6 Mio t lime-sand bricks in Germany in 2021 generated 885000 t CO_2. 27 % originate from fossil energy required for decarbonation of $CaCO_3$ (lime production), 20 % were released during hydrothermal synthesis in the lime-sand brick plants, and about 53% are released by the decarbonation reaction itself [1]. The roadmap [1] also describes that a natural CO_2 sequestration by the lime sand bricks occurs slowly within 50 years from air. However, we could show that accelerated carbonation of hydrothermally produced lime sand bricks lead to a complete recarbonation within hours, which could be used to significantly reduce the CO_2 emission during production. The effect of accelerated recarbonation is investigated using powder XRS (X-Ray Scattering), FTIR absorption, TG/DTA, REM, optical microscopy.It is observed that the primary glue/binder between quartz crystals of the lime sand brick consists of tobermorite nano-crystals and a CSH-gel residual (C=CaO, S=SiO_2, H = H_2O). During recarbonation both of these phases are transformed to a SiO_2-inorganic polymer enclosing freshly formed carbonate crystals (Aragonite, Vaterite and Calcite). Compressive strength experiments of cyclindrical samples with 2 cm diameter and 1 cm height were carried out observed using in situ 3D-XRM (X-ray microscopy, Fig. 1). Both types of samples, carbonated and uncarbonated, show a maximum compressive strength of about 16 MPa. However, the compressive strength is observed at slithly lower deformation displacement for the carbonated sample.

References:

(1) Geres, R.; Lausen, J; Weigert, S.: Roadmap für eine treibhausgasneutrale Kalksandsteinindustrie in Deutschland. Eine Studie für den Bundesverband Kalksandsteinindustrie e.V., München, 2021.

Acknowledgement: XRM measurements at the Bruker XRM Application Lab through V. Vancauwenberghe, and discussion of results with F. Stemme and N. Schott are greatly acknowledged.

Fig. 1 Force versus deformation displacement. Inserts: XRM-on crosssections.

Fig. 1

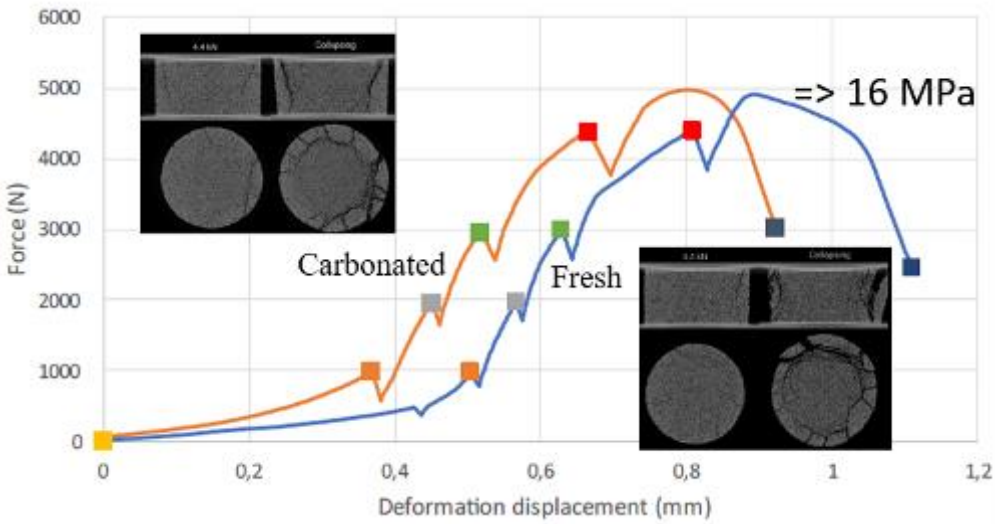

OPo-3

Orthorhombic Symmetry and Anisotropic Properties of Rutile TiO_2

N. Gonzalez Szwacki (Warsaw/PL), P. Fabrykiewicz (Aachen/DE, Garching/DE), I. Sosnowska (Warsaw/PL), F. Fauth (Barcelona/ES), E. Suard (Grenoble/FR), R. Przeniosło (Warsaw/PL)

The symmetry of the material is an important factor determining its properties. In this work, we demonstrate [1] both experimentally and by numerical simulations that the actual symmetry of the rutile phase of TiO_2 is $CaCl_2$-type [2] orthorhombic, described with space group Pnnm, in contrast to what it is commonly believed that rutile TiO_2 has a tetragonal symmetry [2-4], described with space group $P4_2/mnm$. We present very precise first-principles calculations for the determination of the structural properties of rutile TiO_2 and highlight the relevance of using the revised regularized SCAN meta-GGA density functional for the interpretation and analysis of neutron and synchrotron radiation diffraction measurements. We showed that symmetry lowering is present in both lattice constants and atomic positions, see Fig. 1. The lowering of the symmetry has a small but not negligible influence on the elastic, vibrational, and optical properties of rutile TiO_2. Results are discussed in the context of analogous lower symmetry structure description in other rutile-type compounds: β-PbO_2 [5], β-MnO_2 [6] and MnF_2 [6].

References:

(1) N. Gonzalez Szwacki, P. Fabrykiewicz, I. Sosnowska, F. Fauth, E. Suard and R. Przeniosło; *J. Phys. Chem. C* **127** (2023) 19240
(2) W. H. Baur; *Crystallogr. Rev.* **13** (2007) 65
(3) D. T. Cromer and K. Herrington; *J. Am. Chem. Soc.* **77** (1955) 4708
(4) J. K. Burdett, T. Hughbanks, G. J. Miller, J. W. J. Richardson and J. V. Smith; *J. Am. Chem. Soc.* **109** (1987) 3639
(5) P. Fabrykiewicz, R. Przeniosło, N. Gonzalez Szwacki and I. Sosnowska, E. Suard and F. Fauth; *Phys. Rev. B* **103** (2021) 064109
(6) P. Fabrykiewicz, R. Przeniosło, I. Sosnowska, F. Fauth and D. Oleszak; *Acta Cryst. A* **75** (2019) 889

Fig. 1

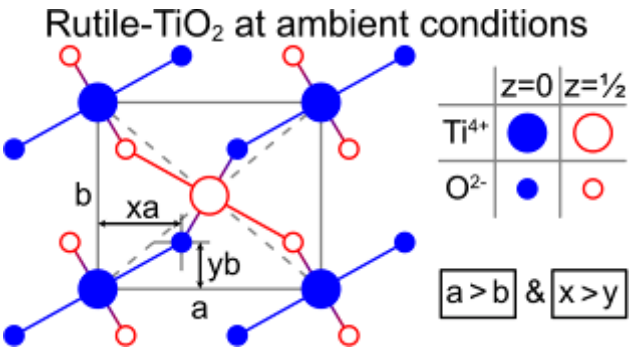

OPo-4

Tl[*Ch*CN] polymorphs – structure determination and phase transitions (*Ch*=O, S, Se)

A. Shlyaykher (Marburg/DE), F. Tambornino (Marburg/DE), D. Fortes (Chilton/GB)

In this work, we present our studies on temperature dependent behaviour of different thallium cyanates Tl[*Ch*CN] (*Ch*=O, S, Se). Whereas the crystal structure of Tl[SCN] has been reported, data on Tl[OCN] and Tl[SeCN] is absent. At 298 K Tl[SCN] crystallizes in the orthorhombic space group *Pbcm* (№ 57, *a*=6.783(1), *b*=6.816(1), *c*=7.606(1) Å, *V*=351.65 Å^3). Here, the S and N atoms of an almost linear [SCN]−-anion can be differentiated from each other without any apparent disorder. By increasing of the temperature to 400 K, Tl[SCN] undergoes an order-disorder transition from *Pbcm* into the higher symmetric tetragonal space group *I*4/*mcm* (№ 140). Due to the head-to-tail disorder of the [SCN]−-anion, S and N atoms occupy the same atomic position.[1,2] Both space groups are related by symmetry, which is described with the aid of the Bärnighausen formalism.

Tl[SeCN] shows similar behaviour. At 298 K it crystallizes isotopically with Tl[SCN] in the space group *Pbcm* (*a*=7.038)1), *b*=6.906(1), *c*=7.724(1) Å, *V*=375.45(9) Å3). At 400 K, due to a significant difference in atomic masses of Se and N atoms only partial disorder of the [SeCN]$^-$-anion can be observed. Se and N atom positions are occupied in the ratio of 0.1 to 0.9 and *vice versa*. It still crystallizes in the space group *Pbcm* (*a*=6.9596(8), *b*=7.0376(8), *c*=7.8570(6) Å, *V*=384.83(7) Å^3). Phase transition to the fully disordered *I4/mcm* phase was studied by ht-PXRD.

From SC-XRD data, the lightest homologue Tl[OCN] is disordered at 298 K. It crystallizes isotopically with ht-Tl[SCN] in the space group *I*4/*mcm* (*a*=6.2437(3), *c*=7.1742(3) Å, *V*=279.68(3) Å3). However, due to a low scattering contrast of O and N atoms, the atomic occupancies cannot be determined exactly. To check if ordering occurs at 298 K or at lower temperatures, we used time-of-flight powder neutron diffraction.

References:

(1) R. Lippman, R. Rudman, *Acta Crystallogr. A.* **1981**, *37*, C106–C106.
(2) R. Lippman, R. Rudman, *J. Chem. Phys.* **1983**, *79*, 3457–3461.

Fig. 1

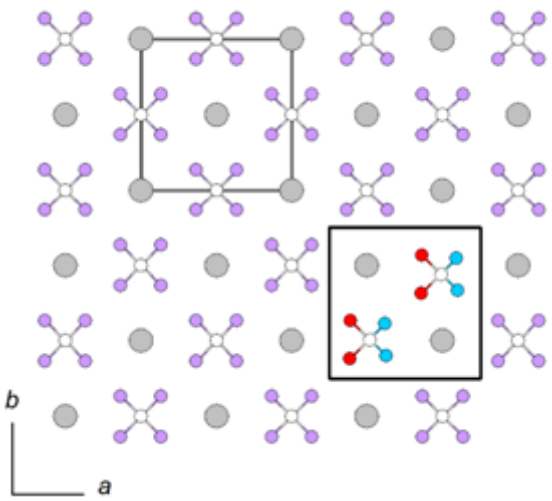

OPo-5

Investigating the mixing of the heavy trielides indium and thallium in the structure type Na_7RbTl_4

M. Janesch (Regensburg/DE), V. Schwinghammer (Regensburg/DE), S. Gärtner (Regensburg/DE)

Alkali metal *Zintl* phases are still the subject of current research as they provide new (semi-) metallic materials of main group elements.[1,2] In this context, we investigated the Na_7ATr_4 structure type (*A*=K, Rb & *Tr*=In, Tl), which crystallizes in the orthorhombic space group *Pbam*.[3,4] The anionic substructure consists of isolated $[Tr_4]^{8-}$ tetrahedra. While tetrahedral clusters of thallium are present in different alkali metal thallides, Na_2In[5] and Na_7KIn_4[4] are the only representatives including $[In_4]^{8-}$ clusters within the alkali metal indium system. While Na_7KTr_4 can be formed by indium as well as by thallium, only the heavier homologue Na_7RbTl_4 is known so far.[3] Thus, the miscibility of the trielides in this structure type was investigated to approximate Na_7RbIn_4. $Na_7RbIn_{2.19}Tl_{1.81}$ provides the highest indium content so far (*a*=16.3721(3) Å, *b*=16.3636(3) Å, *c*=11.3376(2) Å). Similar work was already done e.g. for group 15 elements, where of the vertexes in Pn_4 (*Pn*=P, As) tetrahedra were partially replaced by Ge atoms which leads to a reduced charge of the anionic entity.[6] Also, for the tetrelides mixed atom variants of $(Ge_{4-x}Si_x)^{4-}$ were investigated.[7] As the group 14 tetrahedra show a lower charge than the electron poor trielide clusters, they readily can be dissolved in polar solvents such as liquid ammonia, which was not known for the highly charged trielide tetrahedra. Preliminary experiments in liquid ammonia for Na_2In as well as for Na_7KIn_4 showed a stepwise oxidation of the $[In_4]^{8-}$ clusters to NaIn, elemental indium and alkali metal amide.[4]

References:

(1) E. Zintl, W. Dullenkopf, *Z. Phys Chem*. **1932**, 16B, 195-205.
(2) S. M. Kauzlarich, S. R. Brown, G. J. Snyder, *Dalton Trans.* **2007**, 2099-2107.
(3) V. F. Schwinghammer et al., *ZAAC,* **2022**, 648.
(4) M. Janesch, et al., *ZAAC,* **2023**.
(5) S. C. Sevov, J. D. Corbett, *J. Solid State Chem.* **1993**, 103, 114-130.
(6) F. Pan, L. Guggolz, S. Dehnen, *CCS Chem.* **2022**, 4, 809-824.
(7) M. Waibel et al., *Eur. J. Inorg. Chem.* **2013**, 2013, 5541-5546.

Fig. 1

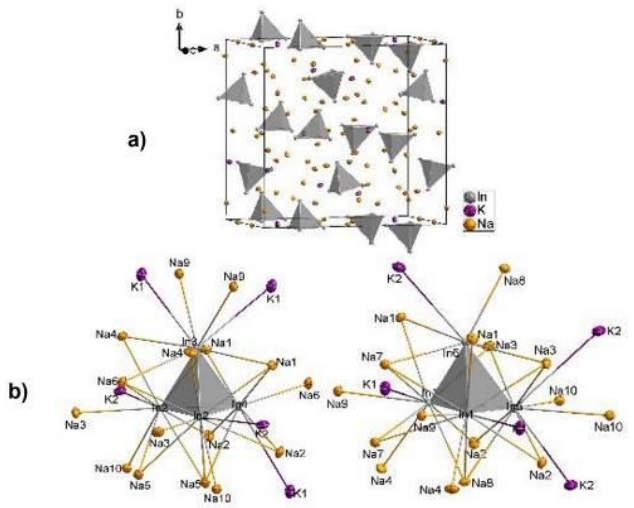

Fig 1: a) Unit cell of the structure type Na_7RbTl_4 b) Coordination sphere of the two crystallographic independent tetrahedra.

OPo-6

Phase Transitions, Structure Evolution, and Thermoelectric Properties based on A_2MnSb_2 (A = Ca, Yb)

K. Liu (Jinan/CN, Beijing/CN), S. Xia (Jinan/CN), H. Gou (Beijing/CN)

Zintl phases are defined as a special type of intermetallic compounds, in which the electronegativity of anions and cations are significantly different. The frameworks of Zintl phases are constructed by anions, while the cations are frequently viewed as charge suppliers and space fillers. Zintl phases with complex crystal structures, dispersive bands, and nonclassical bonding interactions show the diverse physical properties. Herein, we synthesized two Mn-containing metastable Zintl phases Ca_2MnSb_2 and Yb_2MnSb_2 with layered structures through induction melting method for the first time[1]. The structures are determined to be LiZnSb-type (Space group: $P6_3mc$) with partial occupancies of transition-metal sites. Interestingly, these compounds bear broad homogeneity ranges, which enable flexible tuning on the Mn sites. Furthermore, the thermal stability of A_2MnSb_2 (A = Ca, Yb) can be significantly improved through Ag doping on the Mn sites. Single crystals of $Ca_2(Mn_{0.71(1)}Ag_{0.58(3)})Sb_2$ and $Yb_2(Mn_{0.86(2)}Ag_{0.28(3)})Sb_2$ are successfully synthesized through metal flux method and systematic investigations on the crystal structures and thermoelectric properties are carried out. Benefited from the complex anionic structures, the thermal conductivity of these phases is extremely low, and $Yb_2(Mn_{0.9}Ag_{0.2})Sb_2$ features the glasslike thermal conductivity of ~0.5 $W{\cdot}m^{-1}{\cdot}K^{-1}$, and meanwhile, a high Seebeck coefficient of 208 $\mu V{\cdot}K^{-1}$ is obtained at 673 K. The discovery of A_2MnSb_2 (A = Ca, Yb) phases fills in the key missing members of the A−Mn−Sb ternary family, which is crucial for understanding the structures and properties of these phases. The studies provide a basic for further design and synthesis of the state-of-the-art thermoelectric materials based on such Zintl phases.

References:

(1) Liu, K.; Liu, J.; Liu, Q.; Wang, Q.; Yu, F.; Liu, X.-C.; Xia, S.-Q. Phase Transitions, Structure Evolution, and Thermoelectric Properties Based on A_2MnSb_2 (A = Ca, Yb). *Chem. Mater.* **2021**, *33*, 9732–9740.

Fig. 1

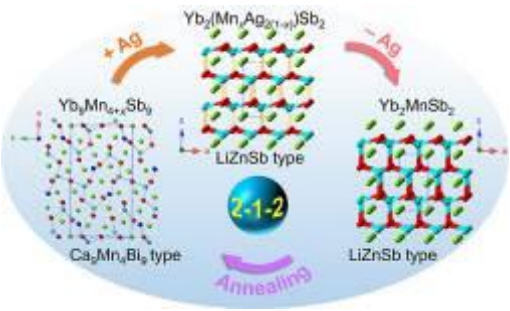

OPo-7

Back and forward: from atomic parameters to crystallographic and cryoEM inhomogeneous-resolution maps for real-space refinement

A. Urzhumtsev (Ourjoumtsev) (Illkirch/FR, Vandoeuvre-lès-Nancy/FR), N. L. Lunina (Pushchino/RU), V. Y. Lunin (Pushchino/RU)

Real-space refinement in crystallography and cryoEM compares model maps with the experimental ones, mimicking imperfections of the latter. The model maps can be calculated as a sum of atomic images given atomic type, position, values of the displacement parameter (*B*), occupancy and a resolution (*D*). The inverse problem is, given a map of a variable resolution, to find the values of all atomic parameters, including the local resolution.

An atomic image is represented by a peak surrounded by Fourier ripples shape of which depends on both *B* and *D*. Describing such images analytically would solve both direct and inverse problems without using reciprocal space data, giving analytic expressions for both the target function and all its partial derivatives.

To model Fourier ripples, a 3D function Ω(x,μ,σ) has been designed [1] such that its convolution with a Gaussian does not change the function itself but only its parameter σ. This means that an image of any atom of any chemical type, at any local resolution *D* and with any *B* value can be expressed analytically as a sum of Ω terms (Fig.1). A model density map, of a variable local resolution, can be calculated in a single run, with no Fourier transform used [2].

As a step toward real-space refinement, we showed that a grid search allows estimating the values of *B* and *D*, assuming that atomic positions are known [3]. Moreover, our procedure succeeded to indicate several examples of incorrectly assigned *B* and *D* values in some deposited models (Fig.2).

The suggested modeling changes the method and the concept of real-space refinement. Being associated with atoms, the local resolution can be refined and reported in the PDB files together with the coordinates and displacement factors.

References:

(1) Urzhumtsev, A., Lunin, V.Y. (2022) *IUCr Journal*, **9**, 728-734
(2) Urzhumtsev, A., Urzhumtseva, L.M., Lunin, V.Y. (2022) *Acta Cryst.,* D**78**,1451-1468
(3) Lunin, V.Y., Lunina, N.L., Urzhumtsev, A. (2023). *Current Res. Struct. Biol.* **6**, 100102

Fig. 1

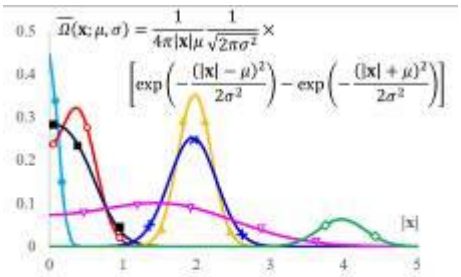

radial component of the function Ω for different sets of its parameters

Fig. 2

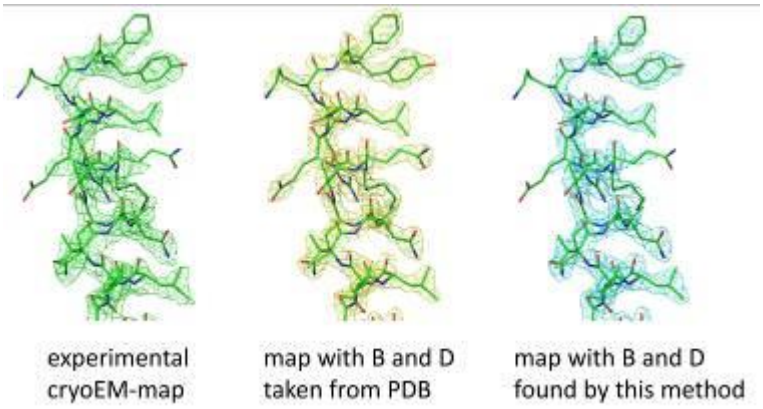
experimental
cryoEM-map
map with B and D
taken from PDB
map with B and D
found by this method

OPo-8

Determination of partial charges with electron diffraction

T. Gruene (Vienna/AT), S. Mahmoudi (Vienna/AT), C. Schröder (Vienna/AT)

It is well know that electron interact with matter through the electrostatic potential. In principle, the map resulting from electron diffraction experiments display the electrostatic potential of the crystalline molecule. For minerals, this fact was demonstrated in the 1990s, pioneered by Spence et al with the development of converged electron beam diffraction. The rise of 3D ED triggered a boost of electron diffraction. Electron diffraction produces a crystal structure, quite similar to X-ray and neutron diffraction, providing information about the 3D atomic coordinates.

Here we present an experimental method to determine partial charges from electron diffraction data. Our method is based on a linear superposition of ionic and atomic scattering factors. We demonstrate that the fraction of ionic scattering factors directly relate to the partial charge of an atom in the crystallographic model. We confirm our result with ED data from a ZSM5, a zeolite of framework MFI with 12 independent T-sites and 26 independent oxygen sites in the asymmetric unit, as well as ED data from L-histidine and D-tyrosine. Quantitatively we confirm our results with quantum chemical computations of the partial charges using a variety of programs and algorithms.

Our method is for sure not as precise as a full multi-pole refinement. However, our method works with data at atomic resolution, i.e., 0.7A - 0.8A. This makes the method applicable to a very broad range of chemical compounds, in particular to systems with a complexity that escapes DFT and similar simulation studies. It is based on refinement with SHELXL, using its concept of free variables, and can be easily adapted by any crystallographer familiar with this concept. Not only does our method provide experimental values of the chemically universal concept of partial charges, it also offers the possibility to improve algorithms for DFT computations and to scale theoretical results.

OPo-9

Bulk High-Entropy Hydrides prepared under High-Pressure High-Temperature

K. Yusenko (Berlin/DE), K. Glazyrin (Hamburg/DE), K. Spektor (Hamburg/DE), W. Dong (Hamburg/DE), M. Bykov (Cologne/DE)

High-entropy alloys (HEAs) have simple crystal structures combining long range periodicity and high degree compositional disorder on the atomic level [1,2]. Structural and mechanical stability of high-entropy alloys under extreme conditions emphasizes their potential for general and special applications. Originally developed as materials for structural applications, HEAs were intensively studied as functional and energy-related materials within the fields of catalysis and energy storage. Here, for the first time, we systematically study an interaction of single phase *fcc*, *hcp* and *bcc* HEAs with hydrogen to obtain HEA hydrides.

Our study of the compression of *hc*-Ir0.19Os0.22Re0.21Rh0.20Ru0.19 and *fcc*-Ir0.26Os0.05Pt0.31Rh0.23Ru0.15 in H2-loaded DACs at RT suggests that HEAs do not form any intermetallics, are stable against H2 at low pressures and absorb detectable amount of H2 above 10 GPa. At higher pressures, the H-rich phase at 53 GPa corresponds to a H:M=0.6:1. Hydrogen uptake upon compression appears efficient and is characterized by a broad hysteresis upon decompression. A study using pulsed laser heating suggests decomposition of *hcp*-PGM HEA in presence of H2 at the area heated by the laser.

Cantor alloy, *fcc*-CoCrFeNiMn, does not absorb hydrogen at RT up to 40 GPa. Such result is unusual while even resistant alloys absorb hydrogen upon compression at RT. Heating above 100 °C resul inrelatively fast hydrogen absorption with a formation of *fcc*–CoCrFeNiMnH high-entropy hydride.

fcc–Al0.3CoCrFeNi HEA shows complex behavior upon hydrogen absorption. Upon heating above 400 °C at 10 GPa the alloy decomposes into two phases: H-rich HEA as a major phase with M:H=1:0.8 and a minor H-deficient HEA with M:H=1:0.2.

References:

(1) A Smekhova, A Kuzmin, KV Yusenko et al. (2023): *Nano Research* 16(4) 5626–5639; [2] A Smekhova, A Kuzmin, KV Yusenko et al. (2021): *Nano Research* 15 4845–4858

OPo-10

Structures of the dedicated futalosine hydrolase and its paralog MTAN from *Thermus thermophilus* provide insights into enzyme evolution

A. Prasad (Halle/DE), C. Cotrim (Halle/DE), D. A. Nguyen (Halle/DE), C. Breithaupt (Halle/DE), J. Ziegler (Halle/DE), H. Lilie (Halle/DE), U. Weininger (Halle/DE), M. T. Stubbs (Halle/DE)

Menaquinone can be synthesized in bacteria via two different pathways: the classical pathway that involves products of the *men* genes [1,2], and the more recently discovered futalosine pathway encoded by mqn genes [3]. The eponymous intermediate futalosine is hydrolyzed to hypoxanthine and dehypoxanthine futalosine (DHFL) by the futalosine hydrolase MqnB, although in some organisms, DHFL is produced directly from the futalosine precursor 6-amino-6-deoxyfutalosine (AFL) by the promiscuous 5"-methylthio adenosine nucleosidase (MTAN) [4,5]. Here we present crystal structures of the *Thermus thermophilus* enzymes *Tt*MTAN and *Tt*MqnB both in the presence and absence of substrates (or analogs) and their nucleotide products. We show that although both enzymes undergo significant structural rearrangements upon ligand binding, these occur via very different routes. Using NMR spectroscopy on *Tt*MqnB, we identify a serine residue near the active site with an unusually low pKa and demonstrate that nucleoside hydrolysis in the two enzymes proceeds via fundamentally different mechanisms.

References:

(1) Meganathan, O. Kwon, Biosynthesis of Menaquinone (Vitamin K 2) and Ubiquinone (Coenzyme Q). *EcoSal Plus* **3** (2009).
(2) Kurosu, E. Begari, Vitamin K2 in Electron Transport System: Are Enzymes Involved in Vitamin K2 Biosynthesis Promising Drug Targets? *Molecules* **15**, 1531–1553 (2010).
(3) Hiratsuka, *et al.*, An Alternative Menaquinone Biosynthetic Pathway Operating in Microorganisms. *Science* **321**, 1670–1673 (2008).
(4) Wang, *et al.*, A Picomolar Transition State Analogue Inhibitor of MTAN as a Specific Antibiotic for *Helicobacter pylori*. *Biochemistry* **51**, 6892–6894 (2012).
(5) Li, D. Apel, E. C. Gaynor, M. E. Tanner, 5′-Methylthioadenosine Nucleosidase Is Implicated in Playing a Key Role in a Modified Futalosine Pathway for Menaquinone Biosynthesis in Campylobacter jejuni. *Journal of Biological Chemistry* **286**, 19392–19398 (2011).

OPo-11

Generation and Crystallographic Screening of a Highly Sociable and Diverse Fragment Library

F. Becker (Münster/DE), P. Janssen (Münster/DE), T. Matviyuk (Lyiv/UA), I. Kondratov (Frankfurt a. M./DE), F. Füsser (Münster/DE), D. Kümmel (Münster/DE), M. S. Weiss (Berlin/DE), O. Koch (Münster/DE)

Fragment-based drug discovery has become an important technique for the development of small molecular probes or drugs.[1] Performing fragment screening with available fragment libraries is often tedious and time-consuming when it comes to fragment extension, as the required direction is often difficult or impossible to access synthetically. St. Denis et al. termed this as non-sociable fragments that lacks the needed growth vector for fragment extensions.[1] The goal of this work was to adress this problem by generating a fragment library that consists of a set of highly sociable and diverse fragments to access a broader range of the chemical space and an easy synthesizability of compounds.

We therefore selected the massive chemical space available via Enamine"s REAL Space approach[2] of 38 billion make-on-demand molecules based on a number of robust reactions combined with a huge number of building blocks. The total in-stock building blocks were clustered according to their shape and features using FastROCS to obtain the widest possible range of fragments. A substructure search was performed in Enamine"s REAL Space S, which was then filtered for fragments with the ability of having a variety of at least 10 substituents for each exit vector. A library of 96 highly sociable fragments has been created, which is about to be screened on an established crystal system on the thioredoxin reductase of *M. Smegmatis* (smTrxR).[3] For some selected Hits, substituted compounds from REAL SPACE S will be purchased and tested to prove the concept.

We will present and discuss the development and application of our highly sociable fragment library that gives an easy access to fragment extension for fast exploration of structure-activity relationships.

References:

(1) St. Denis *et al.*, *RSC Med. Chem.* **2021**, DOI: 10.1039/D0MD00375A.
(2) https://enamine.net/compound-collections/real-compounds, accessed 11.11.2023.
(3) Füsser *et al.*, *Acta Crystallogr D Struct Biol.* **2023**, DOI: 10.1107/S2059798323005223.

OPo-12

Macromolecular Crystallography at Beamline P11

S. Chatziefthymiou (Hamburg/DE), V. Delsoglio (Hamburg/DE), A. Grebentsov (Hamburg/DE), A. Gruzinov (Hamburg/DE), T. Melson (Hamburg/DE), O. Merkulova (Hamburg/DE), J. Song (Hamburg/DE), H. Taberman (Hamburg/DE), G. Pompidor (Hamburg/DE), J. Hakanpää (Hamburg/DE)

DESY"s MX beamline P11 has been operating since 2012 at PETRA III and offers versatile focusing options to match the beam size and desired dose with diverse samples and various kinds of experiments (1). Fast and robust sample changer, in combination with Eiger2 X 16M, allows data collection as fast as 2 min per sample and fits 23 unipucks simultaneously. Remote operation is realised with simple web-browser based solution and authentication through the user portal, DOOR. P11 user laboratory is equipped with the OLT Shifter for semi-automated crystal harvesting and soaking experiments, ideal for drug screening campaigns.

Serial synchrotron crystallography at P11 is enabled mainly with the CFEL tape-drive setup, also capable of time-resolved experiments by the mix-and-diffuse method (2). Real-time autoprocessing of serial data with CrystFEL (3) has been developed within a long-term proposal.

At PETRA IV, we are aiming to form a uniform bio-village at the current location of DESY and EMBL beamlines (P11-P14). P11 has implemented MXCuBE/ISPyB for data acquisition and information management to harmonize the interfaces to the beamlines and is working together with EMBL within a long-term proposal to further develop both software and hardware. Together with EMBL and Hamburg University of Applied Sciences (HAW Hamburg), DESY is currently building up a new logistics chain for MX samples.

In preparation for PETRA IV, P11 is moving to a new access mode in 2024, to pilot the rolling call and project based access.

References:

(1) Burkhardt A., et al., Status of the crystallography beamlines at PETRA III. Eur. Phys. J. Plus 131, 56 (2016)
(2) Beyerlein K. R., et al., Mix-and-diffuse serial synchrotron crystallography. IUCrJ 4, 769-777 (2017)
(3) White T. A., et al., Recent developments in CrystFEL. J. Appl. Cryst. 49, 680-689 (2016)

OPo-13

$Pr_3OI[AsO_3]_2$: The First Oxide Iodide Oxoarsenate of the Rare-Earth Metals

R. J. C. Locke (Stuttgart/DE), T. Schleid (Stuttgart/DE), A. Erden (Stuttgart/DE)

In analogy to the non-centrosymmetric $Ln_3OX[AsO_3]_2$ representatives (*Ln* = Ce–Nd, Sm–Dy; *X* = Cl and Br)[1–4], the isostructural iodide $Pr_3OI[AsO_3]_2$ was obtained in synthetic experiments with Pr, PrI_3, As_2O_3 with CsI as flux by means of a partial metallothermic reduction at 850 °C. The green, needle-shaped crystals could be recovered phase-pure after removal of the resulting monolithic arsenic crystal. $Pr_3OI[AsO_3]_2$ crystallizes in the tetragonal space group $P4_2nm$ with the lattice parameters *a* = 1289.13(9) pm, *c* = 559.24(5) pm and *c/a* = 0.434 for *Z* = 4 (CSD-2306280). The crystal structure contains two positions for the Pr^{3+} cations (Pr1 at 4*c*: 0.24148(8), 0.24148(8), 0.0000(6) and Pr2 at 8*d*: 0.13722(9), 0.45738(9), 0.5286(7)), only one for I^- (I at 4*c*: 0.37891(12), 0.37891(12), 0.4725(5)) and As^{3+} (As at 8*d*: 0.03472(15), 0.21332(15), 0.4988(7)) as well as four O^{2-}-anion sites (O1 at 4*b*: 0, ½, 0.261(5); O2 at 8*d*: 0.2113(12), 0.4201(12), 0.966(4); O3 at 8*d*: 0.0961(13), 0.2768(13), 0.746(3); O4 at 8*d*: 0.0949(14), 0.2916(14), 0.275(3)). $(Pr1)^{3+}$ is surrounded sixfold by O^{2-} anions forming trigonal prisms, which are capped by an I^- anion each ($[(Pr1)O_6I]^{10-}$), whereas $(Pr2)^{3+}$ has also one I^-, but seven O^{2-} anions as coordination sphere resulting in bicapped trigonal prisms $[(Pr2)O_7I]^{12-}$ (Figure 1). These $[(Pr2)O_7I]^{12-}$ polyhedra are stacked alternatingly along [001] to form columns and edge-linked with $[(Pr1)O_6I]^{10-}$ polyhedra, which alternate with each other and form rings parallel to the (001) plane. The non-bonding electron pairs at the ψ^1-tetrahedral $[AsO_3]^{3-}$ anions point into cavities, which run along [001] (Figure 2), as do the chains of trans-edge shared $[OPr_4]^{10+}$ tetrahedra.

References:

(1) D.-H. Kang, *Doctoral Dissertation*, Univ. Stuttgart, **2009**.
(2) D.-H. Kang, T. Komm, Th. Schleid, *Z. Kristallogr.* **2005**, *S 22*,157–157.
(3) H. Ben Yahia, U. Ch. Rodewald, R. Pöttgen, *Z. Naturforsch.* **2009**, *64 b*, 896–900.
(4) F. Ledderboge, *Doctoral Dissertation*, Univ. Stuttgart, **2016**.

Fig. 1

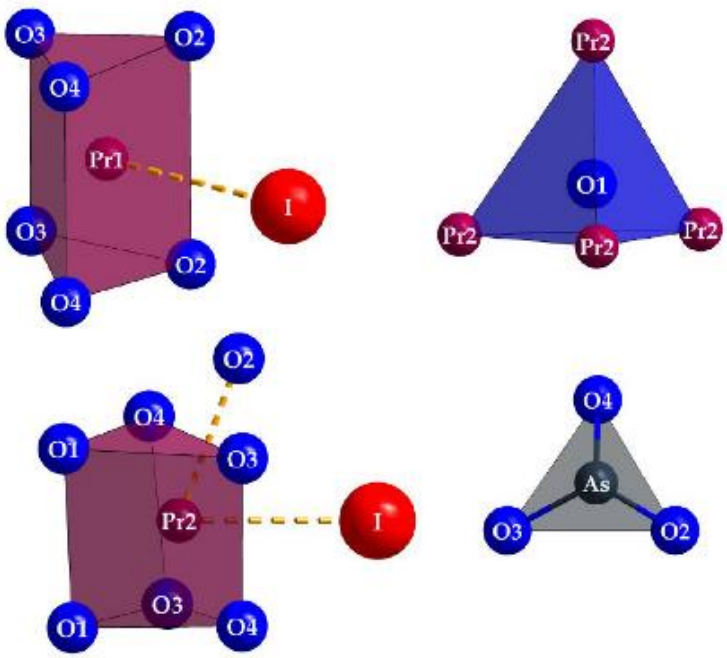

Figure 1. Capped and bicapped trigonal prisms $[(Pr1)O_6I]^{10-}$ and $[(Pr2)O_7I]^{12-}$ (*left*) as well as $[OPr_4]^{10+}$ tetrahedron and ψ^1-tetrahedral $[AsO_3]^{3-}$ anion (*right*) in the crystal structure of $Pr_3OI[AsO_3]_2$.

Fig. 2

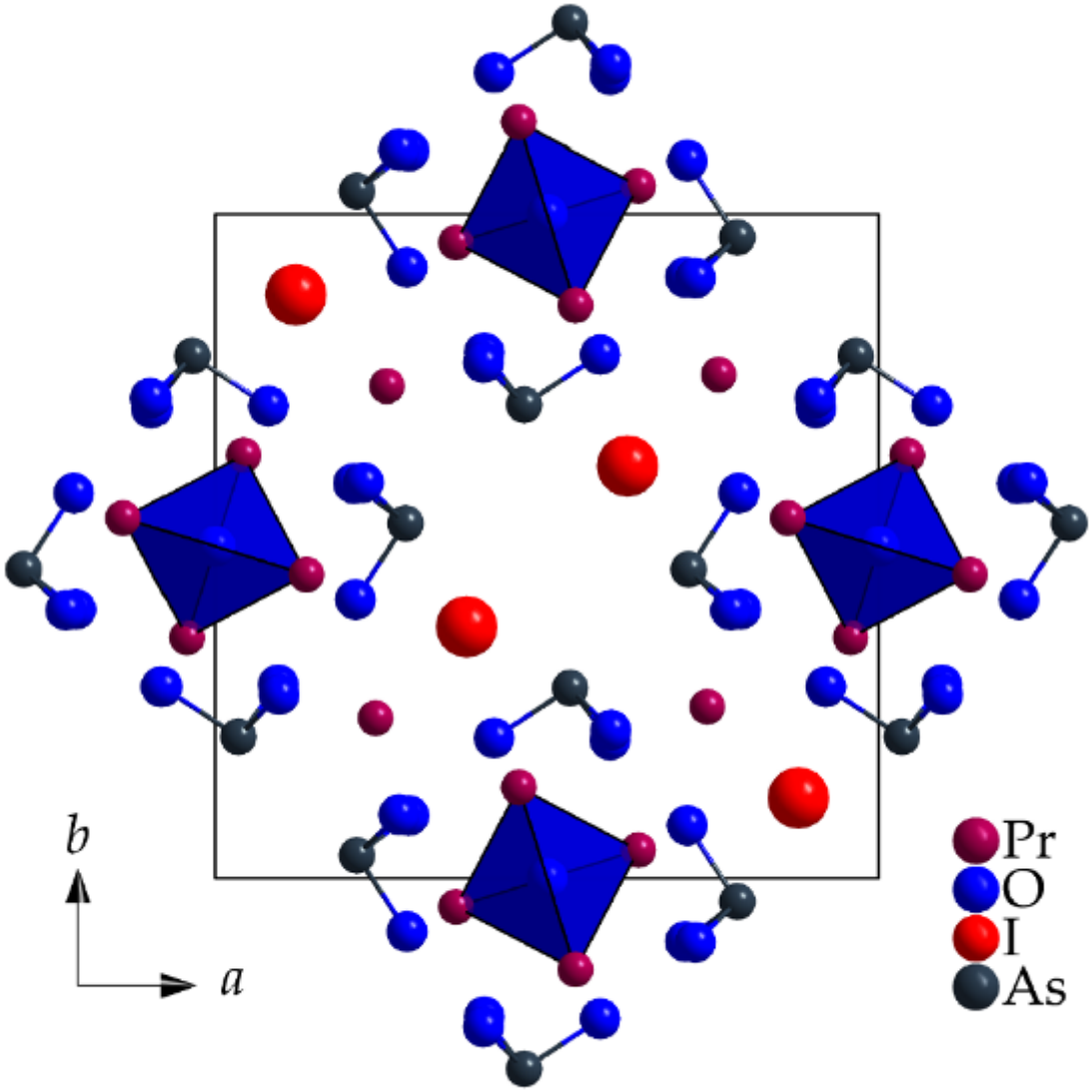

Figure 2. View at the tetragonal crystal structure of $Pr_3OI[AsO_3]_2$ along [001].

OPo-14

Bridging the gap between Electron and X-ray Diffraction

T. Stürzer (Karlsruhe/DE), C. Lenczyk (Karlsruhe/DE), J. Graf (Karlsruhe/DE)

Structure determination on ever smaller and more weakly diffracting crystals is one of the biggest challenges in crystallography. Traditionally, in-house X-ray crystallography covers sample sizes down to a lower limit of approximately 50 µm.[1] Consequently, electron diffraction is receiving a lot of attention, as it promises structure determination on significantly smaller samples. However, while micro-ED can cope with samples in the nm range up to approximately 1 µm, the refined structure models are less accurate compared to X-ray data.[2] Furthermore, the preparation of suitable sub-µm samples is often a challenge, whereas few micrometers sized crystals would be readily available. Therefore, equipment for X-ray structure determination closing the gap for samples between 50 to 1 micrometer in size would be highly desirable.

Exciting developments and latest innovations in X-ray source and detector technology enable the crystallographer to bridge this gap. Crystal sizes in the sub-10 µm range are now routinely accessible by modern instrumentation, while at the same time retaining the convenience and accuracy of single crystal X-ray structure determination. This will be highlighted by single crystal X-ray diffraction data collected on three micro crystals and compared to recently published MicroED Data on the same.[3]

References:

(1) Gruene et al., Angew. Chem. Int. Ed. Engl., **2018**, 57, 16313–16317.
(2) Simoncic et al., Acta Cryst. E, **2023**, E79, 410–422.
(3) Bruhn et al., Front. Mol. Biosci., **2021**, 8, 1– 16

OPo-15

Beyond Single Crystal Diffraction – Advanced Applications

M. Adam (Karlsruhe/DE), M. Evans (Karlsruhe/DE), T. Stürzer (Karlsruhe/DE)

Modern single crystal X-ray diffraction (SC-XRD) solutions allow for reliable structure determination from one small single crystal, routinely within minutes. These systems often feature easy switching between multiple wavelengths including hard radiation from Mo and Ag sources. Complementary to SC-XRD, powder X-ray diffraction (PXRD) is typically used on bulk materials. Advances in X-ray diffraction technology are pushing the limits of what information can be extracted from more complex samples. This development coincides with researchers working on more challenging samples. Compounds may not be amenable to conventional SC-XRD or may require an unreasonable amount of time for obtaining acceptable results. In these situations, PXRD may be an option, but often not enough sample is available, or the dedicated instrument configuration is not accessible. Although SC-XRD solutions often are considered only as dedicated systems for 3D structure analysis, the design features of these systems, including high-intensity sources, small X-ray beams and photon-counting 2D detectors can be advantageous for the investigation of PXRD samples. We will present results from various experiments with a focus on non-ambient temperature dependent micro-PXRD, pair distribution function (PDF) analysis, and high-pressure powder studies.

MS 16: Experimental methods III: Large scale facilities

OP-055

Thermal Diffuse Scattering (TDS) of small Crystals – TDS Experiments using high energy X-rays at Beamline P21.1

K. Köhler (Frankfurt a. M./DE), A. C. Dippel (Hamburg/DE), M. von Zimmermann (Hamburg/DE), A. Mirone (Grenoble/FR), B. Wehinger (Grenoble/FR), B. Winkler (Frankfurt a. M./DE)

The benefits of diffraction experiments with high-energy X-rays (enhanced access to reciprocal space, significant reduction of radiation-induced damage, the ability to study samples containing strongly absorbing elements) have long been recognized[1].

Beamline P21.1 at PETRAIII provides ideal conditions for diffraction experiments with high-energy X-rays. An X-ray beam with photon energies of 54, 88, or 102keV, a beam size of about 1mm², and a hybrid pixel detector (Dectris Pilatus3 X CdTe 2M) were already available.

In our BMBF-funded project, we further optimized the experimental setup at P21.1. We integrated a microscope into the setup to simplify sample alignment, added an open flow cryostreamer to facilitate container-less low-temperature measurements down to 30K, and installed CRL-based focusing optics to realize beam sizes down to 2x70µm. P21.1 now efficiently allows temperature-dependent scattering experiments (diffraction and diffuse) over a wide temperature range, using small crystals.

One set of case studies will focus on the measurement of thermal diffuse scattering to extract the complete elastic stiffness tensor (C_{ij}) from small crystals with low symmetry. A theoretical description of TDS was developed early[2], but only the availability of large detectors allows efficiently mapping the diffuse scattering[3-5]. We now aim to improve the data analysis of TDS measurements at P21.1 to provide a unique setup for TDS studies with high-energy photons.

We are grateful for funding within the BMBF Project (05K22RF1), financial support from the DFG and DESY for their excellent cooperation and support.

References:

(1) Ramsteiner, I. B., et al. J. Appl. Crys. 42.3, 392-400 (2009).
(2) Lonsdale K, Proc. Phys. Soc. 54, 314-353 (1942).
(3) Wehinger B, et al., Phys. Rev. Lett. 118, 035502 (2017).
(4) Mirone, A., Wehinger, B. http://ftp.esrf.fr/scisoft/AB2TDS/index.html (2013); http://ftp.esrf.eu/scisoft/TDS2EL/index.html (2017).
(5) Büscher, et al., J. Appl. Crystallogr. 54, 287-294 (2021).

Fig. 1

New setup in the EH1 of P21.1: Cryo streamer and microscope.

OP-056

Demonstration of non-linear crystallography using valence-specific x-ray-optical wavemixing

D. Krebs (Hamburg/DE), F. Kerker (Hamburg/DE), C. Bömer (Hamburg/DE)

Over the past decade, free-electron lasers (FELs) have been established as x-ray sources of unprecedented brilliance. They enable the study of nonlinear phenomena in the x-ray regime and allow us to transfer nonlinear optics from the visible towards x-ray photon energies.

Among the newly accessible phenomena, we focus in this presentation on x-ray-optical wavemixing (XOWM) processes, which combine diffractive imaging capabilities similar to regular x-ray diffraction with spectroscopic sensitivity.

Specifically, we present an FEL-based approach to x-ray-optical difference-frequency generation (DFG), where a pulsed optical laser drives the valence electrons of a diamond sample, allowing for x-ray diffraction off these excited charges. Combined with theoretical insights from non-relativistic QED [1], we can relate the scattering signal to non-linear structure factors of the underlying valence-response function.

Measuring DFG for several orientations of diamond, we demonstrate this non-linear scattering process for the first time and collect sufficient data to spatially reconstruct the non-linear response at sub-Angstrom resolution (see Figure).

Providing this proof-of-principle for non-linear crystallography, we emphasize that future applications to more complex samples (e.g., semiconductors, correlated materials) will increasingly benefit of the method"s valence-specificity, suggesting investigations into bond-structures, excitation dynamics or electronic correlation properties.

References:

(1) D. Krebs and N. Rohringer, Theory of parametric x-ray optical wavemixing processes, arXiv:2104.05838 (2021)

Figure: Spatial reconstruction of the nonlinear response function probed by x-ray-optical difference-frequency generation in diamond (optical photons at 1.55 eV).

Fig. 1

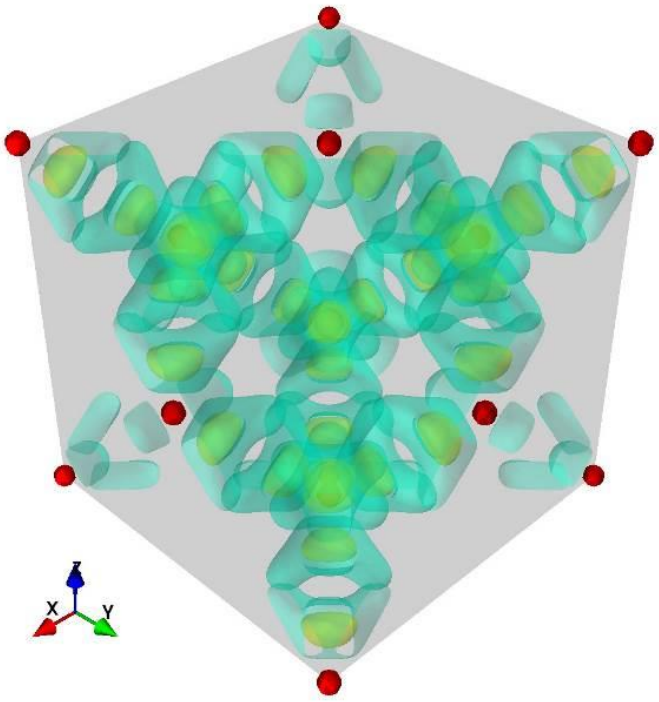

OP-057

Building a dedicated instrument around the Nordseekammer

L. C. Folkers (Darmstadt/DE), T. Weigel (Freiberg/DE), M. Zschornak (Dresden/DE)

Investigations of new materials undergoing structural transitions at the same time as exhibiting a physical phase change to, e.g., a piezoelectric phase require multiple probes to be connected to the sample in question. Thus, Nentwich et al. [1] built the Nordseekammer, which is a dedicated sample chamber allowing to apply electric fields and variable temperatures under ultra-high vacuum while simultaneously measuring X-ray diffraction. The Nordseekammer was built in collaboration with the P23 and P24 beam lines at PETRA III (DESY) and intended for the use at a synchrotron beam line.

However, experimental time at a synchrotron is scarce and requires minute planning. To allow for measurements at home or to investigate samples prior to a synchrotron measurement, the use of this chamber on an in-house diffractometer was required.

We were able to adapt the STOE STADIVARI diffractometer to offer enough space to incorporate the approximately 24x24x20 cm large chamber, while also tackling the necessity to drive the almost 7 kg heavy setup with connected cables and hoses to various angles with maximum precision and incorporating its control with the X-Area software.

This talk will showcase how the STOE STADIVARI was turned into the perfect diffractometer to host the Nordseekammer while continuing to produce the high precision data it is famous for.

References:

(2) M. Nentwich, et al., *J. Synchrotron Radiation*, **2021**, *28*, 158 - 168

OP-058

Insights into the structural dynamics of crystalline porous solids from in situ PXRD techniques

V. Bon (Dresden/DE), A. Khadiev (Hamburg/DE), D. Novikov (Hamburg/DE), J. Weiß (Dresden/DE), D. M. Többens (Berlin/DE), D. Wallacher (Berlin/DE), N. Grimm (Berlin/DE), S. Kaskel (Dresden/DE)

Switchable porous solids are a sub-class of MOFs with adaptable porosity, which undergo stimuli-induced phase transitions between open porous and contracted or even dense phases, typically triggered by guest molecules, temperature, pressure, or light irradiation.[1–3] Such adaptive materials are currently intensively discussed as promising materials for natural gas storage[4] and adsorptive separation.[5] The mechanistic understanding of structural dynamics of these materials requires the development of advanced characterization techniques, which allows to monitor the phase transitions upon adsorption and desorption of fluids.

Herein we present the prototype instrumentations for in situ PXRD in parallel to adsorption of gases and vapors in the broad range of gas pressure and temperature conditions at KMC-2 beamline of HZB and home-built setup, adapted to conventional laboratory powder X-ray diffractometer at TU Dresden. In addition, the instrumentation for time-resolved PXRD studies of adsorption-induced switching in crystalline nanoporous solids, designed at P23 beamline of PETRA III synchrotron will be shown. The representative case studies will be highlighted.

References:

(1) S. Krause, N. Hosono, S. Kitagawa, *Angew. Chem. Int. Ed.*, 2020, **59**, 15325–15341.
(2) Schneemann, V. Bon, I. Schwedler, I. Senkovska, S. Kaskel, R. A. Fischer, *Chem. Soc. Rev.*, 2014, **43**, 6062–6096.
(3) S. Horike, S. Shimomura, S. Kitagawa, *Nat. Chem.*, 2009, **1**, 695–704.
(4) J. A. Mason, J. Oktawiec, M. K. Taylor, M. R. Hudson, J. Rodriguez, J. E. Bachman, M. I. Gonzalez, A. Cervellino, A. Guagliardi, C. M. Brown, P. L. Llewellyn, N. Masciocchi, J. R. Long, *Nature*, 2015, **527**, 357–361.
(5) L. Bondorf, J. L. Fiorio, V. Bon, L. Zhang, M. Maliuta, S. Ehrling, I. Senkovska, J. D. Evans, J.-O. Joswig, S. Kaskel, T. Heine, M. Hirscher, *Sci. Adv.*, 2022, **8**, eabn7035.

MS 17: Structural biology III: Structure-based drug discovery & design

OP-059

Assembly of re-designed protein nanocages into large-scale crystalline structures for applications in optical nanomaterials and nanomedicine

T. Beck (Hamburg/DE), L. Lang (Hamburg/DE), M. Rütten (Hamburg/DE), H. Wagler (Hamburg/DE)

Self-organization of biomolecular building blocks can be harnessed for the construction of functional nanomaterials. We have recently established a novel method for the self-organization of biomolecular building blocks and nanoparticles. Here, protein cages, engineered with opposite surface charge, are used as an atomically precise ligand shell for the assembly of inorganic nanoparticles.[1] The assembly of these protein-nanoparticle composites yields highly ordered nanoparticle superlattices with unprecedented precision.[2] The biohybrid materials show interesting optical properties.[3-4]

We currently investigate the assembly requirements for two-component materials. To achieve this, we designed several variants of ferritin nanocages to determine the surface characteristics necessary for the formation of large-scale binary three-dimensional assemblies. These nanocage variants were employed in protein crystallization experiments and macromolecular crystallography analyses, complemented by computational methods. We identified several essential features for successful assembly.[5]

Moreover, we show the application of crystalline protein materials for the adsorption of uremic toxins, which accumulate in patients with chronic kidney disease. Protein design techniques enabled crafting of defined binding sites for the toxins inside the ferritin cavity.[6]

References:

(1) M. Künzle, T. Eckert, T. Beck, *J. Am. Chem. Soc.* **2016**, *138*, 12731-12734.
(2) M. Künzle, T. Eckert, T. Beck, *Inorg. Chem.* **2018**, *57*, 13431-13436.
(3) M. Lach, C. Strelow, A. Meyer, A. Mews, T. Beck, *ACS Appl. Mater. Interfaces* **2022**, *14*, 10656-10668.
(4) N. O. Junker, A. Lindenau, M. Rütten, M. Lach, A. Nedilko, D. N. Chigrin, G. von Plessen, T. Beck, *Adv. Funct. Mater.* **2023**, 10.1002/adfm.202303260.
(5) L. Lang, H. Böhler, H. Wagler, T. Beck, *in revision*.
(6) H. Böhler, S. Orth-Alampour, C. Baaten, M. Riedner, J. Jankowski, T. Beck, *J. Mater. Chem. B* **2023**, *11*, 55-60.

OP-060

Targeting the Pseudomonas aeruginosa virulence factor LasB - a structure-guided approach to high-affinity inhibitors

D. Kolling (Hannover/DE, Saarbrücken/DE), J. Haupenthal (Saarbrücken/DE), A. Hirsch (Saarbrücken/DE), J. Köhnke (Hannover/DE)

Antimicrobial resistance development is a major and urgent global threat to public health. The standard of care antibiotics used in the clinic are losing their effectiveness and the treatment of serious infections is becoming increasingly difficult. Of special importance are infections with multidrug-resistant bacteria such as carbapenem-resistant variants of the Gram-negative pathogen *Pseudomonas aeruginosa* responsible for hospital-acquired fatal lung infections and cystic fibrosis. *P. aeruginosa* uses the virulence factor LasB, a zinc dependent metalloenzyme, to break down connective tissue through cleavage of elastin and collagen to allow the progression of the infection. Targeting bacterial virulence factors is a new approach to disarm pathogens without creating selection pressure, which avoids or delays the development of mutations leading to antimicrobial resistance.

Over the past six years, we have been pursuing a medicinal chemistry program to develop potent LasB inhibitors. Here, we share the journey from small fragments, via fragment growing and merging, to potent molecules. Over 50 complex structures of LasB with different inhibitor classes have aided drug design: After initial screens yielded molecules inhibiting LasB in the mid-µM range, we now have highly efficacious inhibitors with a 50,000-fold improvement in affinity.

OP-061

The reversible inhibitor SR-4835 binds Cdk12/Cyclin K in a non-canonical G-loop conformation

M. Schmitz (Bonn/DE), I. H. Kaltheuner (Bonn/DE), K. Anand (Bonn/DE), R. Düster (Bonn/DE), J. Moecking (Bonn/DE), A. Monastyrskyi (Tampa. FL/US), D. R. Duckett (Tampa. FL/US), W. R. Roush (Jupiter, CA/US), M. Geyer (Bonn/DE)

Transcription-associated Cyclin-dependent kinases (CDKs) are serine/threonine-directed protein kinases that, upon activation regulate key transcriptional events in higher eukaryotes. Inhibition of CDKs has evolved as an emerging anti-cancer strategy.

Here we present the molecular mechanism of SR-4835, a small molecule inhibitor currently in phase I clinical trials. We determined the crystal structure of SR-4835 bound to the Cdk12/Cyclin K complex at 2.68 Å resolution. The compounds benzimidazole moiety is embedded in a unique hydrogen bond network mediated by the kinase hinge region with flanking hydroxy groups of the Y815 and D819 side chains. Whereas the SR-4835 head group targets the adenine-binding pocket, the kinase"s glycine-rich loop is shifted down towards the activation loop. Additionally, the αC-helix adopts and inward conformation, and the phosphorylated T-loop threonine interacts with all three canonical arginines, a hallmark of CDK activation. Dose-response inhibition measurements with recombinant CMGC kinases show that SR-4835 is highly specific for Cdk12 and Cdk13. Comparing the efficacy of SR-4835 with other CDK-targeting inhibitors highlights its potential as a promising candidate for targeted anti-cancer therapy. Structural insights provide the basis for the selective binding of SR-4835 to Cdk12 and Cdk13, and offer a foundation for optimization and design of reversible Cdk12-specific inhibitors and could facilitate the basis for the development of novel cancer therapeutics. Finally, we identify SR-4835"s molecular glue ability and show SR-4835-induced ternary complex formation between the E3-ligase adaptor protein DDB1 and the Cdk12/CycK heterodimer by biochemical and structural analyses in comparison to known CycK degraders CR8 and dCeMM2.

Fig. 1

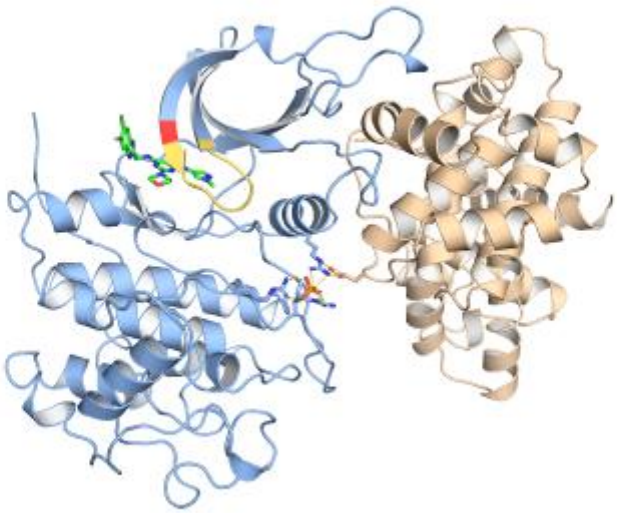

Fig. 2

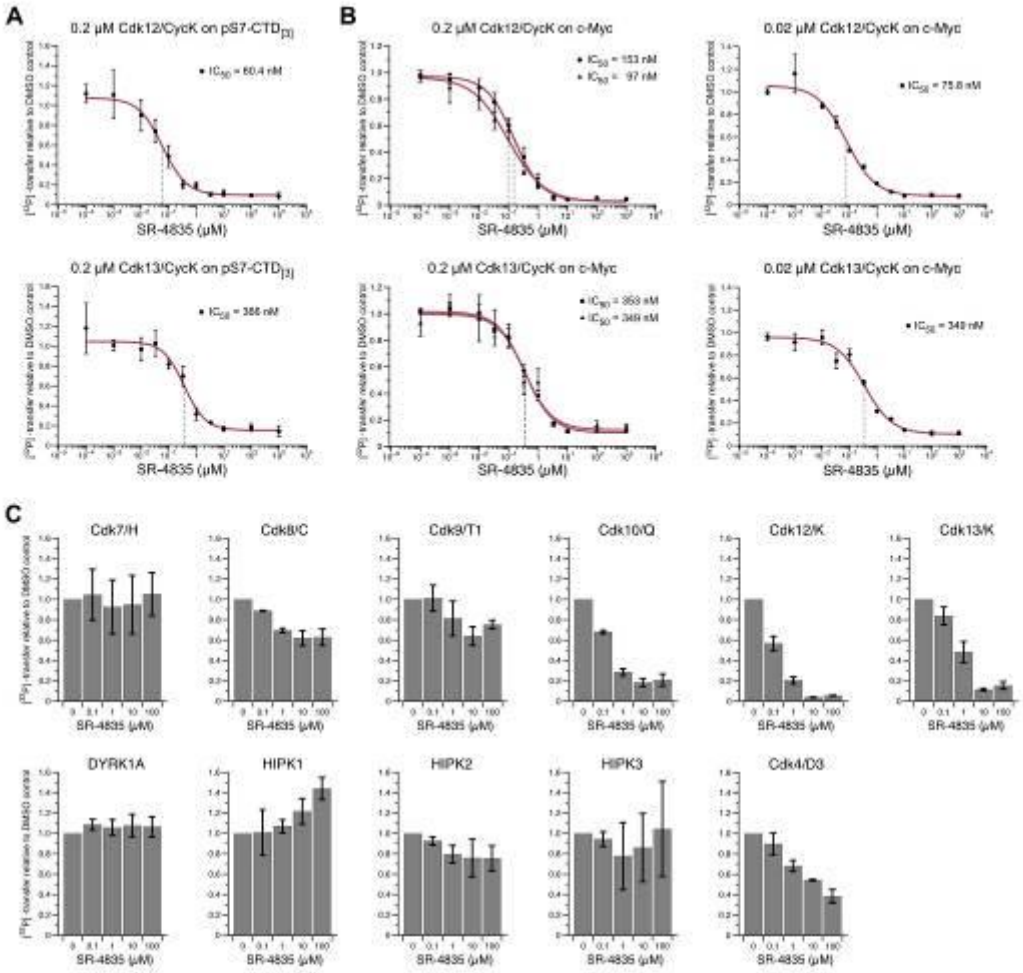
A
0.2 μM Cdk12/CycK on pS7-CTD[3]
0.2 μM Cdk13/CycK on pS7-CTD[3]
B
0.2 μM Cdk12/CycK on c-Myc
0.02 μM Cdk12/CycK on c-Myc
0.2 μM Cdk13/CycK on c-Myc
0.02 μM Cdk13/CycK on c-Myc
SR-4835 (μM)
C
Cdk7/H
Cdk8/C
Cdk9/T1
Cdk10/Q
Cdk12/K
Cdk13/K
DYRK1A
HIPK1
HIPK2
HIPK3
Cdk4/D3

OP-062

Crystal Structure of the Cyclic Peptide Antibiotic Tripropeptin C from *Lysobacter sp.*

P. Hendricks (Bonn/DE), M. Arts (Bonn/DE), T. Schneider (Bonn/DE), G. Hagelueken (Bonn/DE)

Disruption of the cell wall biosynthesis in bacteria is a common mode of action for antibiotics. In this regard, the cell wall precursor lipid II is of great interest, due to its limited biosynthesis resulting in minimal concentration per cell. Tripropeptin C (TPPC), a natural cyclic peptide found in Lysobacter sp., comprises eight amino acids, including five unusual ones like D-prolin or hydroxylated variants. It potentially targets undecaprenyl pyrophosphate (C_{55}-PP), a subunit of lipid II. This leads to accumulation and subsequent inhibition of the lipid cycle by interfering with transport processes. The key to understanding and consequently exploiting the potential antibiotic properties lies in the structure of the macromolecules and the interaction with their target.

We successfully crystallized TPPC in complex with C_{10}-PP and collected a 1.1 Å diffraction data set. Due to the small size of the molecule and the presence of the unusual amino acids, building a model for molecular replacement was not trivial, even with modern AI approaches. However, since the resolution of the diffraction data was sufficiently high and heavy atoms such as phosphorus and calcium were present in the crystal lattice, we could successfully employ single atom molecular replacement, as implemented in Phaser, to determine the structure of the TPPC/C_{10}-PP complex.

Consistent with the known calcium dependence, the cyclic depsipeptide and the phosphate group of the C_{10}-PP moiety coordinate a Ca^{2+} ion in our structure. The crystal packaging exhibits an intriguing feature, where TPP and C_{10}-PP complexes form pseudo-bilayers. In addition, six complexes form ring-like structures along a sixfold crystallographic axis. This structural elucidation is an important step in unraveling the mode of action of TPPC.

MS 18: Materials science crystallography III: In situ/operando characterization - a key to structure-property relationships

OP-063

Interplay of material mechanisms of complex materials and devices for energy conversion

M. Hinterstein (Freiburg i. Br./DE), G. Vajpayee (Freiburg i. Br./DE), L. Lemos da Silva (Freiburg i. Br./DE)

In order to meet the challenges of the future in transforming our society toward sustainable energy sources, technological advances in the area of energy conversion are necessary in addition to the expansion of renewable energies. When converting energy using electrolysis, fuel cells, solar cells or heating elements, efficiency and system reliability play a decisive role in the overall economic assessment. The lower the losses during energy conversion, the less renewable energy needs to be installed and the less space needs to be made available to cover the final energy consumption. The efficiency and reliability of energy conversion systems depend largely on the properties of the functional materials and their internal structure. Examples include ionic conductors in electrolysis and fuel cells, perovskite materials for future solar cells, piezoceramics for energy harvesting and ceramic heating elements with good heat conduction properties. The internal structure ranges from the crystal structure over domain structures inside grain and the microstructure of the grains up to meso-structures such as particle networks and additively manufactured devices. With sophisticated processing methods all length scales of the internal structure can be controlled and tailored for highest properties. With *in situ* structural characterization the crystal structure can be correlated with the macroscopic properties and even fundamental material parameters. This way future functional materials and devices for energy conversion with highest efficiency can be designed. In this contribution we will demonstrate how quantitative analysis of *in situ* experiments of complex materials and devices for energy conversion elucidates the interplay of material mechanisms on different length scales.

OP-064

Structural change in Mo/Rh-doped PtNi nanoparticles during heat treatment in hydrogen atmosphere

O. Prymak (Essen/DE), P. Paciok (Jülich/DE), S. Polani (Berlin/DE), T. Möller (Berlin/DE), J. Kang (Berlin/DE), M. Epple (Essen/DE), M. Klingenhof (Berlin/DE), K. E. MacArthur (Jülich/DE), M. Heggen (Jülich/DE), P. Strasser (Berlin/DE), R. E. Dunin-Borkowski (Jülich/DE)

Platinum-based materials are promising catalysts for the oxygen reduction reaction (ORR) at proton-exchange membrane fuel cells (PEMFCs), and their activity can be increased by the shapes and faceted surfaces as well as by the incorporation of transition metals into the Pt-matrix.

This work focuses on the synthesis and characterization of binary PtNi and Mo/Rh surface-doped PtNi octahedral nanoparticles (NPs). The NPs were heat-treated by in-situ XRD and STEM and further investigated in terms of their stability and activity as revealed from their structural change and electrochemical performance.

PtNi-based NPs were characterized by X-ray powder diffraction (XRD), high-resolution transmission electron microscopy (HRTEM), energy-dispersive X-ray spectroscopy (EDX) and X-ray photoelectron spectroscopy (XPS). The electrochemical surface area (ECSA) during accelerated stress test (AST) in Ar-purged HClO4 was also determined.

HRTEM showed octahedral NPs with a diameter of about 7-9 nm, which all consisted of a hexapodal Pt-rich core and a partially oxidized octahedral Ni-rich shell with (111) facets and a thickness of about 0.5 nm as EDX and XPS confirmed. According to the Rietveld refinement, PtNi-NPs consisted of 85 wt% Ni-rich and 15 wt% Pt-rich phases with a crystallite size of about 2-3 nm, whearas PtNi(Mo/Rh)-NPs had a 96/4 wt% phase composition and crystallite size of about 4-6 nm. Heat treatment at T=350 °C in H2-atmosphere led to recrystallized spherical PtNi-NPs with a Ni-rich phase and a decrease of ECSA by 43%. At the same time, octahedral PtNi(Mo/Rh)-NPs remained structurally almost unchanged, but the ECSA increased by about 30%. In both cases a formation of a Pt-rich shell during heating was observed.

The study showed that the incorporation of 1.4 at% Mo and 0.4 at% Rh into PtNi-NPs significantly increased their electrochemical and thermal stability with a maintained octahedral morphology as an additional important factor for catalytic activity.

OP-065

Monitoring the structure evolution of boron-modulated transition metal oxides for oxygen evolution reaction

H. Cheraparambil (Muhlheim an der Ruhr/DE), Y. Wang (Muhlheim an der Ruhr/DE), M. Gil Sepulcre (Muhlheim an der Ruhr/DE), O. Rüdiger (Muhlheim an der Ruhr/DE), S. DeBeer (Muhlheim an der Ruhr/DE), H. Tüysüz (Muhlheim an der Ruhr/DE), C. Weidenthaler (Muhlheim an der Ruhr/DE)

Oxygen evolution reaction (OER) is considered as the bottleneck of water splitting because of the complex four-electron transfer process.[1] Therefore, intensive research is being conducted to develop efficient and low-cost catalysts, among which transition metal (TM)-based compounds containing some nonmetals such as N, P, S and metalloids (B, Ge As), have recently attracted special interest.[2] It has been shown that the incorporation of more electronegative elements like boron into transition metal oxides facilitates the charge transfer and boosts the OER performance.[3] Our previous work shows that among a series of CoxNi-B oxides synthesized via a simple precipitation method and a post-calcination step, Co_8Ni-B oxides show superior OER activity.[4] In our present work, we have monitored the structure evolution of Co_8Ni-B oxides via in situ X-ray total scattering experiments and subsequent PDF analysis as well as X-ray absorption spectroscopy. The morphology, crystallinity, and surfaces of the samples obtained at different temperatures were studied by electron microscopy and X-ray photoelectron spectroscopy. We show that simple precipitation results in partly amorphous sheet-like structures that are a mixture of Co_3BO_5 and $Ni(OH)_2$. At 550°C, the system transforms to a crystalline mixture of $NiCo_2O_4$ and B_2O_3. Further heating to 800 °C results in the formation of ordered core-shell structures with a composition of $Co_{3-x}Ni_xB_2O_6$ and $NiCo_2O_4$. The structure transformation is summarized in the figure attached. The structural information obtained at different temperatures is further correlated to the OER activity.

References:

(1) Yu, M., *et al. Angew Chem Int Ed Engl*, **61**, e202103824 (2022). 2. Masa, J., *et al*. *Adv. Energy Mater.* **6**, 1502313 (2016). 3. Yu, M., *et al*. *Angew Chem Int Ed*, **61**, e202211543 (2022). 4.Wang et al. submitted

Fig. 1

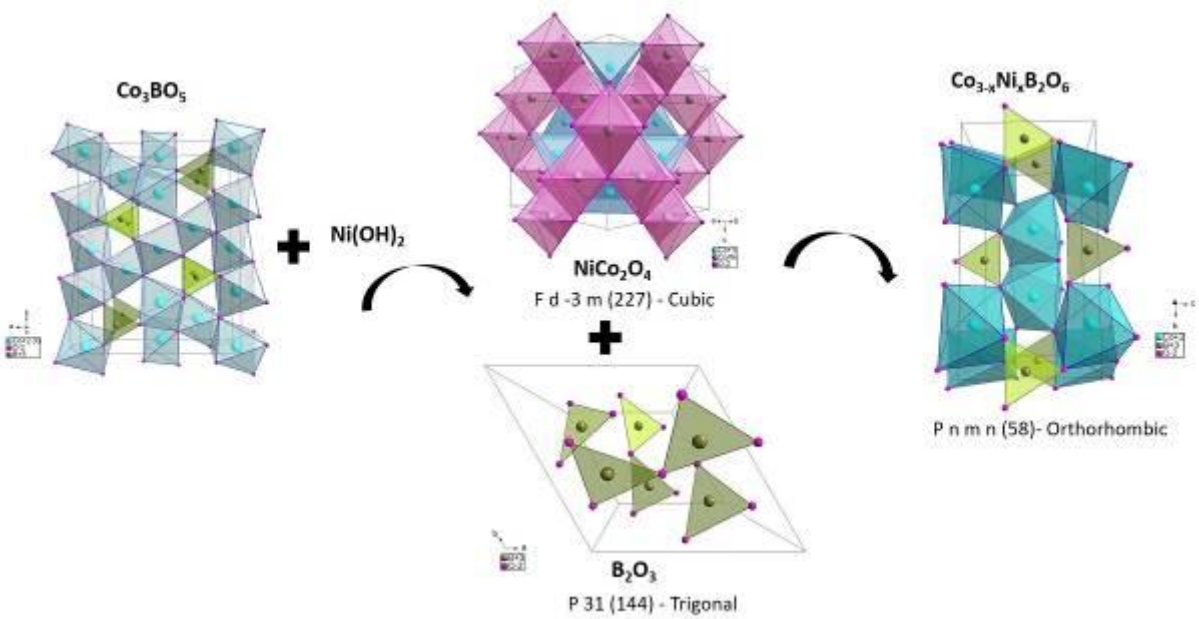

OP-066

Stratlingite: synthesis, structure, and properties of a component of roman cement

A. Shevchenko (Stuttgart/DE), S. Bette (Stuttgart/DE), M. W. Terban (Stuttgart/DE), R. E. Dinnebier (Stuttgart/DE)

One of the mineral phases that is found in ancient Roman cement and is believed to be responsible for its durability and self-healing properties is Stratlingite. According to the published data from the naturally occurring mineral, its chemical formula is $Ca_2Al_2SiO_2(OH)_{10}{\cdot}2.25H_2O$. Stratlingite has a trigonal layered structure composed of brucite-type $[AlCa_2(OH)_6]^+$ and negatively charged double tetrahedra $[AlSiO2(OH)4]^-$ layers stacked along *c*-axis. The published average structure is highly idealized and does not represent the reality giving partial occupancies and disorder in the double-tetrahedra layer (fig. 1). Therefore, a more thorough approach accessing the local structure is required.

In this work we focus on the synthetic aspects of Stratlingite and its structure using different complementary methods like XRPD, PDF-analysis, TG, EDX spectroscopy, solid-state NMR while X-ray diffraction solely is not sensitive enough to describe all features of the real material.

Wet-chemical synthesis of Stratlingite was carried out in ambient or CO_2-free environments with CaO, $NaAlO_2$ and $Na_2SiO_3{\cdot}5H_2O$ as precursors. *In-situ* variable humidity XRPD analyses revealed that Stratlingite reversibly absorbs water resulting in a change of lattice volume. This property seems very important for understanding the mechanism of self-healing properties of Stratlingite-containing cements that are exposed to constantly changing relative humidity. Another previously unknown aspect is the flexibility of cationic composition of Stratlingite. To investigate this further, we used alternative methods that could give additional information about the local structure (e.g. PDF analysis, solid-state NMR) and cation composition (e.g. EDX spectroscopy, TG).

In conclusion, we will describe the water "breathing" behavior of Stratlingite and propose a more realistic structural model that is suitable for modelling more defective materials (faulted, amorphous) as usually encountered in real-life conditions.

Fig. 1

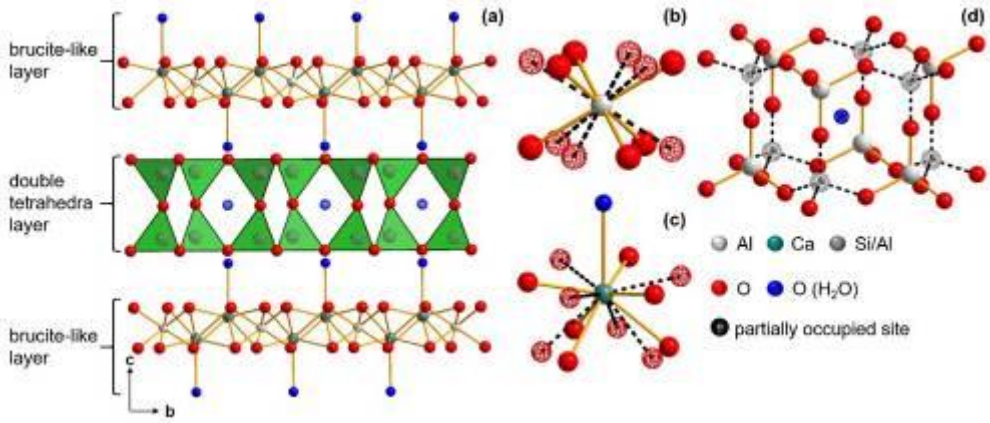

MS 19: Mineralogical crystallography I: Order and disorder in minerals

OP-067

Disorder in minerals: new insights from single-crystal X-ray diffuse scattering

G. O. Lepore (Florence/IT), M. Morana (Florence/IT), A. Minelli (Oak Ridge, TN/US), E. M. Schmidt (Bremen/DE), S. Margheri (Florence/IT)

Crystal structures of minerals are determined routinely to characterize a species and its crystal-chemistry, thus inferring information such as genetic environment and structure-properties correlation. The characterization of the average structure tends to overlook any deviations from this description, whereas key information related to the structural disorder hides in the diffuse scattering (DS) pattern. DS studies have recently gained new attention, thanks to technological and methodological development.

Minerals, due to their structural complexity, have seldom been the subject of DS studies. In this work we selected several mineral groups with known complex structures and different possible origins of DS, such as pyrochlore, hollandite, cupropearceite and members of the layered lead oxychloride (LLO) group. Pyrochlores and hollandites are known for hosting disorder, mainly related to the position of tunnel cations, pearceite-polybasite minerals show composite modulated structures and DS due to the presence of mobile ions, whereas LLO minerals comprise a variety of structures with disorder in the stacking sequence and/or within the layers. To address these questions, we performed X-ray data collection (λ=0.6968 Å) at ID28, ESRF, using the continuous rotation method and a Pilatus 1M detector. Preliminary analyses reveal that DS can provide plenty of information in such complex cases. For example, synthetic Na-bearing elsmoreite present features mainly related to in-phase vibration of neighbouring pairs and some other likely occupational correlations. In the case of LLO, the diffuse features highlight substantial differences on the origin of disorder, so while janchevite is mainly affected by stacking faults, DS in thorikosite and schwartzembergite hints at a partial ordering perpendicular to the stacking direction.

Further data analysis including 3D-ΔPDF maps and modelling of the DS is in progress to better understand and quantify the origin of disorder.

OP-068

Natural As_2S_3 glass from burning mine dumps – powder XRD, Pair Distribution Function and SEM-EDS analyses

T. Witzke (Almelo/NL), G. Nénert (Almelo/NL), M. Gateshki (Almelo/NL)

Introduction

At the mine dumps of the Lichtenberg open cast, Ronneburg, Thuringia, Germany (mined for U-bearing alum shale) and of the Kateřina coal mine, Radvanice, Czech Republic, orange-red to red glassy crusts and droplets were found. Both dumps caught fire by spontaneus self-ignition several decades ago. The mineral was solidified from a melt, which was probably a sublimation product from a gas phase.

Materials & Methods

Four samples were selected for powder XRD and SEM-EDS analyses. To be able to characterize structurally this amorphous mineral, Pair Distribution Function (PDF) analysis has been carried out using a sample from Radvanice.

Results

The chemical composition of the samples from both localities ranges from $As_{1.97}S_{3.03}$ to $As_{2.05}S_{2.95}$, very close to stoichiometric As_2S_3. X-ray diffraction showed that the material is amorphous. No peaks, just flat, broad humps around d = 5 Å, 2.8 Å and 1.68 Å were observed in the diffraction patterns.

Similarly, to previous Raman studies on the synthetic materials (Georgiev et al., 2003), the PDF data show that this mineral is intrinsically phase separated into small As-rich (realgar molecules As_4S_4) and S-rich clusters. Distances in the PDF analysis (Fig. 1) correspond to As-S (2.2 - 2.25 Å), As-As and S-S (3.3 - 3.5 Å) in the the As_4S_4 molecules. The influence of the S-rich clusters on the PDF is small and their structure remains unknown.

Conclusion

The result suggests that an amorphous mineral with a narrow compositional range close to As_2S_3 was formed on two burning mine dumps. A main constituent are As_4S_4 molecules. The mineral is closely related to the synthetic As_2S_3 glass and can be regarded as an amorphous polymorph of orpiment (monoclinic As_2S_3).

References:

(1) Georgiev D G, Boolchand P, Jackson K A (2003): Intrinsic nanoscale phase separation of bulk As_2S_3. – Phil. Mag. 83, 2941

Fig. 1: PDF fit of the experimental data using As_4S_4 molecules.

Fig. 1

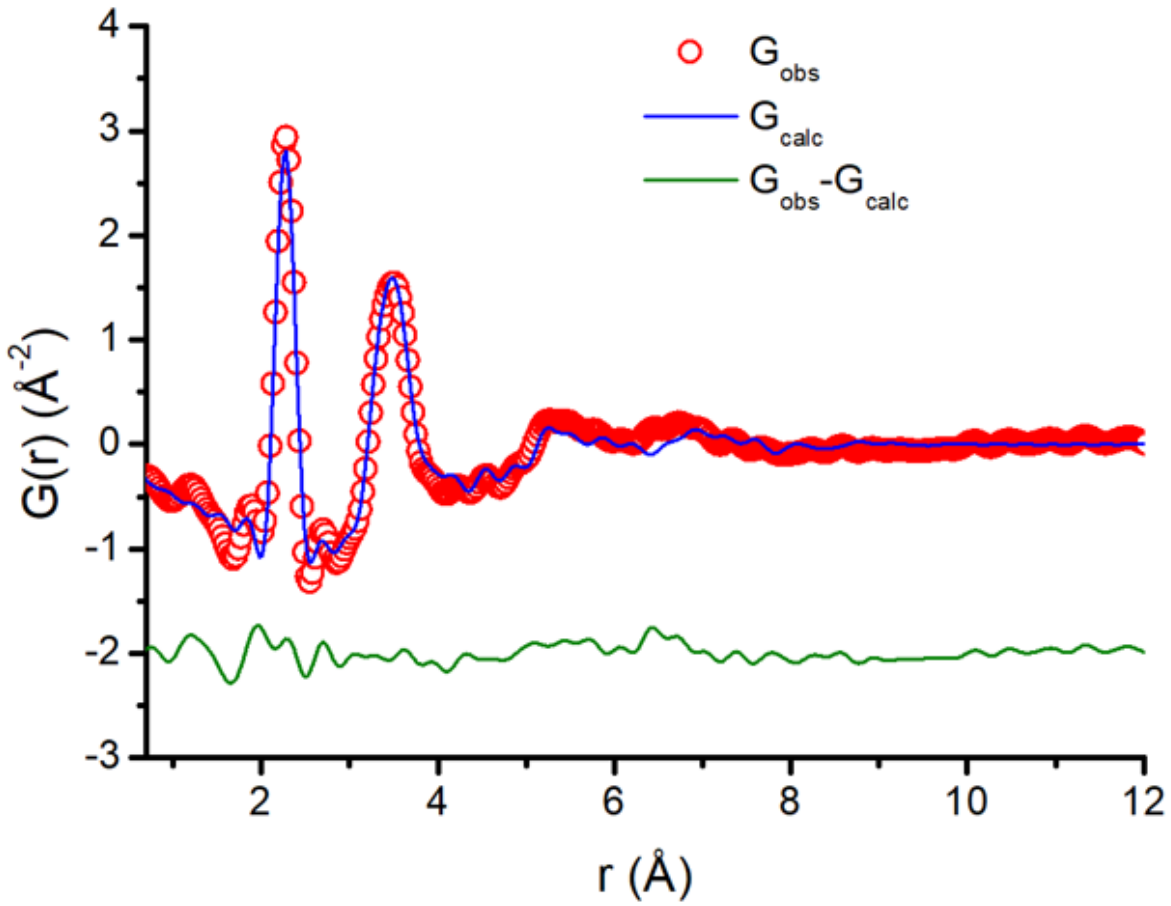

OP-069

Multi-method study of calcium-aluminate cement hydration and its crystal structures.

L. Gemmrich Hernández (Mainz/DE), U. Kolb (Mainz/DE)

Calcium aluminate cement (CAC) presents several advantages in comparison to other types of cement: CO2 incorporation, fast-setting, high-temperature and chemical resistance. However, CAC"s initial setting strength is higher than its strength once dry due to formation and conversion of metastable hydrates into their stable counterparts. Since the structures of the metastable products are not yet well known, the difficulty in predicting the amount of phase formed makes predicting its strength development challenging. Structure solution of the metastable phases would allow quantification and therefore, development of accurate strength prediction of CAC. This study focuses on C2AH8, one of the main hydrates that appear during CAC"s early hydration. C2AH8 forms as small intergrowing, usually twinned and preferentially oriented hexagonal platelets (often disorderly stacked), which is why methods such as single crystal and powder XRD have not been entirely successful in the elucidation of these types of structure. For this reason, 3D electron diffraction has been chosen as the main method of structural investigation (with support of In-situ XRD, EDX, SEM), which has already allowed us to access a large number of different CAC structures. Sample preparation methods have been tested to optimize synthesis and crystal selection and to avoid CO2 contamination, preferential orientation, dehydration, and beam damage. Significantly better data can be achieved when using cryo conditions. With the use of cryo-protection, the information about the ordered water content in the structure remains, leading to superstructure reflections that reflect a 4 fold modulation in a* and b* direction. Due to preferential orientation, space group and correct cell determination are hindered. To overcome this issue, methods such as FIB and Microtomy have been used to access this information, leading to promising advances in the structural elucidation of metastable CAC hydrates.

OP-070

Cation ordering and long-range disorder among cationic columns in fluoralforsite – a new apatite-group mineral

K. Skrzyńska (Sosnowiec/PL), G. Cametti (Bern/CH), A. Krzątała (Sosnowiec/PL), I. Galuskina (Sosnowiec/PL), E. Galuskin (Sosnowiec/PL)

Introduction The apatite-type minerals, described by the general formula $M1_2M2_3(TO_4)_3X$ (where *M* and T are cationic sites, X is the anionic one), may incorporate distinct ions into the structure. Various possible chemical compositions and symmetry changes pose difficulties in the classification and nomenclature.

Objectives The study aims to describe a new mineral species belonging to the apatite group. The new mineral, fluoralforsite with idealized formula $Ba_5(PO_4)_3F$, has been approved by the International Mineralogical Association.

Materials & methods Fluoralforsite was found in high-temperature rocks from the Hatrurim Complex in Israel. The new mineral was associated with other unique Ba-minerals, such as barrioferrite and zadovite. Single-crystal X-ray diffraction data were collected using a four-circle Rigaku Synergy R diffractometer.

Results Diffraction data indicated the following unit cell parameters: $a = b = 10.0031(2)$Å, $c = 7.5382(2)$ Å, V = 653.23(3) Å^3. The structure was solved in the $P6_3/m$ space group. Additionally, test refinements were performed to check symmetry lowering. However, the refinement in $P6_3/m$ was superior, and *R*-value converged to 1.92%. Ba predominantly occupies *M1* and *M2* positions. Albeit, the chemical composition and the mean electron number of the *M*1 site pointed to substitution of Ba by Ca atoms. There are two variants of *M*1 site coordination due to the displacement of the oxygen position (O2) off the mirror plane. Consequently, the *M*1 – O2 distance can be 2.79 Å corresponding to the site occupied by Ba or 2.40 Å, reflecting the substitution of Ca at the *M*1 site (Fig. 1).

Conclusion The ordered arrangement of Ba/Ca at the *M*1 site occurs within individual columns. Nevertheless, the disordered distribution of adjacent columns enables the maintenance of $P6_3/m$ symmetry.

Acknowledgment The research was supported by NCN of Poland, grant no. 2019/35/O/ST10/01015

Fig. 1 (a) coordination of *M*1 site; (b) ordered *M*1 column in fluoralforsite

Fig. 1

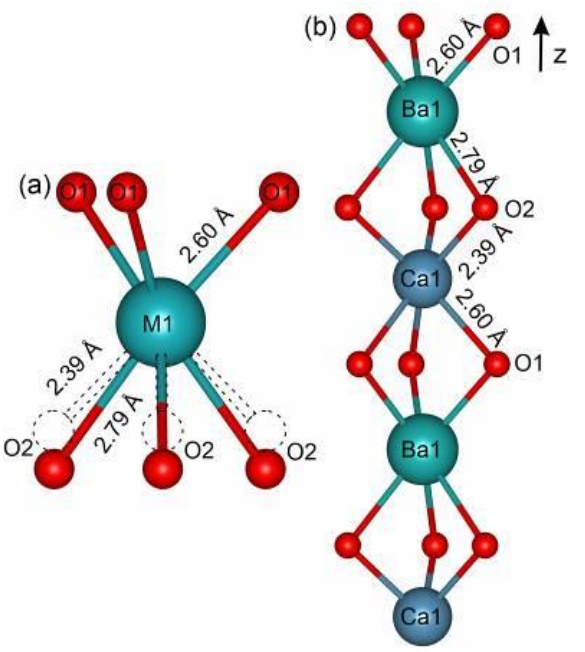

MS 20: Chemical crystallography III: Powder diffraction in chemistry

OP-071

***In-situ* studies on microstructural changes of stacking faulted functional materials by external stimuli using X-ray powder diffraction**

S. Bette (Stuttgart/DE), M. Plass (Stuttgart/DE), S. Emmerling (Stuttgart/DE), M. Däntl (Stuttgart/DE), R. E. Dinnebier (Stuttgart/DE), B. V. Lotsch (Stuttgart/DE)

Crystalline matter responses on external stimuli like temperature, humidity or pressure in various ways ranging from simple expansion/contraction to phase transitions. This response materializes in gradual or rapid changes in the physical properties. In real crystalline materials, in particular in layered materials defects like antisite defects, occupational disorder or stacking fault disorder are omnipresent which creates a microstructure that can also have a significant impact on the material's physical properties. Accordingly the questions on how the microstructure responds on external stimuli and on how microstructural investigation can be carried out *in situ* are of great interest.

In this work, we will present in situ studies on microstructural changes of inorganic materials: ion conducting Li_3HoI_6 (Figure 1, a-c); organic materials: porous, covalent organic framework compounds (COFs) and on spin coated, polycrystalline, $H_3Sb_3P_3O_{14}$ thin films (Figure 1, d-f). We demonstrate how heating can lead to both fault healing and to increased disorder and for $H_3Sb_3P_3O_{14}$ thin films how a mechanism for competing ethanol and amine intercalation can be derived from *in situ* data (Figure 1, g-i).

Figure 1. Li_3HoI_6: (a) honeycomb motifs of layers, occupational disorder cations is indicated by a magenta arrow, (b) temperature dependent *in situ* XRPD patterns (c) analysis of the evolution of cation and stacking fault disorder in Li_3HoI_6 during heating, TAB-COF: (d) layers, random shifting is indicated by green arrows, (e) temperature dependent *in situ* XRPD patterns during heating, (f) quantification of the layer buckling indicated by d(010) and the random layer offset during isothermal heating, $H_3Sb_3P_3O_{14}$ thin films: (g) *in situ* XRPD patterns recording during the ethanol and amine loading, (h) suggested mechanism for competing ethanol and amine intercalation, (i) quantitative analyses of the *in situ* XRPD shown in (g).

Fig. 1

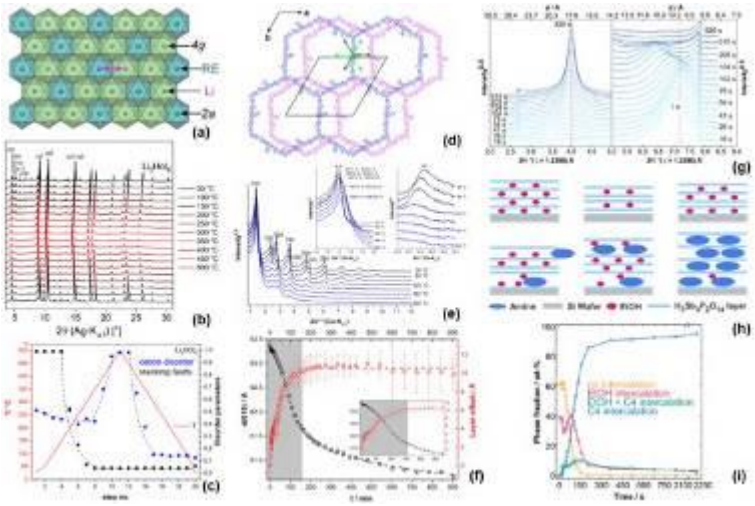

OP-072

CO_2-sorption/desorption studies in zeolites: Formation of new cage filling species in a hydrosodalite framework with unit cell formula $Na_6[Si_6Al_6O_{24}]((H_3O)^+(HCO_3^-)*2H_2O)_2$

B. Hagel (Hannover/DE), C. H. Rüscher (Hannover/DE), N. M. Denda (Hannover/DE), A. M. Schneider (Hannover/DE)

Comparing hydro-sodalites and zeolites Z13X and Z4A could be interesting concerning their de/rehydration and CO_2-sorption/desorption behavior due to their specific structural relationship, i.e. closed packed sodalite cages versus sodalite cages connected via double six-ring windows (Z13X) or double four-ring windows (Z4A). Effects are studied using commercially available Z13X and Z4A and hydrothermally synthesized hydrosodalites. Samples were characterized by XRPD, SEM/EDX and FTIR absorption. De-/rehydration and CO_2-sorption-desorption was followed in-situ by TG/DTA measurements. Heating under N_2 gas (20ml/min 1 bar) showed in all cases typical dehydration curves indicating a complete loss of molecular water at about 400°C and no mass change during cooling. Rehydration occurs at room temperature at atmospheric conditions in a certain time depending on the surrounding humidity. CO_2-sorption/desorption of the dehydrated samples could be observed in successive heating/cooling runs using varying CO_2/N_2 gas-mixtures (1, 5, 10, 20...100% CO_2, 20ml/min, 1bar). In all cases hysteresis type behavior in mass loss/gain during successive cooling/heating runs were observed between 50 and 250°C. Dehydrated hydro sodalites gain up to 6 wt% when exposed to CO_2/N_2 gas-mixtures at > 10wt% CO2 during cooling. Z13X and Z4A gain up to about 15 wt% and 10 wt%, respectively. IR absorption spectra show that the CO_2 sorbed in Z13X and Z4A become completely replaced by H_2O when exposed to to atmospheric conditions at room temperature. In contrast, CO_2 entrapped in the hydro sodalite samples attracts H2O molecules suggesting the formation of $((H_3O)^+(HCO_3^-)*2\ H_2O)$ type species in the cages based on IR absorption peaks (Fig. 1). This could be confirmed by forcefield simulation studies (Fig. 2).

Fig. 1 Typical IR absorption spectra: A, B, C D denote peaks of the newly formed cage species.

Fig. 2 By forcefield method: SOD framework = yellow. Cage filling species: Na_{green}, H_{white}, C_{grey}, O_{red}.

Fig. 1

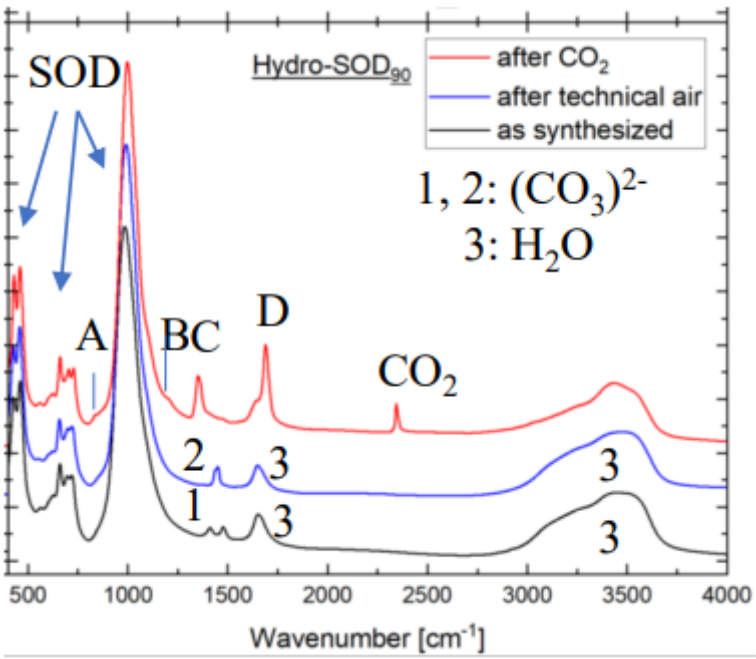

Fig. 2

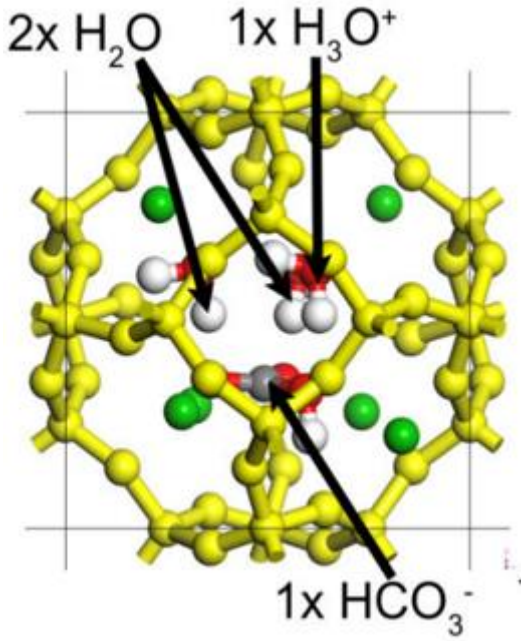

OP-073

Versatility of High-entropy Oxides: Tailoring Structure, Chemical Composition and Oxidation States

A. Kirsch (Copenhagen/DK), K. M. Jensen (Copenhagen/DK)

Introduced in 2004 [1], high-entropy materials have emerged as a fascinating area in materials science, providing a unique approach for material design. High-entropy oxides (HEOs) constitute a novel category of complex solid solutions where five or more metals are distributed in approximately equal proportions within a single crystallographic site. Their adaptable compositions provide a more expansive design space compared to conventional solid solutions and hence increased opportunities for tailoring material properties. HEOs have demonstrated notable characteristics, such as exceptionally low thermal conductivity [2].

We explore novel structure-types for high-entropy oxides (HEOs) and determine their solution limits for specific chemical species [3]. Due to the material"s complex nature, an in-depth analysis of their microstructure, crystal structure and chemistry requires a multimodal characterization approach. More specifically we use a combination of X-ray/neutron diffraction and total scattering, X-ray photoelectron, fluorescence and absorption spectroscopy to characterize our materials. We here give an overview of our recent works regarding the tunablity of structure, size, chemical composition and oxidation states of some high-entropy oxide systems, including spinels and perovskites.

References:

(1) Yeh, J.-W.; Chen, S.-K.; Lin, S.-J.; Gan, J.-Y.; Chin, T.-S.; Shun, T.-T.; Tsau, C.-H.; Chang, S.-Y. *Adv. Eng. Mater.* 2004, 6 (5), 299–303.
(2) Banerjee,R.; Chatterjee, S.; Ranjan, M.; Bhattacharya, T.; Mukherjee, S.; Jana, S.; Dwivedi, A.; Maiti, T. *ACS Sustain. Chem. Eng.* 2020, *8*, 17022.
(3) Kirsch, A.*; Bøjesen, E.D.; Lefeld, N.; Mathiesen, J.K.; Skjærvø, S.L. Pittkowski, R.K.; Sheptyakov, D.; Jensen, K.M.Ø.* *Chem. Mater.* 2023, 35, 20, 8664-8674.

OP-074

Understanding the formation mechanism of intermetallic (nano)particles in polyol processes

M. Smuda (Dresden/DE), J. Ströh (Kiel/DE), N. Pienack (Kiel/DE), A. Khadiev (Hamburg/DE), H. Terraschke (Kiel/DE), M. Ruck (Dresden/DE), T. Doert (Dresden/DE)

Intermetallic (nano)particles have achieved great scientific and technological interest in catalysis and electronics in the last years. One way to obtain such intermetallic (nano)particles is the polyol process, the reduction of metal salts in polyalcohols. This method is able to provide (nano)particles in high yields with controlled size and morphology at low temperatures and in short reaction times. However, a detailed knowledge about the formation mechanism of intermetallic particles under these conditions is lacking, even though a deeper understanding is crucial for targeted synthesis and material design for specific applications.

Therefore, we investigated four intermetallic systems to identify key parameters, such as precursors, temperature or pH value, using ex-situ and in-situ PXRD, SEM, and TEM, e.g. Although using chemically similar systems (Bi-Ni, Bi-Ir, Bi-Rh and Bi-Pd) and largely the same synthesis conditions, we found considerably different reaction behaviour, nucleation. The formation of crystalline BiNi starts with the successive reduction of Bi^{3+} and Ni^{2+}, leading to core-shell nanoparticles "Bi@Ni".[1] Investigations of the formation of Bi_2Ir particles revealed a partial co-reduction of Bi^{3+} and Ir^{3+} and the formation of a hitherto unknown intermetallic suboxide Bi_4Ir_2O.[2] Bi_2Rh particles are obtained via simultaneous co-reduction and an intermediately formed BiRh in a first step.[3] For γ-BiPd formation, Pd was identified as primary reduction product.

References:

(1) M. Smuda, C. Damm, M. Ruck, T. Doert, *ChemistryOpen* 2020, *9*, 1085.
(2) M. Smuda, K. Finzel, M. Hantusch, J. Ströh, N. Pienack, A. Khadiev, H. Terraschke, M. Ruck, T. Doert, *Dalton Trans.* 2021*, 50*, 17665.
(3) M. Smuda, J. Ströh, N. Pienack, A. Khadiev, H. Terraschke, M. Ruck, T. Doert, *Dalton Trans.* 2020, 51, 17405.

Legend: In-situ diffraction of the Bi/Rh reduction

Fig. 1

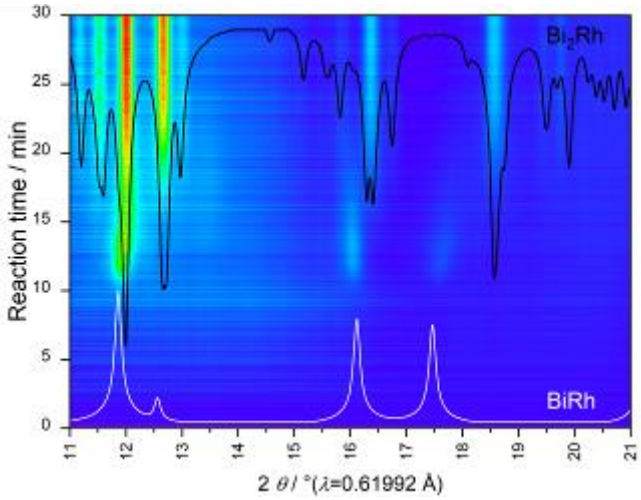

MS 21: Extreme conditions IV: High-pressure phenomena

OP-075

Theoretical simulations of materials at extreme conditions: from crystal structure to advanced functionalities

I. Abrikosov (Linköping/SE)

Recent advances in high-pressure high-temperature (HPHT) experiments allow for materials synthesis at TPa compression and temperature above 2000 K [1], paving the way towards discoveries of new materials with exciting crystal chemistry [2] and physical properties [3]. The main challenge in going from the discoveries towards applications is a need to characterize functionalities of the synthesized materials and retain them at the conditions of the operation in devices and tools. Unfortunately, experiments at HPHT conditions are very demanding, time- and resources consuming, with limited possibilities to perform *in situ* characterization. In this talk we demonstrate capabilities of state-of-the-art theoretical simulations to verify crystal structure of compounds discovered in HPHT experiments, to predict their (meta-)stability at ambient conditions and to disclose materials properties attractive for applications. We review recent advances in theoretical description of materials at extreme conditions, which combines first-principles electronic structure theory with machine learning (ML) tools [4,5]. We demonstrate feasibility of discovering metastable materials with advanced functionalities in HPHT synthesis followed by decompression to ambient conditions [6,7]. Moreover, we show that decompression of materials synthesized at HPHT conditions could lead to phase transitions to metastable polymorphs with properties even more exciting than those of the original HPHT phases [3].

References:

(1) L. Dubrovinsky, *et al.,* Nature **605**, 274 (2022).
(2) D. Laniel, *et al.,* Nature Chem. **15**, 641 (2023).
(3) M. Bykov, *et al.,* Phys. Rev. Lett. **126**, 175501 (2021).
(4) A. V. Shapeev, *et al.,* New J. Phys. **22**, 113005 (2020).
(5) H. Levämäki, *et al.,* NPJ Comp. Mater. 8, 17 (2022).
(6) M. Bykov, *et al.,* Nature Commun. **10**, 2994 (2019).
(7) D. Laniel, *et al.,* Adv. Mater. (2023).

OP-076

Polytypism of Incommensurately Modulated Structures of Crystalline Bromine upon Molecular Dissociation under High Pressure

Y. Yin (Bayreuth/DE, Jinan/CN), A. Aslandukov (Bayreuth/DE), M. Bykov (Cologne/DE), D. Laniel (Edinburgh/GB), A. Aslandukova (Bayreuth/DE), A. Pakhomova (Grenoble/FR), T. Fedotenko (Hamburg/DE), W. Zhou (Bayreuth/DE), F. I. Akbar (Bayreuth/DE), M. Hanfland (Grenoble/FR), K. Glazyrin (Hamburg/DE), C. Giacobbe (Grenoble/FR), E. L. Bright (Grenoble/FR), G. Garbarino (Grenoble/FR), Z. Jia (Jinan/CN), N. Dubrovinskaia (Linköping/SE, Bayreuth/DE), L. Dubrovinsky (Bayreuth/DE)

Polytypes of an element or compound differ only in the stacking sequence of their layers of identical structure and composition. Here, using single-crystal synchrotron X-ray diffraction, we demonstrate the existence of polytypes with incommensurately modulated sequence of layers during bromine"s molecular dissociation. At 81 GPa Br_2-I (*oC*8) transforms to the incommensurately modulated structure *Fmmm*(00γ)s00 Br-II; (γ = 0.493(3)) and, to several polytypes of Br-IIIγ (*Fmmm*(00γ)s00) with values of γ varying within 0.18 to 0.3. The diversity and coexistence of these polytypes, as well as similar behavior of other halogens, suggest that incommensurate polytypism is a common phenomenon for simple halogen systems undergoing transformations from molecular to non-molecular crystal states.

OP-077

Anti-isostructural phase transition and incommensurate magnetic structure of CrAs at high pressures and low temperatures

K. Friese (Jülich/DE), V. Dmitriev (Grenoble/FR), A. Eich (Jülich/DE), A. Grzechnik (Aachen/DE, Jülich/DE)

CrAs becomes superconducting below 2.2 K at about 1.0 GPa. At T_N = 267 K and ambient pressure, it undergoes a phase transition to an incommensurate magnetic structure and exhibits a structural transition of the anti-isostructural type, in which both orthorhombic phases have the same space-group symmetry (*Pnma*, *Z* = 4), but different distortions of the parent hexagonal structure of the NiAs type ($P6_3/mmc$, *Z* = 2). At the anti-isostructural transition, additional twin domains are formed. Our synchrotron single-crystal diffraction studies in diamond anvil cells at high-pressures and low temperatures show that compressing CrAs across T_N at low temperatures is equivalent to warming up the material from the antiferromagnetic to the paramagnetic phases at atmospheric pressure.

The magnetic structure is studied with neutron powder diffraction at ambient pressure in the range 1.5–300 K and neutron single-crystal diffraction to 0.84 GPa at 2 K. The incommensurate magnetization propagation vector is $\boldsymbol{k} = (0,0,k_c)$ with k_c = 0.3807(7) at 260 K and ambient pressure. For the analysis of the magnetic structure, a group-theoretical approach based on the space group of the nuclear structure and its subgroups is used. In the literature, the magnetic structure has been determined on the basis of powder diffraction data as a double helix propagating along the *c* axis. We discard this model based on the neutron single-crystal data. Instead, several other models, each of them spiral-like with directional components in all three directions and with no spin-density wave character that would cause a non-constant magnetic moment, are found. The ordering of the spins is neither a pure helix nor a pure cycloid. The model in superspace group $P21.1'(\alpha 0\gamma)0s$ yields the best agreement factors and is unique, as it is the only one, in which all the magnetic moments rotate with the same chirality.

OP-078

The melting curve and phase stability of diamond

C. Prescher (Freiburg i. Br./DE), O. B. O. EuXFEL#3406 Community Proposal (Freiburg i. Br./DE)

Carbon is one of the most abundant elements in the universe. Thus, the knowledge of its phase diagram, physical properties and reactivity is of fundamental importance for understanding the world around us. Elemental carbon occurs as manifold polymorphs (diamond, graphite, glassy carbon, fullerenes, nanotubes, or graphene etc.), which exhibit a wide range of exceptional mechanical, electrical, and thermal properties for technological use. In addition to industrial applications, carbon is also a major component of planetary interiors.

Despite the importance of carbon in technology, geology and planetary science, the phase diagram of carbon is still widely unexplored. While the phase transition between graphite and diamond has been experimentally well constrained, with strong implications for the synthesis of synthetic diamonds, the melting curves of both phases, graphite and diamond are strongly debated.

In this study, we report findings from experiments conducted using the European X-ray Free Electron Laser (EuXFEL) to explore the phase stability of carbon under extreme conditions, with timescales ranging from nanoseconds to microseconds and pressures up to 150 GPa. To achieve these conditions, we employed diamond anvil cells for pressurization and used a 270-nanosecond pulsed infrared laser to elevate the sample temperatures to a range of 7,000-10,000 K. Leveraging the unparalleled X-ray brilliance of the EuXFEL, we successfully captured real-time diamond formation during cooling of the sample by collecting X-ray diffraction patterns at 220-nanosecond intervals. By comparing the unit cell volumes of the newly formed diamonds to those of fully cooled diamonds after approximately 5 microseconds, we were able to estimate the crystallization temperature using established equations of state.

MS 22: Materials Science Crystallography IV: Structural studies of energy materials

OP-079

Development of indate-based Ruddlesden-Popper-type oxide materials and their topochemical fluorination as the strategy to tailor the optical properties for suitable photocatalyst

S. Perween (Stuttgart/DE), O. Clemens (Stuttgart/DE)

The recent advances of Ruddlesden–Popper–type (RP) materials have attracted particular interest because of their unique structural, electronic, and optical properties that show a high potential as a photocatalyst. A few RP-type materials such as Sr_2TiO_4, and $Li_2CaTa_2O_7$ have been reported to be efficient photocatalysts for hydrogen evolution. This lecture will present the recent results on the development of indate-based intercalation-based oxide materials such as $ABInO_4$ (where A = Lanthanides, Yttrium; and B = Ca, Sr, Ba) as a novel photocatalyst via chemical synthesis routes and the various analytical techniques such as XRD, ADT/TEM, XPS, SEM/EDS, UV-Vis-DRS have been used as the characterization methods. The topochemical fluorination of the synthesized oxide materials such as $LaBaInO_4 \rightarrow LaBaInO_3F_2$,[1] $LaSrInO_4 \rightarrow LaSrInO_3F_2$ as well as $YBaInO_4 \rightarrow YBaInO_3F_2$ (Figs 1 and 2)that shows a strong impact on the structural and optical properties of the materials developed as well as photocatalytic activities for sacrificial hydrogen evolution. The introduction of fluorine via topochemical fluorination reaction (substitution reaction) to the intercalation-based RP-type oxide adds a new dimension to control and tune the electronic and atomic structure of materials therefore affecting the physical properties. The synthesis of oxyfluorides has been obtained successfully via low-temperature topochemical reactions, and characterized by a variety of experimental analytical techniques. The structural-optical impact upon topochemical fluorination suggests a valuable tool to alter the optical properties of the materials developed while maintaining precise control of the fluorine content added to the RP-type oxide materials.

Reference:

(1) Perween et al, Topochemical Fluorination of $LaBaInO_4$ to $LaBaInO_3F_2$, Their Optical Characterization, and Photocatalytic Activities for Hydrogen Evolution *Inorg. Chem.* **2023**, *62*, 40, 16329–16342

Acknowledgment: DFG Fund within Project Number 518952364

Fig. 1

Fig. 2

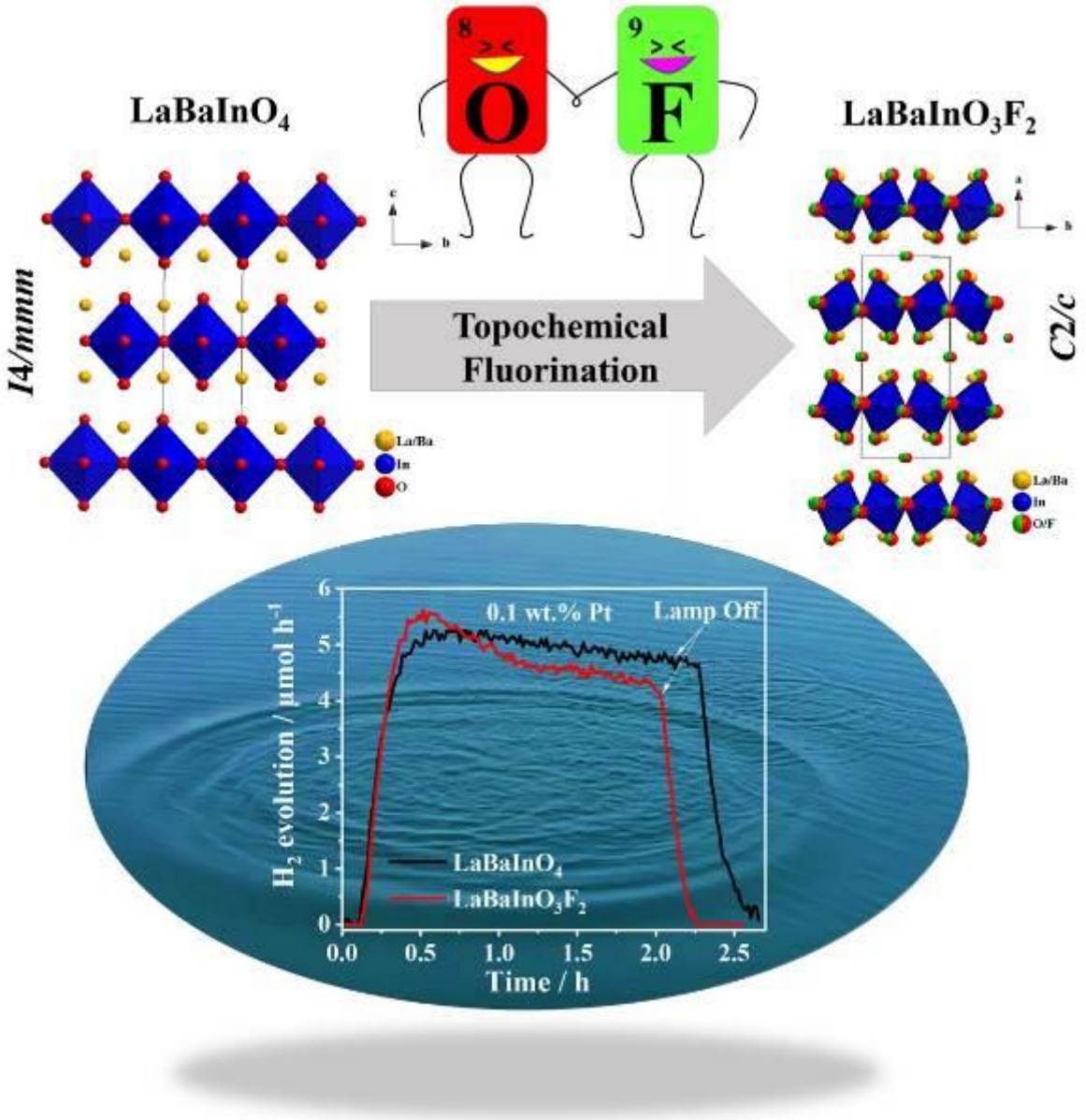
LaBaInO4
LaBaInO3F2
I4/mmm
C2/c
Topochemical Fluorination
La/Ba
In
O
O/F
0.1 wt.% Pt
Lamp Off
H2 evolution / μmol h-1
Time / h
LaBaInO4
LaBaInO3F2

OP-080

Detailed structural investigation, cation distribution model, and opto-electronic properties in alkali doped kesterite-type semiconductors for photovoltaic applications

H. Prell (Berlin/DE), G. Gurieva (Berlin/DE), A. Manjon-Sanz (Oak Ridge, TN/US), M. Kirkham (Oak Ridge, TN/US), S. Schorr (Berlin/DE)

Cost-effective absorber layers for photovoltaic applications are essential for large-scale production of efficient and environmentally friendly solar cells. This study explores the potential of alkali metal doped Cu2ZnSnSe4 (CZTSe) absorbers and focuses on the effects of doping with Li, Na, and K on off-stoichiometric bulk CZTSe. The investigation includes a comprehensive structural analysis using X-ray and neutron powder diffraction at POWGEN1 to reveal effects of doping on lattice parameters, cation distribution, and concentrations of intrinsic point defects. Structural variations induced by these processes are characterized, employing Rietveld2 refinements in combination with the average neutron scattering length method3 to derive a detailed model for the cationic distribution, along with their impact on opto-electronic properties. A post synthesis treatment, with LiF during annealing in evacuated silica glass tubes is compared to a direct incorporation utilizing NaCl and KCl, respectively, mixed with pure elements directly during synthesis. Phase-purity, homogeneity, and chemical composition is analysed employing wavelength dispersive X-ray spectroscopy by electron microprobe analysis. Despite the relatively low efficiency due to a low VOC, most efficient devices to date are based on off-stoichiometric, Cu-rich, Zn-poor material4. This research aims to enhance our understanding of these materials and contribute to the development of efficient low-cost and environmentally friendly solar devices and is founded by the Deutsche Bundesstiftung Umwelt.

References:

(1) Huq, A. et al. 2019. J. of Applied Crystallography, 52(5), 1189-1201.
(2) Rietveld, H. M. 1969. J. applied Crystallography, 2(2), 65-71.
(3) Schorr, S. 2011. Solar Energy Materials & Solar Cells; 95: 1482-1488.
(4) Kumar, M. et al. 2015. Energy & Environmental Science, 8(11), 3134-3159.

A portion of this research used resources at the Spallation Neutron Source, a DOE Office of Science User Facility operated by the ORNL

OP-081

Ternary Hydrides of CrB-type Zintl phases Eu*Tt* (*Tt* = Si, Ge, Sn)

L. Y. Dorsch (Leipzig/DE), H. Kohlmann (Leipzig/DE)

Zintl phases exhibit diverse structure and bonding motifs upon hydrogenation ranging from ionic "interstitial hydrides" to "polyanionic hydrides" containing covalently bound hydrogen in the polyanions.[1] For the CrB-type Zintl phases (space group no. 63, *Cmcm*) of the composition *MTt* (*M* = Ca, Sr, Ba; *Tt* = Si, Ge, Sn) several hydrides $MTtH_x$ are already reported.[2] They are known to incorporate hydrogen subsequently at interstitial sites up to contents of $x = 1$, while higher contents lead to the oxidation of the polyanion and a condensation of the zigzag chains. As the size of the cation increases, the larger gap between chains favors the termination by covalently bound hydrogen atoms rather than condensation of chains, leading to higher hydrogen contents (e.g. $CaSiH_{4/3-y}$, $SrSiH_{5/3-y}$, $BaSiH_{2-y}$). For Eu*Tt* (*Tt* = Si, Ge, Sn) a hydride with the composition $EuSiH_{1.8}$ was reported, but no structure was given.[3] However, as the atomic radii between Sr and Eu are similar, one would expect a hydrogen content of $x = 1.66$ or less. Eu*Tt* (*Tt* = Si, Ge, Sn) were synthesized by solid state methods, hydrogenated in autoclaves, and characterized by X-Ray powder diffraction and Rietveld analysis.The X-Ray powder diffraction data of hydrogenated EuSi suggests a structure isotypic to γ-$SrSiH_{5/3-y}$ in space group *Pnma* (a = 1444.82(9) pm, b = 395.52(2) pm, c = 2414.7(2) pm). Hydrogenation of EuGe led to three X-ray powder diffraction patterns resembling γ-$SrGeH_{4/3-y}$ (*Pnma*, a = 1496.3(2) pm, b = 404.11(3) pm, c = 1163.6(2) pm)), β-$BaGeH_{1-y}$ (*Pnma*, a = 1278.26(5) pm, b = 405.13(2) pm, c = 865.47(3) pm)), and α-$SrGeH_{1-y}$ with (*Cmcm*, a = 456.60(9) pm, b = 1179.3(3) pm, c = 408.30(8) pm)) respectively. Further hydrogenation experiments on EuSn will also be presented.

References:

(1) U. Häussermann *et al.*, *Struct. Bond.* **2011**, *139*, 143–162.
(2) H. Auer *et al.*, *Inorg. Chem.* **2017**, *56*, 1061-1071.
(3) M. Armbruster, *Z. Anorg. Allg. Chem.* **2009**, *635*, 1758–1766.

OP-082

Crystal structure of Cu2Zn(GexSi1-x)Se4 solid solution: the kesterite to wurz-kesterite structural phase transition

G. Gurieva (Berlin/DE), S. Niedenzu (Berlin/DE), A. Manjon-Sanz (Oak Ridge, TN/US), D. Matzdorff (Berlin/DE), M. Kirkham (Oak Ridge, TN/US), S. Schorr (Berlin/DE)

In this work, we explore the potential of tetravalent cation mutation in Cu-based quaternary chalcogenide semiconductors (Cu2ZnSixGe1-xSe4 [1]) with the aim of finding a material with increased bandgap (ideally around 1.7eV) and reduced structural disorder, which is considered to be the main culprit of the low VOC in the only CRM-free material used in PV technology at the moment (Cu2ZnSn(S,Se)4). One of the ways, previously shown to completely block structural disorder, especially the Cu/Zn disorder, is a change of the atomic crystal structure. The substitution of the tetravalent cation in the compound semiconductor brings a drastic structural change from the tetragonal kesterite type structure in Cu2ZnGeSe4 to the monoclinic wurtz-kesterite type structure in Cu2ZnSiSe4, with a significant increase in the bandgap as well [3].

We studied crystal structure, cation distribution and intrinsic point defect scenario in Cu2ZnSixGe1-xSe4 mixed crystals (powder samples) by neutron diffraction. This method enables us to differentiate the isoelectronic cations Cu+, Zn2+ and Ge 4+ in the crystal structure analysis. These investigations enabled us to deduce the structural transition scenario of the Cu2Zn(Ge,Si)Se4, series which is going via a region where two phases with different crystal structures but with the same chemical composition coexist. Interestingly both quaternary phases show the same cation distribution within the element specific cation sites. In the Cu2Zn(Ge,Si)Se4, series the distortion of the coordination tetrahedra is increasing with increasing Si content thus indicating that the structural transition from the kesterite type to the wurtz-kesterite type structure is distortion driven.

References:

(1) Niedenzu, S. et al. In: IEEE, 2018. - ISBN 978-1-5386-8529-7, p. 3290-3293 [2] Schorr, S. Sol. En. Mat. and Sol. Cells 249 (2022), p. 112044

A portion of this research used resources at the Spallation Neutron Source, a DOE Office of Science User Facility operated by the ORNL.

MS 23: Structural biology IV: Fragment-based drug discovery

OP-083

Room temperature X-ray fragment screening with serial crystallography

S. Günther (Hamburg/DE), P. Fischer (Hamburg/DE), M. Galchenkova (Hamburg/DE), P. Y. A. Reinke (Hamburg/DE), S. Falke (Hamburg/DE), S. Thekku Veedu (Hamburg/DE), A. C. Rodrigues (Hamburg/DE), L. Gumprecht (Hamburg/DE), J. Meyer (Hamburg/DE), M. Barthelmess (Hamburg/DE), A. Meents (Hamburg/DE)

Until today the majority of macromolecular X-ray crystallography experiments have been conducted at cryogenic liquid nitrogen temperatures. This has given us tremendous insights into the structure of macromolecules and enabled technological breakthroughs like highly reliable structure prediction by AI. However macromolecules typically function at physiological temperatures. This implies that our picture of proteins is incomplete and might be biased. Indeed structure predictions yield only a single structure per protein sequence which does not reflect the inherent dynamic nature of proteins. Flexible binding sites can be of a particular problem when predicting binding of small molecules as the actual structure of the protein might differ from the one in absence of a ligand.

In X-ray structures from cryogenic data, protein conformations can sometimes be trapped in artificial, normally lowly populated conformations. This can be remedied by collecting data at room-temperature. At the same time, typically, the resolution of derived data is lower because the sample are more radiation-sensitive. This problem can be circumvented using serial crystallography where each crystal is only exposed once and the structure is derived from thousands of crystals.

Here I present data from a fragment screen that was conducted by serial crystallography at room–temperature. The comparison with the same screen conducted using standard single crystal data collection at cryogenic temperatures reveals different conformations of the active site. While the subset of fragments identified binding to the target protein is smaller at room-temperature, the binding mode of these is unchanged from cryogenic conditions.

In summary the data suggest that extending a standard screening campaign conducted at cryogenic temperature by screening at room-temperature may reveal different target protein conformations that can lead to identification of novel binding sites for compounds.

OP-084

The crystallographic fragment screening platform at HZB

T. Barthel (Berlin/DE), W. Scanlan (Berlin/DE), L. S. Benz (Berlin/DE), U. Müller (Berlin/DE), M. S. Weiss (Berlin/DE)

Drug design is a time-consuming process, and incidents like the recent pandemic highlighted how important it is to design drugs in a time-efficient manner. Crystallographic fragment screening (CFS) is an advantageous method to discover starting points for drugs. It allows to detect weak binders and identify their binding mode and site. At HZB we aim to support our users in their endeavors to develop novel drugs.[1]

We offer the structurally and chemically diverse F2X libraries, allowing soaking of fragments in high concentrations (100 mM) and without organic solvents.[2] The EasyAccess Frame, developed at HZB, speeds up crystal manipulation; supporting our users to handle hundreds of crystals.[3] We provide two state-of-the-art beamlines for CFS campaigns. The data analysis and tracking are simplified via the web-based data management platform FragMAXapp.[4] We also offer computational support for the first rounds of optimization with the Frag4Lead workflow.[5]

We performed many successful CFS campaigns with hit rates mainly between 10-25% for diverse protein targets.[6,7] One example is the inhouse campaign of a protein-protein (PP) complex. We screened 1013 fragments and identified 269 fragment hits, pointing us to putative PP interaction sites.[8] Thus, revealing the possibility to investigate a protein"s surface for novel biological functions via CFS.

Our platform supports synchrotron users to perform CFS campaigns in a straight-forward manner and reach first higher affinity binders.

References:

(1) Wollenhaupt, J. et al.; 2021;*J. Vis. Exp.;*2021; 1-19
(2) Wollenhaupt, J. et al.; 2020;*Structure;*28; 694-706
(3) Barthel, T. et al.; 2021;*J. Appl. Crystallogr.;*54; 376-382
(4) Lima, G. M. A. et al.; 2021;*Acta Crystallogr. Sect. D;*77; 799-808
(5) Metz, A. et al.; 2021;*Acta Crystallogr. Sect. D;*77; 1168-1182
(6) Füsser, F. T. et al.; 2023;*Acta Crystallogr. Sect. D;79; 857–865*
(7) Scaletti, E. et al.; 2021;*Purinergic Signalling*;17; 693–704
(8) Barthel, T. et al.; 2022;*J. Med. Chem.;*65; 14630–14641

OP-085

Uncovering novel drug targets of polyprotein precursors of SARS-CoV-2

G. L. von Scholley (Grenoble/FR), C. Mueller-Dieckmann (Grenoble/FR), M. Soler Lopez (Grenoble/FR), M. Schäfer (Berlin/DE), R. Hillig (Berlin/DE), E. Kandiah (Grenoble/FR)

Introduction

The Covid-19 pandemic has been successfully tackled by the quick development of mRNA vaccines. While vaccines are very effective in slowing the viral spreading, therapeutic drugs help deal with severe cases of infection. So far, only one drug has been developed against the SARS-CoV-2 Mpro.

Another theurapeutic target is the Papain-like Protease (PlPro) located on the non-structural protein 3 (NSP3). NSP3 fulfils multiple crucial functions in viral replication. After the genome translation into two polyproteins, PlPro cleaves part of the polyprotein to release the functional NSPs 1-3. PlPro furthermore suppresses the human innate immune system by its deubiquitinating and deISGlating properties. Furthermore, NSP3 together with NSP4 forms so called double membrane vesicles (DMVs) with the ER-membrane, which are a hub for viral RNA replication.

Objectives

Structural and functional studies on PlPro and its neighbouring domains (Ubl2 and NAB) within NSP3 with the goal to perform fragment screening to explore novel small molecule binding sites for antiviral therapeutics development.

Methods

This project is an integrated biology approach using mainly X-ray crystallography for the target domains, as well as SAXS to study domain-domain interactions. Cryo-EM is available as a method for larger construct that are difficult to crystallise.

Results

Fragment screen has been successfully performed on the target domain Ubl2-PlPro, measuring ~800 different fragments that resulted in multiple promising hits. Furthermore, TSA fragment screens with ~2000 fragments were performed against Ubl2-PlPro and its neighbouring NAB domain as well as a Ubl2-PlPro-NAB. Multiple hits were identified for each domain.

Conclusion

Promising fragment hits agains PlPro were determined in crystallographic and TSA fragment screen. Further experiments exploring these fragments and their potential to inhibition of PlPro are undergoing.

Fig. 1

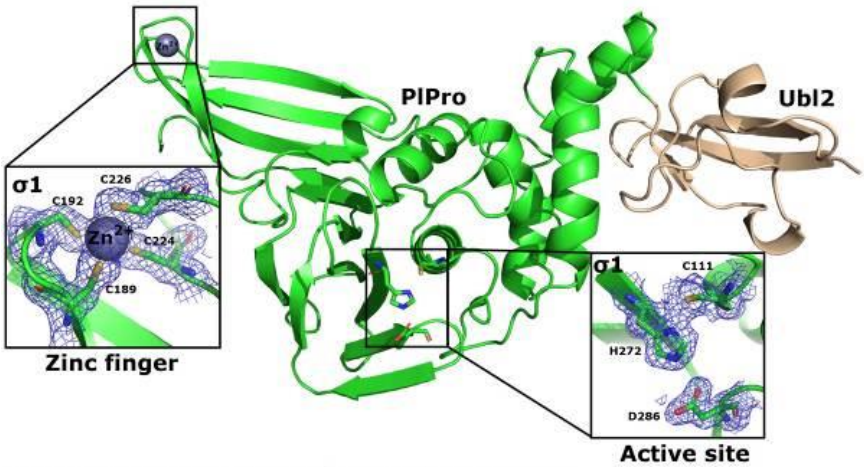

Presentation of Ubl2-Plpro Wildtype Chain A at 1.8 Å with zinc coordination and active site.

Fig. 2

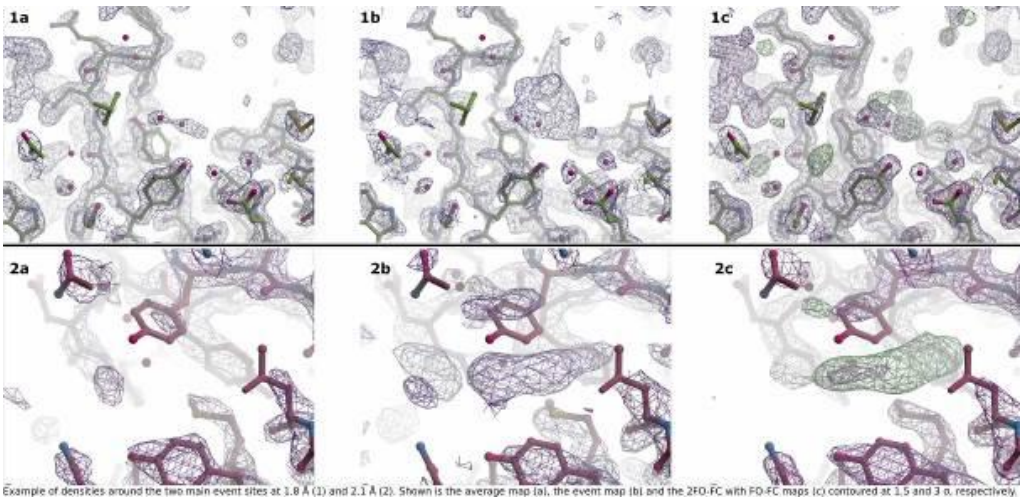

Example of densities around the two main event sites at 1.8 Å (1) and 2.1 Å (2). Shown is the average map (a), the event map (b) and the 2FO-FC with FO-FC maps (c) contoured at 1.5 and 3 σ, respectively.

OP-086

The search for FGE stabilizing molecules: from fragment screen hits to potential lead(s)

J. L. Kowal (Bielefeld/DE), N. Ezzaidi (Southampton/GB), J. Wollenhaupt (Berlin/DE), K. Radhakrishnan (Bielefeld/DE), T. Pietrowski (Bielefeld/DE), M. Thangarasah (Bielefeld/DE), W. Keller (Bielefeld/DE), S. Alam (Bielefeld/DE), M. S. Weiss (Berlin/DE), M. G. J. Baud (Southampton/GB), H. H. Niemann (Bielefeld/DE)

Formylglycine-generating enzyme (FGE) is key to the posttranslational modification of the active site of all known sulfatases. By conversion of a cysteine to formylglycine, FGE activates the sulfatases in the endoplasmic reticulum. Missense mutations in the gene encoding FGE lead to catalytically impaired or unstable protein variants that are prone to degradation. The resulting lack of sulfatase modification leads to the rare disease known as multiple sulfatase deficiency (MSD).[1]

The work presented here is the first structure-based approach to stabilize mutated FGE variants and rescue their activity by development of pharmacological chaperones.[2] Using the F2X-Entry Screen, a subset of the F2X-Universal library, and additional compounds selected from previous experiments, we soaked preformed crystals of human FGE with small molecules to identify hits and interesting binding pockets on the enzyme surface.[3,4] Data collection at BESSY BL 14.2 and multi data set analysis in FragMAXapp[5] revealed several unique fragment hits in four interaction sites, including the active site of FGE. Two compounds with overlapping binding positions in a potential allosteric site were used for merging and synthesis of several follow-ups, based on the structural data. Data collection at DESY P13 revealed *Fo-Fc* density for one of these follow-ups in a data set from a single crystal which suggests stronger interaction with the enzyme. To evaluate whether the discovered hits and follow-up compounds stabilize the protein or not, we obtained first results from differential scanning fluorimetry.[6] Additionally, a bigger crystallographic screen with the full F2X-Universal library is in progress.

References:

(1) Cell. (2005) 121, 541-52. [2] Int J Mol Sci. (2020), 21, 489. [3] Structure. (2020) 28, 694-706. [4] JoVE. (2021) 169, e62208. [5] Acta Cryst. (2021) D77, 799-808. [6] Biophys Rev. (2020) 12, 85-104.

MS 24: Mineralogical crystallography II: Minerals at non-ambient conditions

OP-087

Accurate Crystal Structures of Ices from X-Ray and Electron Diffraction with Hirshfeld Atom Refinement

K. Woźniak (Warszawa/PL), M. Chodkiewicz (Warszawa/PL), R. Gajda (Warszawa/PL), V. B. Prakapenka (Chicago, IL/US), P. Dera (Honolulu, HI/US)

We have applied Hirshfeld Atom Refinement (HAR) against single crystal high pressure (sc HP) synchrotron and laboratory X-ray and electron diffraction data for ice VI, ice VII and hexagonal ice (Ih). This method (HAR) utilizes aspherical atomic scattering factors (X-rays), and aspherical atomic electrostatic potentials (ED), based on so called stockholder (Hirshfeld) partition of electron density and is especially effective in the case of refinement of crystals of H-rich compounds (ices in particular)

We will present details of HAR procedure and accurate crystal structures of H_2O, D_2O and mixed (50%H_2O/50%D_2O) ice VI and ice VII obtained by HAR against sc HP synchrotron and laboratory X-ray diffraction data as well as results of refinement of hexagonal ice obtained by HAR against electron diffraction data. We have performed both kinematic and dynamical refinements for Ih and compared the obtained results with HAR refinement. It was possible to obtain O-H bond lengths and anisotropic ADPs for disordered hydrogen atoms which are in good agreement with the corresponding results of single crystal neutron diffraction data.[1] Our results show that HAR against X-ray diffraction and electron diffraction data is a tool which can compete with neutron diffraction in detailed studies of polymorphic forms of ice and crystals of other hydrogen rich compounds. Cheaper and more accessible X-ray measurements combined with HAR can facilitate the verification of the existing ice polymorphs and the quest for the new ones.[1]

References:

(1) M. L. Chodkiewicz, R. Gajda, B. Lavina, S. Tkachev, V. B. Prakapenka, P. Dera, K. Woźniak, *IUCRJ*, **9**, 573-579 (2022).

Financial support of this work by the National Science Centre, Poland, through OPUS 21 grant number DEC-2021/41/B/ST4/03010 is gratefully acknowledged.

OP-088

Non-ambient and *operando* X-ray diffraction for the investigation of materials of any type (from minerals to batteries)

B. Puhr (Graz/AT), M. Kremer (Graz/AT), A. O. F. Jones (Graz/AT), B. Schrode (Graz/AT), H. Sievers (Ostfildern-Scharnhausen/DE)

Modern powder X-ray diffraction (XRD) systems must nowadays be able to meet the challenges faced by multi-user and multi-application facilities. Instruments must be capable not only of routine XRD measurements, but also have to offer advanced capabilities such as measurements under non-ambient (varying temperature, pressure, gas atmosphere, humidity, ...) or *operando* conditions which can drastically change material properties.

The recently launched XRDynamic 500 automated multipurpose powder X-ray diffractometer from Anton Paar has set new standards in terms of data quality, automation and efficiency for laboratory powder diffractometers. The core of XRDynamic 500 is the TruBeam™ concept that comprises a large goniometer radius and evacuated optics units, automatic change of the beam geometry and all optics components, and automated instrument and sample alignment routines. All of these features combine to deliver outstanding data quality that can be measured with high efficiency in a straight-forward manner. The high level of automation means that you can perform measurements on one or many samples with different geometries and instrument configurations in one batch with no user intervention needed.

XRDynamic 500 can also be equipped with different non-ambient and *operando* XRD attachments to perform measurements under non-ambient conditions or to study materials *operando*. These attachments are perfectly integrated into the hard- and software (plug-and play mode, integrated control unit, built-in connections) and guarantee best-in-class convenience for your non-ambient and *operando* XRD studies.

To highlight the potential of XRDynamic 500, we will present key instrument features and benefits in addition to recent application data on non-ambient XRD and *operando* XRD studies on batteries.

Fig. 1

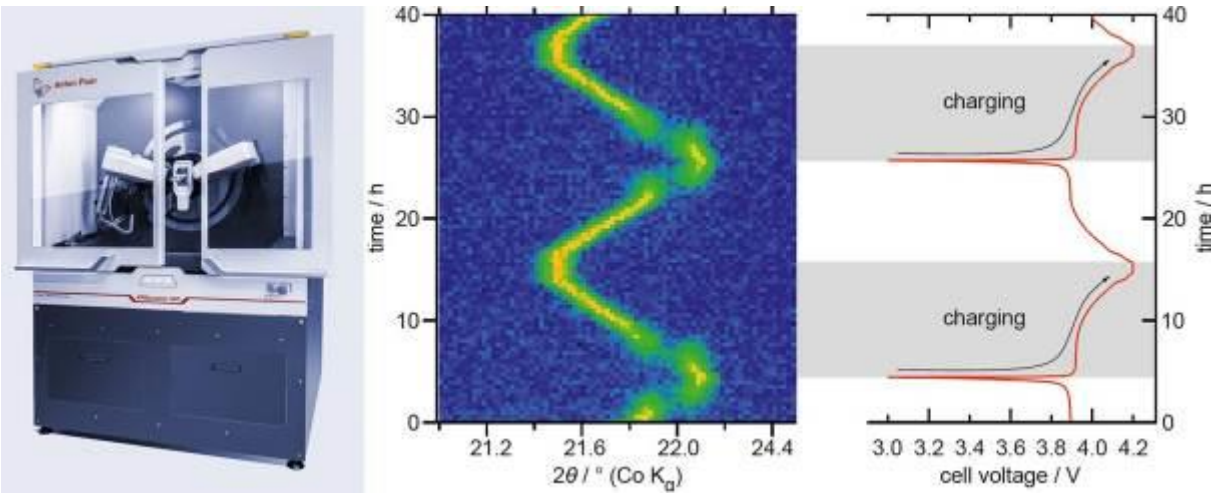

OP-089

Phase evolution and thermal behavior of hydrous Fe sulfate minerals: coquimbite $AlFe_3(SO_4)_6(H_2O)_{18}$, römerite $Fe^{2+}Fe^{3+}{}_2(SO_4)_4(H_2O)_{14}$ and aluminocopiapite $Al^{3+}{}_{2/3}Fe^{3+}{}_4(SO_4)_6(OH)_2(H_2O)_{20}$

V. Abdulina (St. Petersburg/RU), A. Borisov (Kiel/DE), O. Siidra (St. Petersburg/RU), A. Holzheid (Kiel/DE)

Hydrated iron sulfates are essential for acid mine drainage (AMD) precipitation as well as for the formation of oxidation zones of ore deposits. They are subjected to transformations under diverse climatic conditions, which include interactions with precipitation and humid atmosphere. A few of these minerals have been found on the surface of Mars under extraterrestrial conditions. The significance of examining the transformations of sulfate minerals occurring on the Mars has been recognized in the context of the potential implementation of the Mars Sample Return Mission. Due to this relevance of the topic, certain inquiries regarding the properties and phase evolution of numerous minerals belonging to this family remain unresolved and subject to debate at present. In our work we report a comprehensive study of the thermal properties and phase transformations of coquimbite $AlFe_3(SO_4)_6(H_2O)_{18}$, römerite $Fe^{2+}Fe^{3+}{}_2(SO_4)_4(H_2O)_{14}$ and aluminocopiapite $Al^{3+}{}_{2/3}Fe^{3+}{}_4(SO_4)_6(OH)_2(H_2O)_{20}$. The stability limits of the specified minerals are reported, substantiated by high-resolution powder X-ray diffraction and thermal analysis. Based on powder X-ray diffraction data for these minerals, the character of thermal expansion was described for the first time. Of particular interest are the results of investigation of the phase transformations of aluminocopiapite under low vacuum conditions – a rare phenomenon previously described only for a few hydrated sulfates. The obtained results expand the field of mineral evolution with sulfate anion over a wide range of physical and chemical conditions.

OP-090

Low-temperature structural phase transitions in halide perovskites

S. Schorr (Berlin/DE), J. HIdalgo (Georgia, GA/US), J. Breternitz (Berlin/DE), D. M. Többens (Berlin/DE)

Halide perovskites with mixed cations as well as mixed halides have shown to be excellent candidates for solar energy conversion. However, understanding the structural phases of these mixed-ion perovskites across a wide range of operating temperatures, including very low temperatures for space applications, is crucial. In this study, we investigated the crystal structure of formamidinium (FA)-based (Cs,FA)Pb(Br,I)3 perovskites using low-temperature *in-situ* synchrotron powder X-ray diffraction.

The studied compositional range of the halide perovskites were selected to keep an FA-rich composition with an ideal bandgap for single-junction solar cells [1]. The compounds should keep an I-based composition and the known thermodynamic limit to form a single-phase perovskite, when alloying Cs and FA, has been taken into account. Thus 12 (CsyFA1-y)Pb(BrxI1-x)3 powder samples with y=0, 0.05, 0.17 and x=0, 0.05, 0.10, 0.17 have been synthesized by evaporating the solvents from a precursor solution (170°C, 2 hours).

To compose a low-temperature phase diagram for the (Cs,FA)Pb(I,Br)3 compositional space, we performed *in-situ* powder X-ray diffraction experiments at the beamline KMC-2 at the synchrotron radiation source BESSY II by cooling the powders from 300 K to 23 K and measured in steps of 20 K.

Our findings revealed that substituting the iodide ion by bromide suppresses the phase transformation from the tetragonal to the orthorhombic perovskite structure which occurs at low temperatures. The addition of bromide also prevents the occurrence of non-perovskite secondary phases. By creating the phase diagram, we gained fundamental insights into the structural behavior or these materials. This understanding of the structural properties lays the groundwork for designing more robust and efficient energy materials capable of functioning under extreme temperature conditions, including space-based solar energy conversion.

References:

(1) Weber et al., *Chem. Mater.* **2018**, *30*, 3768

MS 25: Structural biology V: Synchrotrons & new methods

OP-091

Probing the modulation of enzyme kinetics by multi-temperature, time-resolved serial crystallography

E. C. Schulz (Hamburg/DE), A. Prester (Hamburg/DE), D. von Stetten (Hamburg/DE), J. P. Leimkohl (Hamburg/DE), H. Schikora (Hamburg/DE), F. Tellkamp (Hamburg/DE), P. Mehrabi (Hamburg/DE)

Although enzymes operate over a wide range of temperatures, the vast majority of protein structures, are acquired under cryo-conditions. However, the conformational dynamics of enzymes are directly correlated with their catalytic rate, and these dynamics are intimately linked to temperature. This mismatch between data collection temperatures and the optimal reaction temperature becomes an acute problem for time-resolved studies that seek to provide detailed structural insight into catalytic mechanisms and allosteric regulation.

We present a new environmental enclosure for fixed-target, serial synchrotron crystallography (TR-SSX) enabling full control of both the temperature and humidity[1]. The setup allows maintaining the relative humidity to within a percent, and provides access to X-ray diffraction experiments in a wide temperature range from below 10° C to above 80° C. Coupled with the liquid application method for time-resolved crystallography (LAMA) [2], TR-SSX experiments can now be carried out at truly physiological temperatures, providing fundamentally new insight into protein function.

For the mesophilic extended-spectrum beta-lactamase CTX-M-14 and the hyperthermophilic enzyme xylose isomerase we show the response of the structures to increasing temperatures from 10°C to 37°C and from 10°C to 60°C, respectively. In addition, we demonstrate for both enzymes the temperature-dependent modulation of turnover kinetics, that is an increase of substrate turnover with increasing temperature. This displays the widespread and convenient applicability of multi-dimensional serial crystallography opening countless new research opportunities.

References:

(1) Mehrabi, P. *et al*. An environmental control box for serial crystallography enables multi-dimensional experiments bioRxiv 2021.11.07.467596
(2) Mehrabi, P. *et al.* Liquid application method for time-resolved analyses by serial synchrotron crystallography, *Nat.Methods* 16, 979–982 (2019)

OP-092

Facilities for Macromolecular Crystallography at the HZB

U. Müller (Berlin/DE), M. S. Weiss (Berlin/DE)

The Macromolecular Crystallography (MX) group at the Helmholtz-Zentrum Berlin (HZB) has been in operation since 2003. Since then, three state-of-the-art synchrotron beam lines (BL14.1-3) for MX have been built up on a 7T-wavelength shifter X-ray source [1-3]. Currently, the three beam lines represent the most productive MX-stations in Germany, with more than 4200 PDB depositions (Status 10/2023). BLs14.1 and 14.2 are energy tunable in the range 5.5-15.5 keV, while beam line 14.3 is a fixed-energy side station operated at 13.8 keV. All three beam lines are equipped with state-of-the-art detectors: BL14.1 with a PILATUS3S 6M detector, BL14.2 with a PILATUS3S 2M and BL14.3 with a PILATUS 6M detector. BL14.1 and BL14.2 are in regular user operation providing close to 200 beam days per year and about 600 user shifts to approximately 100 research groups across Europe. Remote beamline operation has been established and operated successfully at BL14.1 and BL14.2. BL14.3 is been equipped with a MD2 micro-diffractometer, a HC1 crystal dehydration device and a REX nozzle changer making it suitable for room temperature experiments. Additional user facilities include office space adjacent to the beam lines, a sample preparation laboratory, a biology laboratory (safety level 1) and high-end computing resources. Within this presentation a summary on the experimental possibilities of the beam lines, future beamline upgrades and the ancillary equipment provided to the user community will be given.

References:

(1) U. Heinemann, K. Büssow, U. Mueller & P. Umbach (2003). Acc. Chem. Res. 36, 157-163.
(2) U. Mueller, N. Darowski, M. R. Fuchs, R. Förster, M. Hellmig, K. S. Paithankar, S. Pühringer, M. Steffien, G. Zocher & M. S. Weiss (2012). J. Synchr. Rad. 19, 442-449.
(3) U. Mueller, R. Förster, M. Hellmig, F. U. Huschmann, A. Kastner, P. Malecki, S. Pühringer, M. Röwer, K. Sparta, M. Steffien, M. Ühlein & M. S. Weiss (2015). Eur. Phys. J. Plus 130, 141-150.

OP-093

Better understanding solvent in macromolecular crystals

M. Edich (Hamburg/DE), A. Wagner (Didcot/GB), M. Hough (Didcot/GB), A. Thorn (Hamburg/DE)

The average discrepancy between models and diffraction data in macromolecular crystallography, as evidenced by R-value, is 24%. [1]. Structures solved from small molecule crystals, however, lead to relatively small R values [2], indicating the source of the R value gap to emerge from a property specific to macromolecular crystals. One of such properties is the presence of solvent channels and their large contribution to the crystal"s volume.

State-of-the-art phasing methods flatten the electron density surrounding the macromolecule and hance, we lose information about the solvent area [3]. However, we found a way to preserve this information, generating maps with little or no model bias. These maps show a greater number of features from the solvent. Here, we will discuss what we have found in the maps so far and show how this could lead to a better understanding of macromolecular structures in general.

References:

(1) Gao, Yunyun, Volker Thorn, and Andrea Thorn. "Errors in structural biology are not the exception." Acta Crystallographica Section D: Structural Biology 79.3 (2023).
(2) Holton, James M., et al. "The R-factor gap in macromolecular crystallography: an untapped potential for insights on accurate structures." The FEBS journal 281.18 (2014): 4046-4060.
(3) Weichenberger, Christian X., et al. "The solvent component of macromolecular crystals." Acta Crystallographica Section D: Biological Crystallography 71.5 (2015): 1023-1038.

This work was supported by BMBF [grant number 05K19WWA and 05K22GU5] and the DFG [project TH2135/2-1].

OP-094

Towards High throughput Fragment Screening at the beamline P11, DESY

G. Pompidor (Hamburg/DE), S. Chatziefthymiou (Hamburg/DE), V. Delsoglio (Hamburg/DE), A. Grebentsov (Hamburg/DE), A. Gruzinov (Hamburg/DE), T. Melson (Hamburg/DE), O. Merkulova (Hamburg/DE), J. Song (Hamburg/DE), H. Taberman (Hamburg/DE), J. Hakanpää (Hamburg/DE)

P11 is a Macromolecular Crystallography (MX) beamline at PETRA III (DESY, Hamburg). The instrument can provide variable experimental setups with multiple focus sizes (from 200 x 200 to 5 x 10 μm^2) in an energy range from 6 to 28 keV. With a high flux of 10^{13} ph/s, the beamline can be used to perform serial crystallography and high throughput crystallography.

Equipped with an EIGER2 X 16M detector (133Hz data acquisition) and an automated sample changer (368 samples capacity and 20 s mounting time), P11 is ideal for large campaigns of fragment or ligand screening with a the total time per sample reduced to less than 2 minutes. To complement these capabilities, the P11 laboratory offers the possibility to use the OLT Crystal Shifter for semi-automated crystal harvesting and soaking of crystals from 96 well crystallization plates. The system can export the sample information to ISPYB to facilitate sample tracking during data collection.

In September 2023, the P11 team and the company CrystalFirst, hosted on the DESY campus, have started a project called "LigandML" whichaims to use AI to increase the success rates of Fragment Based Drug Design campaigns. The first screening campaign will start at the end of the year on a WDR5, a highly conserved human nuclear protein which has been identified as an interesting target for inhibition in several cancer types. The campaign will make use the Echo Liquid Handler which can precisely deliver nanoliters scale to prepare to soak crystals in numerous conditions. The experiments will be used as test cases to develop the fragment screening at P11 from the sample preparation to the implementation of a pipeline for automated ligand/fragment identification.

MS 26: Chemical crystallography IV: Complex, aperiodic and disordered structures

OP-095

Interaction space modelling for ultra-fast diffuse scattering map calculations

E. M. Schmidt (Bremen/DE), A. Simonov (Zurich/CH)

Advances in neutron, X-ray and electron diffraction setups have made the routine collection of single crystal diffuse scattering data possible. However, the interpretation of single crystal diffuse scattering is still regarded as a complex problem, where the determination of meaningful descriptors that describe the disorder causing the diffuse scattering is a challenge. Here, we show how our recently introduced interaction space modelling approach [1] can be applied to derive meaningful descriptors.

In this approach we utilize a simple interaction Hamiltonian and apply a mean filed approximation to calculate the expected diffuse scattering without the need to generate large supercells. The parametrization of the disorder model in terms of only a few terms in the interaction Hamiltonian makes this approach not only efficient in terms of parameters but also fast for the calculation of the diffuse scattering. Hence, a big parameter space can be probed with little computational effort.

Here, we use this approach for the ultra-fast calculation of diffuse scattering maps of disordered rocksalt structures [2], and Prussian blue analogues [3] (see Figure 1). We demonstrate that by applying this simple and easy calculation approach, the diffuse scattering for many systems cannot just be predicted accurately but also the interaction parameters can be refined, as long as the disorder sill lies within the stability regime of the mean field approximation.

Figure 1: *hk*0-layer of single crystal diffuse scattering from Prussian blue analogues as a function of interaction parameters *b j*1 (drive for local electroneutrality) and *b j*2 (drive for local centro-symmetry). For comparison see the phase diagram based on Monte Carlo simulations in [3], red part indicates the boundary of the mean-field stability regime [1].

References:

(1) Schmidt, E.M. *et al.* (2022) *IUCrJ* **9**(1), 21-30.
(2) Withers, R. (2015) *IUCrJ* **2**(1), 74-84.
(3) Simonov, A. *et al.* (2020) *Nature* **578**, 256–260.

Fig. 1

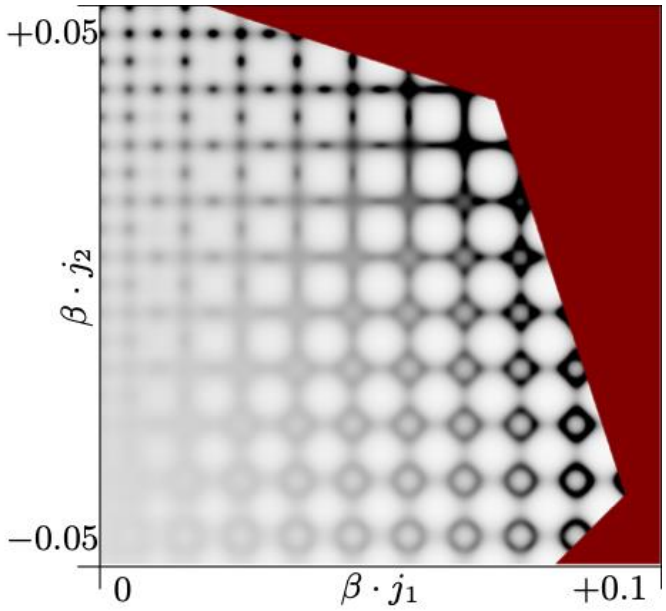

OP-096

Twinning of owyheeite: the case for a generalized order-disorder (OD) theory

B. Stöger (Vienna/AT), D. Topa (Vienna/AT)

Owing to systematic twinning, the complete crystal structure of the sulfosalt mineral owyheeite [$Cu_{0.09}Ag_{2.77}Pb_{10.23}Sb_{10.89}S_{28.00}$] has reamained unknown for many decades. Only a subcell has been derived from synchrotron poowder data [1]. Recently, we were able to elucidate the twofold superstructure based on a tiny crystal [2]. Systematic twinning is often rationalized by application of he order-disorder (OD) theory [3]. In a classical OD description, the structure is considered as being built of layers. Adjacent layers can connect in different, albeit geometrically equivalent, ways. This gives rise to a family of polytypes, which are locally equivalent. An OD twin is such a polytype, where the twin interface constitutes a fragment of a different polytype.

Owyheeite possesses pseudo-symmetry that is indicative of an OD structure. However, the putative OD layers and the symmetry elements of the domains are inclined. A full OD description is therefore only possible in terms of rods. Indeed, the structure can be `sliced' into two kinds of rods *A* and *B*, as shown in Fig. 1. The trigonal pseudo-symmetry of the A rods ultimately explains the observed systematic twinning. Yet, this decomposition does not represent a classical OD structure, because the *A* rod can contact in non-equivalent ways to other *A* and *B* rods. It has "OD character" though in the sense that all possible rod arrangements are locally equivalent. We therefore propose a generalized OD theory that is not based on disjoint rods, but on overlapping *equivalence regions* .

This generalized OD theory directly expresses the crucial point of *local equivalence*. Moreover, it can be used to describe more relaxed structure families.

References:

(1) Laufek, F., Pažout, R. & Makovicky, E. (2007). *Eur. J. Mineral.* **19**, 557–566.
(2) Stöger,B. Göb, Ch., Topa. D. (2023). *Acta Cryst. B***79**, 271–280.
(3) Dornberger-Schiff, K. & Grell-Niemann, H.. *Acta Cryst.* **14**, 167–177.

Fig. 1 The structure of owyheeite interpreted in terms of OD rods.

Fig. 1

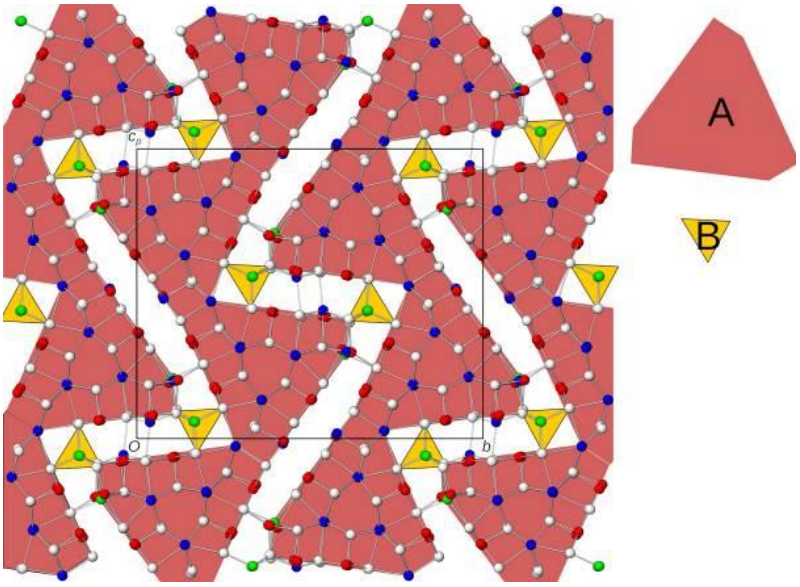

OP-097

Incommensurately modulated structure of $RAl_{1-x}Ga_x$ (R = Eu, Sr)

H. Agarwal (Bayreuth/DE), S. R. Kotla (Bayreuth/DE), S. Ramakrishnan (Higashi-Hiroshima/JP), C. Eisele (Bayreuth/DE), L. Noohinejad (Hamburg/DE), M. Tolkiehn (Hamburg/DE), C. Paulmann (Hamburg/DE), B. Bag (Jharkhand/IN), B. Baran Maity (Mumbai/IN), S. Dan (Mumbai/IN), A. Thamizhavel (Mumbai/IN), S. Ramakrishnan (Pune/IN), S. van Smaalen (Bayreuth/DE)

Intermetallic materials with a centrosymmetric square net structural motif having the $BaAl_4$ or $ThCr_2Si_2$ structure type [1] are perfect cases of quantum materials that exhibit superconductivity, charge density wave (CDW) ordering, ferromagnetism (FM), or heavy fermionic activity [2]. The compounds $R(Al_{1-x}Ga_x)_4$ (where R= Eu, Sr) have a tetragonal crystal structure with space group *I4/mmm* at room temperature [3, 4]. The temperature dependence of electrical resistivity of these compounds suggests the formation of a CDW in $EuAl_4$ at T_{CDW} = 145 K, in $SrAl_4$ at T_{CDW} = 243 K [5] and in $EuGa_2Al_2$ at T_{CDW} = 51 K [3]. Single crystal X-ray diffraction reveals incommensurately modulated orthorhombic CDW phase transition in EuAl4 with modulation vector q = (0, 0, 0.187) at 145 K and (0, 0, 0.174) at 20 K having superspace group *Fmmm(00g)s00* [6].

We have observed an incommensurately modulated CDW phase in $EuAl_2Ga_2$. X-ray diffraction was performed at beamline P24 of PETRA-III at DESY (Hamburg, Germany) in the 300 K – 18 K temperature range with radiation of wavelength 0.5 Å. We will present the incommensurately modulated crystal structure as a function of temperature in $EuAl_2Ga_2$ and compare it to the CDW structures of $EuAl_4$ [6] and $SrAl_4$ [7].

References:

(1) Klemenz, S. *et al. J. Am. Chem. Soc.* **142**, 6350–6359 (2020).
(2) Shatruk, M. *J. Solid State Chem.* **272**, 198–209 (2019).
(3) Stavinoha, M. *et al. Phys. Rev. B* **97**, 195146 (2018).
(4) S. Engel et al. *Inorg. Chem.* 62, 4260 (2023).
(5) Nakamura, A. *et al. J. Alloys Compd.* **654**, 290–299 (2016).
(6) Ramakrishnan, S. *et al. IUCrJ* **9**, 378–385 (2022).
(7) Ramakrishnan, S. *et al.* arXiv: 2309.08959 (2023).

OP-098

Monoclinic symmetry of the hcp-type ordered areas in bulk cobalt

P. Kozłowski (Warsaw/PL), P. Fabrykiewicz (Aachen/DE, Garching/DE), I. Sosnowska (Warsaw/PL), F. Fauth (Barcelona/ES), A. Senyshyn (Garching/DE), E. Suard (Grenoble/FR), D. Oleszak (Warsaw/PL), R. Przeniosło (Warsaw/PL)

The gradual ferromagnetic spin reorientation in the hcp phase of cobalt between 230°C and 330°C reported for a Co single crystal [1] suggests that this phase cannot have a hexagonal symmetry [2,3]. This hypothesis is verified positively by synchrotron radiation diffraction and neutron diffraction on powder of cobalt [4]. The hexagonal close packed phase of cobalt (hcp-Co) is associated with numerous stacking faults while the face centered cubic phase of cobalt (fcc-Co) has considerably less stacking faults, as shown e.g. in [5,6]. The analysis of diffraction data has been done by using a specific set of Bragg peaks, which are not affected by the stacking faults. The crystal structure of the hcp-type ordered areas of cobalt is described by a monoclinic symmetry with the magnetic space group C2'/m', where the former hexagonal [001] axis is no longer perpendicular to the hexagonal layers. The hexagonal [001] and [010] axes make an angle equal $\alpha \approx 90.10(1)°$, while the angle between in-plane [100] and [010] axes equals $\gamma \approx 120.11(1)°$. The monoclinic symmetry provides an approximate description of the crystal structure of the stacking faulted hcp-Co areas coexisting with fcc-Co areas [4].

References:

(1) E. Bertaut, A. Delapalme and R. Pauthenet; *Solid State Commun.* 1 (1963) 81
(2) R. Przeniosło, P. Fabrykiewicz and I. Sosnowska; *Acta Cryst. A* **74** (2018) 705
(3) P. Fabrykiewicz, R. Przeniosło and I. Sosnowska; *Acta Cryst. A* **77** (2021) 327
(4) P. Kozłowski, P. Fabrykiewicz, I. Sosnowska, F. Fauth, A. Senyshyn, E. Suard, D. Oleszak and R. Przeniosło; *Phys Rev. B* **107** (2023) 104104
(5) O. S. Edwards and H. Lipson; *Proc. R. Soc. Lond. Ser. A-Math. Phys. Sci.* **180** (1942) 268
(6) O. Blaschko, G. Krexner, J. Pleschiutschnig, G. Ernst, C. Hitzenberger, H. P. Karnthaler and A. Korner; *Phys. Rev. Lett.* **60** (1988) 2800

MS 27: Experimental methods IV: Electron diffraction

OP-099

PyFast-ADT: Python-Driven Advancements in Automated Crystal Tracking and 3DED Data Collection

M. Santucci (Mainz/IT), U. Kolb (Mainz/IT)

3-Dimensional Electron Diffraction (3DED) is a powerful tool for nano crystalline material structure determination [1]. Challenges arise due to hardware and software limitations, particularly in the context of nano crystals. The absence of nanoscale goniometers forces to track the diffracting volume over a wide tilt range. Automating data acquisition is crucial to overcome these mechanical constraints [2]. Our solution is pyFast-ADT, a versatile Python-based software designed for data collection and crystal tracking.

We've developed pyFast-ADT for FEI Tecnai SPIRIT and Tecnai F30 Transmission Electron Microscopes operating at 120 and 300 kV. These instruments are equipped with a TVIPS XF416R camera and a Timepix 1 Hybrid Pixel Detector.

PyFast-ADT employs a flexible, adaptor-based structure that simplifies the integration of new devices. This design ensures our software can continually evolve to control various experimental setups.

During data collection, pyFast-ADT uses a novel automatic crystal tracking algorithm. We've improved the tracking method, transitioning from a semi-automatic to a fully automatic approach. This enhancement is achieved through a robust routine for object detection and tracking adaptable to both Continuous Rotation Electron Diffraction and Stepwise Electron Diffraction, resulting in a more consistent behavior of the goniometer.

In conclusion, our work aims to lay the foundation for implementing new tracking routines and data acquisition methods in 3DED. The Python environment is necessary to overcome past hardware limitations, thereby facilitating the software's adoption within the electron diffraction community. Additionally, the ease of accessing powerful packages optimized for computer vision and image recognition empowers us to develop new features that other languages struggle to match.

References:

(1) M. Gemmi, et al. https://doi.org/10.1021/acscentsci.9b00394.
(2) S. Plana-Ruiz et al. https://doi.org/10.1016/j.ultramic.2020.112951.

Fig. 1

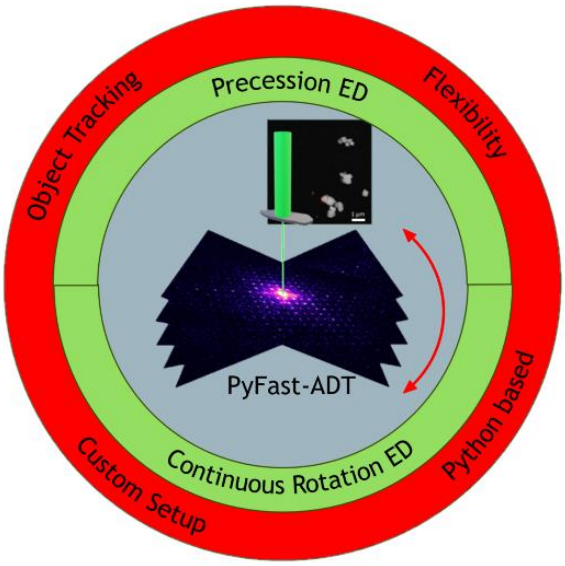

OP-100

XtaLAB Synergy-ED: A Journey Through the 'Highs' and 'Lows' of Variable Temperature Diffraction

K. N. Truong (Neu-Isenburg/DE), R. Bücker (Neu-Isenburg/DE), C. Göb (Neu-Isenburg/DE), C. Schürmann (Neu-Isenburg/DE), J. Wojciechowski (Neu-Isenburg/DE), M. Jasnowski (Wrocław/PL), M. Meyer (Wrocław/PL), F. White (Neu-Isenburg/DE)

Since its launch in 2021, the XtaLAB Synergy-ED has produced many structures, with over 400 unique structures from Rigaku labs alone. The majority of those structures have been conducted at ambient temperature, lately with low temperature, particularly cryo-transfer, showing considerable usefulness for preservation of sensitive samples both those sensitive to vacuum and those sensitive to electron beam damage.

Thanks to its compatibility with the existing ecosystem of holders available for TEM instruments, the XtaLAB Synergy-ED is able to provide structural scientists with access to several experiment types already used in X-ray crystallography.

Cryo-transfer specimen holders such as the Gatan ELSA enable the protection of samples1 before introduction to the vacuum, allowing the study of solvates and other vacuum-sensitive species, in addition to allowing exploration of phase behaviour. Some results from samples for which cryo-transfer proved essential are discussed.

In addition, the Hummingbird Scientific MEMS biasing/heating holder offers the possibility to *increase* temperature, allowing for exploration of the phase behaviour of materials such as porous materials. Our recent results using single-crystal data from electron diffraction on a MOF system, Cu(ta)2 (Hta = 1*H*-1,2,3-triazole), at room temperature and at 200 °C were compared to a previous study by Grzywa *et al*2 of the same material from 2012 done using SC-XRD and PXRD.

Figure 1 Overlays of the ambient and high temperature phases of Cu(ta)2 from the XtaLAB Synergy-ED (blue) and the X-ray structures by Grzywa *et al.* (orange).

References:

(1) Truong *et al.*, *Symmetry* **2023**, *15(8)*, 1555.
(2) Grzywa *et al.*, *Dalton Trans.* **2012**, *41*, 4239.

Fig. 1

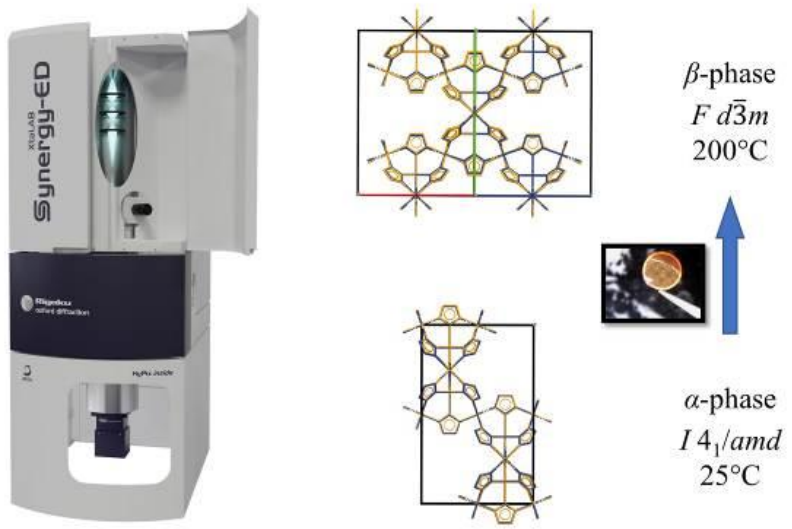

OP-101

Investigating the Structure of Synthetic Ye'elimite with 3D Electron Diffraction

C. Jandl (Villigen/CH), W. Depmeier (Kiel/DE), L. Samperisi (Villigen/CH), G. Santiso-Quinones (Villigen/CH), G. Steinfeld (Villigen/CH)

Ye'elimite – $Ca_4(AlO_2)_6SO_4$ – is the main component in calcium sulphoaluminate (CSA) based cements, which are seen as an environmentally friendly alternative to Portland cement due to their lower energy consumption and CO2 footprint during production. The structure of such synthetic Ye'elimite, however, is still uncertain and different models derived from the basic sodalite cage structure have been suggested ranging from cubic to orthorhombic symmetry.

So far, all diffraction studies on this topic were based on powder samples due to the unavailability of large enough single crystals. With the development of 3D electron diffraction (3D ED, microED) it became possible to measure crystals below 1 µm in size and thus obtain single crystal diffraction data from synthetic Ye'elimite (prepared according to *J. Chem Phys. C* **2018**, *122*, 12077 and kindly provided by Jørgen Skibsted). Our results support the proposed orthorhombic structure in space group *P*cc2. However, they still represent an averaged structure of multidomain crystals as indicated by the sulfate ion, which is disordered over two positions by rotation around one S-O bond with a slight additional tilt. Limitations of probing a single domain are given by the size of the illuminating beam and crystallite thickness. Domain formation likely originates from cooling of a higher symmetry phase obtained during the synthesis at up to 1350°C.

In addition, a related second phase was found which is formed as a by-product and might explain some of the difficulties in elucidating the structure from powder diffraction data. The results will allow a better understanding of CSA cements and can serve as models for their analysis using Rietveld refinement.

Figure 1: Representation of the unit cell of synthetic Ye'elimite crystallising in *P*cc2 with disordered sulfate ions.

Fig. 1

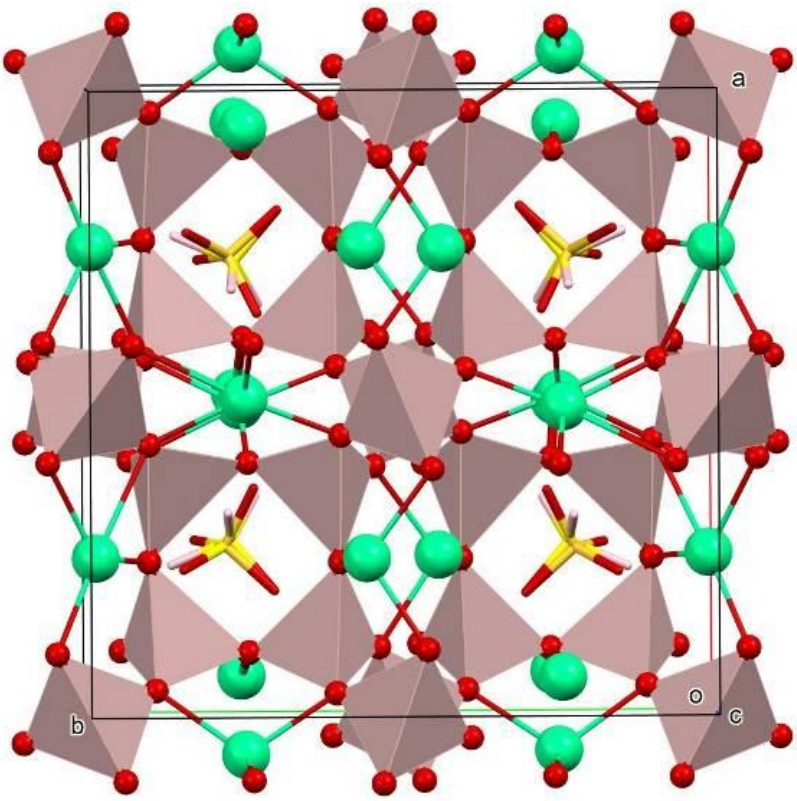

OP-102

Continuous rotation electron diffraction with the MerlinEM

G. Mangan (Oxford/GB)

The MerlinEM is a versatile hybrid pixel electron detector capable of noiseless, continuous readout. The sensor of the MerlinEM can tolerate high intensity direct electron probes with energies ranging between 30 keV and 300 keV, without the need for a beam stop. Moreover, the dynamic range of the detector is sufficiently high to record both the high intensity direct beam and low intensity high-resolution reflections simultaneously [1]. These properties of the MerlinEM make it ideal for (low-dose) three-dimensional electron diffraction (3D ED) experiments. 3D ED is an umbrella term for a set of data collection and analysis protocols involving the sequential acquisition of electron diffraction patterns and the necessary metadata for atomic structure solution [2].

Here, we focus on continuous rotation electron diffraction (cRED), -also known as MicroED- a data collection protocol in which a crystal is continuously rotated under a static parallel electron beam while electron diffraction patterns and metadata are simultaneously recorded [3]. This method is analogous to conventional single crystal X-ray diffraction (SC-XRD). However, the properties of electrons enable acquisition from nanocrystalline volumes, making 3D ED the only method suitable for data acquisition from crystals that are difficult to grow large enough for SC-XRD.

While dedicated electron diffractometers are on the market, conventional older imaging TEMs with stable goniometers can be equipped with the MerlinEM and dedicated data acquisition software to achieve comparable results at a much lower cost. We describe the implementation of cRED on a conventional TEM equipped with the MerlinEM and the freely available open-source Python software Instamatic [3] for data collection. Then, we present atomic structures of small molecules solved using direct methods from electron diffraction data collected with this protocol.

References:

(1) J.A. Mir, R. Clough, R. MacInnes, C. Gough, R. Plackett, I. Shipsey, H. Sawada, I. MacLaren, R. Ballabriga, D. Maneuski, V. O'Shea, D. McGrouther, A.I. Kirkland. Medipix3 Demonstration and understanding of near ideal detector performance for 60 & 80 keV electrons. Ultramicroscopy Volume 182, November 2017, Pages 44 - 53.

(2) Gemmi, M., Mugnaioli, E., Gorelik, T.E., Kolb, U., Palatinus, L., Boullay, P., Hovmöller, S. and Abrahams, J.P. (2019). 3D Electron Diffraction: The Nanocrystallography Revolution. *ACS Central Science*, 5(8), pp.1315–1329. doi:https://doi.org/10.1021/acscentsci.9b00394.

(3) Magdalena Ola Cichocka, Ångström, J., Wang, B., Zou, X. and Smeets, S. (2018). High-throughput continuous rotation electron diffraction data acquisition *via* software automation. *Journal of Applied Crystallography*, 51(6), pp.1652–1661. doi:https://doi.org/10.1107/s1600576718015145.

MS 28: Experimental methods V: Improvement of methods

OP-103

Refinement of anomalous dispersion parameters - more than model improvement

M. Bodensteiner (Regensburg/DE), F. Meurer (Regensburg/DE), O. V. Dolomanov (Durham/GB), F. Kleemiss (Aachen/DE), N. Peyerimhoff (Durham/GB), H. Puschmann (Durham/GB), C. Hennig (Dresden/DE, Grenoble/FR)

Correcting for anomalous dispersion takes the inelastic scattering in the diffraction experiment into account.[1] This effect, which relates closely to X-ray absorption, is specific to each chemical compound and particularly sensitive to radiation energies near the absorption edges of the elements in the compound. The widely used tabulated values for these corrections are only approximations, as they are based on calculations for isolated atoms.[2] Features of the unique spatial and electronic environment are ignored, although these can be spectroscopically observed. This significantly affects the fit between the crystallographic model and the measured intensities. The dispersive (*f'*) and absorptive (*f''*) terms of the anomalous dispersion can be refined as independent parameters in the full-matrix least-squares refinement.[3] This procedure has now been implemented as a new feature in the well-established Olex2 software.[4]

The presentation will report on synchrotron multi-wavelength single-crystal X-ray diffraction as well as X-ray absorption spectroscopy experiments. It will further show strong deviations observed with home laboratory sources even far from an absorption edge and provide an outlook for determining oxidation states in organometallic compounds. The figure shows the changes of *f'* and *f''* depending on the oxidation state of Co obtained from in-house experiments using Cu-K_α radiation.

References:

(1) S. Caticha-Ellis, *Anomalous Dispersion of X-rays in Crystallography* **1981;** [2] a) B. L. Henke, E. M. Gullikson, J. C. Davis, *At. Data Nucl. Data Tables* **1993**, *54*, 181–342; b) S. Brennan, P. L. Cowan, Rev. Sci. Instrum. **1992**, *63*, 850–853; c) S. Sasaki, *KEK Report* **1989**, *88*, 1–136; [3] O. Einsle, S. L. A. Andrade, H. Dobbek, J. Meyer, D. C. Rees, *J. Am. Chem. Soc.* **2007**, *129*, 2210–2211; [4] F. Meurer, O. V. Dolomanov, C. Hennig, N. Peyerimhoff, F. Kleemiss, H. Puschmann, M. Bodensteiner, *IUCrJ* **2022**, *9*, 604– 609.

Fig. 1

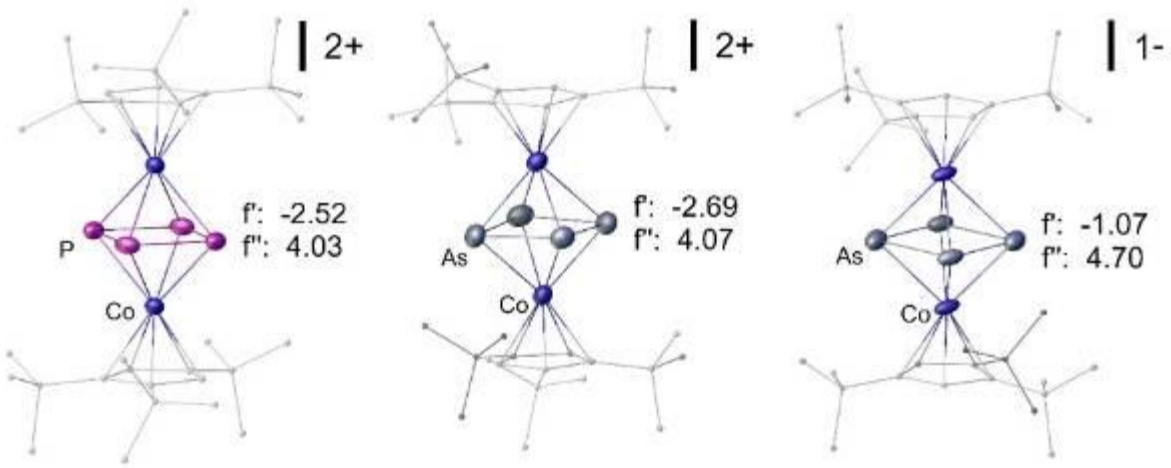

OP-104

How to harness In K_α radiation from a METALJET for high resolution experiments

D. Stalke (Göttingen/DE)

The MetalJet source provides new available K_α radiation wavelength for use in X-ray diffraction experiments.[1] Here we want to demonstrate the application of using indium K_α radiation in independent atom model refinement, as well as approaches using aspherical atomic form factors. Results vary strongly with the employed detector as the energy cut-off of the Eiger2 CdTe provides a solution to a unique energy contamination problem of the MetalJet In radiation, which the Photon III detector cannot provide.[2]

References:

(1) Nico Graw, Paul Niklas Ruth, Tobias Ernemann, Regine Herbst-Irmer, Dietmar Stalke "Indium *K*α radiation from MetalJet X-ray source: The long way to a successful charge density investigation" *J. Appl. Cryst.* 2023, *56,* 1315-1321; https://doi.org/10.1107/S1600576723007203.

(2) Paul Niklas Ruth, Nico Graw, Tobias Ernemann, Regine Herbst-Irmer, Dietmar Stalke "Indium *K*α radiation from MetalJet X-ray source: Comparison of the Eiger2 CdTe and Photon III detectors" *J. Appl. Cryst.* **2023**, *56,* 1322-1329; https://doi.org/10.1107/S1600576723007215.

Fig. 1

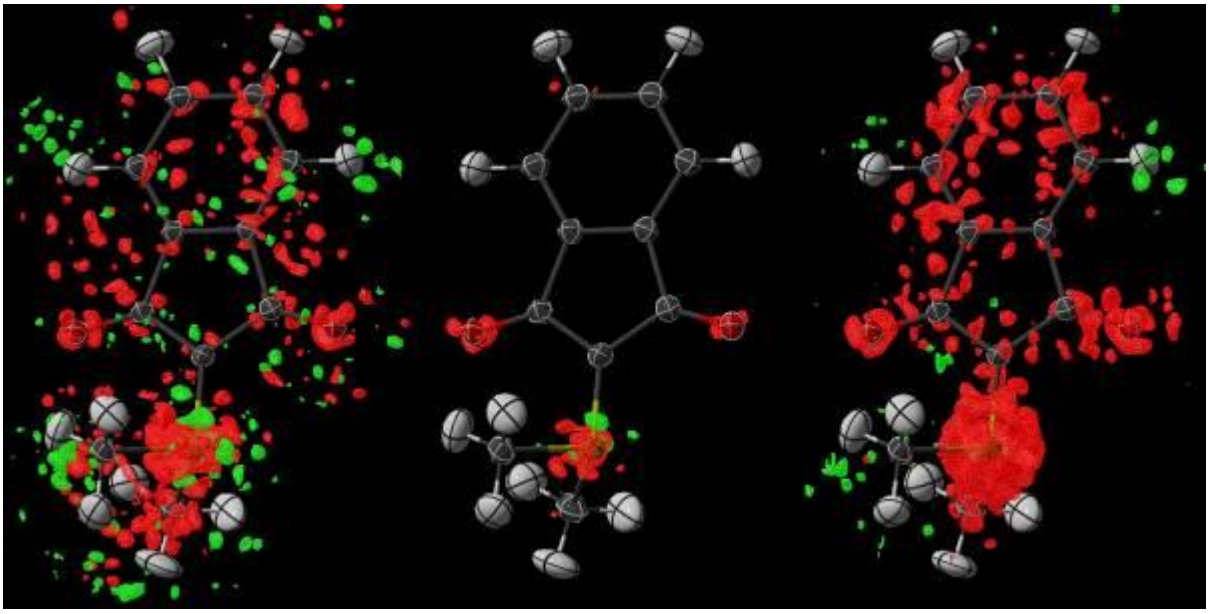

OP-105

A new approach for high-resolution powder diffraction with a small 2-D detector

C. Hennig (Grenoble/FR), V. Svitlyk (Grenoble/FR), M. Feig (Grenoble/FR), R. Gumeniuk (Freiberg/DE), J. Kieffer (Grenoble/DE)

The highest resolution in powder diffraction is nowadays achieved at the synchrotron diffractometers equipped with analyzer crystals [1,2]. These diffractometers usually use a fixed wavelength because the setting of the analyser is very complex. A weak point for diffractometers located on bending magnets is that a large part of intensity is lost at the analyzer. A new development in recent years is the use of very large single photon counting detectors, which can record a complete diffractogram in a few milliseconds. Since these detectors have to be placed close to the sample, the achieved resolution is not high.

Fig. 1. Left: Section of LaB6 scattering cone. Right: Result of the radial integration.

A new powder diffraction unit was developed, with the ability to scan a small 2D detector at a very large distance to the sample stepwise to high scattering angles. All individual angular positions of the detector must be precisely calibrated. This is achieved in a semi-atomic routine and multiple standards [3]. The resolution (see Fig. 1) reaches that of some synchrotron diffractometers with analyzer crystals [4]. The high efficiency of the detector enables a very high count rate. Diffraction with analyzers suffer often at small scattering angles from asymmetric peaks due to axial divergence. This is avoided by radial integration of the detector content. By using a small detector on a rotating detector arm, the x-rays always hit the detector perpendicularly. This excludes peak asymmetry at low scattering angles. The applied technique and selected examples will be discussed.

References:

(1) Hodeau, J. L., et al., Proc. SPIE 3448 (1998) 353–361.
(2) Dejoie, C. J. et al., Appl. Cryst. 51 (2018) 1721-1733
(3) Kieffer J. et al., J. Synchrotron Rad. 27 (2020) 558-566
(4) Sitaud B. et al. *J. Nucl. Materials* 425 (2012) 238-243

Fig. 1

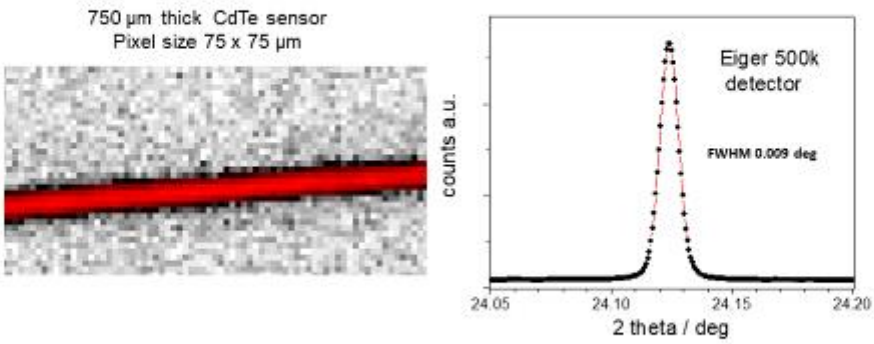

Page 2

OP-106

Direct detection in CdTe enables high efficiency for short- and dual-wavelength instruments

M. Müller (Baden-Daettwil/CH)

The use of short wavelengths can make the difference between failure and success or have a substantial effect on the data quality in different kinds of diffraction experiments. This applies in particular in the fields of high-pressure and quantum crystallography or when strongly absorbing samples are investigated. However, the measurement of short-wavelength data is often hampered by the lower quantum efficiency for short-wavelength radiation compared to copper radiation that various types of detectors commonly used in X-ray diffraction exhibit. Optimizing the detectors" efficiency for short wavelengths usually comes at the expense of reduced efficiency for copper radiation.

Recent advances in the use of cadmium telluride as a sensor material for Hybrid Photon Counting (HPC) detectors provide a solution to the problem of reduced efficiency for either short wavelength or copper radiation. HPC technology and direct detection in CdTe sensors enables high efficiency for both short wavelength and copper radiation.

This presentation will highlight why HPC detectors equipped with CdTe sensors are a universal solution for high efficiency with any radiation type commonly used in single-crystal diffraction and will outline some of the other benefits of HPC technology and direct detection.

Poster session I: Chemical crystallography

PP-001

Synthesis and characterization of tin- and zirconium-substituted ferrites

Y. M. Dreer (Stuttgart/DE), R. Niewa (Stuttgart/DE)

The synthesis of substituted hexaferrites is an ongoing field of interest due to their tunable magnetic properties. Their applications range from data storage, permanent magnets and waste water treatment to microwave, optical and diagnostic devices [1]. The aim of this work was the synthesis and crystal growth of the M-type ferrite $BaFe_{12-x}M_xO_{19}$ with M = Sn, Zr and $0.1 \leq x \leq 1.6$, in order to investigate the influence of the substitution on the structure. Via flux growth, single crystals with edge lengths up to 1.0 mm were obtained.

Both structure refinements based on powder and single crystal XRD show that the lattice parameters of $BaFe_{12-x}M_xO_{19}$ increase with increasing degree of substitution. Furthermore, the Fe(4)-atoms (Wyckoff site 4*f*) in the center of face-sharing octahedra doubles from oxide anions were determined as the preferred position of the M^{4+}-cations for mixed site occupation. Due to the substitution of Fe^{3+} with M^{4+}-ions, it is most likely that some iron ions are reduced to Fe^{2+} to maintain charge neutrality, as it was already investigated in the corresponding system with titanium. Additionally, defects can occur in the structure as counterbalance to the positive charges brought in by the M^{4+}-ions [2].

Microprobe analyses indicate that the maximum degree of substitution is around $x_{Sn} = 1.3$ for tin and $x_{Zr} = 0.8$ for zirconium at a synthesis temperature of $T = 1300$ °C, which is in good agreement with SCXRD results. A qualitative mapping via microprobe shows, that the elements are distributed homogeneously throughout the crystals surfaces. However, WDX measurements also indicate that various crystals from the same synthesis experiment can vary in composition.

Literature:

(1) R. C. Pullar, *Prog. Mater. Sci.* **2012**, 57, 1191. [2] K.-I. Mehnert, M. Häßner, Y. M. Dreer, I. Biswas, R. Niewa, *Inorganics* **2023**, *11*, 207.

PP-002

Crystal structure redetermination of tetragonal $LiSr_2NH_2$

C. Liang (Stuttgart/DE), R. Niewa (Stuttgart/DE)

For $LiSr_2NH_2$ two modifications were reported in literature, namely an orthorhombic one in *Pnma* [1] and a tetragonal one in *I4/mmm* [2, 3]. We have synthesized the tetragonal form in single phase bulk through ball milling of $LiNH_2$ with SrH_2 and grown single crystals via the reaction of strontium metal with LiH and Li_3N in a sealed niobium ampoule using lithium flux at 600 °C. The crystal structure was determined via powder and single crystal X-ray diffraction. The obtained structural data reveals that $LiSr_2NH_2$ crystallizes in space group *I4mm* (No. 107), with lattice constants of a = 3.7877(3) Å, c = 13.4093(8) Å, in contrast to the previous structural model, derived solely from powder diffraction in the centrosymmetric space group *I4/mmm* [2, 3].

The crystal structure solution in the non-centrosymmetric space group resolves the partial occupation and disorder in the previous reports [2, 3]. The structure of $LiSr_2NH_2$ can be considered as a stuffed variant of the K_2NiF_4 type. Rocksalt-kind layers of N-centered edge-sharing distorted octahedra $^{2}_{\infty}[Li_{1/1}Sr_{1/1}Sr_{4/4}N]$ are stacked along c, with the lithium vertices all pointing in the same direction, leaving ample space for hydride ions in between. Hydride ions in turn connect the former layers by a $^{2}_{\infty}[Li_{2/4}Sr_{4/4}H]$ layer of mutually face-sharing octahedra.

We compare structures of the two tetragonal models and the orthorhombic form and discuss thermodynamic phase relations.

References:

(1) B. Blaschkowski. Th. Schleid, *Z. Anorg. Allg. Chem*. **2007**, *633*, 2644.
(2) D.M. Liu, Q.Q. Liu, T.Z. Si, Q.A. Zhang, *J. Alloys Compd.* **2010**, *495*, 272.
(3) G. Jiang, N. Matsui, T. Mezaki, Y. Toda, K. Suzuki, M. Hirayama, T. Saito, T. Kamiyama, R. Kanno, *J. Solid State Chem.* **2022**, *310*, No.123051.

PP-003

Metal-organic frameworks for gas storage applications

A. Kochel (Wrocław/PL), M. Hołyńska (Eindhoven/NL)

Metal-organic frameworks (MOFs) have 1D-3D structures comprising metal ions linked with organic ligands and being porous subgroup of coordination polymers. Their potential applications include reversible gas exchange which is of relevance for mixture separation and energy storage. Recently also water adsorption and heat exchange have become relevant motivation to study MOFs.

In our studies, MOFs are obtained solvothermally in Berghoff pressure reactor. Polydentate ligands are used, mainly aminocarboxylate acids with multiple N/O donor atoms. The synthesis is one-pot and leads to crystalline products. The reaction outcomes are influenced by reaction time, amounts of the reagents, pH and temperature values. The scheme below shows example of luminescent Cu(I,II) coordination polymer.

Figure: 3D coordination polymer with aminocarboxylate ligand and Cu(I)(II).

Fig. 1

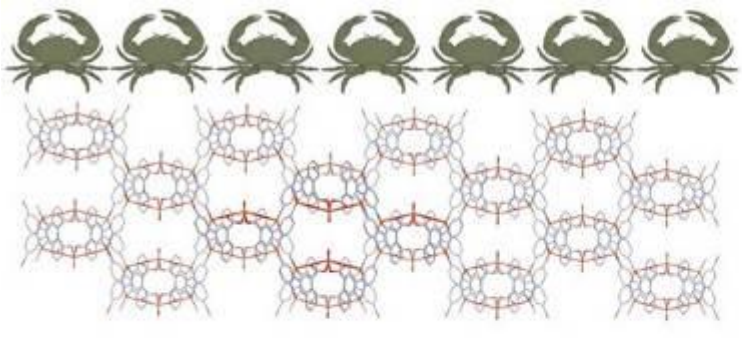

PP-004

$(Sr_9N_{1.34(8)})[SrIn_3](CN_3)$ - a new guanidinate accessible from pressure-less sodium flux synthesis

R. Stelzer (Stuttgart/DE), Y. Wang (Aachen/DE), R. Dronskowski (Aachen/DE), R. Niewa (Stuttgart/DE)

As the sphere of nitrides is explored, the quest for new classes of compounds becomes a vital part for successful research as nitride compared to oxide chemistry still remains less explored. Recently, the fully deprotonated guanidinate anion was discovered by synthesis in a diamond anvil cell at high pressure and found to be relatively stable at ambient pressure and temperature [1]. Herein, we present a guanidinate compound accessible from alkali metal flux synthesis in metal ampoules and interpret the structure through wavefunction-based COHP [2] and COBI [3] analysis.

This new compound with the chemical formula $(Sr_9N_{1.34(8)})[SrIn_3](CN_3)$ consists of threefold capped trigonal prismatic coordinated (CN_3) units, $(Sr_9N_{1.34(8)})$ octahedra doubles and $[SrIn_3]$ chains along *c*. Synthesis was achieved in Ni ampoules with sodium flux. The compound is highly sensitive to irradiation at ambient temperatures.

The planar $(CN_3)^{5-}$ unit is located on a center of symmetry which leads to a (N–C–N)-angle of 120° and C–N distances of 1.387(9) Å, which is consistent with recent findings in compounds synthesized under high pressures [1]. The C–N distance is longer than those found in guanidine and the C–O distance in carbonates. The chemical bonding analysis implemented in LOBSTER [4] was performed in both two center and multicenter manners, showcasing significant multicenter interactions in the $(CN_3)^{5-}$ anion. Further charge analysis also suggests negatively charged In atoms.

We conclude that we made the new class of guanidinates more accessible by a pressure-less synthetic route. This opens the possibility to explore metathesis reaction and coordination behavior of the $(CN_3)^{5-}$ ion.

References:

(1) Aslandukov *et al.*, *Angew. Chem. Int. Ed.* 2023, e202311516; Brüning *et al.*, *Angew. Chem. Int. Ed.* 2023, e202305585.
(2) Dronskowski *et al.*, *J. Phys. Chem.* 1993, ***97**, 8617–8624.*
(3) Müller *et al.*, *J. Phys. Chem. C* 2021, ***125**, 7959–7970.*
(4) Nelson *et al.*, *Journal of Comput. Chem.* 2020, ***41**, 1931–1940.*

Fig. 1

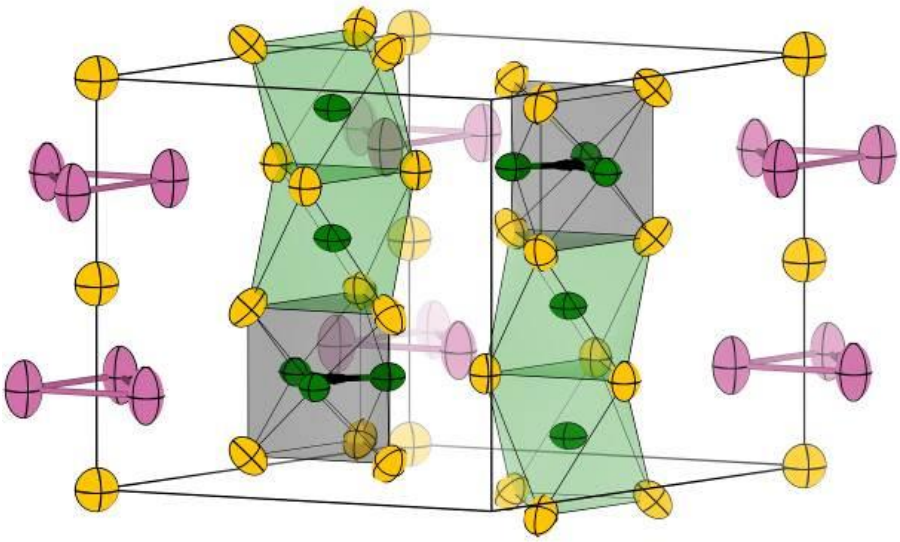

Fig. 2

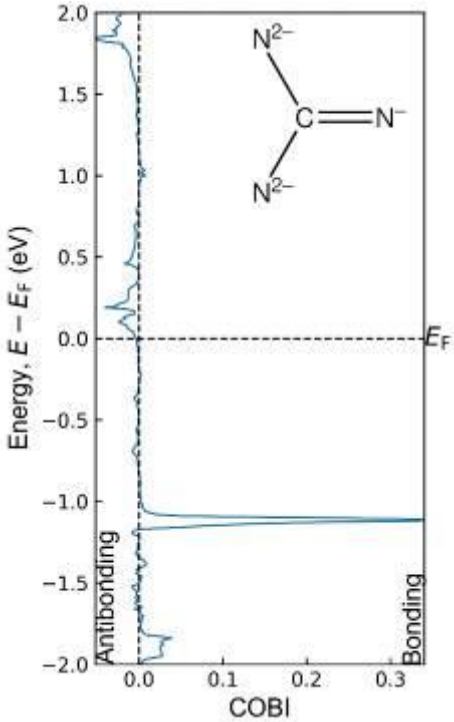
2.0
1.5
1.0
0.5
0.0
−0.5
−1.0
−1.5
−2.0
Energy, $E - E_F$ (eV)
E_F
Antibonding
Bonding
0.0
0.1
0.2
0.3
COBI
N^{2-}
C
N⁻
N^{2-}

PP-005

Investigations on Compounds related to the Structure Type $Na_2K_{21}Tl_{19}$

V. Schwinghammer (Regensburg/DE), S. Gärtner (Regensburg/DE)

The combination of alkali metals with the more electronegative group 13 element thallium became of greater interest after the discovery of NaTl by *E. Zintl* in the early 1930s.[1] The investigations on this class of compound resulted in various binary and ternary materials with different A_xTl_y (*A*=Li-Cs) compositions.[2] In case of a single type of alkali metal, there are so far only five phases with discrete clusters known so far, which include four different types of clusters, $[Tl_4]^{4-}$ in Na_2Tl[3], $[Tl_{11}]^{7-}$ in A_8Tl_{11} (*A*=K-Cs)[4,5], $[Tl_7]^{7-}$ in $K_{10}Tl_7$[6] and the compressed $[Tl_6]^{6-}$ in KTl[7] and CsTl[8]. Combining two alkali metals allows for the observation of additional cluster types, as Tl_5 and Tl_9 are only present in the crystal structures of mixed alkali metal thallides. Both, $[Tl_5]^{7-}$ and $[Tl_9]^{9-}$ are observed in the compound $K_{21}Na_2Tl_{19}$ on which the group of *J. D. Corbett* reported in 1994.[9]

During our investigations on the role of the different alkali metals in alkali metal thallides, we prepared binary and ternary approaches according to the $A_{23}Tl_{19}$ (*A*=Na-Cs) stoichiometry. EDS was applied to confirm the right composition, additionally DFT calculations were carried out to allow deeper insight in the electronic structure of the compounds.

References:

(1) E. Zintl, W. Dullenkopf, *Z. phys. Chem.* **1932**, *B16*, 195-205.;
(2) S. Gärtner, *Crystals* **2020**, 10, 1013.;
(3) D.A. Hansen, J.F. Smith, *Acta Crystallogr.* **1967**, 22, 836-845.;
(4) W. Blase et al., *Z. Naturforsch.* **1993**, *48b*, 754-760.;
(5) Z.-C. Dong, J.D. Corbett, *J. Clust. Sci.* **1995**, 6, 187-201.;
(6) S. Kaskel, J. D. Corbett, *Inorg. Chem.* **2000**, *39*, 778-782.;
(7) Z. C. Dong, J. D. Corbett, *J. Am. Chem. Soc.* **1993**, *115*, 11299-11303.;
(8) Z. C. Dong, J. D. Corbett, *Inorg. Chem.* **1996**, *35*, 2301-2306.;
(9) Z. C. Dong, J. D. Corbett, *J. Am. Chem. Soc.* **1994**, *116*, 3429-3435.

Fig. 1

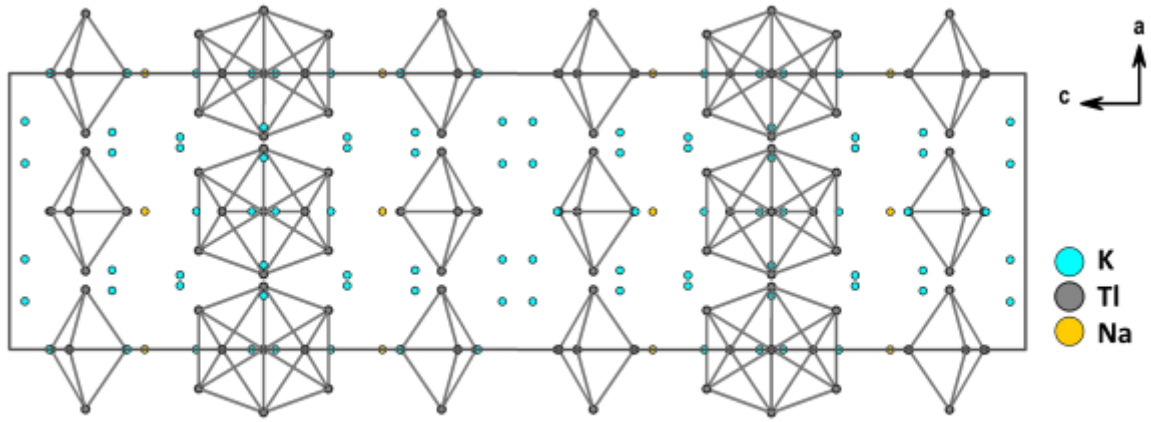

Figure 1: Unit cell of $Na_2K_{21}Tl_{19}$ in crystallographic *b* direction.

PP-006

Hydrogen Bonding in the Solid State of *N*,*N*'-biscarbamoyl ureas, *N*,*N*'-Carbonyl bis(carbamates) and -(*S*-thiocarbamates)

J. Pfeiffer (Marburg/DE), M. Möbs (Marburg/DE), S. Reith (Marburg/DE), M. Diels (Marburg/DE), F. Tambornino (Marburg/DE)

The derivatives of triurea, tri carbonyl group containing molecules, are known, but the present studies do not focus on the characterisation of their crystal structures. Until today, the crystal structures of only three molecules were analysed in the solid state.[1,2] Within this work we fill this gap and present the crystal structures of *N*,*N*'-biscarbamoyl ureas, *N*,*N*'-carbonyl bis(carbamates) and *N*,*N*'-carbonyl bis(*S*-thiocarbamates), focusing both on the intramolecular hydrogen bonding and their extended hydrogen bonding networks.[3]

All compounds form a six membered ring *via* an intramolecular hydrogen bond from an N–H to a O=C moiety. This motif is more stable than the open-chain form, as has already been shown.[4] In addition, they form *via* intermolecular hydrogen bonds either dimers, or extended networks in the form of strands by connection to neighbouring molecules. This leads to stacking of the molecules in the extended crystal structure along specific crystallographic axes. Together with Hirshfeld surface analysis, the influence of the substituted group (amide, alkoxide or sulfide) for the hydrogen bond formation is showcased. Bulkier aryl or alkyl groups lead to a change from polar interactions being prominent, to increasingly higher non-polar van der Waals interactions.

References:

(1) A. D. Mahapatra, A. Shaik, V. Thiruvenkatam, B. Datta, *J. Mol. Struct.* **2021**, *1233*, 130158.
(2) T. M. Klapötke, B. Krumm, S. F. Rest, M. Sućeska, *Z. Anorg. Allg. Chem.* **2014**, *640*, 84–92.
(3) J. Pfeiffer, M. Möbs, S. Reith, M. Diels, F. Tambornino, *J. Mol. Struct.* **2023**, *submitted*.
(4) J. Pfeiffer, H. Günther, L. Völlinger, D. Botros, B. Scheibe, M. Möbs, F. Kraus, F. Weigend, F. Tambornino, *Chem. – A Eur. J.* **2023**, e202203983.

PP-007

First molecular structure elucidation of a geminal and a vicinal bis(triflate) ester

T. Pickl (Garching/DE), J. Zuber (Garching/DE), J. Stephan (Garching/DE), A. Pöthig (Garching/DE)

The trifluoromethanesulfonate group (–OTf) is an important functional group in organic chemistry because of its strong electron-withdrawing nature.[1] Thus, derived triflyl esters (R–OTf) are potent electrophiles. Pushing the reactivity of these compounds to an extreme, two triflate groups can be attached to the same carbon to form a geminal bis(triflate) ester, TfO–CH2–OTf (**1**), which has been used as an extremely electrophilic C1 synthon for the construction of macrocyclic molecules.[2] Similarly, vicinal bis(triflate) ester TfO–(CH2)2–OTf (**2**) has been used as an analogous C2 fragment in chemical synthesis.[3] To find relationships between the extreme electrophilicity of these alkylene sources and their solid-state properties, we aimed to elucidate the molecular structure by SC-XRD. While analogous mesylates and tosylates have already been investigated structurally, this study presents the first structures of a geminal and vicinal bis(triflate). Single crystals of **1** and **2** suitable for SC-XRD were grown by allowing the liquids to solidify over several hours at 4 °C. Well-diffracting thin plates of **1** and **2** were measured as two-component twins on a *Bruker* D8 Venture SC-XRD equipped with a *Bruker* Photon III CPAD detector, a TXS rotating anode with MoKα radiation (λ = 0.71073 Å) and *Helios* optics. Geminal bis(triflate) **1** crystallized in the space group $P2_1$ while vicinal bis(triflate) **2** crystallized in *P*-1. The packing of **1** and **2** is dominated by intermolecular F–F interactions closer than the sum of the *vdW* radii, created by the spatial arrangement of trifluoromethyl residues. For **1**, the respective bis(triflates) form alternating 2D layers of fluorous and non-fluorous domains, while for **2**, packing is completely dominated by fluorous domains between triflate groups of the molecules.

References:

(1) *Chem. Rev.* **1977,** *77* (1), 69-92.
(2) *Inorg. Chem.* **2015,** *54* (8), 3797-3804.
(3) *Synthesis* **2006,** *2006* (01), 146-150.

Bis(triflates) **1** and **2**.

Fig. 1

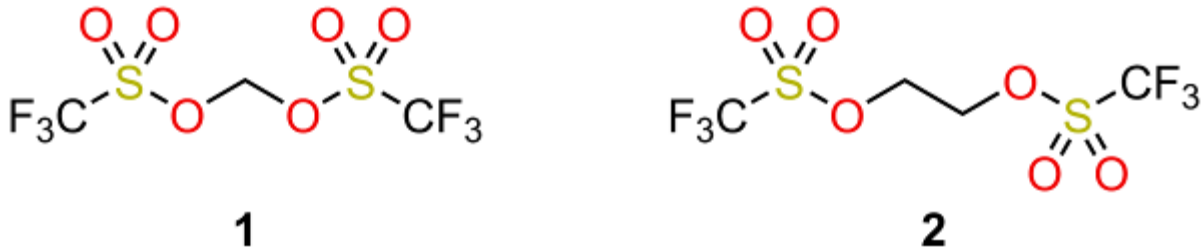

PP-008

Structure determination of liquid compounds using capillary crystallisation

N. Nöthling (Muhlheim an der Ruhr/DE)

A limiting factor in crystal structure determination is often the growth of suitable single crystals. In particular, when the compounds are in a liquid state at room temperature, it is not possible to use conventional crystallisation methods. To obtain detailed crystallographic information from such liquid compounds, capillary crystallisation is a simple and powerful tool in chemical science. The first developments in capillary crystallography took place over 70 years ago.[1] Our work focuses on the determination of new crystal structures of chemically and industrially relevant compounds. The crystals are grown from the neat liquid by capillary crystallisation via zone freezing in a cold N2 gas stream. This method provides a rapid and non-destructive way of determining molecular structures. Further advantages are the small sample size and the fact that no additives or host compounds are required. Here we report our experience of growing single crystals in glass capillaries in a cold N2 gas stream (Figure 1).

Figure 1. Experimental set up and procedure for crystal growth in a capillary.

Since the beginning of our work, we have already been able to clarify several unknown structures. Structures have been obtained from chemical precursors, highly reactive compounds, mixtures, and fragrances and flavourings [2-5]. Studies on quantitative mixtures of two different compounds are currently underway.

References:

(1) Kaufman, H. S. & Fankuchen, I. **1949** *Rev. Sci. Instrum.*, 20, 733-734.
(2) Seidel, R. W., Goddard, R., Nöthling, N. & Lehmann, C. W. **2016** *Acta Crystallogr. C*, 72, 753–757.
(3) Bodach, A., Nöthling, N. & Felderhoff, M. **2021** *Eur. J. Inorg. Chem.*, 2021, 1240 – 1243.
(4) Patzer, M., Nöthling, N., Goddard, R. & Lehmann, C. W. **2021** *Chemistry*, 3, 578-584.
(5) Seidel, R. W., Goddard, R., Nöthling, N. & Lehmann, C. W. **2019** *CrystEngComm.*, 21, 3295-3303.

Fig. 1

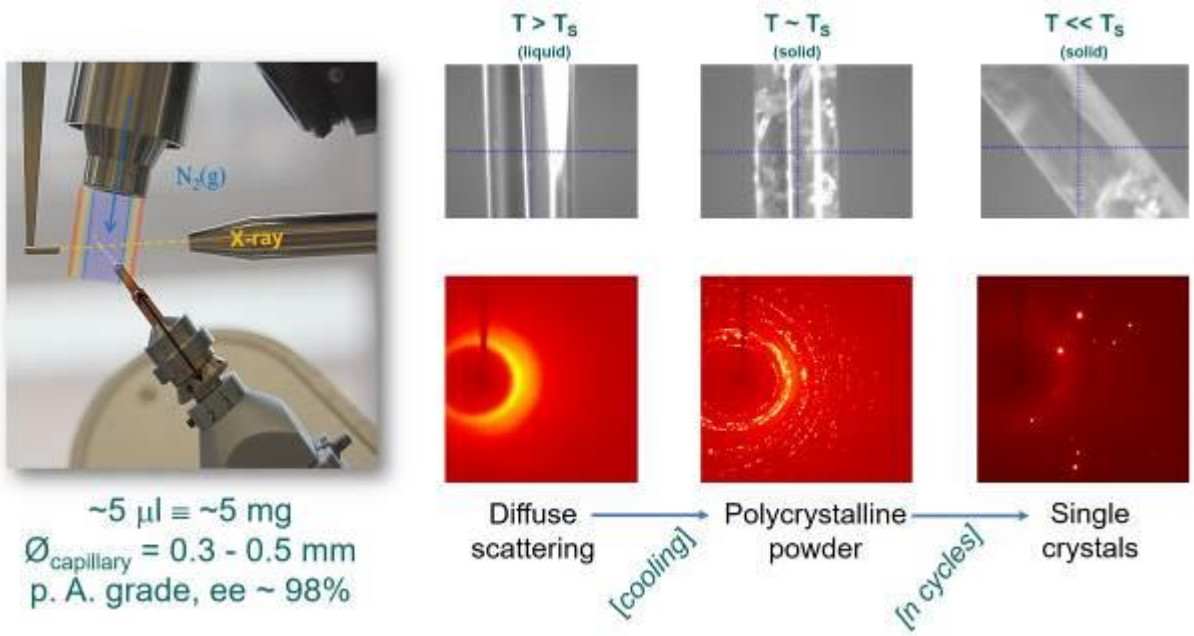

PP-009

$Pb_2(Pb_{1-x}Sn_x)O_4$: characterization of temperature-dependent structure-property relations

C. S. Reuter (Bremen/DE), M. M. Murshed (Bremen/DE), T. M. Gesing (Bremen/DE)

The known schafarzikite mineral group members of O8 mullite-type, Pb_2MO_4 crystallize in space group *P4₂/mbc* and *Pbam*, respectively, for M = Pb and Sn. The successful synthesis by solid-state reactions in sealed quartz tubes and subsequent characterization of the $Pb_2(Pb_{1-x}Sn_x)O_4$ solid solution indicated a room-temperature symmetry change from tetragonal to orthorhombic for compounds with x > 0. Pb_2PbO_4 itself shows a symmetry reduction from tetragonal to orthorhombic at 170 K [1] and being then isostructural to the room-temperature polymorph of Pb_2SnO_4. This phase doesn"t show any symmetry changes at low temperatures [2]. Through XRPD measurements between 300 K and 1250 K as well as DTA investigations significant changes in the behavior within the solid solution could be obtained. While heating Pb_2PbO_4 results in the formation of β-PbO, Pb_2SnO_4 performs a symmetry change from orthorhombic to tetragonal above 1050(10) K, which is identical with the low-temperature phase transition of Pb_3O_4. Further heating led to its decomposition to β-PbO and SnO_2 at 1340(10) K. Samples of the solid solution with x < 0.8 show slow decomposition above 900(10) K, leading to the release of β-PbO and formation of orthorhombic Pb_2SnO_4 which then undergoes a phase-transition to the tetragonal phase. For x ≥ 0.8, a direct phase transition from the orthorhombic to tetragonal $Pb_2(Pb_{1-x}Sn_x)O_4$ is observed without any observable decomposition steps. Temperature-dependent Raman spectroscopy compliment the results.

Figure 1: Crystal structure of $Pb_2(Pb_{0.5}Sn_{0.5})O_4$ and formation of tetragonal Pb_2SnO_4 and β-PbO

References:

(1) J.R. Gavarri, D. Weigel, A.W. Hewat, J Solid State Chem 23(3-4) (1978) 327-339.
(2) J.P. Vigouroux, E. Husson, G. Calvarin, N.Q. Dao, Spectrochim. Acta A 38 (1981) 393-398.

We gratefully acknowledge the DFG for financial support withing the Project GE1981/18-1

Fig. 1

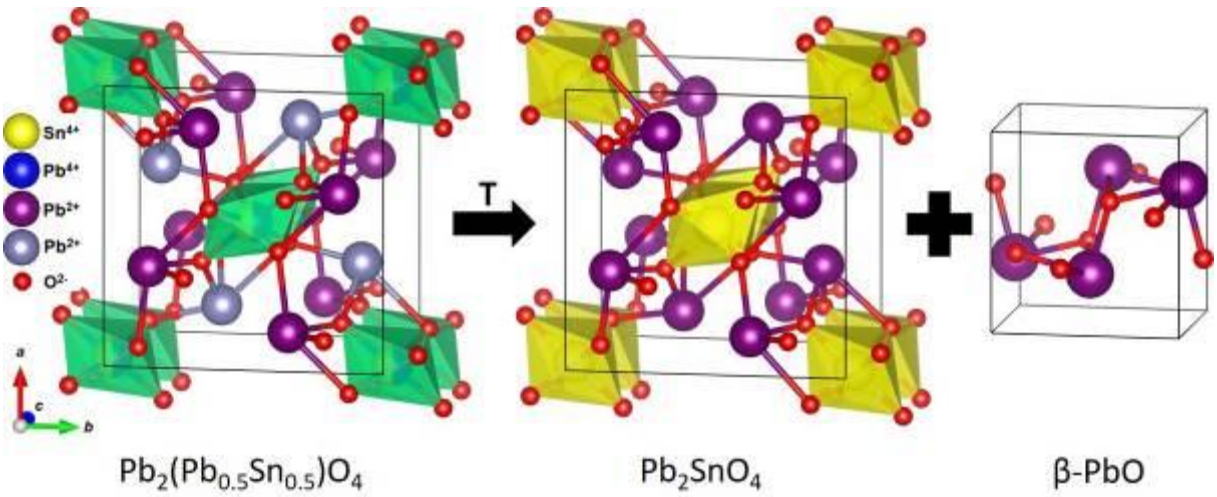

PP-010

Two New Iodate Selenites in Search for Non-linear Optical Properties

K. Eble (Freiburg i. Br./DE), H. Hillebrecht (Freiburg i. Br./DE)

Non-linear optics play a large role in the development and improvement of lasers, one of the most important technologies of today and the future. Currently, much research is being done in the field of non-linear optical materials, with a primary focus on finding and developing new materials which can be used with lasers to produce non-linear optical effects, such as second harmonic generation (SHG). This is due to limitations found in many available materials, such as poor physical or chemical stability, low SHG response, or a low laser damage threshold. Finding suitable candidates for use as non-linear optical materials proves to be a large challenge, however, as such materials must fulfill certain criteria in order to show effects such as SHG, the most important of which is lacking an inversion center in the unit cell.

One group of materials which shows much promise is that of iodate selenites. Besides compounds which we have previously presented, there are now two new compounds of the rare iodate selenite group which we are presenting in this work, namely $In(IO_3)(SeO_3)$ and $Ho(IO_3)(SeO_3)$.

$In(IO_3)(SeO_3)$ and was found using a similar strategy as illustrated by Wang et al., namely orientating around a known compound, replacing an anion with the desired one and balancing the created difference in charge with a cation of now fitting charge and similar size to the original cation, this technique is known as aliovalent substitution.[1] Here, hexagonal ($P6_3$) $Mg(IO_3)_2$ served as the inspiration for $In(IO_3)(SeO_3)$, whereby one $(SeO_3)^{2-}$ unit was replaced by $(IO_3)^-$, and Mg^{2+} by the appropriately charged In^{3+}, which also happens to be similar in size to its role model. This lead to hexagonal ($P6_3$) $In(IO_3)(SeO_3)$, which shares the same space group and very similar cell parameters with $Mg(IO_3)_2$. Monoclinic ($P2_1/c$) $Ho(IO_3)(SeO_3)$ was found individually, without using aliovalent substitution.

References:

(1) Y. Wang et al., *Inorg. Chem.* **56**(6), *2017,* 3702

PP-011

Crystal Structures of the Phosphidosilicates $Mg_2Sr_3Si_{20}P_{30}$ and $MgSr_3Si_3P_7$

J. Aicher (Munich/DE), D. Johrendt (Munich/DE)

Relatively few quaternary phosphidosilicates have been published so far. The fundamental building unit within these compounds are $[SiP_4]$-tetrahedra, making them structurally related to the silicates. A condensation of the tetrahedrons via edges or vertices, forming negatively charged chains or networks and the ability to form P-P bonds allows for a large structural variety.[1-2]

While three quaternary magnesium phosphidosilicates have been reported, only one quaternary strontium phosphidosilicate is known, namely $Na_3(Na_{1.15}Sr_{1.85})SiP_4$.[3-5] Here we report two new quaternary phosphidosilicates with magnesium and strontium crystallizing in the hexagonal space group $P6_3$ and the trigonal space group $P31m$, respectively.

$Mg_2Sr_3Si_{20}P_{30}$ and $MgSr_3Si_3P_7$ were obtained by solid state reaction at 850 °C. In $Mg_2Sr_3Si_{20}P_{30}$ ($P6_3$, a = 15.7767(4) Å, c = 11.7407(4) Å), the $[SiP_4]$-tetrahedra are connected via vertices forming a highly condensed network. $MgSr_3Si_3P_7$ ($P31m$, a = 18.7339(5) Å, c = 6.1393(3) Å) crystallizes likewise in a new structure type with a network of three $[SiP_4]$-tetrahedra connected by vertices. Three units of this motive are repeatedly connected via vertices building a network in which the magnesium is located. One phosphorus position is not bonded to silicon but resides in Sr6 octahedra, which form chains via common faces. These P-atoms are shifted from the octahedron centres and form chains of P-P dumbbells running along the *c*-axis.

References:

(1) B. Eisenmann, M. Somer, *Z. Naturforsch. B: Anorg. Chem. Org. Chem. Biochem. Biophys. Biol.* **1984**, *39*, 736–738.
(2) J. Mark, J. Wang, K. Wu, J. G. Lo, S. Lee, K. Kovnir, *J. Am. Chem. Soc.* **2019**, *141*, 11976–11983.
(3) J. Chen, H. Chen, F. Xu, L. Cao, X. Jiang, S. Yang, Y. Sun, X. Zhao, C. Lin, N. Ye, *J. Am. Chem. Soc.* **2021**, *143*, 10309–10316.
(4) J. Wang, J. T. Greenfield, K. Kovnir, *Inorg. Chem.* **2017**, *56*, 8348–8354.
(5) J. Nuss, H. Kalpen, W. Hönle, M. Hartweg, H. Von Schnering, *Z. Anorg. Allg. Chem.* **1997**, *623*, 205–211.

PP-012

$Rb_4[As_2S_{10}]$: A Rubidium Polythioarsenate(V) with an Unusual Discrete $[S_3AsS(S_2)SAsS_3]^{4-}$ Anion

K. Engel (Stuttgart/DE), T. Schleid (Stuttgart/DE)

Since polythioarsenate and -phosphate fluxes were successfully used during the syntheses of quaternary thioarsenates and -phosphates in the past, it is surprising that for thioarsenates just a few $[As_xS_y]^{n-}$ anions such as $[AsS_4]^{3-}$ and $[AsS_3]^{3-}$ are known [1,2]. In an attempt to expand the diversity of thioarsenates, $Rb_4[As_2S_{10}]$ as the first alkali-metal polythioarsenate(V) that includes discrete $[S_3AsS(S_2)SAsS_3]^{4-}$ anions occurred.

$Rb_4[As_2S_{10}]$ was synthesized from a mixture of Rb_2S:As_2S_5:S in a molar ratio of 2:1:7, which was heated up to 500 °C in a glassy silica ampoule. Single-crystal XRD shows that $Rb_4[As_2S_{10}]$ crystallizes monoclinically in the space group $P2_1/c$ with a = 1735.21(9) pm, b = 699.36(4) pm, c = 2355.83(12) pm and β = 93.975(3)° for Z = 6. The crystal structure is characterized by discrete $[As_2S_{10}]^{4-}$ units, so far unknown for arsenic compounds, separated by Rb^+ cations with C.N.(Rb^+) = 8 – 10. These anions are built by two $[AsS_4]^{3-}$ tetrahedra linked by a disulfide unit $(S_2)^{2-}$ forming a tetrasulfide chain in the center of each $[S_3AsS(S_2)SAsS_3]^{4-}$ entity. This As^{5+}-bridging chain occurs in different conformations, since the torsion angle in $[(As1)(As2)S_{10}]^{4-}$ equals 89.7°, but is 180° for $[(As3)_2S_{10}]^{4-}$. Compared with similar polythiophosphates(V) $A_4[P_2S_{10}]$ (A = Rb, Cs), the crystal structure differs with respect to the connecting tetrasulfide chains. While for the thiophosphates the chain in $[(Pn3)_2S_{10}]^{4-}$ (Pn = P and As) is reported to have unequally occupied split positions[3,4], the crystal structure of $Rb_4[As_2S_{10}]$ appears to be well ordered. The corresponding Raman spectrum is very unique and could be used as a fingerprint.

References:

(1) T. K. Bera, M. G. Kanatzidis, *Inorg. Chem.* **2008**, 47, 7068.
(2) Y. Wu, C. Näther, W. Bensch, *Inorg. Chem.* **2006**, 45, 8835.
(3) J. A. Aitken, C. Canlas, D. P. Weliky, M. G. Kanatzidis, *Inorg. Chem.* **2001**, 40, 6496.
(4) F. Alahmari, B. Davaasuren, J. Khanderi, A. Rothenberger, *Z. Anorg. Allg. Chem.* **2016**, 642, 361.

Fig. 1

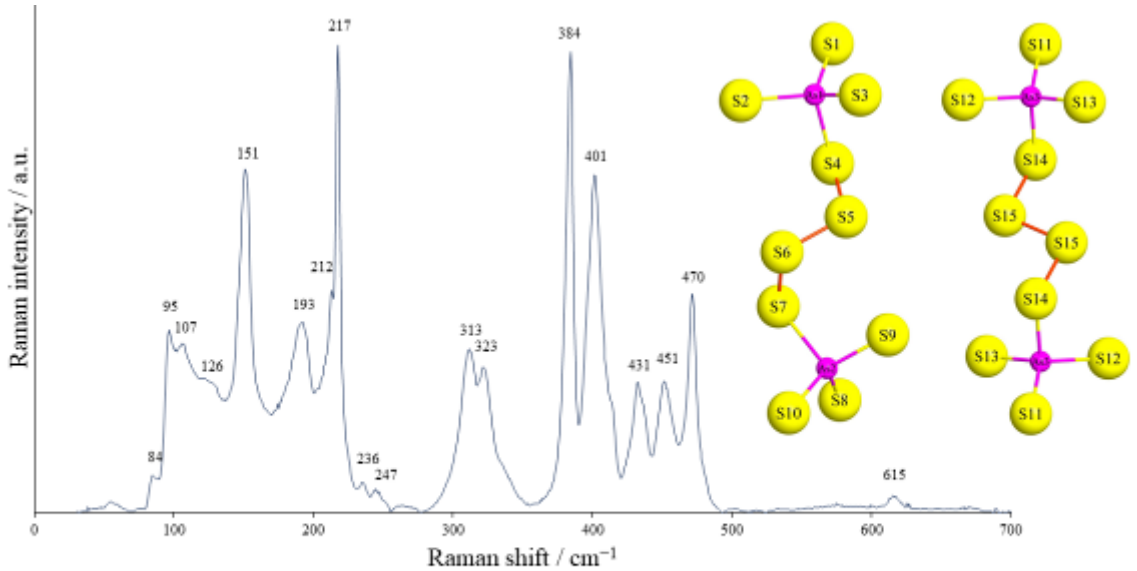

Figure 1: Raman spectrum of $Rb_4[As_2S_{10}]$ with two structurally different $[As_2S_{10}]^{4-}$ units.

Fig. 2

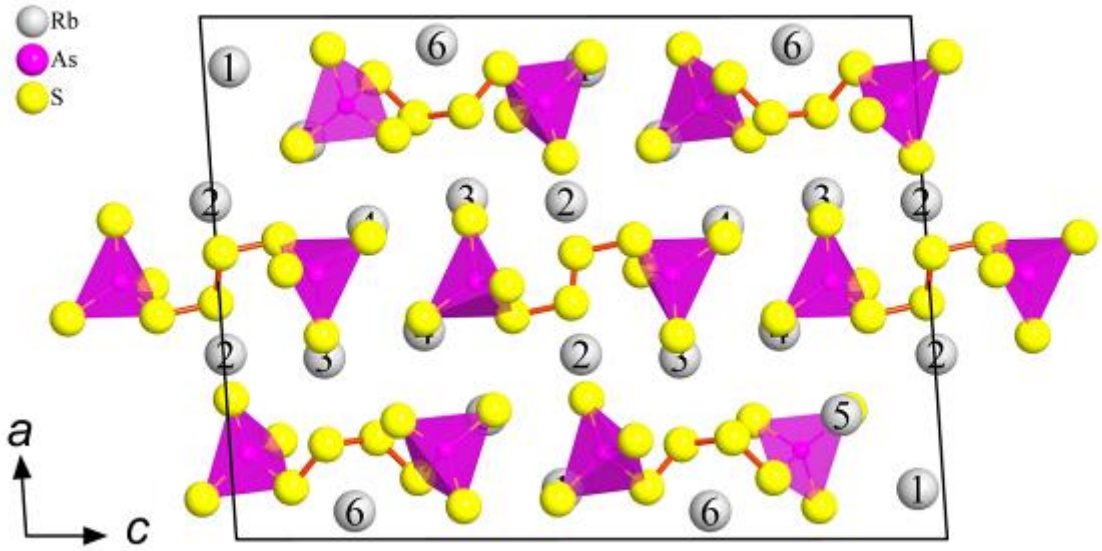

Figure 2: Unit-cell content of $Rb_4[As_2S_{10}]$ with highlighted $[As_2S_{10}]^{4-}$ anions.

PP-013

Crystal structures, polymorphism, and computational studies of oxalyl halides $(COX)_2$ (X = F, Cl, Br)

S. Ringelband (Marburg/DE), F. Tambornino (Marburg/DE), P. Moths (Marburg/DE)

The syntheses of oxalyl chloride $(COCl)_2$ and -bromide $(COBr)_2$ have been well known for more than 40 years.[1,2] Both compounds have been characterized by single crystal X-ray diffraction in 1962.[3] In contrast, the crystal structure of oxalyl fluoride $(COF)_2$ has not been reported, yet. Herein, we report on the crystal structure of $(COF)_2$, revisit the crystal structures of $(COCl)_2$ and $(COBr)_2$, and present the newly discovered polymorphism for all three compounds. $(COF)_2$ crystallizes in space group *Cmce* (No. 64) with a = 8.2641(7) Å, b = 6.3299(5) Å, c = 6.3729(4) Å, V = 333.37(4) Å^3, Z = 4, T = 200 K. At 250 K, $(COCl)_2$ crystallizes with its high temperature polymorph (*Pbca*, No. 61, a = 6.44(3) Å, b = 6.030(17) Å, c = 11.94(10) Å, V = 463.67(463) Å^3, Z = 4) and in contrast to literature we found an overlooked disorder, leading to substantially improved atomic coordinates. At 100 K, oxalyl chloride crystallizes *iso*-structural with $(COBr)_2$ in space group $P2_1/c$ (No. 14) with a = 6.0241(1) Å, b = 5.3184(1) Å, c = 7.1949(1) Å, β = 113.2192(12)°, V = 211.85(1) Å^3, Z = 2. Oxalyl bromide crystallizes in space group $P2_1/c$ (No. 14) with a = 6.1016(16) Å, b = 5.4752(9) Å, c = 7.6591(19) Å, β =111.804(19)°, V = 237.57(10) Å^3, Z = 2. The structure of $(COF)_2$ (*Cmce*) and the high temperature modification of oxalyl chloride (*Pbca*) are linked by symmetry relationships and, additionally, the high and low temperature polymorphs of $(COCl)_2$ are also symmetry related. All symmetry relations are presented with the aid of Bärnighausen formalism. Periodical quantum mechanical calculations were performed to verify determined structures and provide further insights into vibrational spectroscopic data.

References:

(1) A. Fauconnier, *C. R. Hebd. Seances Acad. Sci.* **1892**, *114*, 122–123.
(2) A. H. Schmidt, M. Russ and D. Grosse, *Synthesis* **1981**, *3*, 216–218.
(3) P. Groth, O. Hassel, *Acta. Chem. Scand.* **1962**, *16*, 2311.

PP-014

Synchrotron small molecule crystallography beyond Ewald's sphere

L. Noohinejad (Hamburg/DE), C. Paulmann (Hamburg/DE), M. Tolkiehn (Hamburg/DE)

A brief overview of beamline P24, a dedicated facility for small-molecule crystallography at Deutsches Elektronen-Synchrotron DESY, will be given.

Synchrotron radiation (SR) has a profound impact on the field of small molecule crystallography. Unlike laboratory-based X-ray sources, the synchrotron provides high brightness and energy tuneability (8 keV-40 keV). This allows us to obtain higher-quality data even from small and weakly diffracting crystals, whilst sensitive crystals can be measured faster. Twinned crystals, diffuse scattering samples, incommensurately modulated crystals, and quasi-crystals can be easily identified and handled using high-brilliance SR X-ray diffraction together with high-resolution and fast photon counting detectors e.g., Lambda 7.5M CdTe detector which is available at P24.

The importance of using synchrotron X-ray diffraction for understanding the crystal chemistry and the functional properties will be presented using examples of the aperiodic organic ferroelectric, 5,5´-dimethyl-2,2´-bipyridine (55DMBP) and bromanilic acid (H_2ba) [1]. It is found that the proton dynamic has a great role in phase transition sequences from paraelectric to ferroelectric phases between 100 to 380 K. I will present recent advances in the field of aperiodic molecular ferroelectrics with an emphasis on the links between incommensurability, intermolecular interactions and ferroelectric properties of the materials.

References:

(1) L. Noohinejad, S. van Smaalen, C. Paulmann, and M Tolkiehn, CrystEngComm, 2023,25, 4539-4549

PP-015

Changing the structure of Tb-Eu carboxylates as a way to increase temperature sensitivity

L. Tcelykh (Karlsruhe/DE, Moscow/RU), V. Kozhevnikova (Khudoleeva) (Moscow/RU), V. Utochnikova (Moscow/RU), S. Bräse (Karlsruhe/DE)

Temperature is the most frequently measured parameter in all natural and engineering systems. At the same time, most known temperature sensors are not applicable for measuring moving objects, or with limited access to the surface and micro level. Non-contact luminescent thermometry is the solution to such problems due to its fast response, high thermal and spatial resolution, and high temperature sensitivity (Sr). Tb-Eu complexes are promising luminescent materials due to their narrow luminescence bands, Stokes shift, long lifetimes, and bright luminescence, as well as the possibility of using the ratio of luminescence bands of two metals ions (LIR) as a response, eliminating the need for additional sensor calibration. Nevertheless, luminescent materials based on lanthanide complexes, whose sensory response is based only on the efficiency of temperature-dependent energy transfers, have low values of temperature sensitivity. A way to increase sensitivity may be the introduction of an additional temperature-dependent process that occurs with different efficiencies for Tb3+ and Eu3+. Such a process can be a change in the structure.

We assumed that since the water molecules in the complexes quench the luminescence of Tb3+ and Eu3+ with different efficiencies, dehydration during heating will significantly affect the luminescence spectrum. Hydrated heterometallic benzoates were used to test this hypothesis. The maximum Sr of Tb0.97Eu0.03(bz)3(H2O)n water suspension is due to the processes of cleavage and attachment of water molecules, which occur in different temperature ranges during the heating and cooling of the suspension. In this case, Sr reaches 55 %/C at 65C, which is the maximum value for luminescent thermometers. The powders of the coordination compounds showed temperature sensitivity in the range of 25-400C. At the same time, the maximum temperature sensitivity is observed precisely with structural changes in the complexes - with dehydration (50-100C).

Fig. 1

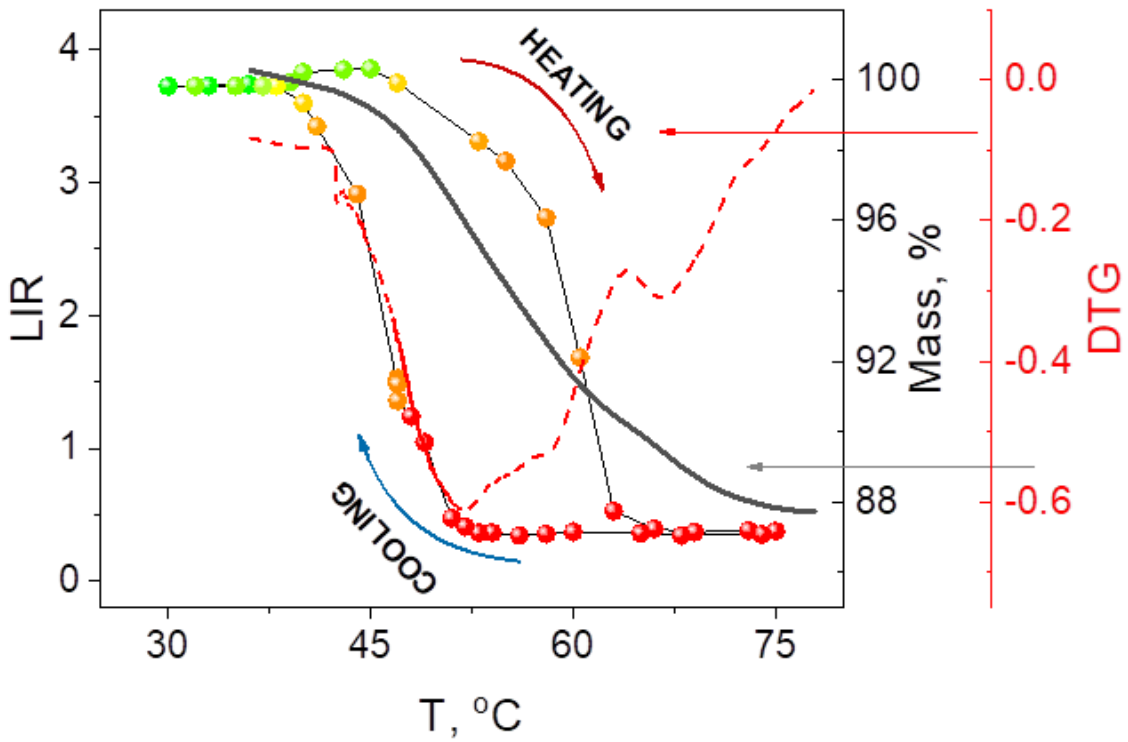

Fig. 2

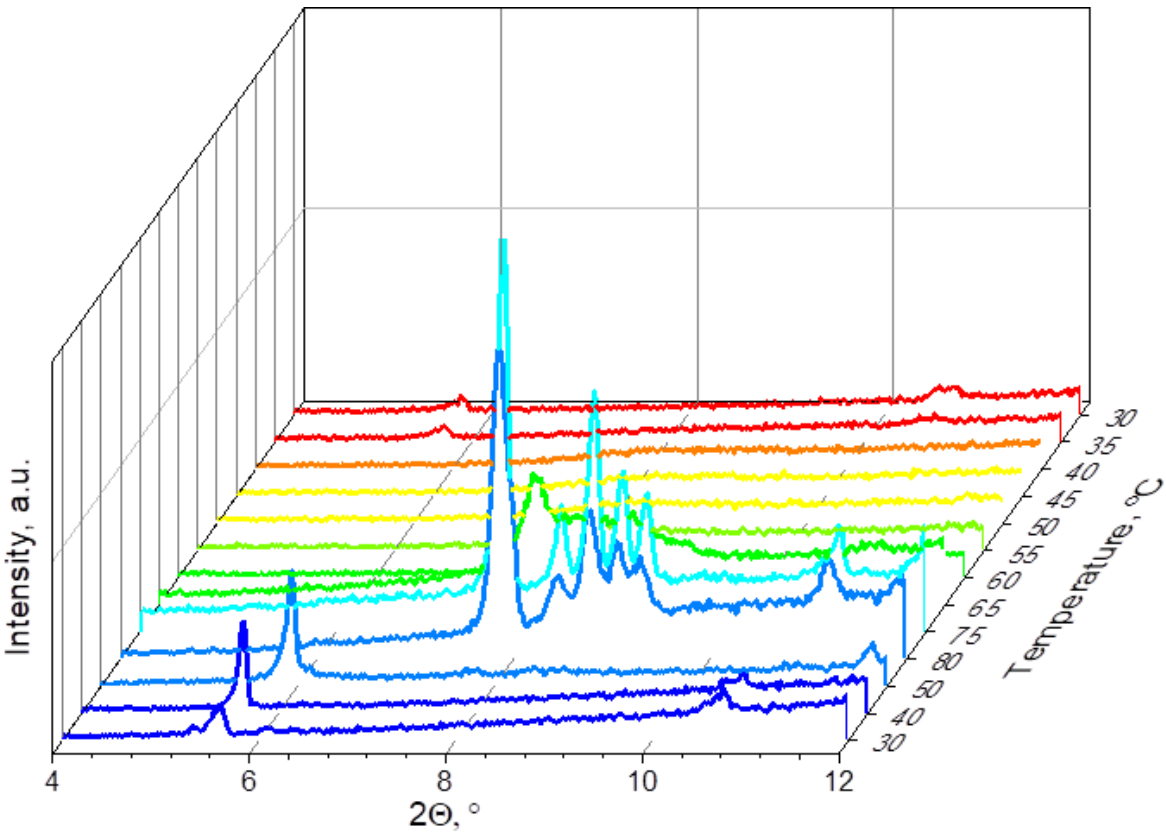
Intensity, a.u.
4
6
8
10
12
2Θ, °
30
35
40
45
50
55
60
65
75
80
50
40
30
Temperature, °C

PP-016

(3+2) D modulated low temperature phase of Rb_2ZnCl_4

S. R. Kotla (Bayreuth/DE), S. Ramakrishnan (Higashihiroshima/JP), T. Rekis (København/DK), A. M. Schaller (Bayreuth/DE), J. K. Bao (Shanghai/CN), C. Eisele (Bayreuth/DE), L. Noohinejad (Hamburg/DE), G. de Laitre (Saint-Martin-d'Hères, Grenoble/FR), M. de Boissieu (Saint-Martin-d'Hères, Grenoble/FR), S. van Smaalen (Bayreuth/DE)

Rubidium Zinc Chloride (Rb_2ZnCl_4) has the β-K_2SO_4 type crystal structure and belongs to the A_2BX_4 crystal family, which are known to exhibit successive phase transitions. Above room temperature it has an orthorhombic structure with space group *Pmcn* and disorder associated with the ZnCl4 tetrahedra A structural phase transition at 303 K, driven by the disordered tetrahedra, takes the structure into an incommensurately modulated phase. This modulation is a described with the wavevector **q** = (1/3 – *δ*) **c***, where *δ* decreases with decreasing temperature. At around Tc = 192 K, *δ* becomes zero as Rb2ZnCl4 undergoes a lock-in transition [1]. Lastly, Rb2ZnCl4 undergoes an additional phase transition around 75 K [2] with a monoclinic lattice distortion. The modulation wave function is highly anharmonic near the lock-in phase at Tc [3-4]. In the low temperature phase (T<75 K), additional satellites appear in the **ab** plane with the wavevector **q** = 0.5**a***+0.5**b*** revealing a second modulation wave, thereby breaking the orthorhombic symmetry. A detailed structural analysis in the low temperature phase (T<75 K), is performed using single crystal X-ray diffraction experiments with synchrotron radiation. This (3+2)D modulated structure has *P1c1*(α2, 0, γ2)s(1/2,β1, 0)*0* as its super spacegroup and the structure can also be described as 2***a*** x 2***b*** x 3***c*** supercell in *C1c1* spacegroup. The ZnCl4 tetrahedra now has 12 orientations as opposed to 3 in its higher symmetry modulated structure and could still be the driving force for the modulation.

References:

(1) Gesi, K. & Iizumi, M. (1979). *J. Phys. Soc. Jpn* **46(2)**, 697-698.
(2) Bagautdinov B. Sh., Shekhtman, V. Sh., (1999) *Physics of Solid State*, **41(6)**: 987-993.
(3) Aramburu, I., Friese, K., Perez-Mato, J. M., Morgenroth, W., Aroyo, M., Breczewski, T. & Madariaga, G. (2006). *Phys. Rev. B* **73**, 014112.
(4) Li, L., Wölfel, A., Schönleber, A., Mondal, S., Schreurs, A. M. M., Kroon-Batenburg, L. M. J. & van Smaalen, S. (2011). *Acta. Cryst. B* **67**, 205-217.

PP-017

X-ray-optical wavemixing – From theory to application in non-linear crystallography

D. Krebs (Hamburg/DE), F. Kerker (Hamburg/DE), C. Bömer (Hamburg/DE)

With the emergence of free-electron lasers (FELs) as brilliant new x-ray sources, the study of nonlinear phenomena in the x-ray regime has become feasible, allowing the transfer of nonlinear optics from the visible regime towards unprecedentedly high photon energies.

Among the newly accessible phenomena, we focus in this poster-presentation on x-ray-optical wavemixing (XOWM) processes, which combine diffractive imaging capabilities similar to regular x-ray diffraction with spectroscopic sensitivity.

Specifically, we focus on the theoretical description of x-ray-optical difference-frequency generation (DFG), complementing its experimental demonstration by C. Bömer et al. [1]. In this process, a pulsed optical laser drives the valence electrons of a diamond sample, while an x-ray-FEL pulse diffracts off the excited charges.

Starting from non-relativistic QED, we have derived a quantitative theory for XOWM, which allows us to relate the scattering signal to an electronic correlation function (i.e., density—current-density correlator) at the microscopic level [2]. Presenting this theoretical framework, we connect to the experimental results [1] and explore interpretations of the novel observable.

With future XOWM experiments forthcoming, we emphasize that our theoretical framework can readily incorporate new materials on the basis of suitable electronic structure calculations.

References:

(1) C. Bömer et al., in prep. 2023; accompanying talk: Demonstration of non-linear crystallography using valence-specific x-ray-optical wavemixing
(2) D. Krebs and N. Rohringer, Theory of parametric x-ray optical wavemixing processes, arXiv:2104.05838 (2021)

PP-018

Towards the spatial resolution of photosystem II charge states from XFEL diffraction data

D. Tchon (Berkeley, CA/US), J. Blaschke (Berkeley, CA/US), V. Ganapati (Berkeley, CA/US), D. Paley (Berkeley, CA/US), B. Poon (Berkeley, CA/US), F. Wittwer (Berkeley, CA/US), I. Young (Berkeley, CA/US), A. Brewster (Berkeley, CA/US), J. Yano (Berkeley, CA/US), J. Kern (Berkeley, CA/US), V. Yachandra (Berkeley, CA/US), N. Sauter (Berkeley, CA/US)

Photosynthesis provides most of the bio-available energy and oxygen to our planet. Yet, while several other mechanisms in oxygenic and anoxygenic photosynthesis have been thoroughly investigated, the core water-splitting reaction of photosystem II (PSII) remains largely uncharacterized. The recent advent of X-ray free-electron lasers has provided us with a tool to probe the structure of PSII's oxygen-evolving complex under ambient conditions and with microsecond time resolution. Still, the quality of diffraction data offered by these experiments is insufficient to reliably observe one-electron differences between individual time points.[1]

Instead of probing the imprecise scatterer distribution, oxidation states of individual metal atoms can be assigned by investigating their X-ray absorption edges. Information from classical spectroscopy can not be matched to individual atoms; however, by performing serial diffraction experiments with a pink beam tuned to the metal absorption edge, the anomalous dispersion of each atom becomes embedded in the diffraction image. A careful analysis of Bragg reflection profiles can be thus applied to retrieve the atomic form factors as a function of energy. Refined absorption curves can be then used to characterize the electronic structure of each atom.

This spatially resolved anomalous dispersion (SPREAD) technique has been previously successfully applied to data simulated for ferredoxin: a 25 kDa protein containing two differently charged iron centers.[2] The present work describes our recent advances in scaling the pipeline for a 750 kDa PSII with a four-manganese cluster and adapting it to experimental data. In particular, we describe the first working refinement of experimental data, as well as issues encountered with reliability, restraints, mosaicity, and memory use.+

References:

(1) Bhowmick, A., Hussein, R., Bogacz, I. et al. *Nature* **617**, 629–636 (2023).
(2) N. K. Sauter, J. Kern, J. Yano, J. M. Holton, *Acta Cryst.*, **D76**, 176–192 (2020).

PP-019

Automated sample change systems for thermal neutron powder diffractometers at the FRM2

C. Hauf (Garching/DE), A. Senyshyn (Garching/DE), M. Hölzel (Garching/DE)

At large-scale facilities, a growing demand for automated measurements in combination with mail-in services for samples has long since been observed. Automatized systems significantly improve the efficiency in the usage of measurement slots, and simultaneously also widen the scope of scientific applications. In particular, they enable to measure large series of samples prepared by different processing routes or varying the chemical composition.

Small series of such measurements at room temperature have already been carried out at the thermal neutron powder diffractometer SPODI at the research neutron source Heinz Maier-Leibnitz (FRM II). Here a semi-automated 10-sample carousel was used, which is also the basis for the very successful rapid access program.

However, there is an increasing demand to extend rapid access measurements to non-ambient temperatures, in particular for large serial measurements that only require one temperature point above and one below a certain phase transition temperature for each sample. Rapid measurements of such type are not yet routinely feasible with the current state of the instruments. These would benefit greatly from a fully automatized non-ambient sample change setup.

We plan employ a common pool of automatized sample environment setups for the diffractometers SPODI, ErwiN and FIREPOD at the beamport SR8 at the FRM2, which is presented in this contribution. The core of the concept is the use of a multi axis robotic arm equipped by a sample magazine, one at each of the three instruments. In the first step, this serves as an automatized sample changer at ambient conditions. In the next step, this is extended to combinations of the robot coupled with dedicated sample environment. These must be suitable for swift automatic sample change at elevated and cryogenic temperatures. The planned capabilities are described in detail.

PP-020

Why Do We Need Synchrotron for Small Molecules?

A. Virovets (Frankfurt a. M./DE), E. Peresypkina (Frankfurt a. M./DE)

Crystallographic community usually considers usage of synchrotron radiation for single-crystal X-ray diffraction (SC-XRD) in the context of macromolecular crystallography. However, high flux sources can be also useful and even obligatory for SC-XRD of "small molecules" [1].

We are going to summarize our experience in using *DESY* beamlines *P11* and *P24* to solve crystal structures of giant non-biological supramolecules based on the organometallic *cyclo*-P_n complexes (Prof.Dr. M. Scheer, Univ. Regensburg) and $\{Si_{20}\}$ cages (Prof.Dr. M. Wagner, Goethe Univ. Frankfurt).[2,3] Being compatible in size with small proteins, they possess much more complicated composition and structure that cannot be derived otherwise than from SC-XRD. Crystals frequently demonstrate weak scattering power due to the severe crystallographic disorder, and only with the use of synchrotron sources we can ensure adequate quality of the diffraction data.

To be able to handle the samples that are prone to oxidation and/or hydrolysis in air, we had to develop special protocols. Thus, we have installed a vacuum-argon (Schlenk) line in the sample preparation lab of P24 beamline to allow handling of air-sensitive samples, developed optimal experimental strategies and protocols for the data finalization using *CrysAlisPro* software (Rigaku OD).

High flux, ability to perform experiments at Helium temperatures, as well as excellent direct photon counting detectors allowed advancing in our research. We not only published dozens of crystal structures of nano-sized supramolecules, but also studied such subtle effects as superstructural ordering, OD-effects and temperature-driven crystallographic disorder.[4]

References:

(1) A. V. Virovets, E. Peresypkina, M. Scheer (2021) *Chem. Rev.*, ***121***, 14485
(2) E. Peresypkina, A. V. Virovets, M. Scheer (2021) *Coord. Chem. Rev.*, **446**:21399
(3) M. Bamberg, T. Gasevic, M. Bolte, A. Virovets, et al *JACS* (2023) **145**, 11440
(4) E. Peresypkina, B. Stöger, A. Virovets (2023) *CrystEngComm*. **24**, 7118

Fig. 1

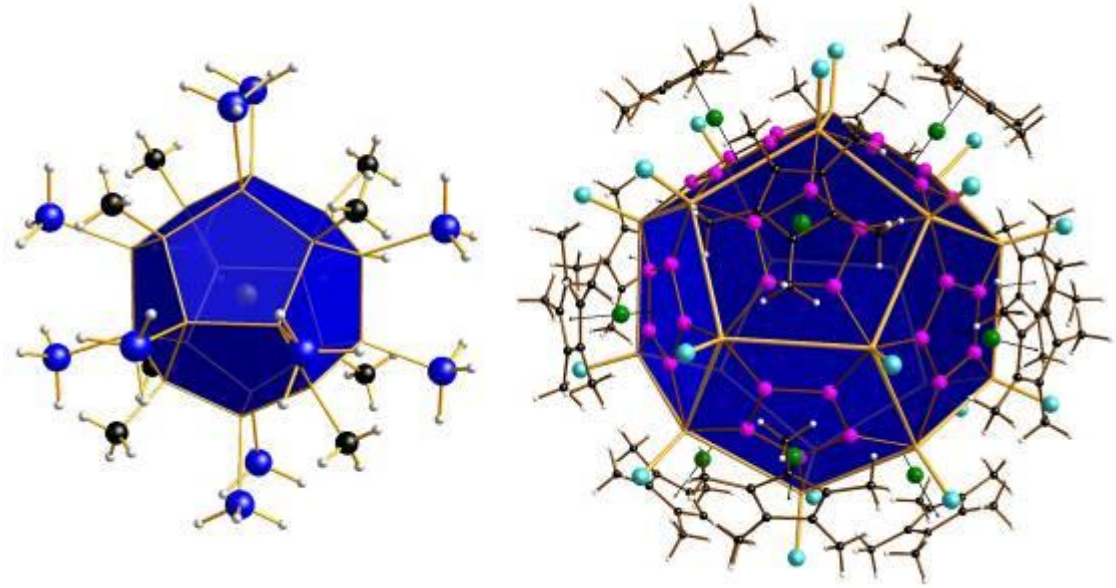

PP-021

Isothermal Compressibility and Isobaric Thermal Expansion of Liquid Trans-1,2-Dichloroethene at Low Temperatures

R. Belikov (Frankfurt a. M./DE), D. Merges (Frankfurt a. M./DE), I. Josipovic (Gent/BE), L. Schröer (Gent/BE), B. Winkler (Frankfurt a. M./DE)

Density of trans-1,2-dichloroethene under pressures up to 150 bar and temperature down to -30 °C was investigated with X-ray radiography. The thermal expansion coefficient and isothermal compressibility are crucial parameters for understanding the thermophysical properties of material, particularly in extreme environments. X-ray tomography set-up from Gent University was used for pressure measurements of the density of the compound inside the metal reservoir at high pressures and low temperatures. Figure 1 shows a photo of the experimental set-up.

In this study we determined the thermal expansion behavior of trans-1,2-dichloroethene and its dependence on pressure and temperature. Isothermal compressibility and isobaric thermal expansion were measured. The observed temperature and pressure dependencies of these parameters align well with existing literature data.

This experimental set-up could be used also for viscosity measurements. Time-resolved radiographic imaging of falling sphere experiments at moderate pressures (up to 200 bar) and variable temperatures (150 < T < 900 K) allows to determine viscosities and densities of liquids and melts and to characterise pressure-induced liquid-to-liquid phase transitions in molecular liquids thus providing an insight into the pressure-dependence of the fragility of liquids and melts. Moreover, the successful application of X-ray radiography highlights its potential as a valuable tool for studying the density, viscosity, and other properties of complex molecular compounds, as well as dense mediums like carbonate melts for fundamental geophysical applications.

Authors acknowledge support by BMBF under grant number 05P21RFFA2.

Fig. 1

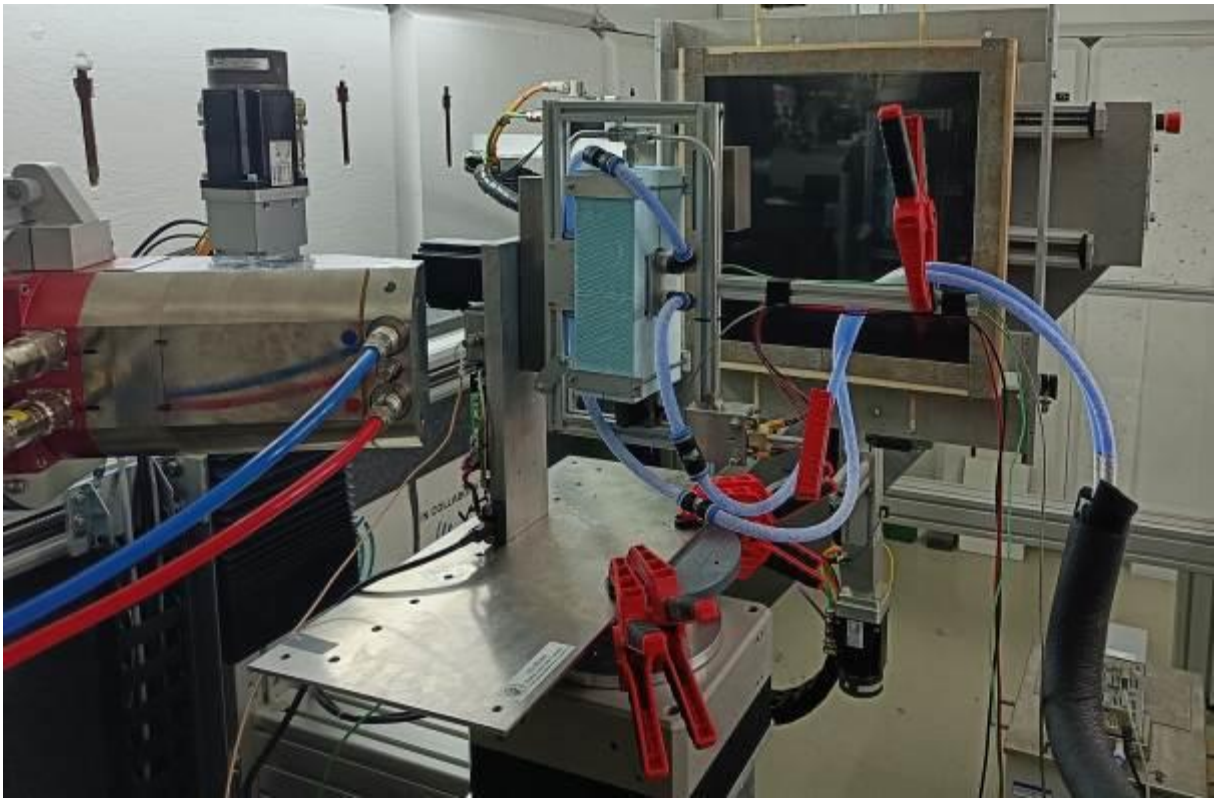

PP-022

On the state of the art and future of electron crystallography in Germany

T. Gorelik (Saarbrücken/DE), M. S. Weiss (Berlin/DE), W. Blankenfeldt (Braunschweig/BE), P. Klar (Bremen/BE), U. Kolb (Braunschweig/DE)

Over the past decade, electron crystallography (3D ED/MicroED) has emerged as a valuable addition to the array of methods for 3D structure determination. ED has transformed from a specialized technique into a highly efficient and reliable method for elucidating crystal structures in minerals, inorganic materials, organic molecules, and even biological macromolecules[1], allowing for structure determination of from crystals smaller than one µm in size. Such size range is not amenable to synchrotron-based X-ray scattering, and significantly extends the range of materials accessible for structure determination. The ability to focus the electron beam on small volumes enables the analysis of individual crystals within mixtures. Furthermore, the principles of dynamical scattering enable reliable absolute structure determination, which is crucial for pharmaceutical research[2].

Traditionally, electron diffraction experiments have been conducted using transmission electron microscopes (TEMs). The initial ED measurement technique, Automated Diffraction Tomography (ATD), was pioneered in Mainz[3], featuring a stepwise frame collection. Precession electron diffraction was utilized for thin wedge integration within each frame. With the advent of fast detectors, the continuous rotation technique[4] gained prominence due to its simplicity, gradually becoming the dominant strategy for ED measurements.

This presentation will delve into the strengths and limitations of various TEM-based measurement strategies. The landscape of ED expertise laboratories in Germany, showcasing their core competencies, will be outlined. Finally, we will discuss a vision for the future development and expansion of a National Electron Diffraction Infrastructure.

References:

(1) Gemmi et al. (2019). ACS Cent. Sci., 5, 1315.

(2) Klar et al. (2023). Nat. Chem. 15, 848.

(3) Kolb et al. (2007) Ultramicroscopy, 107, 507.

(4) Nederlof et al. (2013). Acta Crystallogr., D69, 1223; Nannenga et al. (2014). Nat. Methods, 11, 927.

PP-023

X-RAY CORELAB at HZB: Modern X-ray diffraction infrastructure for materials research

M. Tovar (Berlin/DE), R. Schwiddessen (Berlin/DE), S. Schorr (Berlin/DE)

As one of the various user platforms established at HZB, the X-RAY CORELAB (LMC) aims at meeting the demand in modern infrastructure for materials research with emphasis on phase and structure analysis, respectively. Versatile instrumentation is made available to everyone in need of laboratory-based X-ray diffraction techniques, be it the characterization of single-crystals, polycrystalline or epitaxial thin films, or powder specimen. In the X-RAY CORELAB one can find a wide variety of equipment and accessories, accompanied with personal support to tackle scientific problems in question. After being individually trained users can carry out their experiments self-dependently and at its own pace while the staff is at your service whenever necessary. In annual schools, users are trained in handling the instruments and analysing the data with applying phase analysis and crystal structure refinement software. Our article presents the laboratory options and some examples of scientific results.

Fig. 1

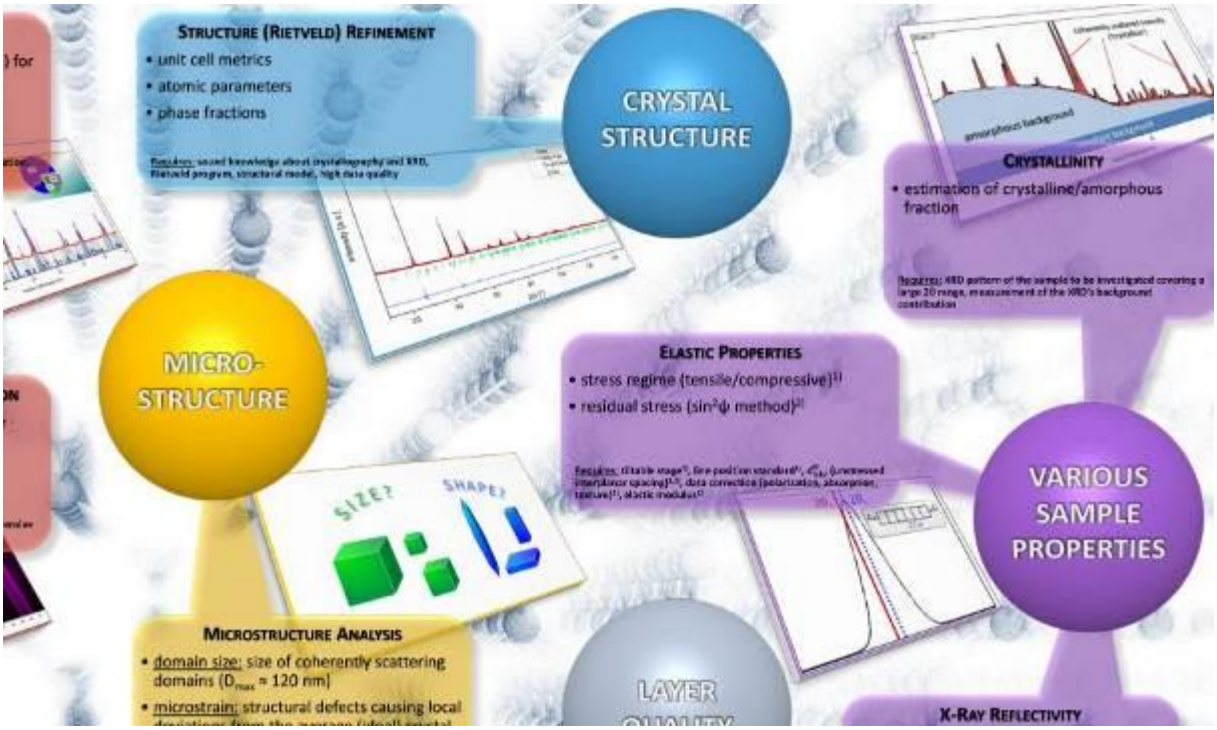

PP-024

Progress Report on the 120 kV MetalJet for Chemical Crystallography

N. Nöthling (Muhlheim an der Ruhr/DE), M. Patzer (Muhlheim an der Ruhr/DE), C. Schäfer (Muhlheim an der Ruhr/DE), C. W. Lehmann (Muhlheim an der Ruhr/DE)

Providing the most brilliant X-ray source for chemical crystallography and quantum crystallography was and is the aim of this project. At the outset a decision to maximize the indium content of the MetalJet alloy, in addition to gallium and zinc, was made. Recent reports by Stalke et al. have illustrated the benefits of this technology.[1] However, in addition to the requirement of heating an indium rich alloy permanently to well above room temperature an acceleration voltage in excess of 70 kV is recommended in order to optimize the emission of X-rays. Since this modification was not available commercially, it was necessary to design and construct this system from individual components. The main stages involved radiation protection, characterization of beam optics, testing of detectors and proof-of-principle experiments.[2] Subsequent steps, which are reported here, are the utilization of an existing kappa-goniometer and the adaptation of software to integrate all components into a diffraction system with a degree of automation comparable to synchrotron beamline instrumentation. Results of some successful crystal structure determinations in addition to a comparision of this design to other standard laboratory set-ups will be shown.

References:

(1) Graw, N., Ruth, P. N., Ernemann, T., Herbst-Irmer, R., Stalke D. J. App. Cryst. **56**, 1315-1321 (2023), Ruth, P. N., Graw, N., Ernemann, T., Herbst-Irmer, R., Stalke D. J. App. Cryst. **56**, 1322-1329 (2023)

(2) Nöthling, N. (2021). Dissertation, University of Duisburg-Essen, Germany DOI: 10.17185/duepublico/74968

PP-025

Insights into the exsolution process using synchrotron radiation methods

S. Mascotto (Koblenz/DE, Hamburg/DE), P. Inangha (Koblenz/DE), F. Colombo (Hamburg/DE), E. Fezai (Hamburg/DE)

The process of metal exsolution attracts since several years the interest of the scientific community because it represents a smart approach to prepare advanced metal-oxide nanocomposites through dopant segregation from a mixed conducting oxide matrix for applications in energy conversion, catalysis, and data storage. In spite of the outstanding number of publications in the past 5 years, still little is known about the formation mechanism of exsolved metal nanoparticles, and particularly about the interplay between the different steps of the process, i.e. dopant reduction, nucleation and nanoparticle growth. To tackle this, synchrotron methods represent a unique opportunity because they enable comprehensive understanding of the nanoparticle segregation process due to their high statistical significance and real-time operation.

In the present paper, the analysis of the exsolution of mono and bimetallic nanoparticles will be addressed by combining small-angle X-ray scattering (SAXS), X-ray diffraction (XRD) and X-ray absorption spectroscopy (XAS). Due to the high complementary character of these techniques it was possible to understand the correlation between the reduction and growth mechanisms during the exsolution of bimetallic Fe-Ni nanoparticles. Also, the use of SAXS combined with XRD enabled to obtain information about the size, shape and distribution of both surface- and bulk-segregated nanoparticles in powder and thin-film materials, providing insightful morphological information at different scales. Finally, the execution of real-time experiments demonstrated to be a highly promising approach to tackle the kinetics of nanoparticle formation, dissolution and self-regeneration.

Fig. 1

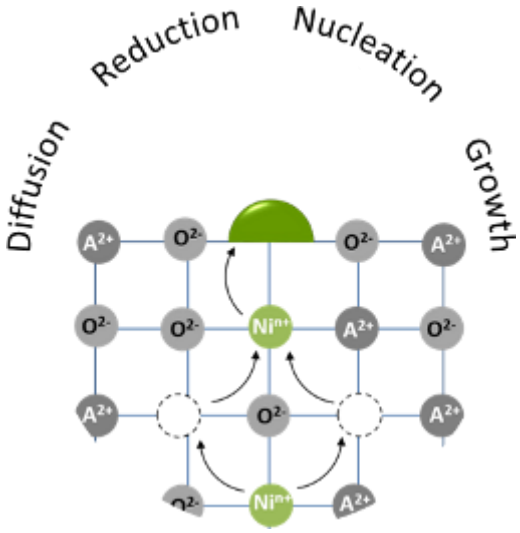

PP-027

Exploring the conformational space of proteins by systematic variation of the relative humidity

P. Y. A. Reinke (Hamburg/DE), S. Günther (Hamburg/DE), S. Falke (Hamburg/DE), M. Galchenkova (Hamburg/DE), A. Rahmani Mashhour (Hamburg/DE), A. Creon (Hamburg/DE), J. Lieske (Hamburg/DE), W. Ewert (Hamburg/DE), A. C. Rodrigues (Hamburg/DE), S. Thekku Veedu (Hamburg/DE), P. Fischer (Hamburg/DE), A. Meents (Hamburg/DE)

The relationship between hydration and the crystal anatomy of proteins is a long-known fact that has been observed since the early days of protein crystallography. Different hydration states influence the activity of enzymes and modulate the interaction landscape. In addition, dehydration of protein crystals has been used to improve the resolution of protein crystals and to induce conformational changes in the protein. Here we present dehydration studies using a newly developed humidity chamber with unprecedented precision. We have used it to perform dehydration studies on proteins to investigate structural dynamics. Dehydration series of lysozymes, the SARS-CoV-2 main protease, and a lignin-interacting peroxidase were performed in the range between 99 % and 34 % relative humidity. We observed not only reorientations of residues and protein surface changes, but also a peptide flip event in lysozyme spanning over several intermediate states. The highly controlled humidity not only allows us to control the dehydration of protein crystals during room temperature experiments, but also provides precise insights into the dynamic nature of the protein during dehydration series.

PP-028

Structural characterization of mofs by diffraction methods

M. Grzywa (Neu-Isenburg/DE), J. Wojciechowski (Neu-Isenburg/DE)

MOFs consist of secondary building units (SBUs) (e.g. metal ions or metal clusters) and organic ligands that can be assembled into periodic networked crystalline structures with high porosity and high surface area. MOFs are known to be one of the most extensively studied materials of the 21st century, due to their wide range of applications in gas storage and separation, drug delivery, imaging, radio- and photo-therapy, water cleaning and harvesting, catalysis, carbon capture, electrochemistry, sensing [1].

The determination of the crystal structure is a key element in the characterisation of any new compound and the first step towards tailoring its properties. Single-crystal X-ray diffraction is the most reliable and fastest technique for the determination of crystal structure. The technique requires suitable crystals in terms of both size and quality, and it is often a limiting factor for application in MOFs studies. The synthesis methods (solvothermal, hydrothermal, microwave-assisted, electrochemical, mechanochemical, sonochemical) affect the crystallization process and quality of the crystalline product. Gas-, temperature- and solvent-induced reactions make single crystals unsuitable for XRD analysis. Thermally activated MOFs often loose crystallinity at least partially. An alternative is to use the X-ray powder diffraction methods or electron 3DED technique for structure determination and characterization of the compounds.

This presentation will show results of structural characterizations of MOFs using the X-ray powder diffraction methods and powder electron-diffraction.

References:

(1) R. Freund, et al. *Angew. Chem. Int Ed.* **2021**, 45, 23975-24001.

Fig. 1

PP-029

Picometer atomic displacements behind ferroelectricity in the commensurate low temperature phase in multiferroic YMn_2O_5

T. Weigel (Freiberg/DE), C. Richter (Berlin/DE), M. Nentwich (Hamburg/DE), D. C. Meyer (Freiberg/DE), M. Zschornak (Dresden/DE, Freiberg/DE)

The material system YMn_2O_5 has several low temperatures phases, where magnetism and ferroelectricity occur. Especially, the origin of ferroelectricity in the commensurate phase is an open question. Literature agrees upon a magnetically driven principal mechanism from changes in the Mn spin configuration, which may be based either on magnetostriction due to symmetric exchange, the antisymmetric inverse Dzyaloshinskii-Moriya interaction or a combination of the two. Both mechanisms are accompanied by specific atomic displacements of ions in the structure. The space group *Pbam* (55) of the paraelectric phase does not allow the respective polar displacements and a refinement of the charge structure in a lower symmetric phase has not been successful so far, mostly because conventional structure analysis lacks the sensitivity required to resolve the expected positional displacements.

We applied the new *Resonantly Suppressed Diffraction* (RSD) [1] method, which is sensitive to minuscule structural changes in the sub-pm range, in order to resolve potential ionic displacements within a polar space group and shed new light on this controversial discussion. The method is based on the destructive interference of structure factors causing the intensity of a Bragg reflection to approach zero.

We measured the energy dependent RSD spectra of carefully selected reflections above and below the phase transition temperature T_{CM} = 39 K. With the data above T_{CM}, we refined the static and dynamic displacements of the paraelectric phase to receive an improved starting model for the structural characterization of the ferroelectric phase. With the improved starting model and the data below T_{CM} we were able to refine the static displacements of the ferroelectric phase. Therefore, we can present the first structure refinement for the ferroelectric commensurate phase and and gain insight into the structural origin of ferroeletricity in YMn_2O_5.

References:

(1) C. Richter *et al.* (2018), *Nat. Commun.*, **9**, 178.

PP-030

The Versatile High-Energy X-ray Scattering Beamline P21.1 at PETRAIII, DESY

F. Igoa (Hamburg/DE), J. Liu (Hamburg/DE), K. Köhler (Hamburg/DE, Frankfurt a. M./DE), K. Iskhakova (Hamburg/DE, Karlsruhe/DE), O. Gutowski (Hamburg/DE), A. C. Dippel (Hamburg/DE), M. von Zimmermann (Hamburg/DE)

The beamline P21.1, located at the PETRA III synchrotron radiation source in Hamburg, Germany, stands as a versatile platform for high-energy X-ray scattering studies. This beamline is designed to cater to a diverse range of materials, offering comprehensive insights through total scattering, powder diffraction, and single crystal diffraction techniques.

The beamline operates at energies of 52 keV, 87 or 100 keV. Such high energies permit the measurement through complex and voluminous sample environments, while still being able to access high *q* ranges. Therefore, the beamline is particularly active in carrying out *in situ* scattering experiments.

The experimental hutch at P21.1 houses a heavy load diffractometer with a remarkable capacity, capable of carrying loads up to 600 kg. Standard sample environments include magnetic fields (up to 10 T), high temperature furnaces (up to 800 °C), low temperature cryostats (down to 2 K) and scattering chambers for low background measurements. Various other equipments can be adapted from laboratories or from the synchrotron pool.

This diffractometer boasts a vertical rotation axis and a double tilt stage, offering flexibility for various sample orientations. Multiple capillaries can be measured automatically, single crystals" reciprocal space can be easily harvested in standard or high resolution, and thin films can be measured in both transmission and grazing incidence geometry thanks to beam focusing.

In this poster session, the P21.1 beamline capabilities are presented to demonstrate the array of techniques available for the crystallographic user community.

PP-031

High temperature electron diffraction on organic crystals: *In situ* crystal structure determination of pigment orange 34

Y. Krysiak (Hannover/DE), S. Plana-Ruiz (Tarragona/ES), L. Fink (Frankfurt a. M./DE), E. Alig (Frankfurt a. M./DE), U. Bahnmüller (Hannover/DE), U. Kolb (Mainz/DE), M. U. Schmidt (Frankfurt a. M./DE)

Small molecule structures and their applications rely on a good knowledge of their atomic arrangements. However, the crystal structure of these compounds and materials, which are often composed of fine crystalline domains, cannot be determined with single-crystal X-ray diffraction. Three-dimensional electron diffraction (3D ED) is already becoming a reliable method for the structure analysis of submicron-sized organic materials (Klar *et al.*, 2023). The reduction of electron beam damage is essential for successful structure determination and often prevents the analysis of organic materials at room temperature, not to mention high temperature studies (Fillafer *et al.*, 2022; Hindricks *et al.*, 2024). In this work, we apply advanced 3D ED methods at different temperatures enabling the accurate structure determination of two phases of Pigment Orange 34 ($C_{34}H_{28}N_8O_2Cl_2$), a biphenyl pyrazolone pigment that has been industrially produced for more than 80 years and used for plastics application. The crystal structure of the high-temperature phase was determined at 220 °C. For the first time, we were able to observe a reversible phase transition in an industrial organic pigment in the solid state despite crystallites are submicron in size. By localising hydrogen atoms, we were even able to detect the tautomeric state of the molecules at different temperatures.

References:

(1) Fillafer, N., Kuper, H., Schaate, A., Locmelis, S., Becker, J. A., Krysiak, Y. & Polarz, S. (2022). *Advanced Functional Materials* **32**, 2201126.
(2) Hindricks, K. D. J., Bon, V., Treske, O., Hannebauer, A., Schaate, A., Krysiak, Y. & Kaskel, S. (2024). *Chem. Mater.*
(3) Klar, P. B., Krysiak, Y., Xu, H., Steciuk, G., Cho, J., Zou, X. & Palatinus, L. (2023). *Nat. Chem.* 1–8.

Fig 1. Localisation of the H atoms of the hydrazone groups from difference Fourier maps obtained by 3D ED. (a) LT phase at -180 °C. (b) HT phase, measured at 220°C. Red isosurfaces correspond to the $3\sigma[\Delta V(\boldsymbol{r})]$ level.

Fig. 1

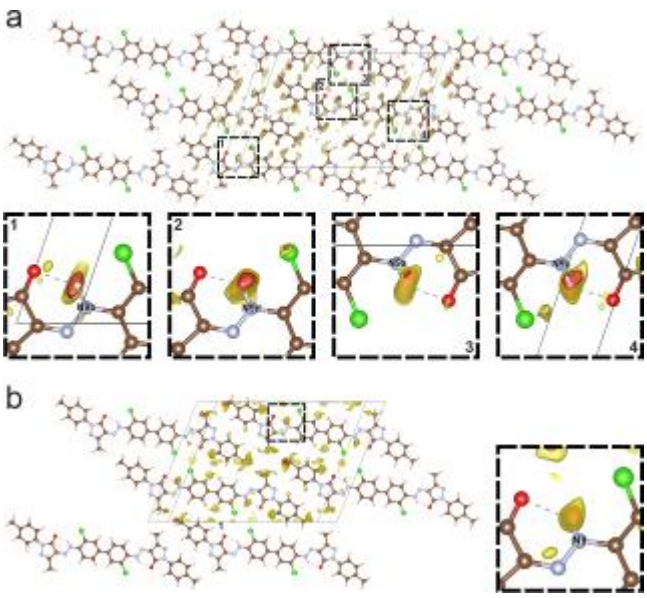

PP-032

Investigation of lens material for X-ray polarization microscopy

J. Görs (Jena/DE), B. Marx-Glowna (Jena/DE, Jena/DE), R. Lötzsch (Jena/DE), W. Hippler (Jena/DE), T. Wunderlich (Jena/DE), S. Sadashivaiah (Jena/DE), Y. Yoshida (Jena/DE), G. G. Paulus (Jena/DE, Jena/DE)

Polarimetry in the visible regime of light is already a widely used technic in material science, while X-ray polarimetry is still a relatively young and underutilized field. With the development of X-ray polarimetry in the last couple of years, we achieved polarization extinction ratios in the order of (10^{-11}). This renders the method sensitive to probe tiniest optical anisotropies for example due to vacuum birefringence and dichroism[1].

Most materials are not polarization-preserving. Therefore, due to the high sensitivity for polarizational change inside the X-ray polarimeter, the usage of opticale elements such as X-ray lenses becomes quite difficult. Recently we could discover a polarization-preserving lens material which allows for the first time the combination of precision polarimetry with micro-focused beams without compromising its polarization purity. This breakthrough opens many new fields of application at synchrotrons and XFEL's, because the new technique allows for the first time to investigate small samples, or tiny regions of interest.

Present fields of application are the investigation of disordered structures such as polycrystalline material. We studied the polarization change, dependent on the crystallite size in powdered samples, as well as the polarization change dependent on the thickness of polycrystalline material. The investigation of the polarization change in polycrystalline material is very important, e.g. for the construction of polarization conserving X-ray lenses, and therefore for the future development of X-ray polarization microscopes.

References:

(1) Schmitt, A.T. et. al. 2020: Disentangling X-ray dichroism and birefringence via high-purity polarimetry. Optica. 8. 10.1364/OPTICA.410357.

PP-033

On the difference pair distribution function method to extract localized structure

M. W. Terban (Mannheim/DE)

Extracting structural information out of the scattering from single molecules or ultrasmall nanoparticles is difficult enough in the first place. It is even more difficult when such species are embedded, for instance, in a microporous host. In recent years, the difference pair distribution function has shown to be an effective tool for gaining insights in this area, notably even for discerning single atom environments, binding behavior of adsorbed species, and changes in molecular interactions. Here, I will showcase some applications of the method along with aspects of interpretation and limitations.

PP-034

Deep insights into energy materials utilizing anomalous X-ray diffraction

D. M. Többens (Berlin/DE), Y. Tomm (Berlin/DE), D. G. Porter (Didcot/GB), S. Niedenzu (Berlin/DE), A. Nicolson (London/GB), G. Gurieva (Berlin/DE), J. Breternitz (Steinfurt/DE), S. Schorr (Berlin/DE, Berlin/DE)

Cation arrangement, disorder and defects substantially impact the optoelectronic properties of multinary semiconductors [1]. Improvement of optical transition like absorption coefficient and photovoltaic device efficiency thus requires solid knowledge of the atomistic material structure. Isoelectric cations are hard to distinguish by laboratory X-ray diffraction. Besides neutron radiation, anomalous X-ray diffraction is commonly used to overcome this problem, utilizing the strong energy dependency of scattering factors close to the element-specific X-ray absorption edges. A variant of this, Multiple Edge Anomalous Diffraction (MEAD) [2] was found by us to work particularly well for determination of cation arrangements within a known parent structure.

The energy range of 5 – 14 keV of beamline KMC-2 at BESSY II, HZB, Berlin [4] allows measurements at the absorption edges of many technically relevant elements, in particular the transition metals of the 4th period. We recently utilized this to measure $CuGaGeS_4$ (see figure) and off-stoichometric Cu_2ZnGeS_4 compounds.

Measurements on $Sn_2SbS_2I_3$ required lower energies, as the L-edges of Sn and Sb lie between 3.9 and 4.7 keV. These experiments were conducted on beamline I16 at Diamond Light Source, Didcot, UK [5], in deviation from our usual procedure using single crystals. As the measurement geometry of MEAD keeps the diffraction vector constant, the method is unaffected by preferred orientation and can be applied to samples of any degree of graininess.

References:

(1) S. Schorr, G. Gurieva, in Crystallography in Materials Science: From Structure-Property Relationships to Engineering, S. Schorr & C. Weidenthaler, Editors. 123 (2021)
(2) D.M. Többens *et al.*, *Acta Cryst.* B76, 1027 (2020)
(3) Y. Tomm *et al.*, Crystal Growth and Structure of a New Quaternary Adamantine $CuGaGeS_4$. *Crystals* 13, 1545 (2023)
(4) HZB, *Journal of large-scale research facilities*, 2, A49 (2016)
(5) S.P. Collins *et al.*, *AIP Conf. Proc.* 1234, 303 (2010)

Fig. 1

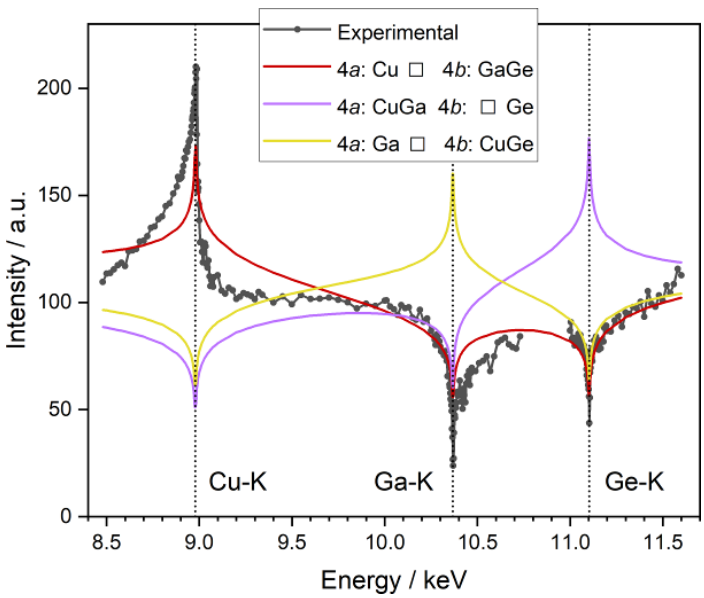

PP-035

Diffraction Studies of the Anisotropy in Advanced High Strength Steel Grades

C. Commenda (Linz/AT)

Introduction

Thermomechanically processed Advanced High Strength Steel (AHSS) grades show strongly preferred crystallographic orientations far from the random distribution. As a consequence the mechanical and magnetic properties of a sheet material are anisotropic.

Objectives

In order to take account of the anisotropy, the structure-property relationship has to be expanded to different orientations in space. Short process times and high cooling rates lead to highly inhomogeneous multi phase micro structures out of thermodynamic equilibrium.

Materials and methods

As representatives for the AHSS grades martensitic and medium manganese materials are chosen. For the quantification of the phase fractions a novel X-Ray diffraction (XRD) method is presented that is based on the measured texture data. By a geometrical averaging procedure in a large area of the reciprocal space it is possible to define an orientation dependent phase fraction that can be related to the anisotropic mechanical and magnetic properties. The structural information from XRD of the phases ferrite, martensite, retained austenite and epsilon martensite is used to setup a combined Electron Backscatter Diffraction (EBSD) and Energy Dispersive X-Ray detection (EDX) measurement on the scanning electron microscope (SEM).

Results and Concluding Remarks

The results of this orientation dependent analysis can be used to improve the understanding of the physical phenomena and mechanical strengthening mechanisms of anisotropic materials on a more general basis. There is an attempt to introduce new orientation dependent quantities to describe the structure property relations in the materials with a complex micro structure.In order to get more insight to the magneto-elastic interaction the samples are analyzed in a pristine, in situ magnetized and a state with remanent magnetization without external field.

PP-036

Determination of atomic arrangement from glassy SiO_2 via machine-learning assisted DFT-PDF fitting

P. Diephaus (Bremen/DE), W. Dononelli (Bremen/DE), T. M. Gesing (Bremen/DE)

The determination of the atomic arrangement is fundamental to understand the properties of any phase or material. Solving crystal structures from 3D single-crystal or 1D micro-crystal data using the Shelx or Rietveld method, respectively, is standard nowadays. However, challenges emerge when working with smaller nano-crystalline powders showing strong reflection broadening and overlapping or even quantum-crystalline (QC) or glassy phases (GP), causing both amorphous scattering only. In such cases, the pair distribution function (PDF) analysis becomes crucial [1]. Yet, many PDF analyses still depend on prior structural information and resemble real-space versions of Rietveld like refinements (PDF-Rietveld). Nevertheless, PDF-Rietveld fails for small long-range ordered QC phases as well as short-range order GP's.

To tackle these challenges, we introduce a machine learning (ML) algorithm for solving atomic arrangements and crystal structures from experimental PDF's, combined with density functional theory (DFT) calculations [2]. By integrating DFT calculations and PDF modelling (DFT-PDF), the ML algorithm is trained within a unified artificial R_{PDF}-factor/DFT landscape, allowing it to accurately determine even metastable phases' structures. Additionally, the method excels in identifying multiple phases or stacking motifs through consecutive multi-phase refinement.

By applying this method, we were able to determine the multiple phases of glassy SiO_2. Different atomic arrangement with average crystallite sizes of ~ 1.4 nm were fitted against the PDF data and possible candidates optimized and pre-selected using DFT energies and chemical criteria. The finally remaining candidates were stepwise combined in a multi-phase refinement till the best solution was obtained.

References:

(1) E. D. Bøjesen, B. B. Iversen, *Cryst. Eng. Comm.* (2016), **18**, 8332.
(2) M. Kløve, S. Sommer, B. B. Iversen, B. Hammer, W. Dononelli, *Adv. Mater.,* (2023), **35**, 2208220.

PP-037

Multi-scale analysis of the high-pressure behaviour of (1-*x*)$Na_{0.5}Bi_{0.5}TiO_3$-*x*$BaTiO_3$ at the morphotropic phase boundary

C. Rösche (Hamburg/DE), T. Boffa Ballaran (Bayreuth/DE), T. Malcherek (Hamburg/DE), C. Paulmann (Hamburg/DE), R. J. Angel (Padova/IT), B. Mihailova (Hamburg/DE)

The perovskite-type (ABO_3) solid solution (1-*x*)$Na_{0.5}Bi_{0.5}TiO_3$-*x*$BaTiO_3$ (NBT-*x*BT) is considered as an environmentally friendly replacement for currently market-leading Pb-based ferroelectric materials. At the morphotropic phase boundary (MPB) (x_{MPB} ~ 0.05-0.06 for NBT-*x*BT) the material properties are strongly boosted. Efficient modification of the material requires a better understanding of the relation between the chemical composition and the nanoscale structure of the corresponding solid solution. To elucidate this, we have conducted high-pressure X-ray diffraction and Raman spectroscopic experiments with NBT-0.048BT single crystals up to 9 GPa using the diamond-anvil-cell technique. The complementary analyses of Bragg scattering, X-ray diffuse scattering and Raman scattering allows a comprehensive picture to be obtained of the pressure-induced structural alterations ranging from the local to the long-range scale. At ambient and low pressure the deviations from the average pseudo-cubic perovskite structure produce strong diffuse scattering that evolves into sharp Bragg peaks with increasing pressure. A phase transition takes place at 4.4-5.5 GPa, as indicated by the appearance of additional Bragg peaks. At the same pressure, pre-existing reflections that are characteristic of distortions at the R-, M- and X-points (in Pm-3m) sharpen and increase strongly in intensity, showing that incipient intermediate range order evolves into long range order. The new high-pressure phase is characterised by a mixed octahedral tilt pattern and antipolar A-cation shifts. The multistep local scale structural transformations that lead to the phase transition are resolved by the Raman data: at 0.5-0.9 GPa the Ba-induced local BO_6 anisotropy is reduced and antipolar order of A-cation off-centre displacements develops above 1.9 GPa. A strong enhancement of octahedral tilting vibrations is observed above 2.7 GPa followed by a change in the tilt pattern at 4-4.5 GPa.

PP-038

New Frontiers in nuclear magnetic resonance for high-pressure research and Geoscience

T. Meier (Beijing/CN)

Nuclear Magnetic Resonance (NMR) is one of the most widespread and versatile spectroscopic probes of contemporary natural sciences. An application in high-pressure or experimental geosciences was however regarded unfeasible until recently. In this talk, I will summarize recent developments in both experiment and method of high-pressure small-scale NMR methods. These developments include the implementation of NMR-crystallographic methods using a combination of high- and low-resolution techniques as well as the opportunity for hydrogen or water quantification in in-situ DAC based experiments or nominally anhydrous minerals under ex-situ investigation.

References:

(1) Meier, T., et al., (2020). Nuclear spin coupling crossover in dense molecular hydrogen. Nature Communications, 11(1).

(2) Meier, T., et al., (2020). Proton mobility in metallic copper hydride from high-pressure nuclear magnetic resonance.
Physical Review B, 102(16).

(3) Meier, T., et al., (2021). In situ high-pressure nuclear magnetic resonance crystallography in one and two dimensions.
Matter and Radiation at Extremes, 6(6), 068402.

(4) Meier, T., et al., (2022). Structural independence of hydrogen-bond symmetrisation dynamics at extreme pressure
conditions. Nature Communications, 13(1).

(5) Meier, T., Laniel, D., & Trybel, F. (2023). Direct Hydrogen Quantification in High-pressure Metal Hydrides, Matter and
Radiation at Extremes, 8.

Fig. 1

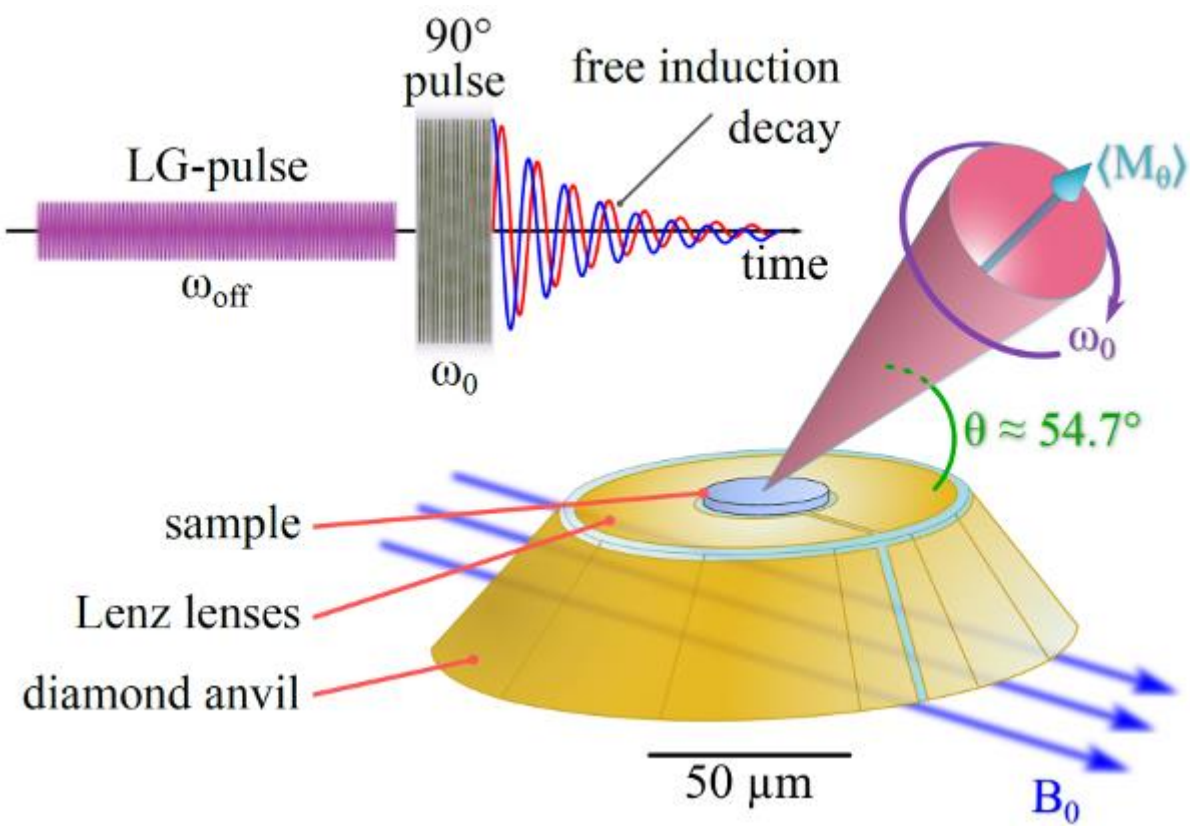

Fig. 2

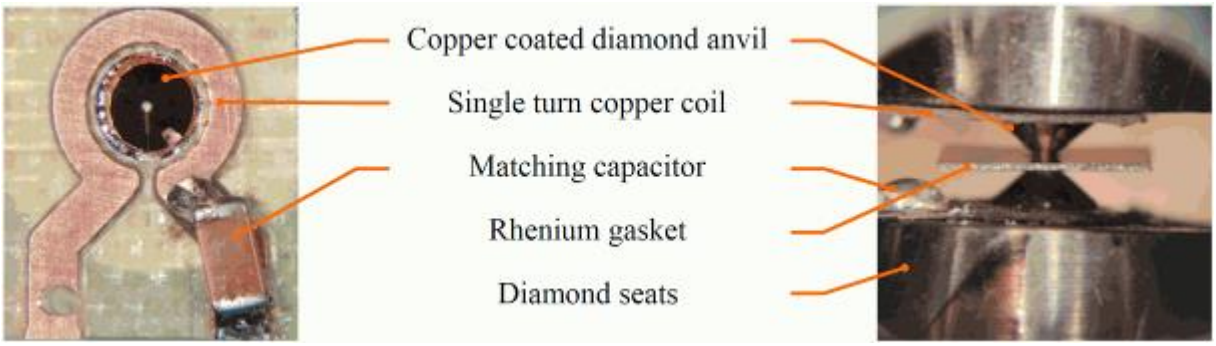
Copper coated diamond anvil
Single turn copper coil
Matching capacitor
Rhenium gasket
Diamond seats

PP-039

X-ray diffraction and electron microscopy study of high-temperature treated Al layers deposited on TiO_2 substrate

P. Cejpek (Freiberg/DE), D. Rafaja (Freiberg/DE), M. Motylenko (Freiberg/DE), A. Leuteritz (Freiberg/DE)

The most pronounced inclusions, which are present in the cast components made of steels or aluminum alloys, are aluminum oxides. These inclusions can significantly worsen the mechanical properties of the components. The usage of a functional filter is necessary to remove these unwanted inclusions from the melt by attaching the oxide particles to the filter surface or by dissolving them in a chemical reaction between the filter and the melt. The study presented here was focused on the Al layer deposited by magnetron sputtering on a single-crystalline α-TiO_2 (rutile) substrate, where Al plays a role of the melt and a rutile substrate serves as the filter.

This system was then study by X-ray diffraction measured in-situ at high temperatures and afterwards by electron microscopy to study the reaction between melted Al and rutile. Both experimental methods showed the growth of single-crystalline α-Al_2O_3 (corundum) which grows on the substrate in the form of small islands of approximately 2-3 µm size. The orientation relation between the substrate and the islands is: $(001)_{rutile}$ parallel to $(100)_{corundum}$, $[010]_{rutile}$ parallel to $[001]_{corundum}$.

The transmission electron microscopy revealed the possibility that the islands do not grow directly from the substrate but the formation of a thin interlayer of Ti-O phases is present. The oxygen atoms from TiO_2 substrate are presumably taken by Al melt which leads to the formation of Al_2O_3 and various titanium oxides.

Poster Session I: Mineralogical crystallography

PP-040

Cation and anion ordering in synthetic lepidolites and lithian muscovites: Influence of the OH/F and Li/Al ratios on the mica formation studied by NMR spectroscopy and X-ray diffraction

M. Fechtelkord (Bochum/DE), B. Marler (Bochum/DE), L. Sulcek (Bochum/DE)

A large number of lepidolites $K(Li_xAl_{3-x})[Si_{2x}Al_{4-2x}O_{10}](OH)_yF_{2-y}$ and Li-muscovites $K(Li_xAl_{2-x/3}\square_{1-2x/3})[Si_3AlO_{10}](OH)yF_{2-y}$ were synthesised by a gelling method in combination with hydrothermal syntheses at a pressure of 2 kbar and a temperature of 873 K. The nominal composition ranged between $0.0 \leq x \leq 2.0$ and $0.0 \leq y \leq 2.0$, i.e., from polylithionite $K[Li_{2.0}Al][Si_{4.0}O10](OH)_yF_{2-y}$ over trilithionite $K[Li_{1.5}Al_{1.5}][AlSi_{3.0}O_{10}](OH)_yF_{2-y}$ to muscovite $K[Al_{2.0}\square][AlSi_{3.0}O_10](OH)_yF_{2-y}$. ^{1}H, ^{19}F, ^{29}Si, ^{27}Al MAS NMR and MQMAS NMR spectroscopy has been performed to investigate the order/disorder state of Si and Al in the tetrahedral layers and of Li, Al, OH and F in the octahedral layer. The synthetic mica crystals are very small, ranging from 0.1 µm to 5 µm. With increasing Al content, the crystal sizes decrease. Rietveld structure analyses showed that nearly all samples consist of two mica polytypes (1M and 2M1) of varying proportions. In the case of lepidolites, the 1M/2M1-ratio depends on the Li/Al ratio of the reaction mixture. The refinement of the occupancy factors of octahedral sites shows that lepidolites ($1.5 \leq x \leq 2.0$) represent a solid solution series with polylithionite and trilithionite as the endmembers. In the case of the Li-muscovites ($0.0 \leq x \leq 1.5$) the 1M/2M1-ratio depends on the amount of impurity phases like eucryptite or sanidine depleting the reaction mixture of Li or Al. There is no solid solution between trilithionite and muscovite, instead, the Li-muscovite crystals consist of domains differing in the relative proportions of muscovite and trilithionite.

The overall composition of the synthesized micas which consist of two polytypes can be characterised by ^{29}Si, ^{1}H and ^{19}F MAS NMR spectroscopy. The Si/Al ratio in the tetrahedral layers and thus the content of $^{[4]}Al$ was calculated by analysing the signal intensities of the ^{29}Si MAS NMR experiments. The Li content *xest* was calculated from the measured tetrahedral Si/Al ratio of the ^{29}Si MAS NMR signals.

PP-041

Synthesis, structural and spectroscopic characterizations of $(Mg_{1-x}Fe_x)_2SiO_4$ olivines for the characterization of Martian regolith

M. I. Jundullah Hanafi (Bremen/DE), M. M. Murshed (Bremen/DE), L. Robben (Bremen/DE), T. M. Gesing (Bremen/DE)

Olivines $(Mg,Fe)_2SiO_4$ are important planetary and terrestrial rock-forming minerals, identified also on the Martian surface [1, 2]. For possible usages of olivines as base materials to fabricate metals in future Mars exploration, synthesis of representative olivines and their detailed structural and spectroscopic characterizations are of crucial importance. As such, a solid solution $(Mg_{1-x}Fe_x)_2SiO_4$ has been synthesized to investigate the influence of substituted iron on the structure within the series. Each member of the series is produced by high-energy ball milling with subsequent heating. X-ray powder diffraction Rietveld analysis confirm that each polycrystalline sample crystallizes in the *Pbnm* space group. The obtained average crystallite size ranges between 80(1) nm and 216(5) nm. Each lattice parameter increases with increasing Fe-content due to larger Fe^{2+} radius than that of Mg^{2+}, following the Vegard"s rule. For a given nominal x-value, substitution of Mg with Fe at the M1-site (4*a*: 0,0,0) is preferred against the M2-site (4*c*: x,y,¼). For instance, for x = 0.5, the Fe/Mg ratio at the M1- and M2-site is found to be 1 and 0.75, respectively. As such, average Fe-content lies below the equivalence line for x = 0.3 – 0.9, indicating the Fe/Mg ratio in the amorphous scattering content is most likely greater than unity. Characteristic Raman spectral features of olivines are observed at 813 cm^{-1} - 825 cm^{-1} and 838 cm^{-1} - 857 cm^{-1}. Changes in the low-frequency region < 400 cm^{-1} are associated with the substitution of the lighter Mg by heavier Fe in the octahedral sites. The global red-shift can be explained by the quasi-harmonic approach. This study keeps valuable information to relevant database for future human mission on Mars.

References:

(1) Y. Liu *et al*. Science 377(6614) (2022) 1513.
(2) Z. Váci *et al*. Meteorit. Planet. Sci. 55 (2020) 1011.

We acknowledge support by the state of Bremen within the "Humans on Mars" initiative for APF "Materials on demand" S1P3.

Fig. 1

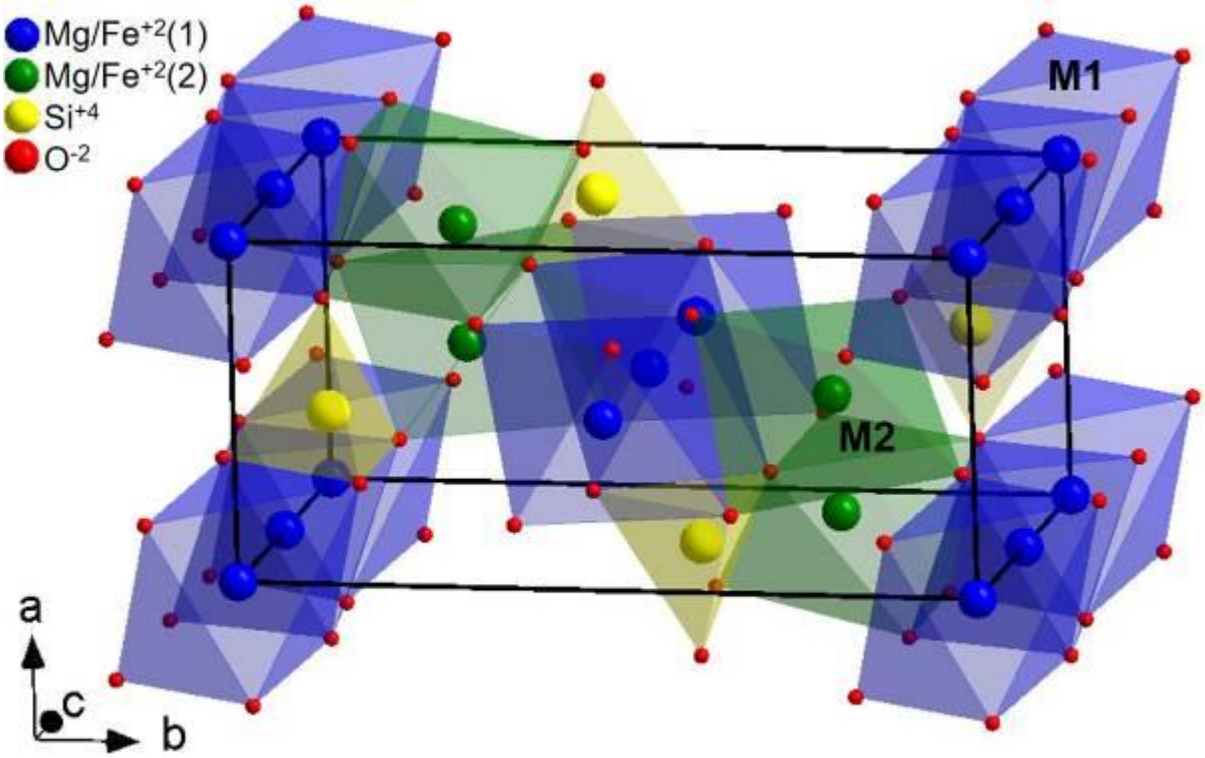

Figure 1. Crystal structure of $(Mg_{1-x}Fe_x)_2SiO_4$ olivine

PP-042

The Trigonal Crystal Structure of Matildite-Type $AgBiS_2$ Revisited

F. Lissner (Stuttgart/DE), K. Walenta (Stuttgart/DE), T. Schleid (Stuttgart/DE)

If it appears as a mineral, the ternary sulfide $AgBiS_2$ can crystallize as schapbachite (cubic, space group: *Fm*-3*m*, *a* = 564.8(3) pm, *Z* = 2) with a cation-disordered rock-salt structure (Ag^+/Bi^{3+} at 4*a*, S^{2-} at 4*b*) [1] or as an ordered trigonal variety (matildite). The latter was first considered as adopting the delafossite structure of α-$NaFeO_2$ with layerwise ordering of the still octahedrally coordinated cations within a cubic close packing of the S^{2-} anions [1]. The space group, however, given as *P*-3*m*1 instead of *R*-3*m*, was conflicting with this structure model. We now were able to refine the crystal structure of maltildite-type $AgBiS_2$ in a similar trigonal unit cell (*a* = 407.75(4) pm, *c* = 1898.3(2) pm) again, but with an ordered cinnabar-related set up, adopting the space group $P3_221$. The ordering of the involved ions on the Wyckoff positions 3*b* (Ag^+), 3*a* (Bi^{3+}) and 6*c* (S^{2-}) brings several advantages for the cations. Their different sizes is nicely reflected by the individual distances (*d*(Ag–S) = 253.0 pm (2×), 285.5 pm (2×) and 312.7 pm (2×) versus *d*(Bi–S) = 267.8 pm (2×), 286.3 pm (2×) and 304.8 pm (2×)) and their stereochemical demands are fulfilled by their local geometry (short linear S–Ag–S links for *C.N.* = 2 (Ag^+: [Kr]$4d^{10}$) versus four rather similar Bi–S contacts for *C.N.* = 4 with a sew-saw conformation allowing for the development of stereochemically active lone-pair of electrons at the Bi^{3+} cation ([Xe]$6sp5d^{10}$) pointing to the remote edge of the distorted $[BiS_6]^{9-}$ octahedron (Figure 1, top). This is illustrated in Figure 1 as compared to the cinnabar-type structure of HgS (a = 414.89(2) pm, c = 949.47(5) pm [2]), where the diversification is hidden behind the Hg–S distances (*d*(Hg–S) = 237.7 pm (2×), 309.3 pm (2×) and 327.9 pm (2×)) for the unique Hg^{2+} cation ([Xe]$5d^{10}$).

References:

(1) S. Geller, J. H. Wernick, *Acta Crystallogr.* **1959**, *12*, 46–54.
(2) Th. Schleid, P. Lauxmann, C. Schneck, *Z. Kristallogr.* **1999**, *S 16*, 95–95.

Fig. 1

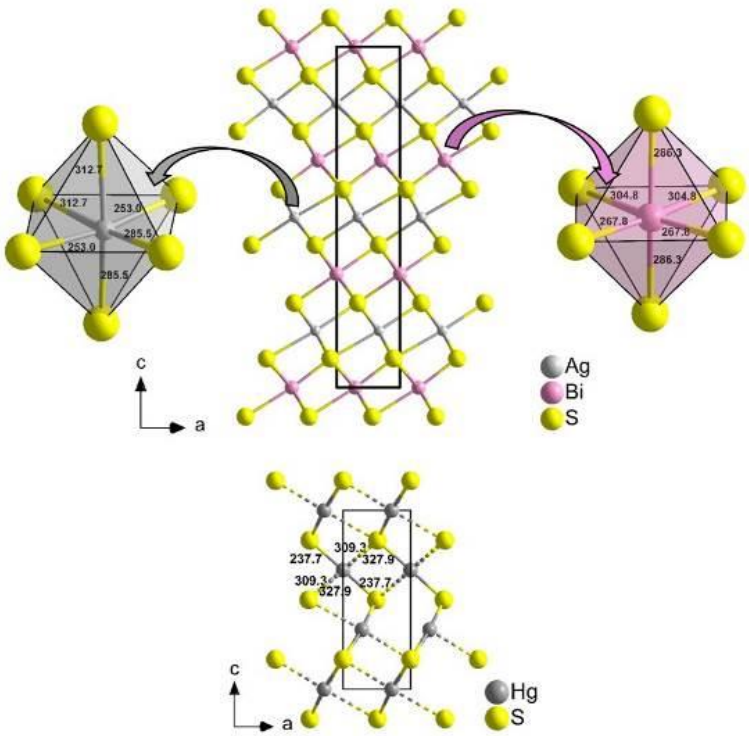

PP-043

Natural ammonium-iron-sulfites

H. Effenberger (Wien/AT)

At a burning dump from an abandoned open-coal pit three ammonium-iron-sulfites were identified (Pécs-Vasas, Mecsek Mountains, South Hungary).

$(NH_4)_9Fe^{3+}(SO_3)_6$ is metastable and decomposes quickly. **$(NH_4)_2Fe^{2+}(SO_3)_2$** crystallizes in the bütschliite-structure type. $[Fe^{3+}(SO_3)_6]^{9-}$ clusters respectively $[Fe^{2+}(SO_3)_2]^{2-}$ layers are linked *via* hydrogen bonds to the ammonium cations. In $(NH_4)_2Fe(SO_3)_2$ about 8 % of the Fe atoms are displaced (Fe–Fe' = 0.64 Å).

$(NH_4)_2Fe^{3+}(OH)(SO_3)_2 \cdot H_2O$ (mineral name kollerite, space group *Cmcm*) exhibits a new structure type. Corner linked FeO_6 octahedra form buckled $[Fe^{3+}(OH)(SO_3)_2]^{2-}$ chains. The chains are linked by clearly defined hydrogen bonds. As the O_w atom has site symmetry *m*2*m*, the H_2O molecule exhibit an orientational disorder violating at least locally *centro*symmetry. Neither a reduction of symmetry nor an enlargement of the unit cell could be verified.

It is remarkable that for a crystal with a size of only 6×7×65 μm^3 it was possible to refine the half occupied H atom position without any restrictions (*i.e.*, with variable atomic coordinates and a variable isotropic displacement parameter). X-ray data were collected with a Stoe-StadiVari diffractometer (Dectris Pilatus 300 K pixel detector, 100 W air-cooled Incoatec IμS micro-focus MoKα X-ray tube).

For details see: B. Fehér, S. Szakáll, M. Ende, H.S. Effenberger, J. Mihály, I. Sajó, L. Kótai, D. Szabó (2023): Three ammonium-iron-sulfite phases from a burning dump of the Vasas abandoned opencast coal mine (Pécs, Mecsek Mountains, Hungary) and the new mineral kollerite. - Mineralogy and Petrology 117, 231–245.

Financial support by the University of Vienna (grants BE532003, IP532010, and IP532022) is acknowledged.

PP-044

Surprising Formation of a $[Bi_6O_4(OH)_4]^{6+}$ Cation in the Dodecahydro-*closo*-Dodecaborate Hydrate: $[Bi_6O_4(OH)_4][B_{12}H_{12}]_3 \cdot 10\ H_2O$

A. Friedly (Stuttgart/DE), L. W. Zimmermann (Stuttgart/DE), T. Schleid (Stuttgart/DE)

Introduction and Objectives

Previous studies showed that cations with polarizing properties can lead to B−H bond activation of hydroborates, as evidenced by a shift of the B−H stretching vibration band in the Raman spectra[1]. In extreme cases, this bond activation results in a substitution reaction as the reaction between Bi^{3+} cations and $[B_{12}H_{12}]^{2-}$ anions to the neutral molecule $BiB_{12}H_{11}$ has shown[2]. In addition to this substitution, other reactions can also take place, as it occurs to the salt $[Bi_6O_4(OH)_4][B_{12}H_{12}]_3 \cdot 10\ H_2O$ under basic conditions.

Materials and Methods

The new compound was obtained by the reaction of $(H_3O)_2[B_{12}H_{12}]$ with an excess of $Bi_2O_2[CO_3]$ in aqueous solution at 40 °C. The free acid of the dodecahydro-*closo*-dodecaborate was produced before by an acidic cation exchanger from $Cs_2[B_{12}H_{12}]$. From the obtained sample, a prism-shaped single crystal was separated and measured at low temperature.

Results and Conclusion

$[Bi_6O_4(OH)_4][B_{12}H_{12}]_3 \cdot 10\ H_2O$ crystallizes monoclinically in the space group $P2_1/c$ with the unit-cell parameters a = 1823.04(9) pm, b = 1794.86(9) pm, c = 1358.31(7) pm and β = 91.023(3)° at 100 K for four formula unit per unit cell. In its structure, the complex cation $[Bi_6O_4(OH)_4]^{6+}$ is present, which consists of a distorted heterocubane made from four oxide with shorter (d(Bi−O) = 207 – 230 pm) and four hydroxide anions with longer distances (d(Bi−OH) = 226 – 260 pm) surrounding a $(Bi^{3+})_6$ octahedron (Figure 1). The coordination spheres of the Bi^{3+} lone-pair cations are completed by water molecules and Bi^{3+}−$H^{\delta-}$ contacts to the negatively polarized hydrogen atoms of the icosahedral $[B_{12}H_{12}]^{2-}$ anions (Figure 2).

References:

(1) E. L. Muetteries, J. H. Balthis, Y. T. Chia, W. H. Knoth, H. C Miller: *Inorg. Chem.* **1964**, *3*, 444−451.
(2) L. W. Zimmermann, Ng.-D. Van, D. Gudat, Th. Schleid: *Angew. Chem. Int. Ed.* **2016**, *55*, 1909−1911.

Fig. 1

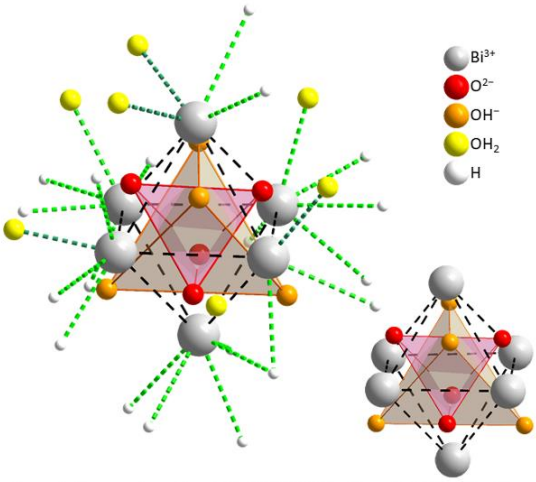

Figure 1. The complex cation $[Bi_6O_4(OH)_4]^{6+}$ (left) with and (right) without the complete Bi^{3+} coodination sphere in the crystal structure of $[Bi_6O_4(OH)_4][B_{12}H_{12}]_3 \cdot 10\,H_2O$.

Fig. 2

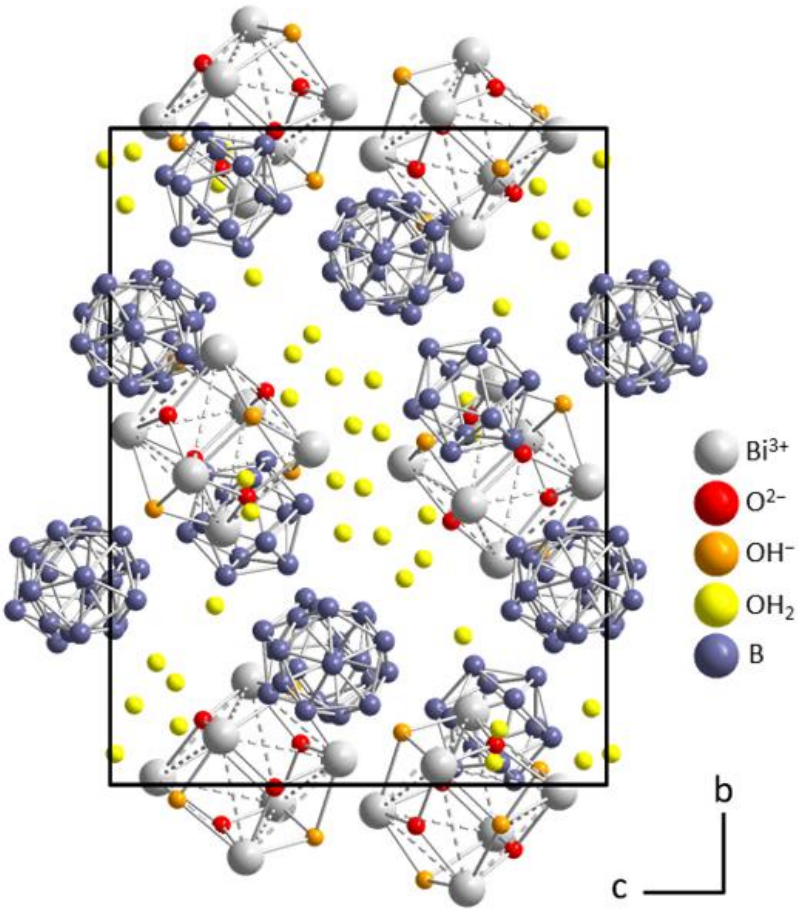

Figure 2. Extended unit cell of $[Bi_6O_4(OH)_4][B_{12}H_{12}]_3 \cdot 10\,H_2O$.

PP-046

$Gd_2F[CO_3][AsO_3]$: A Serendipitously Formed Gadolinium Fluoride Oxocarbonate Oxoarsenate(III)

F. C. Goerigk (Stuttgart/DE), R. J. C. Locke (Stuttgart/DE), T. Schleid (Stuttgart/DE)

In an attempt to synthesize $Gd_5F_3[AsO_3]_4$[1–4] under high-pressure conditions from appropriate molar mixtures of GdF_3, Gd_2O_3 and As_2O_3, which were filled into a gold ampoule with a drop of deionized water, colorless lath-shaped crystals of what turned out to be $Gd_2F[CO_3][AsO_3]$ emerged. After seven days in a piston-cylinder high-pressure cell at 10 kbar and 850 °C, some CO_2 dissolved in the applied water must have served as source for the oxocarbonate formation. The mixed-anionic $Gd_2F[CO_3][AsO_3]$ crystallizes in the monoclinic space group $P2_1/c$ with the lattice parameters a = 1015.04(6) pm, b = 772.56(4) pm, c = 775.85(4) pm and β = 109.629(3)° for Z = 4. Its crystal structure contains two positions for the Gd^{3+} cations, only one for F^-, C^{4+} and As^{3+} each, as well as six O^{2-}-anion sites, all at general Wyckoff positions 4*e*. $(Gd1)^{3+}$ is surrounded by six O^{2-} and two F^- anions, while $(Gd2)^{3+}$ has only one F^-, but seven O^{2-} anions as coordination sphere, both in the shape of distorted square antiprisms (Figure 1, left). All oxygen atoms belong to either carbon (O1 – O3) or arsenic (O4 – O6) to form planar $[CO_3]^{2-}$ triangles or $[AsO_3]^{3-}$ ψ1-tetrahedra (Figure 1, right). The fluoride anions reside in quasi-planar coordination of three Gd^{3+} cations and two of the resulting $[FGd_3]^{8+}$ triangles share a common edge (Gd1–Gd1) to assemble as discrete $[F_2Gd_4]^{10+}$ dimers (Figure 1, mid). A view of the complete crystal structure of $Gd_2F[CO_3][AsO_3]$ along [010] is shown in Figure 2. Wavelength-dispersive electron-beam X-ray microprobe analyses confirmed the composition and Raman spectra the presence of discrete $[CO_3]^{2-}$ and $[AsO_3]^{3-}$ anions as well as the absence of $(OH)^-$ groups, which could isomorphically replace part of the F^- positions.

References:

(1) F. Ledderboge, Th. Schleid, *Z. Anorg. Allg. Chem.* **2014**, *640*, 2350.
(2) F. Ledderboge, *Dissertation*, Univ. Stuttgart, **2016**.
(3) F. C. Goerigk, *Dissertation*, Univ. Stuttgart, **2021**.
(4) R. J. C. Locke, *Dissertation*, Univ. Stuttgart, **2024**.

Fig. 1

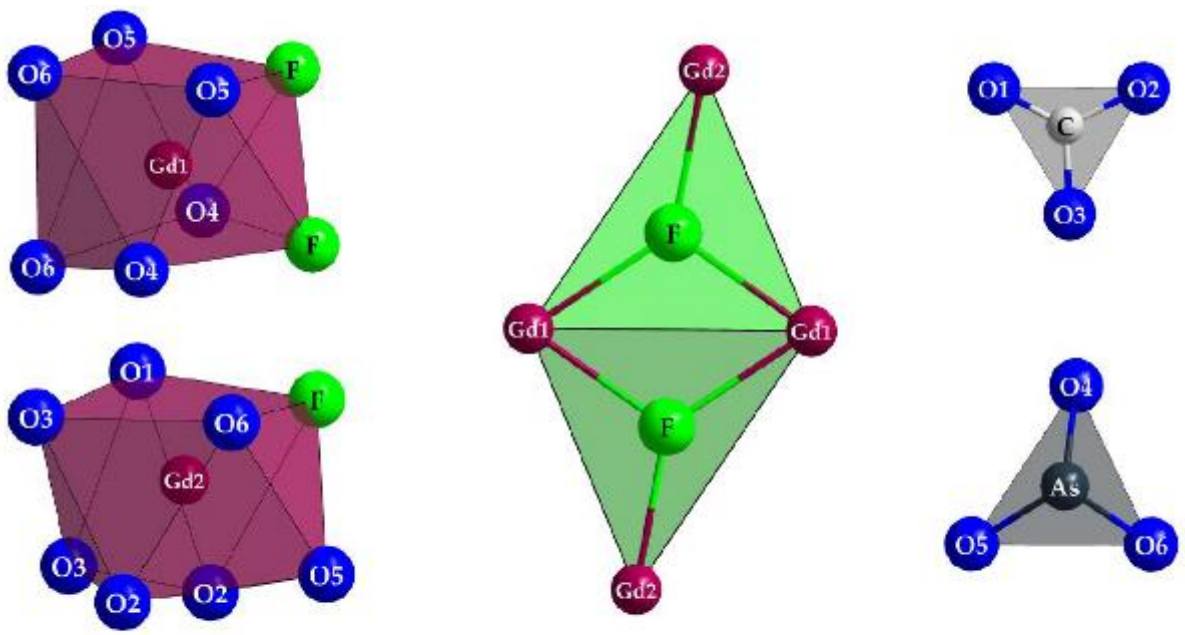

Figure 1. Distorted square antiprisms $[(Gd1)O_6F_2]^{11-}$ and $[(Gd2)O_7F]^{12-}$ (*left*), $[F_2Gd_4]^{10+}$ congonial bitriangle (mid) as well as triangular $[CO_3]^{2-}$ and ψ¹-tetrahedral $[AsO_3]^{3-}$ anion (*right*) in the crystal structure of $Gd_2F[CO_3][AsO_3]$.

Fig. 2

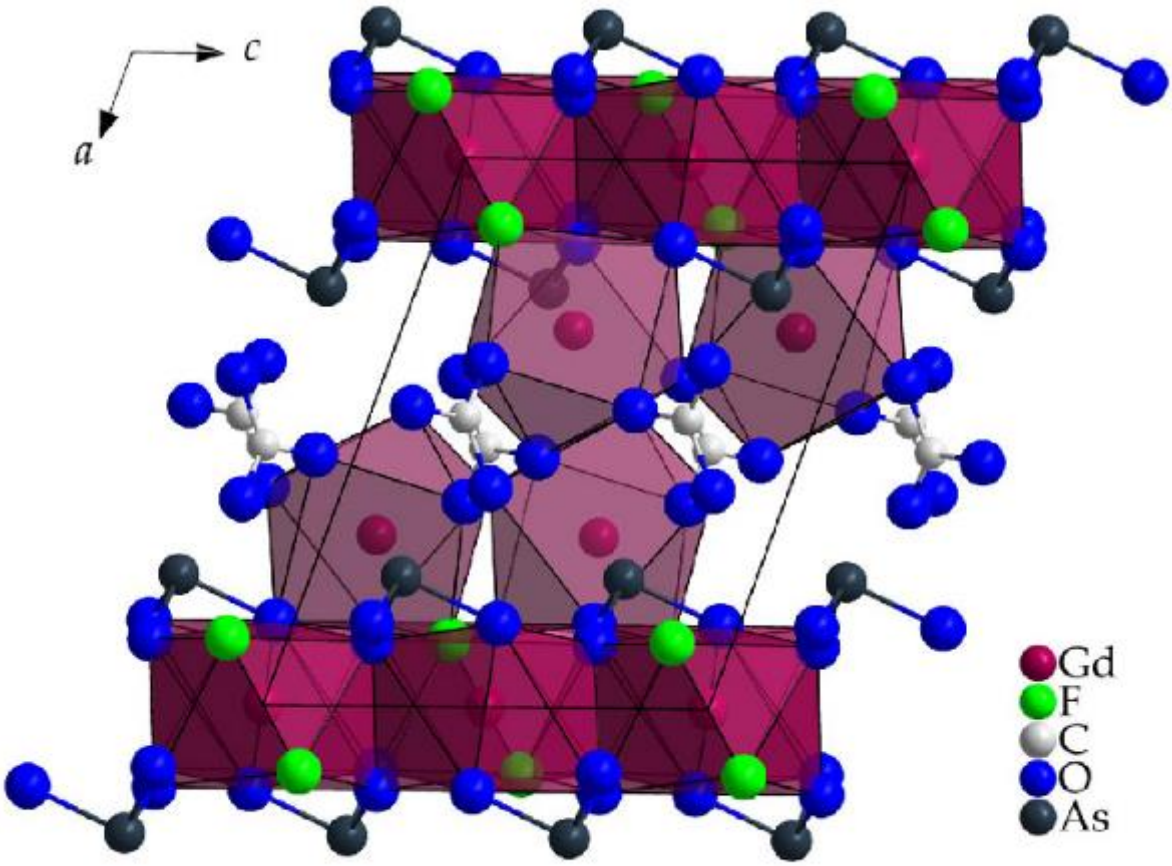

Figure 2. View at the monoclinic crystal structure of $Gd_2F[CO_3][AsO_3]$ along [010].

PP-047

$Ca_3Mg_8In_4$ and $Ca_2Mg_{4-x}In_{3+x}$ (x = 0.26): The first mixed Ca/Mg indides, including a new structure type

M. Otteny (Freiburg i. Br./DE), C. Röhr (Freiburg i. Br./DE)

In contrast to the heavy alkaline-earth metals Sr and Ba, Ca forms only very few binary phases with Mg and In, with $CaMg_2$ and $CaIn_2$ being the *A*-richest compounds [1]. Despite this, our systematic experimental investigation of the system Ca-Mg-In yielded the two Ca-poor new orthorhombic title compounds, which were obtained by slowly cooling stoichiometric melts of the elements. The new structures can be described either by their In anion packing (with Ca/Mg stuffed voids) or by a Mg/In heteropolar anionic network. The first Zintl-like description follows from the calculated Bader charges, whereas the second one is justified by the Mg-In bcp's of the electron density maps.

$Ca_2Mg_{4-x}In_{3+x}$ (x=0.26, *Ima*2, a=762.46(5), b=1433.8(1), c=823.33(5) pm, $R1$=0.0309) crystallises in the TiFeSi-type, a superstructure of Fe_2P/ZrNiAl [2]. Here, In atoms are arranged in distorted (In_2 dumbbells) $3^3{\cdot}4^2{+}3^6$ (1:2) nets, |:AB:| stacked ⊥ *c* (Fig. 1, left). Ca occupies octahedral voids, whereas the smaller Mg cations exhibit a tetrahedral as well as a square planar coordination by In (Fig. 1, right). The Mg/In polyanion consists of edge-sharing $MgIn_4$ tetrahedra and MgIn(In2)In(2) pyramids.

The Mg-rich phase $Ca_3Mg_8In_4$ forms a new structure type (*Fdd*2, a=1762.13(6), b=3321.1(1), c=1016.81(4) pm, $R1$=0.0231) with In arranged in h.c.p. layers, which are $(hc)_2$ stacked ⊥ *b*. All Ca and one Mg atom fill up all octahedral voids, the remaining Mg atoms occupy 7/8 of the tetrahedral voids (Fig.2, left). The Mg/In network consists of corner-sharing building blocks: In-centered cubes $In@Mg_2Mg_{6/2}$ (M_6, *C*, blue) and μ_3 capped icosahedra halfs $Mg_4In_{5/2}Mg_{3/2}In$ (M_9, μ_3 *I*/2, red) in a 1:2 ratio.The μ_3 *I*/2 clusters are again arranged in pseudo hexagonal layers ⊥ *b* which are **ADD'D"** stacked (γ-Pu type, Fig. 2, right).

References:

(1) M.O., K. Köhler, M. Wendorff, C.R.,*Acta Crystallogr.* **A78**, e554 (2022).; *Z. Naturforsch.* **59b**, 619 (2004).

(2) R. Kraft et. al, *Z. Naturforsch.* **59b**, 513 (2004).

Fig. 1

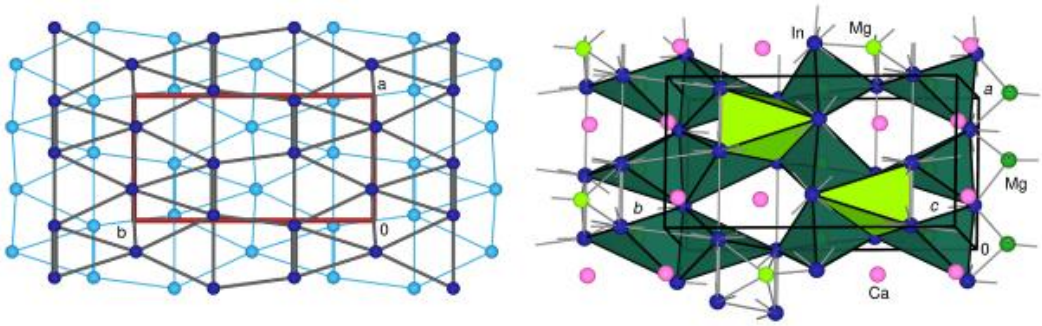

Fig. 2

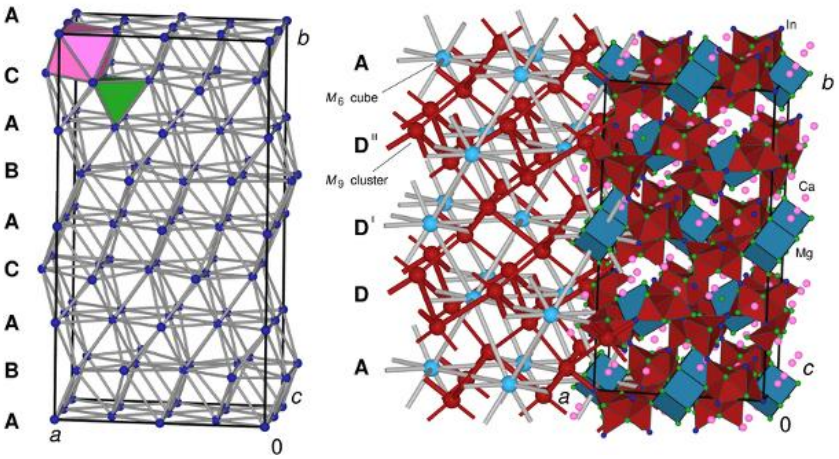

PP-048

Structural relations in the A_2MO_3 family on the example of Cs_2CeO_3

I. Zaytseva (Munich/DE), L. Nusser (Munich/DE), C. Hoch (Munich/DE)

The oxocerate(IV) Cs_2CeO_3 has been synthesised by reacting Cs_2O with cerium metal at 650 °C. The series A_2MO_3 (with A = Li – Cs, and M = Ge, Sn, Pb, Zr and more) comprises a variety of structure types [1–3]. On the example of the first single crystals of Cs_3CeO_2 (colourless transparent air-sensitive crystals, orthorhombic, space group $Cmc2_1$, a = 11.493(3) Å, b = 7.7429(15) Å, c = 6.4321(12) Å, V = 572.4(2) Å^3, Z = 4) we discuss (pseudo)inversion symmetry. The structure is built from $^1_\infty[CeOO_{4/2}]^{2-}$ chains of $[CeO_5]$ square pyramids with common square edges and alternatingly oriented apical O atoms. The main group analogue of this compound is Cs_2PbO_3, first published in the centrocymmetrical space group *Cmcm,* later corrected to $Cmc2_1$ [3, 4]. There is no difference in the reflection conditions of the two possible space groups *Cmcm* and $Cmc2_1$, the *E*-value statistics can be impaired by twinning, and the difference in powder patterns of Cs_3CeO_2 in these space groups manifests only in a marginal variation of intensities. Therefore, geometry and distortion of the anions as well as the observed electron density distribution must be considered. The presence of an inversion centre necessitates a mirror plane in between the $[CeO_5]$ pyramids, fixing the distortion angle to 180 °, and moving the apical oxygen atoms from a general position to the special position 4*c* with point symmetry *m*2*m*. We give a comprehensive overview over the A_2MO_3 structure family and discuss the structure of Cs_2CeO_3 with the help of single crystal X-ray diffraction, assisted by experimental and simulated vibrational spectra.

IZ acknowledges support by DFG under grant number 444769550.

Reference:

(1) B. M. Gatehouse, D. J. Lloyd, *J. Solid State Chem.* (1970) **2**, 410.
(2) C. Brink, N.F. Binnendijk, J. van de Linde, *Acta Cryst.* (1954) **7**, 176.
(3) [3] P. Panek, R. Hoppe, *Z. Anorg. Allg. Chem.* (1972) **393**, 13.
(4) [4] H. Stoll, R. Hoppe, *Z. Anorg. Allg. Chem.* (1987) **551**, 151.

Fig. 1

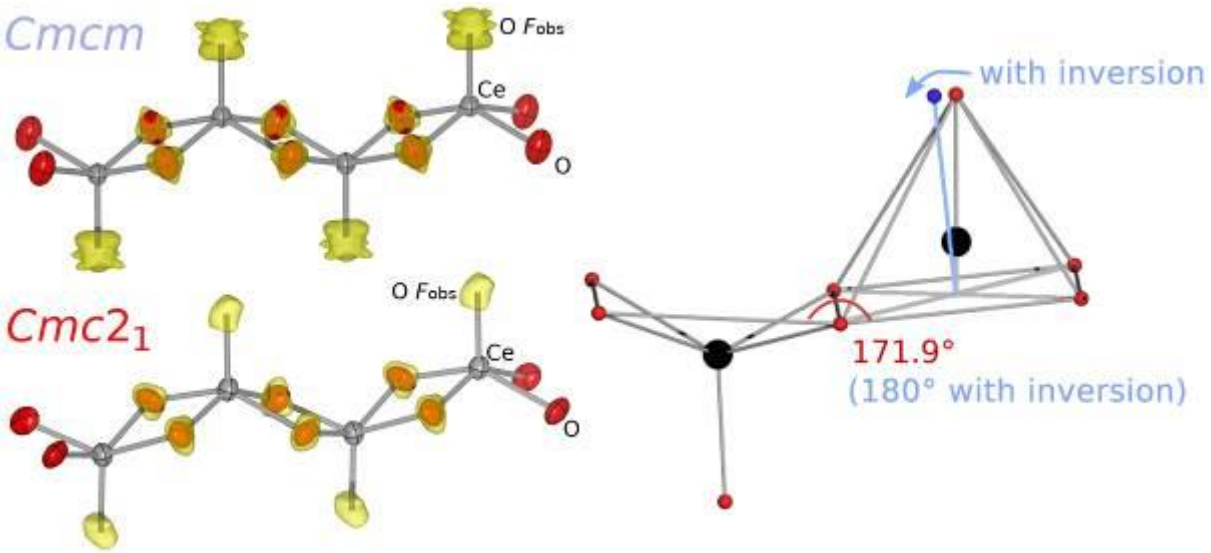

PP-049

$KAlS_2$, $KAlSe_2$ and $RbAlTe_2$: New members of the alkali dichalcogenido metallate series $AM^{III}Q_2$

M. Schwarz (Freiburg i. Br./DE), V. Daiber (Freiburg i. Br./DE), C. Röhr (Freiburg i. Br./DE)

In the course of our investigations of alkali chalcogenido ferrates [1] a comparison of the structure chemistry with the related diamagnetic Al, Ga and In compounds is suitable to further explore the geometric (and magnetic) parameters that determine the crystal chemistry of common compounds series like A_5MQ_4, $A_6M_2Q_6$ [2] and finally AMQ_2. The structures occuring in the latter series are summarized in Fig. 1: Whereas all ferrates(III) (with AFM coupled HS-d^5 Fe) show SiS_2 analogous chains (red symbols, **1**-**5**), this structure motif is only found for some tellurido trielates (**1**) and the HT forms of $CsGa(S/Se)_2$ (**3**) [3]. For all remaining trielates, the $KInS_2$-type [4], with sheets of T_2 supertetrahedra (Fig. 2), i.e. cornersharing tetrahedra only, is the dominant structure type (green, **6**). This structure family was now completed by the aluminates $KAlS_2$, $KAlSe_2$ and $RbAlTe_2$, which were synthesized from melts of the elements. Whereas the data of the two potassium compounds could be refined conventionally [e.g. $KAlS_2$: a=1034.6, b=1033.8, c=1469.2, β=100.16°, $R1$=0.0620, cf. Fig. 2], the *hhl* sections of $RbAlTe_2$ (a=1181.4, b=1182.3, c=1704.6 pm, β=99.999°) show very strong diffuse scattering with streaks along c^*. Similar to $K(Ga/Al)(Se/Te)_2$ [5], the intensity distribution is simulated by stacking faults ⊥ to the *ab* plane. For the AMQ_2 compounds of Fig. 1, a full literature survey and a structural map, which takes geometric criteria into account, are presented.

References:

(1) M. Schwarz, P. Stüble, K. Köhler, C. Röhr, *Z. Kristallogr.* **235**, 275 (2020).

(2) M. Langenmaier, S. Wissinger, C. Röhr, *Z. Anorg. Allg. Chem.* **646**, 138 (2020).

(3) D. Friedrich, M. Schlosser, A. Pfitzner, *Cryst. Growth Des.* **16**, 3983 (2016).

(4) H. Schubert, R. Hoppe, *Z. Naturforsch.* **25b**, 886 (1970).

(5) J. Kim, T. Hughbanks, *J. Solid State Chem.* **149**, 242 (2000).

(6) S. Balijapelly et al., *Inorg. Chem.* **62**, 3886 (2023).

(7) H. Lin, J.-N. Shen, W. Ling. L.-M. Wu, *Inorg. Chem.* **52**, 10726 (2013).

Fig. 1

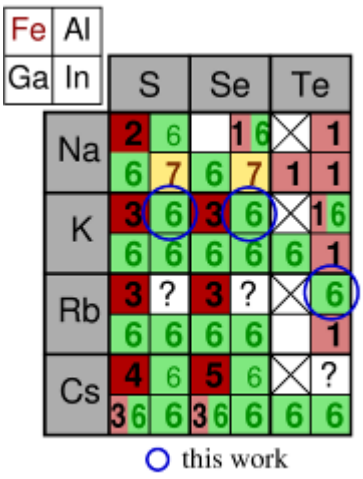

Fe	M	structure type	spacegroup	CN(A)	polyanion
	1	$TlTlSe_2$	$I4/mcm$	8	linear chains
2		$NaFeS_2$	$I222$	4	
3	3	$KFeS_2$	$C2/c$	8	
4		$CsFeS_2$	$Immm$	8	
5		$TlFeS_2$	$C2/m$	6	
	6	$KInS_2$	$C2/c$	6+2	sheets of T2 supertetrahedra
	7	$NaCrS_2$	$R\bar{3}m$	6	octahedra

Fig. 2

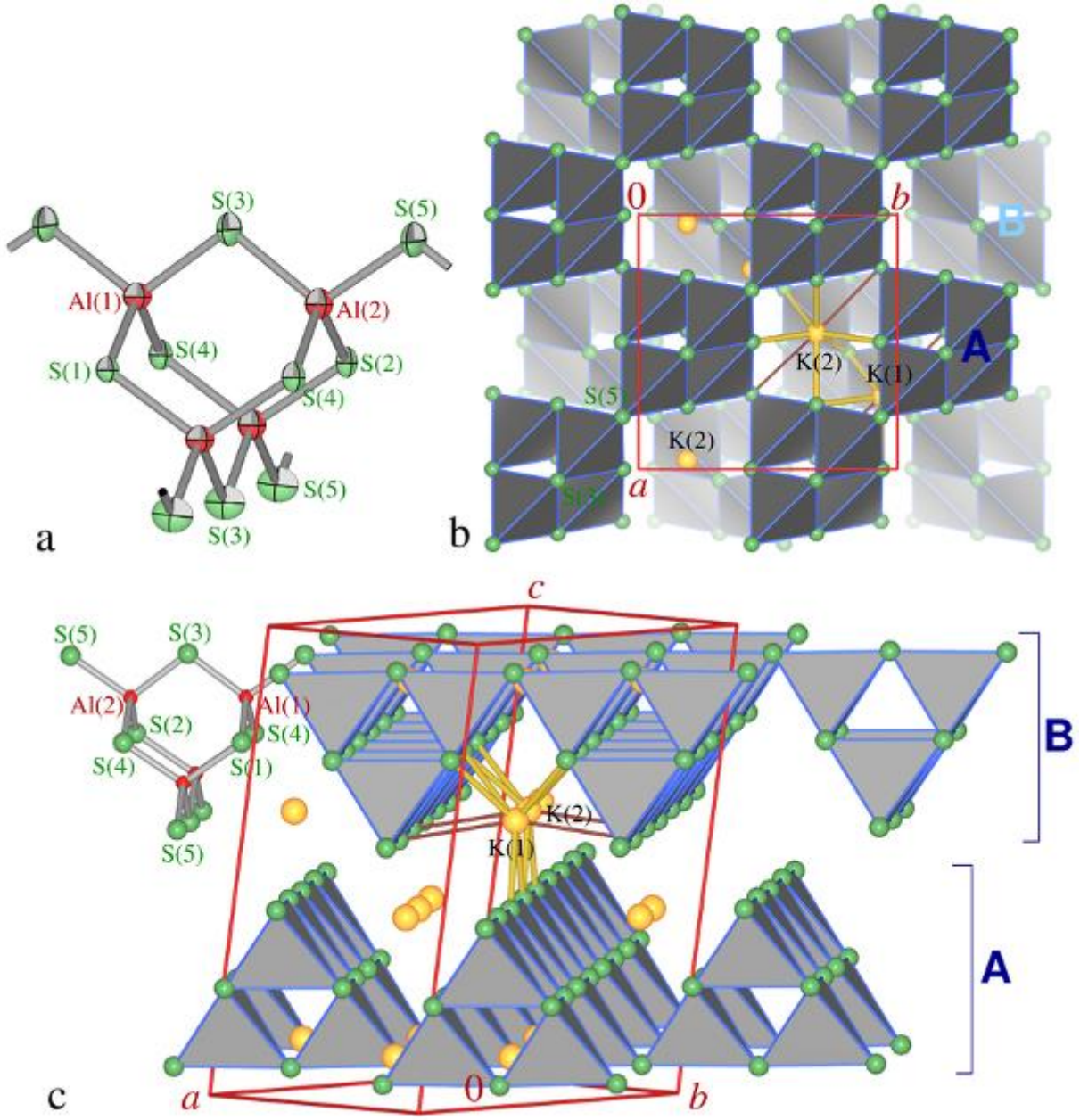
S(3)
S(5)
Al(1)
Al(2)
S(4)
S(1)
S(2)
S(4)
S(5)
S(3)
a
0
b
B
A
K(2)
K(1)
S(5)
K(2)
a
b
S(5)
S(3)
Al(2)
Al(1)
S(2)
S(4)
S(4)
S(1)
S(5)
c
K(2)
K(1)
B
A
c
a
0
b

PP-050

Crystal structure determination of $Rb[SbO(OH)_4]$ – a hitherto new structural set-up for alkali metal hydroxidoantimonates(V)

T. Wolflehner (Vienna/AT), M. Weil (Vienna/AT), B. Stöger (Vienna/AT)

Due to their comparatively good solubility in water, oxidic alkali metal hydroxidoantimonates(V) are important precursor compounds for the synthesis of oxidic antimony compounds under hydrothermal conditions. Our knowledge of the family of alkali metal hydroxidoantimonates(V) is restricted to the phases $K_2[Sb(O)(OH)_5]$, $Na[Sb(OH)_6]$, Cs[Sb(OH)6] and $Cs_2[Sb_2(\mu\text{-}O)_2(OH)_8]$ [1]. A corresponding rubidium salt has not been reported so far, which motivated us to start phase formation studies in the system $Rb/Sb^V/O/OH$. Indeed, it was possible to obtain a previously undescribed salt with the composition $Rb[SbO(OH)_4]$ and to determine its crystal structure.

$Rb[SbO(OH)_4]$ was obtained hydrothermally at 210 °C, starting from RbOH, $Te(OH)_6$ and Sb_2O_3 at pH ~10. Under these conditions, $Te(OH)_6$ oxidizes Sb_2O_3 under formation of elementary tellurium. The grown colourless $Rb[SbO(OH)_4]$ crystals had a needle- to block-like form and showed extensive intergrowth, which complicated crystal structure determination and refinement due to the presence of multiple domains. For the final structure solution, a data set originating from three domains was used. The diffraction pattern showed pseudo-orthorhombic symmetry (a ~ 5.66 Å, b ~ 7.29 Å, c ~ 5.67 Å, β ~ 90°), with the crystals in fact being monoclinic ($P2_1/m$, Z = 2).

The asymmetric unit of $Rb[SbO(OH)_4]$ comprises of one Sb atom (site symmetry 1), one Rb atom (m), one O atom (m), two O atoms belonging to hydroxyl groups (1) and two H atoms (1). The Sb^V exhibits a slightly distorted octahedral $[Sb(OH)_4O_2]$ coordination environment with a mean Sb–O distance of ~1.98 Å. By corner-sharing the oxygen atoms, straight $[SbO_{2/2}(OH)_{4/1}]^-_\infty$ chains extending parallel to [010] are formed. The Rb^+ ions are situated between these chains and have contacts to 12 oxygen atoms within a range between 3.00 and 3.40 Å. O–H…O hydrogen-bonding interactions of medium strengths consolidate the crystal packing.

PP-051

Novel rubidium-antimony-chlorides with unusual structural motives

M. Bravic (Freiburg i. Br./DE), M. Daub (Freiburg i. Br./DE), H. Hillebrecht (Freiburg i. Br./DE)

Antimony- and bismuth halides are present in a variety of perovskite-like compounds, such as $Cs_2AgSbCl_6$, Cs_2SbCl_6, $Rb_3Sb_2Br_9$ and $Cs_4CuSb_2Cl_{12}$ to name a few [1]. Due to the lone-pair effect, antimony- and bismuth halides could occur in square pyramidal and octahedral configurations. These polyhedra can form a multitude of anionic sublattices through combination of multiple units by sharing common corners, edges or faces [2,3]. However, with the combination of rubidium, antimony and chloride, several new compounds with uncommon structural units could be discovered.

We accomplished to determine the crystal structure of $Rb_4CuSb_2Cl_{12}$, which was first synthesized by Vargas et. al. [4]. The structure is similar to the structure <111>-vacancy–ordered 2D perovskites as $Cs_4CuSb_2Cl_{12}$, but due to the rotation of half the $[CuCl_6]^{4-}$–octahedra, the antimony occurs in $[SbCl_5]^{2-}$–square pyramids instead of $[SbCl6]^{3-}$–octahedra. This leads to a reduction of the symmetry to the triclinic space group *P*(2).

One newfound compound includes the motiv of an $[Sb_{18}Cl_{84}]^{30-}$–polyhedron, which can be found in $Rb_{26}Sb_{16}Cl_{75}$. It is composed of corner sharing $[SbCl_6]^{3-}$–octahedral. The crystal structure can be described as a complex variant of a cubic perovskite with additional Rb^+ and Cl^-.

In $Rb_{19}Cd_4Sb_5Cl_{42}$ there are isolated face-sharing dioctahedra $[M_2Cl_9]$ combined with pentameric units of five $[MCl_6]$–octahedra connected by common corners to a $[M_5Cl_{24}]$ cluster. It is not possible to distinguish Cd/Sb, but an electron-precise composition is obtained with the assumption of the units $[Cd_2Cl_9]^{5-}$ and $[Sb_5Cl_{24}]^{9-}$. The crystal structure still shows some similarities to the closest packing AX_3 of the perovskite type, but the differences are now more significant.

References:

(1) Q. A. Akkerman, L. Manna, *ACS energy letters* **2020**, *5*, 604.
(2) N. Shen, et al., *CrystEngComm* **2020**, *22*, 3395.
(3) K. M. McCall, et al. , *ACS materials letters* **2020**, *2*, 1218.
(4) B. Vargas, R. et. al, *Chem. Mater.* **2020**, *32*, 424.

PP-052

***RE*-Fe-Sb compounds – crystal structure and magnetic interactions of two representative groups**

M. Schulze (Dresden/DE), F. Pabst (Amsterdam/NL), T. Doert (Dresden/DE), M. Ruck (Dresden/DE)

Intermetallic *RE-TM*-antimonides containing rare-earth metal *RE* and transition metal ions *TM* show a large variety of crystal structures. Single crystals of these compounds can be grown in multiple ways. This study used Bi flux syntheses followed by hot centrifugation, which gives access to representatives of the $RE_3TM_3Sb_7$ and $RETMSb_3$ compounds. Large needle-shaped single crystals of $RE_3Fe_3Sb_7$ can be obtained for *RE* = Pr, Nd and Sm. Further substitutions are strongly restricted for all structure sites, probably due to particular atomic interactions in the complex $RE_3Fe_3Sb_7$ crystal structure. The $RETMSb_3$ compounds show a more pronounced compositional diversity. Single crystals of $REFeSb_3$ were already described for *RE* = Pr, Nd, Sm, Gd and Tb, while the Ce-member was newly discovered in this study. As *RE-TM*-Sb representatives host *RE* and *TM* atoms in variable arrangements, they can show complex 3*d* and 4*f* electron interactions, resulting in exotic magnetic behaviour. Accordingly, the $RE_3Fe_3Sb_7$ compounds show anti-ferromagnetic ordering of the *RE* and *TM* substructures, which induces spontaneous negative magnetisation (e.g. $Pr_3Fe_3Sb_7$). In contrast to that, the $REFeSb_3$ compounds show seemingly no *TM* contribution to the magnetic behaviour. As this phenomenon is poorly understood, the magnetic properties of the $REFeSb_3$ compounds are about to be further investigated.

PP-053

Survey of zirconium-containing NaSICON-type solid-state Li+ ion conductors with the aim of increasing reduction stability by partial cation substitution

A. Loutati (Titz/DE, Duisburg-Essen/DE)

Various compositions of the series Li1+xM3+xZr2-x(PO4)3 where M3+ = Al3+, Sc3+, Y3+ were prepared by solution-assisted solid-state reaction, since they could have a higher reduction stability as solid electrolytes in lithium batteries than in germanium- or titanium-containing materials. The influence of substitution on crystallographic parameters, density, and ionic conductivity were investigated. The cation substitution of M3+ (M = Al, Sc, Y) for Zr4+ in LiZr2(PO4)3 stabilizes the rhombohedral NaSICON structure (space group) at room temperature and increases the ionic conductivity significantly. Here, at 25 °C and with a consistent relative density of 94-96 %, an ionic conductivity of 2.7 × 10-5 S cm-1, 6.7 × 10-5 S cm-1, and 3.6 × 10-6 S cm-1 was achieved with the compositions Li1.2Sc0.2Zr1.8(PO4)3, Li1.2Y0.2Zr1.8(PO4)3, and Li1.2Al0.2Zr1.8(PO4)3, respectively. In comparison with Li1+xScxZr2-x(PO4)3, the Y3+ substitution in LiZr2(PO4)3 enhanced the ionic conductivity slightly and denoted the maximum Li+ ionic conductivity obtained at room temperature. However, substitution with Al3+ decreased the ionic conductivity.

For the first time, this work provides a complete overview of three series of solid Li-ion conductors in the Li2O-M2O3-ZrO2-P2O5 system where M = Al, Sc, Y. Noticeable differences in the chemistry of resulting compounds were observed, which likely depend on the ionic radius of the cations being substituted. The series with Sc showed complete miscibility from x = 0 to x = 2 with a continuous change of the NaSICON polymorphs. The series with Y showed a solubility limit at about x = 0.3 and higher substitution levels led to the increasing formation of YPO4. The series with Al exhibited continuously decreasing ionic conductivity until x = 1, whereupon the investigation was terminated due to its very low conductivity of about 10-10 S cm-1

PP-054

Synthesis and characterization of sulfido silicates

I. Dimitrova (Berlin/DE), G. Thiele (Berlin/DE)

Inspired by the family of lithium superionic conductors and the sodium ion conductors based on the A-Si-S (A = Li, Na) systems, we extend the search for solid state electrolytes for all-solid-state batteries to further members of the A-Si-S (A = Li, Na, K, Rb, Cs) compound class. As only five ternary alkali metal sulfido silicates have been reported so far, the initial focus lies on the synthesis and characterization of new compounds of this class. Herein we present the synthesis and characterization of four new ternary alkali metal sulfido silicates.

PP-055

Halogen bonds vs. hydrogen bonds in the crystal packing formation of halogen substituted anilines

I. Konovalova (Kharkiv/UA, Dusseldorf/DE), G. J. Reiss (Dusseldorf/DE)

The halogen substituted anilines (Fig.1) are key structural blocks of bioactive products, medically important compounds and organic functional materials. Therefore, the study of molecular and crystal structure of such a type of compounds has an immense importance.

Fig. 1 Crystal packing (on the left) and the energetic vector diagram (on the right) of o-chloroaniline.

All modern approaches to the molecular crystal structure analysis base on the comparison of the geometric characteristics of intermolecular interactions. However, these approaches are useless in many cases: a lot of weak interactions presence, the specific directed interactions absence etc.

In the case of halogen substituted anilines the presence only of weak (N/C-H...π, N-H...N and halogen bonds) types of intermolecular interactions complicates the description of the crystal structures. It is difficult to define the main structural motif in the solid state just on the basis of geometrical considerations. Taking into account the significant attention to halogen bonds in recent years, it is interesting to compare the crystal structures of the isomers of halogen substituted anilines from energetic viewpoint and analyze the role of different types of intermolecular interactions. The crystal packing analysis from energetic viewpoint indicates that the role of halogen bonds in supramolecular architecture depends on the position of halogen atom in the aromatic cycle.

Fig. 1

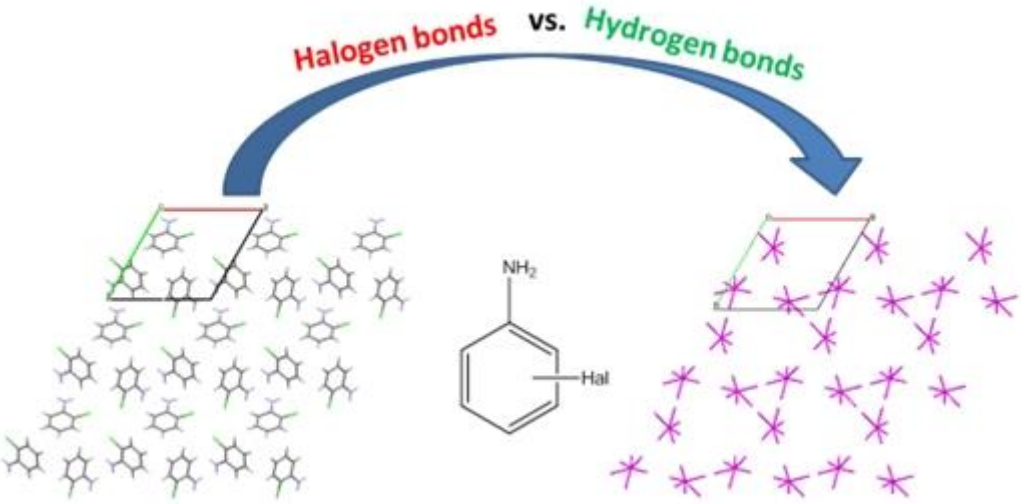

PP-056

A structural study of the isomers of the aminopyridine using non-spherical atomic form factors

G. J. Reiss (Düsseldorf/DE), I. Konovalova (Düsseldorf/DE, Kharkiv/UA)

Aminopyridines possessing biological activities are of general interest. For example, the 4-aminopyridine is used in MS therapy. The structures of the three isomers of amino-pyridine are known since the 70th of the last century [1-3]. Crystal structure re-determinations with quality data are limited to two cases [4, 5]. New crystallographic methods like the usage of non-spherical atom form factors [6] for quality standard datasets opens the possibility to do re-determinations on a much higher level. Thus we have collected new diffraction data for the three isomers of aminopyridine (*ap*) and re-refined the crystal structures using the NoSpherA2 option of the OLEX2 program system (see Figure 1).

Our previous crystal structure organization analysis for the isomers of mono-aminopyridines (2-*ap*, 3-*ap*, 4-*ap*) were studied using an approach based on comparison of interaction energies between molecules calculated by *ab initio* quantum chemical methods [7]. The presence of the pyridine nitrogen atom causes the formation of a typical N-H...N_{pyr} hydrogen bond, which is the strongest intermolecular interaction in all the studied structures. The donor acceptor distances for the N-H...N hydrogen bonds are 2.9773(8) Å for 4-*ap*, 3.0699(8) Å for 2-*ap and* 3.09773(8) Å for 3-*ap*. Being amphiphilic in hydrogen bond formation, the amino group possesses acceptor properties only in the *meta*-position in mono-aminopyridines. Additionally, C/N-H...π hydrogen bonds were observed in all isomers of aminopyridines. It should be noted that stacking interactions are absent in mono-aminopyridines despite the presence of the aromatic π-system.

Fig. 1. The aminopyridine isomers (2-*ap*, 3-*ap*, 4-*ap*) re-determined from standard diffraction datasets using non-spherical atom form factors

References:

(1) M.Chao, E.Schempp, R.D.Rosenstein, *Acta Crystallogr. B,* **31** (1975) 2922.
(2) M.Chao, E.Schempp, R.D.Rosenstein, *Acta Crystallogr. B* **31** (1975) 2924.
(3) M.Chao, E.Schempp, *Acta Crystallogr. B,* **33** (1977) 1557,
(4) Ilyukhin, P. Koroteev, CCDC 2170593: *Experimental Crystal Structure Determination*, 2022.
(5) F .P. Anderson, J. F. Gallagher, P. T. M.Kenny, A .J. Lough, *Acta Crystallogr. E,* **61** (2005) o1350.
(6) L. Midgley, L. J. Bourhis, O. V. Dolomanov, S. Grabowsky, F. Kleemiss, H. Puschmann and N. Peyerimhoff Acta Crystallogr. A, **77** (2021) 519.
(7) S. Konovalova,, E. N. Muzyka, V. V. Urzhuntseva, S.V. Shishkina, Struct. Chem. **32** (2021) 235.

Fig. 1

PP-057

Stabilization of Guanidinate Anions $[CN_3]^{5-}$ in Calcite-Type $SbCN_3$

L. Brüning (Cologne/DE), N. Jena (Linköping/SE), E. Bykova (Frankfurt a. M./DE), P. Jurzick (Cologne/DE), N. Flosbach (Cologne/DE), B. Winkler (Frankfurt a. M./DE), I. Abrikosov (Linköping/SE), M. Bykov (Cologne/DE)

The stabilization of nitrogen-rich phases presents a significant chemical challenge due to the inherent stability of the dinitrogen molecule. Since synthesized N-based materials have a wide range of applications, such as the ultra-high hardness of nitrides, this opens the motivation for new synthetic routes to N-based materials.

The stabilization of nitrogen rich phases can be achieved by utilizing strong covalent bonds in complex anions with carbon, such as cyanide $[CN]^{1-}$ and $[NCN]^{2-}$ carbodiimide, while more nitrogen-rich carbonitrides with higher dimensionality like guanidinate $[CN_3]^{5-}$ and ortho-nitrodocarbonate $[CN_4]^{8-}$ are hitherto unknown. A straightforward approach to synthesizing guanidinates involves the deprotonation of guanidine, which can be performed by strong bases in ammonothermal reactions in autoclaves. This method allowed to achieve double-deprotonated guanidinates in solid phases. However, achieving full deprotonation of guanidine proves impossible due to guanidine's inherent properties as a very strong base itself. Our thermodynamically and pressure-driven synthesis approach in laser-heated diamond anvil cells leads to fully deprotonated guanidinate $[CN_3]^{5-}$ from elements or C-N containing precursors in a hydrogen-free environment. The crystal structure of $SbCN_3$ was solved and refined from synchrotron single-crystal X-ray diffraction data. $SbCN_3$, which is isostructural to calcite $CaCO_3$, can be recovered under ambient conditions and is a predicted direct bandgap semiconductor, making it a promising candidate for optoelectronic applications. This study opens a straightforward route to the entire new family of inorganic nitridocarbonates with higher dimensionality.

https://doi.org/10.1002/anie.202311519

Fig. 1

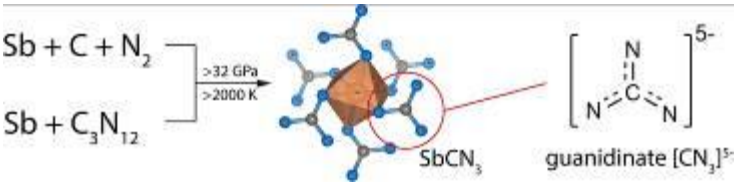

PP-058

Neutron diffraction studies of high pressure effects on some complex cobalt oxides.

V. Sikolenko (Leipzig/DE)

Here we present the results of neutron diffraction studies of magnetic properties and crystal strucure of some complex cobalt oxides under high external pressure up to 8 GPa and low temperatures. As object of studies were chosen: oxygen deficient doped compex cobalt oxides La(Ba)CoO3-x, tetragonal Nd-doped cobalt oxides, layered Y and Ca doped cobalt oxides. It was shown, that applying of high pressure leads to induce of ferromagnetic orderng in initially antiferromagnetic ordered oxygen deficient cobalites, suppressing of ferromagnetic ordering in layered cobaltites and inducing of magnetic ordering in Nd subblattice in Nd-Ba-Co-O complex system. Mechanisms of superexchange interaction of cobalt ions and influence of rare earth subblatice are discussed

PP-059

Hydrogenation Reactions at High Pressures and High Temperatures: *In situ* Synchrotron Diffraction Studies of the Formation and Polymorphism of K_2SiH_6

D. C. Beyer (Leipzig/DE), K. Spektor (Hamburg/DE), H. Kohlmann (Leipzig/DE), U. Häussermann (Stockholm/SE)

Here we report on *in situ* observations at gigapascal pressures based on the large volume press (LVP) high-pressure methodology employing ammonia borane, BH_3NH_3, as a hydrogen source. LVPs provide a well controllable and stable reaction environment at high *p* and *T* for extended periods of time. The application of high pressures (ranging from 4 to 10 GPa) in hydrogenation reactions using KH/Si mixtures or KSi as starting materials affords the crystalline hydridosilicate K_2SiH_6, which possesses unique hypervalent $[SiH_6]^{2-}$ complexes and is quenchable to ambient pressures.[1] In these previous investigations it was found, that Si is rather unreactive and KSi forms byproducts with the hydrogen source. Therefore, we report on *in situ* diffraction studies of hydrogenation reactions using the silanide $KSiH_3$ as a precursor at 8 and 13 GPa.[2] Upon heating the formation of K_2SiH_6 adopting a trigonal $(NH_4)_2SiF_6$ structure type (*P*-3*m*1) was observed at 260 °C and was stable up to 725 °C at 13 GPa. After pressure release at room temperature, it transforms into a cubic polymorph below 6.7 GPa adopting the K_2PtCl_6 type structure, which is recoverable at ambient pressure. Theoretical calculations suggest that a third polymorph with a hexagonal structure is stable in the narrow pressure range 3 – 5 GPa. K_2SiH_6 is a semiconductor with a calculated (indirect) band gap of about 2 eV. In addition, the possible existence of metallic substitution variants $K_2Si_{1-x}Al_xH_6$ and $K_2Si_{1-x}P_xH_6$ is suggested by theoretical calculations.[2]

References:

(1) K. Puhakainen, D. Benson, J. Nylén, S. Konar, E. Stoyanov, K. Leinenweber, U. Häussermann *Angew. Chem. Int. Ed.* **2012** *51* 3156-3160.
(2) O. Yu. Vekilova, D. C. Beyer, S. Bhat, R. Farla, V. Baran, S. I. Simak, H. Kohlmann, U. Häussermann, K. Spektor *Inorganic Chemistry* **2023** *62* (21), 8093-8100.

PP-060

Structural Evolutions and Superconductivity of Quasi-One-Dimensional (NbSe4)3I under pressure

D. Jia (Beijing/CN), H. Gou (Beijing/CN), X. Wang (Beijing/CN), Q. Zhao (Beijing/CN)

Long-range ordered materials with amorphous building blocks discovered under pressure are unique class of materials that exhibits intriguing physical properties, such as ultrahardness and superconductivity. However, the structural pathway to the order-disordered formation of these materials under pressure remains poorly understood. Here we perform the systematic investigations of the structural and transport behaviors of (NbSe4)3I under high pressure through a thorough combination of in-situ high-pressure powder and single-crystal X-ray diffraction, Raman spectroscopy, and resistance measurements, together with transmission electron microscopy (TEM) analysis and ab initio simulations. Upon compression, (NbSe4)3I undergoes two phase transitions, an order-disordered intermediate phase and then completely transform into an amorphous phase that retains to ambient pressure. Superconductivity emerges upon partial amorphization and superconducting transition temperature Tc shows unusual linear relation with the external pressure. Single-crystal analysis and ab initio simulations reveal that disordering of compressed (NbSe4)3I originates from the decreasing distances between quasi-one-dimensional chains, leading to the enhancement of Se-Se and I-Se interactions between the chains as pressure increases. Furthermore, the superconductivity is derived from the transition from the semimetal phase to metal with a relatively higher density of states at the Fermi level after amorphization, where Se dominates at the Fermi level, rather than Nb. Our findings improve our understanding of order-disordered formation mechanism in such quasi-one-dimensional materials and provide a key insight into the correlation between superconductivity and disordered structure.

PP-061

Assessing structure of $Mg_3Bi_{2-x}Sb_x$ ($0 \leq x \leq 2$) at pressures below 40 GPa

K. Glazyrin (Hamburg/DE), W. Dong (Hamburg/DE, Beijing/CN), W. Xu (Beijing/CN, Rome/IT), Z. Guo (Beijing/CN), W. Liu (Shenzhen/CN), Y. Pan (Dresden/DE), S. Kulkarni (Dresden/DE, Hamburg/DE), X. Li (Beijing/CN)

$Mg_3Bi_{2-x}Sb_x$ ($0 \leq x \leq 2$) have gained significant attention due to their potential in thermoelectric (TE) applications. Here, we fill blanks in the phase diagram considering the space of $Mg_3(Bi,Sb)_2$ solid solutions to pressures up-to 40 GPa at room temperature. With the help of high-pressure X-ray diffraction, we describe a succession of structural transitions below 40 GPa, namely P3m1->C2/m-> $P2_1/n$ with the latter being valid for the full range of compositions. We explore in greater detail the low-pressure phase and characterize the influence of composition on $Mg_3Bi_{2-}Sb_x$ crystal structure and compressibility. Our study offers a comprehensive picture of $Mg_3Bi_{2-x}Sb_x$ as a function of pressure and chemical composition providing a solid foundation for the future experimental and theoretical studies searching for the most efficient TE compound within the compositional space of $Mg_3Bi_{2-x}Sb_x$ ($0 \leq x \leq 2$).

PP-062

Pressure-induced emission enhancement and bandgap narrowing: experimental investigations and first-principles theoretical simulations on the model halide perovskite $Cs_3Sb_2Br_9$

D. Samanta (Kalyani/IN), S. P. Chaudhary (Kalyani/IN), B. Ghosh (Kalyani/IN), S. Bhattacharyya (Kalyani/IN), G. D. Mukherjee (Kalyani/IN)

Halide perovskites have drawn significant attention due to their potential application in multiple research fields starting from photovoltaics to light emission, ferroelectricity, thermoelectric, etc. Most of the researchers have been trying to tune photovoltaic properties by using traditional ways like chemical manipulation and different processing conditions. In this work, we use pressure as a parameter and try correlating structural, optical, and electronic properties of $Cs_3Sb_2Br_9$ through **high-pressure photoluminescence, Raman scattering, and x-ray diffraction measurements.** At about 3 GPa, an **electronic transition** manifests through a broad minimum in linewidth, a maximum in the intensity of E_g, A_{1g} Raman modes, and an unusual change in the c/a ratio of the trigonal lattice. The large compressibility and observed Raman anomalies indicate a soft material with strong **electron-phonon coupling**. The observed below bandgap broadband emission in the photoluminescence measurement indicates the recombination of **self-trapped excitons**. A first-order **trigonal to a monoclinic structural transition** is also seen at 8 GPa. The first-principles density functional theory (DFT) calculations reveal that the electronic transition is associated with **direct-to-indirect bandgap transition** due to changes in the hybridization of *Sb-5s* and *Br-4p* orbitals near the Fermi level in the valence band. In addition, the DFT calculations predict a **27.5% reduction of the bandgap** in the pressure range of 0-8 GPa. This work not only provides a relationship between optical properties and structural evolution of the $Cs_3Sb_2Br_9$ under pressure but also shows an effective way to achieve high optical response by tuning interatomic distances without changing the material composition [1].

References:

(1) D. Samanta et al., Phys. Rev. B **105**, 104103 (2022).

PP-063

Compressibility of N-bearing talc: Insight into the deep nitrogen cycle

A. Minchenkova (Bayreuth/DE), D. J. Frost (Bayreuth/DE), T. Boffa Ballaran (Bayreuth/DE), A. Kurnosov (Bayreuth/DE), G. Criniti (Bayreuth/DE), C. Melai (Bayreuth/DE), W. Zhou (Bayreuth/DE), M. Hanfland (Grenoble/FR)

Xenoliths from the Earth"s upper mantle have varying nitrogen levels ranging from a few parts per million (ppm) in the sub-ridge mantle, to nearly 100 ppm in mantle-enriched areas created by recycling organic materials drawn down to the deep mantle through subduction. There is, however, a limited understanding of nitrogen partitioning among the different mantle mineral phases. Recent high-pressure experiments conducted using as starting materials of antigorite and glycine (as nitrogen source) and performed at 2.5 GPa and at 500-700°C resulted in the formation of N-bearing mineral with a chemical composition resembling that of talc. Nitrogen appears to be incorporated as NH_4^+ atoms between the T-M-T layers, where T stands for tetrahedral and M stands for octahedral sites. These layers are usually empty in the talc structures, whereas they contain NH_4^+ and K in the tobelite structure. The recovered crystals have a monoclinic symmetry and the incorporation of NH_4^+ results in a larger c-axis with respect to that of talc and severe diffuse scattering which is at the moment being evaluated. Single-crystals of N-bearing talc were selected and loaded in a diamond anvil cell (DAC) with He as pressure transmitting medium and a ruby chip for pressure determination. Single-crystal X-ray diffraction was performed at pressures up to 10.2 GPa at the ESRF ID15B beam line in order to investigate the effect of NH_4^+ incorporation on the compressibility of talc. The axial compressibility is very anisotropic as observed for all phyllosilicate minerals with the c-axis, i.e. the direction perpendicular to the layers, being the most compressible direction. The N-bearing talc structure appears much more compressible than talc however it has a very large first pressure derivative of the bulk modulus (K'=17(1)) suggesting that the small amount of NH_4^+ present in the interlayer sites affect drastically the response of the talc structure to the increase of pressure.

PP-064

High-pressure *oC*16-YBr_3 polymorph recoverable to ambient conditions: from 3D framework to layered material

A. Aslandukova (Bayreuth/DE), A. Aslandukov (Bayreuth/DE), F. I. Akbar (Bayreuth/DE), N. Dubrovinskaia (Bayreuth/DE, Linköping/SE), L. Dubrovinsky (Bayreuth/DE)

Exfoliation of graphite and the discovery of unique properties of graphene – graphite"s single layer – raised significant attention to layered compounds as precursors of 2D materials with potential applications in optoelectronics, spintronics, sensors, and solar cells. In this work, a new orthorhombic polymorph of yttrium bromide, *oC*16-YBr_3 was synthesized from yttrium and CBr_4 in a laser-heated diamond anvil cell at 45 GPa and 3000 K. The structure of *oC*16-YBr_3 was solved and refined using *in situ* synchrotron single-crystal X-ray diffraction. At high pressure it can be described as a 3D framework of YBr9 polyhedra. Upon releasing pressure, the Y-Br network changes in such a way that below 25 GPa the structure can be considered as layered. The layers are comprised of edge-sharing YBr8 polyhedra, weakly bonded by van der Waals and non-covalent Br-Br interactions (Fig. 1). According to DFT calculations, *oC*16-YBr_3 is a semiconductor with a band gap significantly sensitive to pressure. The layered material can be recovered to ambient conditions and the calculations show that it has a low exfoliation energy of 0.30 J/m^2. Our results expand the list of layered trivalent rare-earth metals halides and provide insight into how high pressure alters their structural motif and physical properties.

Figure 1. Illustration of the change in the oC16-YBr3 structural motif from a 3D framework of Y-Br polyhedra to a layered structure.

Fig. 1

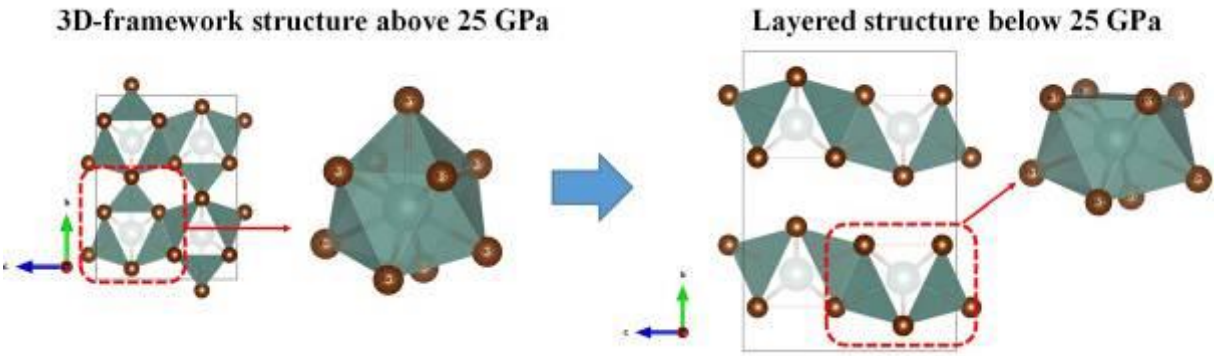

PP-065

Swift heavy ion irradiation of bismuth nanowire networks pressurized in diamond anvil cells

C. Schroeck (Frankfurt a. M./DE, Darmstadt/DE), I. Tzifas (Darmstadt/DE), L. Bayarjargal (Frankfurt a. M./DE), K. O. Voss (Darmstadt/DE), I. Schubert (Darmstadt/DE), M. Wagner (Darmstadt/DE), W. Sigle (Stuttgart/DE), I. Armstrong-Cowell (Darmstadt/DE), J. Marquardt (Frankfurt a. M./DE), C. Trautmann (Darmstadt/DE), B. Winkler (Frankfurt a. M./DE), M. E. Toimil-Molares (Darmstadt/DE)

The simultaneous exposure of materials to multiple extreme conditions is a field of increasing interest in modern high pressure (HP) research. Concomitantly applying HP using diamond anvil cells (DACs) and irradiation with swift heavy ions (SHI) of GeV energies represents a worldwide unique approach, that has been pioneered at GSI Helmholtz Centre Darmstadt. Ground-breaking experiments revealed new effects such as the generation of new phases far from thermodynamic equilibrium or the stabilization of HP phases at ambient conditions [1,2].

This report presents our activities to explore intrinsic properties of nanomaterials that facilitate the modification of HPof HP phase diagrams in order to establish nano-structuring as an additional tool in HP research to explore ion-induced effects. We studied Bismuth (Bi), due to its complex and well-characterized HP phase diagram [3] and its sensitivity to SHI irradiation [4]. Bi-nanowire networks (Bi-NWNWs) of various diameter were fabricated by electrodeposition in etched ion-track membranes [5] and exposed to various extreme conditions. Here, we will discuss the size-dependent HP phase transitions of Bi-NWNWs, as well as their respective behavior when being irradiated using SHI in both, ambient and HP conditions. Ion-induced effects were investigated applying in-situ Raman spectroscopy, offline synchrotron-XRD, secondary and transmission electron microscopy.

The authors gratefully acknowledge funding and beamtime provided by the GSI Helmholtz Centre, as well as synchrotron beamtime at PETRA-III, DESY (Hamburg, Germany).

References:

(1) Glasmacher, U.A. et al., PHYS REV LETT, 96(19), (2006), p. 195701
(2) Lang, M. et al., NAT MAT, 8(10), (2009), p. 793
(3) Ono, S. et al., HIGH PRESSURE RES, 38(4), (2018), p. 414
(4) Dufour, C. et al., J PHYS-CONDENS MAT, 5(26), (1993), p. 4573
(5) Wagner, M.F.P. et al., ADV. ELECTRON. MATER., 7(3), (2021), p. 2001069

PP-066

Stabilization of the CN_3^{5-} anion in recoverable high-pressure $Ln_3O_2(CN_3)$ (Ln = La, Eu, Gd, Tb, Ho, Yb) oxoguanidinates

A. Aslandukov (Bayreuth/DE), N. Dubrovinskaia (Bayreuth/DE, Linköping/SE), L. Dubrovinsky (Bayreuth/DE)

Inorganic ternary metal-C-N compounds with covalently bonded C-N anions encompass important classes of solids. The most investigated classes are cyanides (CN^-) and carbodiimides (NCN^{2-}), which are used in a plethora of applications. While CN^- and CN_2^{2-} anions are well-known, the next member of this series — the CN_3^{5-} anion, a completely deprotonated guanidine, has hitherto been unknown. Despite numerous attempts to synthesize gaunidinate anion by deprotonation of guanidine molecule using strong bases, only partially deprotonated guanidine has been stabilized

Here, we present the successful stabilization of CN_3^{5-} guanidinate anion using not a classic "wet chemistry" approach, but rather a non-conventional route of solid-state synthesis under extreme conditions. A series of isostructural $Ln_3O_2(CN_3)$ (Ln = La, Eu, Gd, Tb, Ho, Yb) oxoguanidinates was synthesized under high-pressure (25-54 GPa) high-temperature (2000-3000 K) conditions in laser-heated diamond anvil cells [1]. The crystal structure of this novel class of compounds was determined *via* synchrotron single-crystal X-ray diffraction as well as corroborated by X-ray absorption near edge structure measurements and density functional theory calculations. Decompression experiments show that $Ln_3O_2(CN_3)$ compounds are recoverable to ambient conditions. The synthesis of the CN_3^{5-} guanidinate anion extends the list of carbon-nitrogen inorganic anions and its stabilization at ambient conditions provides new opportunities for inorganic and organic synthetic chemistry.

References:

(1) A. Aslandukov et al. Stabilization of the CN_3^{5-} anion in recoverable high-pressure $Ln_3O_2(CN_3)$ (Ln = La, Eu, Gd, Tb, Ho, Yb) oxoguanidinates, 2023, *Angewandte Chemie International Edition,* e202311516.

PP-067

Novel High-Pressure Rare-Earth Carbides with Diverse Carbon Atoms Arrangements

F. I. Akbar (Bayreuth/DE), A. Aslandukova (Bayreuth/DE), A. Aslandukov (Bayreuth/DE), Y. Yin (Bayreuth/DE, Linköping/SE), M. Bykov (Frankfurt a. M./DE), N. Dubrovinskaia (Bayreuth/DE, Linköping/SE), L. Dubrovinsky (Bayreuth/DE)

High-pressure methods enable synthesis of novel carbides with unique chemistry and properties relevant in science and technology. In this work, several dysprosium carbides were synthesized by laser heating of Dy up to ~2800 K at ~20-95 GPa in a diamond anvil cell. Sodium chloride was used as a pressure transmitting medium and a thermoinsulator. Chemical reaction between Dy and carbon from diamond anvils resulted in formation of several dysprosium carbides (Fig. 1) as revealed by the analysis of single-crystal synchrotron X-ray diffraction data.

Dysprosium carbide Dy_3C_2 (*P4/mbm*) was discovered at ~55-70 GPa (Fig. 1a). Its structure contains C-C dumbbells with the C-C distance of 1.49(4) Å at 70 GPa. Dy_4C_3 (*I*-43*d*) synthesised at 19-95 GPa was found to have the anti-Th_3P_4-type structure (Fig. 1b), which has been described for scandium carbide, Sc_4C_3, but not observed in lanthanide or Y carbides[1]. γ-Dy_4C_5 is isostructural to γ-Y_4C_5 (*Cmce*), recently discovered at ~50 GPa, and contains carbon dumbbells (C-C = 1.38(4) Å at 70 GPa) and trimers (C-C = 1.428(19) Å at 70 GPa) (Fig. 1c). Dy_5C_9 (*P4/mnc*) was synthesised at 70 GPa (Fig. 1d). It contains polymeric carbon chains with the C-C distance of ~1.46(2) Å at this pressure. γ-DyC_2 (*Immm*) was observed at 70 GPa. In the structure of γ-DyC_2 carbon atoms polymerize to form flat ribbons with the C-C distances of 1.47(3) Å and 1.501(10) Å at 70 GPa (Fig. 1e).

Density functional theory calculations agree with the experimental data and suggest the dynamical stability of γ-DyC_2, γ-Dy_4C_5 and Dy_4C_3 at ambient conditions. The identification of polycarbon anions, previously unobserved in rare-earth carbide systems, significantly broadens carbides chemistry.

Fig. 1. Structures of the synthesized carbides: a) Dy_3C_2, b) Dy_4C_3, c) γ-Dy_4C_5, d) Dy_5C_9, e) γ-DyC_2. The blue and brown spheres represent dysprosium and carbon, respectively.

References:

(1) Akbar, F. I. *et al.* High-pressure synthesis of dysprosium carbides. *Front. Chem.* **11**, 1–9 (2023).

Fig. 1

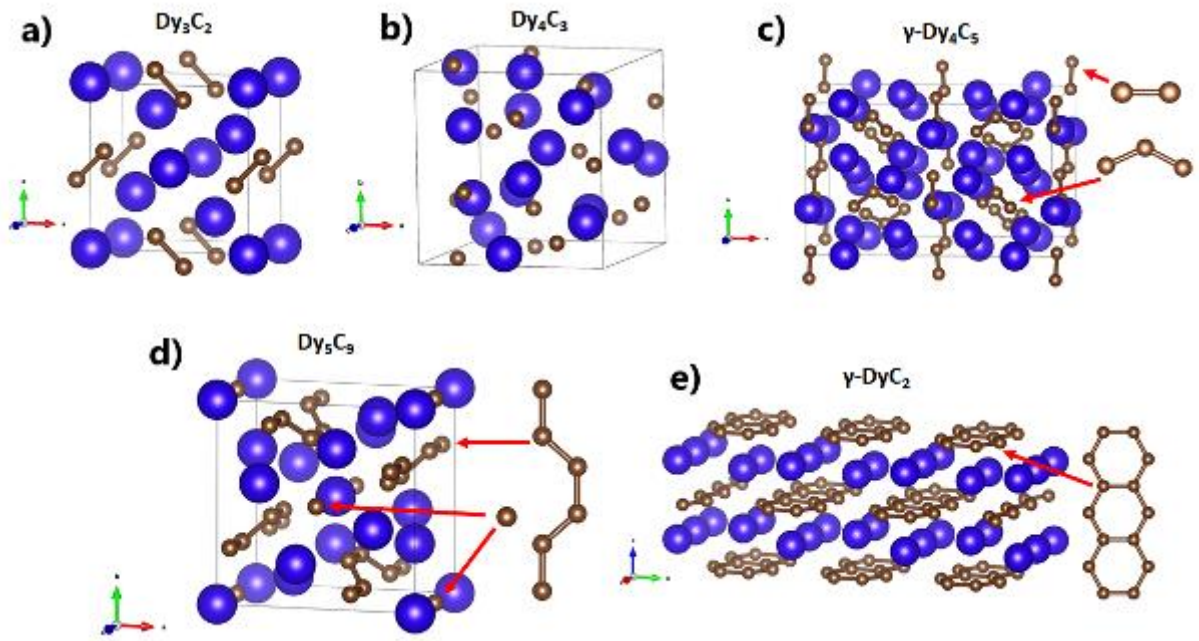

PP-068

High-pressure synthesis of novel manganese nitrides and polynitrides

P. Jurzick (Cologne/DE), L. Brüning (Cologne/DE), Y. Wang (Frankfurt a. M./DE), N. Flosbach (Cologne/DE), M. Bykov (Frankfurt a. M./DE)

The synthesis of polynitrogen compounds is a fundamental challenge due to their intrinsic thermodynamically instability. Here we report the synthesis and crystal structures of several novel manganese nitrides and polynitrides, including Mn5N, Mn3N2, MnN, MnN2 and MnN8 · N2. These compounds were synthesized via direct reactions between manganese and nitrogen in a laser-heated diamond anvil cell (LHDAC) at pressures ranging between 52 and 112 GPa. The compounds were studied by means of multigrain single-crystal X-ray diffraction. Synthesis at lower pressures yielded Mn-rich nitrides, whereas at pressures increased to 112 GPa, the polynitride compounds MnN2 and MnN8·N2 were formed. Notably, MnN8 · N2 is a metal−inorganic framework with conjugated polydiazenediyl chains [–N=N–]∞. The synthesis is in agreement with previously reported ReN8·xN2 and WN8·xN2, synthesized at 105 GPa [1,2]. These nitrogen-rich compounds are of great importance due to their potential as high-energy-density materials (HEDM) featuring metallic properties.

References:

(1) M. Bykov, E. Bykova, E. Koemets, T. Fedotenko, G. Aprilis, K. Glazyrin, H. P. Liermann, A. V. Ponomareva, J. Tidholm, F. Tasnádi, I. A. Abrikosov, N. Dubrovinskaia, L. Dubrovinsky, *Angew. Chemie - Int. Ed.* **2018**, *57*, 9048–9053.

(2) M. Bykov, S. Chariton, E. Bykova, S. Khandarkhaeva, T. Fedotenko, A. V. Ponomareva, J. Tidholm, F. Tasnádi, I. A. Abrikosov, P. Sedmak, V. Prakapenka, M. Hanfland, H. Liermann, M. Mahmood, A. F. Goncharov, N. Dubrovinskaia, L. Dubrovinsky, *Angew. Chemie* **2020**, *132*, 10407–10412.

Fig. 1

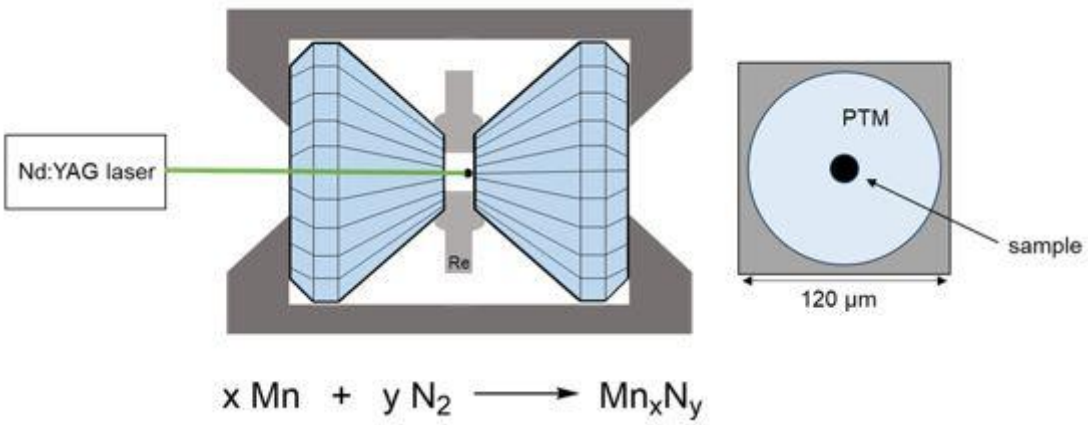

PP-069

Synthesis of magnesium (II) orthocarbonate, Mg_2CO_4, from different precursors

L. Dubrovinsky (Bayreuth/DE)

Deep-mantle diamonds, carbon rich mantle-derived magmas, carbonate rocks in subduction zones, even carbonates and carbides inclusions in diamonds from the transition zone, provide numerous lines of evidence point to the early and continuing long-term exchange of substantial carbon between Earth"s surface and its interior. Mineral(s) form of carbonate(s) in deep Earth interior remain debatable.

In our experiments we used large opening BX-90 type diamond anvil cells equipped with Boehler-Almax type diamonds. The plates of MgO were mounted on the both sides of the DACs. The DACs were cryogenically loaded with oxygen, which served as a chemical reactant, pressure-transmitting medium and absorber of NIR laser radiation at high-pressures. In another experiment the 50-50 wt.% mixture of MgO and $MgCO_3$ powders were prepared and loaded into the sample chamber of the DAC along with a piece of platinum.

We observed new monoclinic phase with the space group symmetry $P2_1/c$. High quality single crystal data allowed solve and refine the crystal structure, and determine chemical composition of the phase as magnesium (II) orthocarbonate, Mg_2CO_4. Notably, we were not able to find structural analog of the new orthocarbonate among orthosilicates.

At 120 GPa, the CO_4 forms distorted tetrahedra isolated from each other while sharing corners and edges with both MgO_7 and MgO_9 polyhedra. The CO_4 tetrahedra has four C-O bonds with lengths of varying from ~1.30 to ~1.36 Å; the angles between C-O bonds vary in the range of 104.32 ° to 111.93 ° with the average value of 109.45 °, as expected for carbon in sp^3 hybridization state.

Thus, we demonstrate that $MgCO_3$ and MgO react with formation of novel magnesium (II) orthocarbonate, and in pyrolite mantle dominated by Mg-rich oxide (ferropericlase) and bridgmanite, not a $MgCO_3$-II but the Mg_2CO_4 (or it Fe-baring analog) will be major host of carbon.

PP-070

The crystal structure of new high-pressure silicate $Fe_{1.5}Si_2O_6$, a novel compound with Eskola-like stoichiometry

V. Kovalev (Frankfurt a. M./DE), P. Jurzick (Cologne/DE), M. Bykov (Frankfurt a. M./DE, Cologne/DE), Y. Wang (Frankfurt a. M./DE), B. Winkler (Frankfurt a. M./DE), A. Aslandukova (Bayreuth/DE), I. Kupenko (Grenoble/FR), G. Aprilis (Grenoble/FR), P. O. Autran (Grenoble/FR), J. Wright (Grenoble/FR), E. Bykova (Frankfurt a. M./DE)

Pyroxenes are one of the major constituents of the Earth"s interiors, composing about 50% of the Earth"s upper mantle (Frost, 2008). Representatives of this mineral group may accumulate various species-defining elements (Morimoto, 1988) as well as vacancies (Ma et al., 2015) in their M1 and M2 sites. Different distribution of cations over the M1 and M2 sites in pyroxene crystal structure leads to the segregation of $M1^{II}$-$M2^{II}$, $M2^{I}$-$M1^{III}$, $M2^{I}$-($M1^{II}$/$M1^{IV}$) subgroups (Morimoto, 1988). In addition to full occupation of M1 and M2 sites, formation of vacancy-rich pyroxenes is also possible and may serve as an indicator of high-pressure conditions (Ma et al., 2015). In the case of calcium-rich pyroxenes, the content of defect-bearing Ca-Eskola component $(Ca_{0.5}\square_{0.5})AlSi_2O_6$ is an essential object for estimating deep Earth conditions in approach to eclogite formation (Schröder-Frerkes et al., 2016). Hence, it is interesting to investigate the formation of compounds with similar stoichiometry with iron as one of the most abundant chemical elements in the Earth"s upper mantle

A mixture of $^{57}Fe_2O_3$ and quartz loaded in BX90 DAC was laser-heated to 2500 K at 20 GPa. We applied methods of multi-grain single-crystal X-ray diffraction and Mössbauer spectroscopy in order to study the reaction products. This reaction yielded a single product: a novel compound exhibiting $(Fe^{2+}_{0.5}\square_{0.5})Fe^{3+}Si_2O_6$ with Eskola-like stoichiometry. It crystallizes in monoclinic C2/c space group with a = 9.333(8) Å, b = 8.4371(18) Å, c = 5.102(2) Å, β = 105.47(7)°. The crystal structure was solved and refined with the following R_1 = 5.58%, wR_2 = 14.21%. We will discuss the magnetic and electronic properties of the Fe-clinopyroxene and the results of the DFT calculations.

Our new Eskola-like compound together with recently discovered mineral tissintite $(Ca,Na,\square)AlSi_2O_6$ may provide insights into the crystal chemistry of vacancy-rich clinopyroxenes and high-pressure conditions on planets interiors and surfaces.

PP-071

Effect of nitrogen saturation on the phase composition of TI40ZR20NB20HF5TA15 high-entropy alloy

L. Rogal (Krakow/PL), J. Kasprzycki (Krakow/PL), G. Garzel (Krakow/PL), U. A. Wdowik (Ostrava/PL), T. A. Strobel (Washington, DC/US), J. Dutkiewicz (Krakow/PL)

Introduction

Currently, *binary transition metal nitrides or pernitrides*, the synthesis of which is possible by high-pressure and high-temperature conditions, represent a prominent class of materials. They are extremely useful in various industrial applications due to their superior mechanical properties, such as high hardness and refractoriness, and functional features: refractivity, superconductivity, and electrocatalytic activity **[1].** Extension composition **nitrides up to 5 elements in the range of 5-35 %at. open new ways for the formation of High Entropy Nitrides (HEN)**, allowing to obtaining of new functional properties. Up to now, they are predominantly produced as thin films [2, 3] and mechanical alloying [4] due to their enhanced methods of high solubility (concerns simple TM nitride compounds). Developing appropriate chemical composition and condition parameters for producing ***bulk materials*** with ***stable multicomponent/high entropy nitrides/pernitrides*** is a significant challenge in materials science [5-7]. Very often, thermodynamically metastable phases are observed during materials synthesis and may possess excellent properties for some applications compared to their corresponding equilibrium states. Moreover, the nitrides remain relatively unexplored, with fewer than 400 unique ternary metal nitrides cataloged in the Inorganic Crystal Structure Database (ICSD), in contrast to over 4,000 ternary metal oxides [8]. *The paucity of known nitrides can largely be attributed to the challenging requirements of* ***nitride/pernitrides synthesis.***

Objectives

The objective of this study is to investigate the impact of high pressure (up to 35 GPa) and temperature (2,500 K) on the formation of non-equilibrium stable nitrides in the Ti40Zr20Nb20Hf5Ta15 High-Entropy Alloy.

Materials & methods

The Ti40Zr20Nb20Hf5Ta15 at.% high entropy alloy was cast using elemental precursors of Ti, Zr, Hf, Ta, and Nb with a purity of 99.99 wt.% in an arc melting furnace, utilizing a water-cooled copper plate under a protective Ar atmosphere. To ensure sufficient homogenization, the alloys were re-melted five times. The overall alloy compositions were determined through large area analysis of 1600 µm x 1600 µm, resulting in the following chemical composition: Ti - 39.5%, Zr - 21%, Nb - 19.2%, Hf - 5.1%, Ta - 15.2% (at.%).

A laser-heated diamond anvil cell with a nitrogen-loaded chamber was used to lead the reaction of Ti40Zr20Nb20Hf5Ta15 HEA and synthesized nitrides. High-pressure experiments were conducted using symmetric diamond anvil cells with 400 µm culets. The sample chamber was filled with N2 gas (99.999% pure) as the pressure-transmitting medium. The samples were compressed up to 35 GPa while collecting in situ synchrotron X-ray diffraction. At 35 GPa, the sample was heated up to 2 500 K. After the DAC experiment, the chamber was reloaded, and a grain rectangular in shape of approximately 15 ´18 µm was recovered for further study.

TEM thin foils were also prepared from the recovered sample after DAC experiments. A lamella for TEM investigations was cut out using the Ga+ focused ion beam (FIB) method with a Thermo-Fisher Scios microscope. It was then thinned down to a thickness of approximately 100 nm from an area of 4 ´ 8 µm. The microstructure of the foil was examined using a Thermo-Fisher Themis G2 200 kV S-corrected X-FEG transmission electron microscope.

Results

A detailed characterization of the Ti40Zr20Nb20Hf5Ta15 at.% HEA sample, which serves as the precursor for our high-pressure studies, revealed that it is composed of a single bcc solid solution with a lattice parameter of 0.3404 nm (space group *Imm).* Synthesis of Ti40Zr20Nb20Hf5Ta15 (at.%) with N2 in a laser-heated diamond anvil cell (35 GPa, 2500K) formed a complex structure. The reaction products typically contained numerous single-crystalline grains of several nitride phases (Fig. 1), identified using synchrotron single-crystal X-ray diffraction and electron diffraction patterns (Fig. 2). A direct reaction between alloy

components and N2 resulted in the synthesis of three kinds of nitrides M2N3, M3N5, MN where M corresponds Ti, Zr, Ta, Nb Hf.

Figure 1 In situ synchrotron x-ray diffraction pattern of Ti40Zr20Nb20Hf5Ta15 at.% after laser heated at 2 500 K and pressure to 35 GPa. Measurements registered at 2 GPa.

TEM studies have been carried out to describe the evolution of the post-process DAC microstructure of synthesized Ti40Zr20Nb20Hf5Ta15 at.%, at nitrogen. Results of these examinations are displayed in Fig. 2. The bright field image reveals a mixture of irregular grains with an average size of 98 nm and various diffraction contrasts, suggesting differences in phase composition. Selected area diffraction patterns from various grains revealed the formation of nitrides M_3N_5 (Pmnb), M_2N_3 (Pnma), which agree with previous synchrotron studies and theoretical calculations.

Figure 2 (a) TEM bright image of the Ti40Zr20Nb20Hf5Ta15 at.% alloy isostatically compressed at 35 GPa and electron diffraction patterns (b, d) from the areas marked as the circle.

Conclusion

Synthesis of Ti40Zr20Nb20Hf5Ta15 at.% HEA at nitrogen leads to the formation of numerous complex nitrides instead of a single solid solution. Optymalistion of chemical composition HEA alloy is required to obtain a single high entropy nitride. For this purpose, the chemical composition of a single grain/phase has been conducted to determine the optimal chemical composition of a new HEA for further studies.

References:

(1) M, Bykov, et al. High-pressure synthesis of ultraincompressible hard rhenium nitride pernitride Re2(N2)(N)2 stable at ambient conditions, Nat. Commun, 10: 2994 (2019).
(2) T.-K Chen et al. Nanostructured nitride films of multi-element high entropy alloys by reactive DC sputtering. Surf. Coat. Technol. 188–189, 193–200 (2004).
(3) Chen, T.-K., et al. Nanostructured nitride films of multi-element high-entropy alloys by reactive DC sputtering. Surf. Coat. Technol. 200, 1361–1365 (2005).
(4) Jin, T. et al. Mechanochemical-assisted synthesis of high-entropy metal nitride via a soft urea strategy. Adv. Mater. 30, 1707512 (2018).
(5) D. B. Miracle, High entropy alloys as a bold step forward in alloy development. Nat. Commun. 10, 1805 (2019).
(6) C. Oses, et.al High-entropy ceramics, Nature Reviews Materials, 5; 295–309, (2020).
(7) P. Sarker, et al. High-entropy high-hardness metal carbides discovered by entropy descriptors. Nat. Commun. 9, 4980 (2018).
(8) W. Sun, et al. A Map of the Inorganic Ternary Metal Nitrides, Nat Mater 18/7:732-739, (2019).

Acknowledgments

This research was supported by Polish science financial resources The National Science Centre, Poland, project No. 2021/41/B/ST8/03758 entitled: *Development of new high entropy nitrides composites synthesized at high pressure and temperature.*

Fig. 1

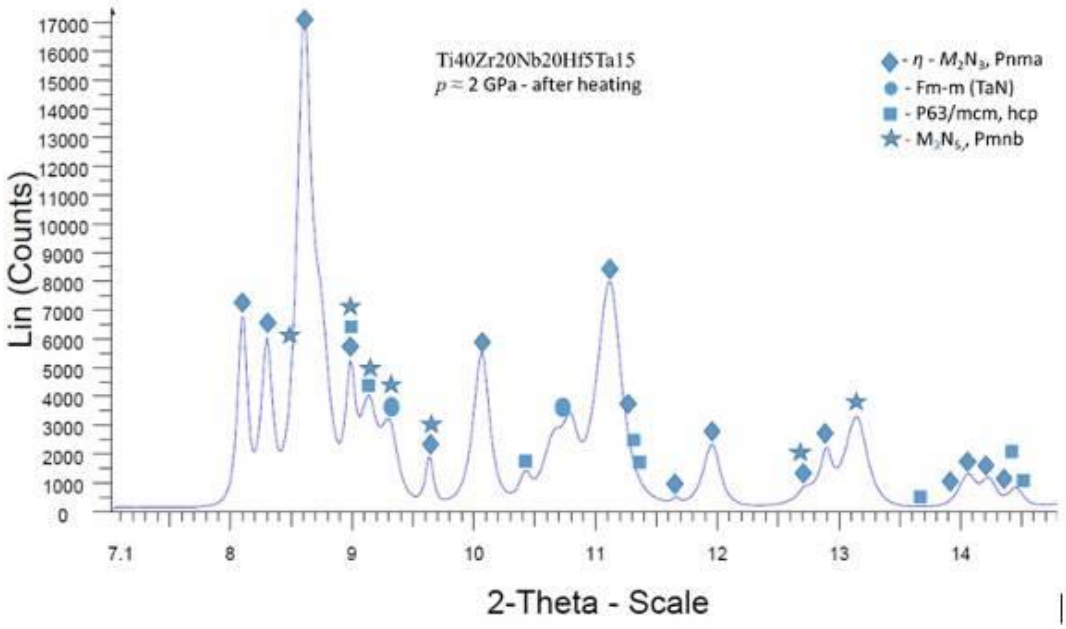
Ti40Zr20Nb20Hf5Ta15
p = 2 GPa - after heating
- η - M2N3, Pnma
- Fm-m (TaN)
- P63/mcm, hcp
- M3N5, Pmnb
Lin (Counts)
2-Theta - Scale

Fig. 2

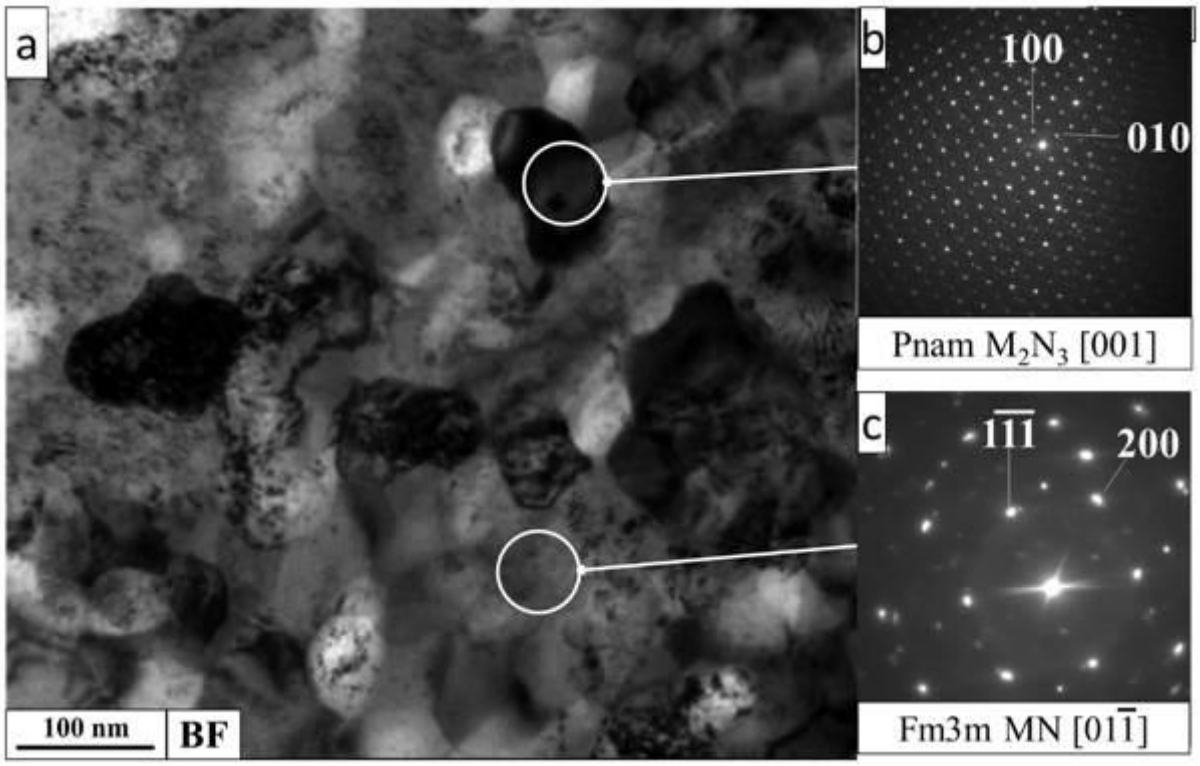
a
b
100
010
Pnam M2N3 [001]
c
1̄11̄
200
Fm3m MN [01̄1̄]
100 nm
BF

Poster Session II: New structures and mechanisms

PP-072

Stepwise O_2-Induced Rearrangement and Disassembly of the [$NiFe_4(OH)(\mu_3\text{-}S)_4$] Active Site Cluster of CO Dehydrogenase

Y. Basak (Berlin/DE), J. H. Jeoung (Berlin/DE), L. Domnik (Berlin/DE), H. Dobbek (Berlin/DE)

Carbon monoxide dehydrogenases (CODHs) catalyse the reversible reduction of CO_2 to CO and water at a unique [$NiFe_4(OH)(\mu_3\text{-}S)_4$]-cluster, called cluster C. CODHs found in anaerobic microbes are of high interest as they are able to catalyse these reactions at relatively high velocities at virtually no overpotentials. However, one of the major caveats faced is their rapid loss of activity when exposed to air. Variations in loss and recovery of activity amongst CODHs have been shown as well. Here we study the time-dependant structural changes of the metal centres of CODH-II by air, to give a clearer understanding behind possible unknown structural changes behind this major hurdle. We were able to show that inactivation is a multistep process, which can be divided into a reversible and an irreversible phase. In the reversible phase, the Ni ion of the active site cluster has its open coordination site blocked by a Ni,Fe-bridging μ-sulfido or chlorido ligand. Subsequent snapshots of cluster C on prolonged O_2 exposure depict an irreversible inactivation phase, where nickel and sulfido ligands in cluster C disappear while the Fe ions are completely rearranged. When the aforementioned open coordination site of Ni is blocked using a cyanide ligand, cluster C is stabilized against dioxygen induced decomposition, indicating that the breakdown of cluster C and, therefore, one of the causes of the loss of CO/CO_2 redox activity of CODHs in air, is induced by this attack of the Ni ion by O_2. Our data is consistent with a reversible reactivation mechanism under reducing condition proposed to safeguard CODHs against transient dioxygen exposure.

References:

(1) Appel, Aaron M., et al. *Chem Rev.*113.8 (2013): 6621-6658
(2) Lazarus, Oliver, et al. *JACS.*131.40 (2009): 14154-14155
(3) Domnik, Lilith, et al. *ACIE.*56.48 (2017): 15466-15469
(4) Svetlitchnyi, Vitali, et al. *J Bacteriol.*183.17 (2001): 5134-5144
(5) Wittenborn, Elizabeth C., et al. *Elife*7 (2018): e39451
(6) Basak, Yudhajeet, et al. *ACIE* 135.32 (2023): e202305341

PP-073

Implementation of a standardized assay for the characterization of newly developed PET hydrolases

Parinita Singh, Da'san Jaradat, Manfred Weiss and Gert Weber
P. Singh (Berlin/DE), D. Jaradat (Berlin/DE), M. S. Weiss (Berlin/DE), G. Weber (Berlin/DE)

Production and usage of plastic polymers lead to large amounts of waste, increasing at a rate of 9% annually. Various polymer types, contaminated with food, additives, packaging labels, and blending materials present a great challenge for their thermal or chemical recycling, which was a sustainable way of waste management in the recent past[1]. To overcome this issue for hydrolyzable polymers like polyethylene terephthalate or PET, is to use efficient polymer degrading enzymes, like, PET hydrolases, to deploy strategies for a bio-based circular economy. The number of new or enhanced PET hydrolases has been growing drastically and a lack of standardized experimental methods draws attention to the reliability of these enzymes for an efficient industrial biodegradation.

In a recent study, 4 PET hydrolases, HotPETase, FAST-PETase, PES-H1$^{L92F/Q94Y}$, LCC^{ICCG}, were compared for their efficacy based on parameters decisive for an upscaling towards industrial applications, like reproducibility, thermostability or product inhibition[2].

We have set out to employ these standardized protocols as a benchmark for our newly developed PET hydrolases. For this, the aforementioned enzymes will be produced and purified, assessed for their activity and, consecutively compared to novel PET hydrolases. For further improvement of in-house developed enzymes, structural characterization in their substrate-bound state is pivotal.

Protein expression of these enzymes in *E.coli* (containing the gene with a terminal 6x His-tag), and thereafter purification with Ni-NTA affinity chromatography have been performed so far. Size exclusion was done to acquire pure enzymes for standardized assays and crystallography.

Large-scale PET degradation will benefit from the comprehensive comparison of PET hydrolases based on feasible common parameters that can also be conventionally implemented on the newly discovered or engineered hydrolases in the future.

References:

(1) 10.1126/sciadv.1700782
(2) 10.1021/acscatal.3c02922

PP-074

Structural insights into ATP-driven electron transfer in the double cubane cluster protein and its reductase complex.

J. H. Jeoung (Berlin/DE), H. Dobbek (Berlin/DE)

Metalloenzymes often need to couple reductions at low redox potentials with ATP hydrolysis to make them thermodynamically favorable. There are three electron-transferring metallo-ATPases in biology that support such thermodynamically unfavorable reactions: Fe-proteins of nitrogenase and activators of Co-corrinoid-containing proteins and radical enzymes. Recently, a protein of a double-cubane cluster protein (DCCP) with two [4Fe4S] subclusters bridged by a sulfide ligand was found, which is novel in biology while the cluster has long existed in chemistry. The DCCP reduces small molecules like acetylene and hydrazine using using electrons from its metallo-ATPase reductase (DCCP-R).

However, the mechanism of ATP-driven electron transfer remains unknown.

Our biochemical and structural studies revealed that DCCP and DCCP-R form a tight complex; nucleotide binding alone doesn't initiate electron transfer; ATP hydrolysis is essential. We studied the complex structures in three states: nucleotide-bound (MgADPNP, MgADPAlF4), and nucleotide-free. The MgADPNP-bound complex indicates DCCP-R homodimer with a [4Fe4S] cluster sits at the two-fold axis of the DCCP homodimer. The ADPAlF4-bound resembles the nucleophilic water attack transition state.

In the nucleotide-free complex, DCCP-R structure expands while DCCP remains unchanged. Comparing these structures suggests a signal transduction pathway with hydrogen-bonding networks linking ATP actions, [4Fe4S] cluster site, and the DCCs together with the angle between cluster helices for electron transfer.

This work enhances our understanding of these vital biological processes.

Jeoung, J.-H.; Dobbek, H. *PNAS* 2018, 115:2994

Jeoung, J.-H.; Nicklisch, S.; Dobbek, H. *PNAS* 2022, 115:e2203576119

Einsle, O.; Rees, D. C. Chem. Rev. 2020, 120:4969

Hennig et al. Nat. Commun. 2014, 5:4626

PP-075

Structural characterization and classification of TRIM family PRY(SPRY) domains

R. Zhubi (Frankfurt a. M./DE)

The SPRY domain is an evolutionarily-conserved protein-protein interaction motif, firstly identified in dual-specificity kinase SPLA of Dictyostelium and rabbit RYanodine receptor. The SPRY family can be divided into two subfamilies: B30.2, so-called PRYSPRY, subfamily which contains an N-terminal PRY motif, and the other is SPRY-only class which nevertheless also has an N-terminal extension that is structurally similar to PRY. More than 40 TRIMs harbor the SPRY domain at their C-terminus, most of which belong to the PRYSPRY subfamily. However, they exhibit low sequence homology, consistent with diverse interaction partners of the SPRY domains. This is exemplified for example by the structures of TRIM21-IgG Fc, TRIM65-MDA5-dsRNA and SPSB2-peptide complexes revealing distinct recognition mechanisms between substrates, range from loops, β-turns, helical motifs or a stretch of short peptides.Several crystal structures of TRIM (PRY)SPRY are currently available, however these only represent <20% of the subfamily. Due to high diversity, we did family-wide structural study program to enable our understanding on this large group of TRIM substrate recognition module.We successfully have determined additional nine novel crystal structures, including MID1 (TRIM18), MID2 (TRIM1), TRIM9, TRIM10, TRIM11, TRIM15, TRIM16, TRIM36 and TRIM67, most of which belong to Class I TRIM. Similarly, all of them share a conserved core bent β-sandwich topology comprised of two β-sheets, and their N-terminal subdomains, mainly PRY, consist of three β strands that are tightly packed onto both SPRY core β-sheets. Nonetheless, structural comparison revealed high diversity at both the N-terminal subdomain and the substrate binding site located on top of the β-sheets of the central SPRY region, caused mainly by different lengths and structural motif of the connecting loops. Such structural alterations thus define distinct characteristics of the substrate binding sites of these TRIM (PRY)SPRYs.

Fig. 1

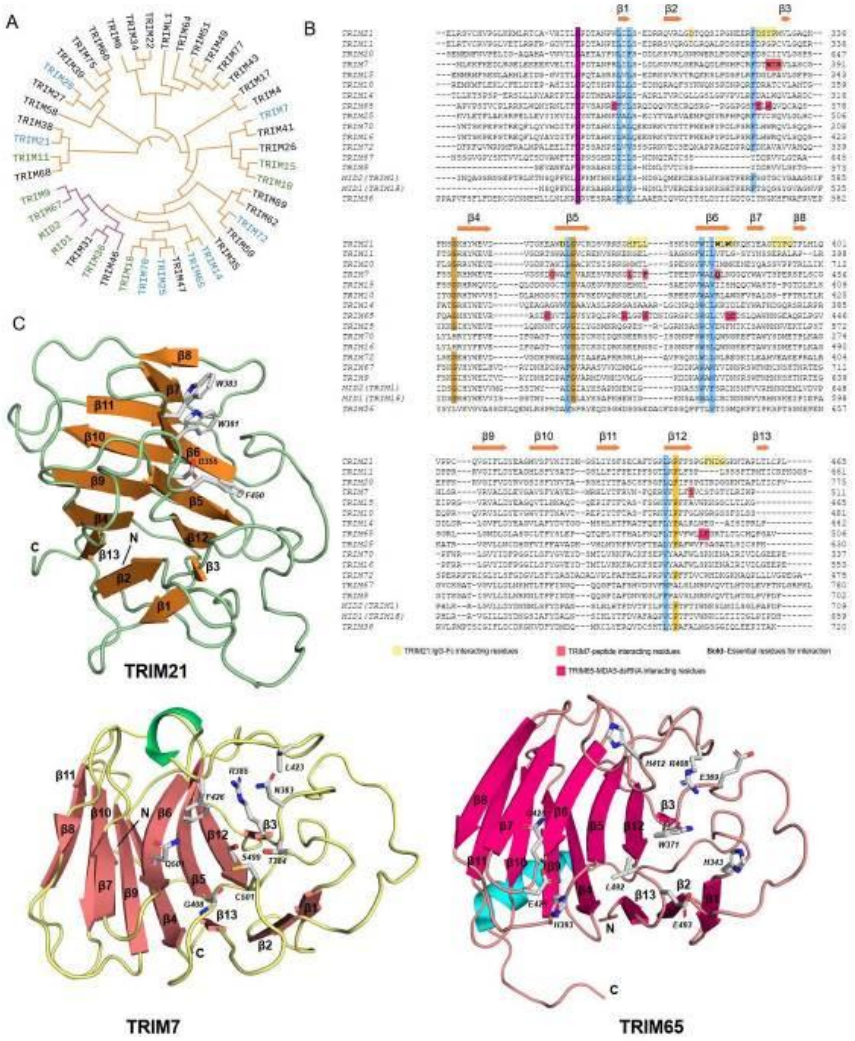

Fig. 2

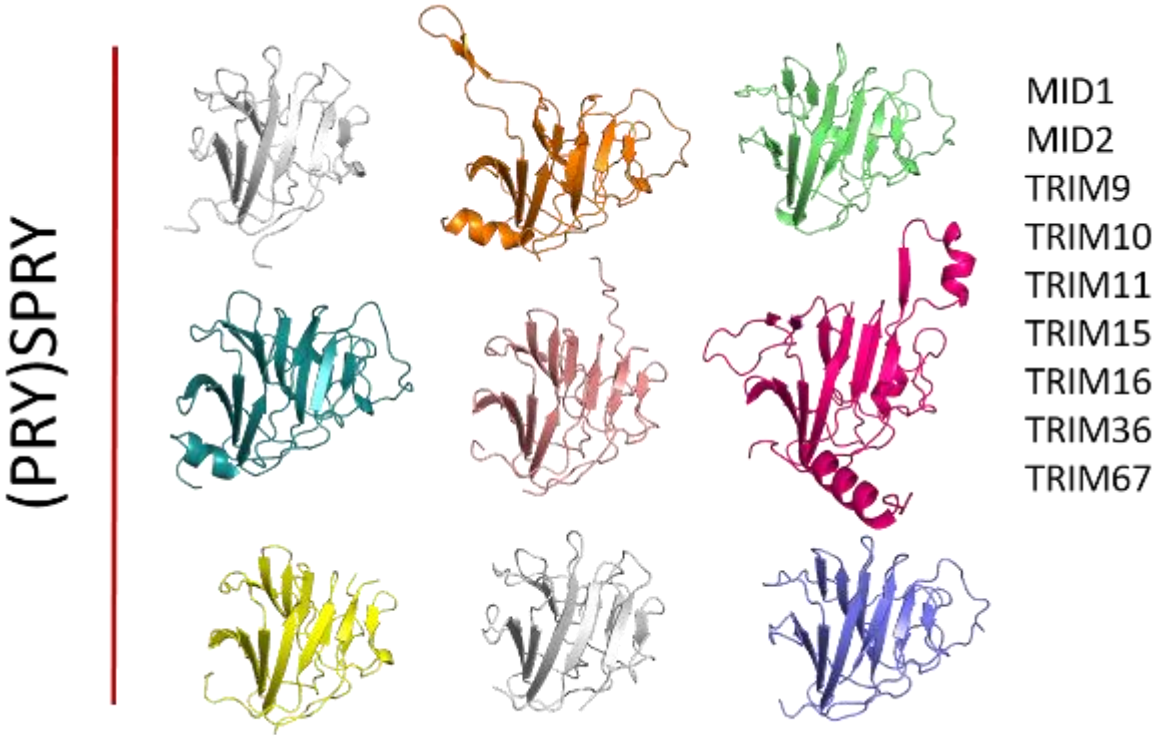
(PRY)SPRY
MID1
MID2
TRIM9
TRIM10
TRIM11
TRIM15
TRIM16
TRIM36
TRIM67

PP-076

MqnA Structure Determination by Electron Crystallography: Toward a Better Understanding of Chorismate Dehydratase Mechanism

A. Shaikhqasem (Halle/DE), F. Hamdi (Halle/DE), P. L. Kastritis (Halle/DE), M. T. Stubbs (Halle/DE)

MqnA is an enzyme that catalyzes the first reaction in the futalosine pathway by dehydrating the substrate chorismate to produce 3-enolpyruvyl-benzoate (3-EPB). Recently we solved the structure of MqnA from *Streptomyces coelicolor* in complex with 3-EPB and with chorismate by X-ray crystallography. The structural analysis indicated a unique mechanism of substrate-assisted catalysis, thought to involve the deprotonation of a water molecule coordinated by hydrogen bonding with an asparagine residue in the active site [1]. Over the last few years electron diffraction has gained prominence as a powerful method in biological macromolecule crystallography [2], [3]. Furthermore, electron crystallography has been proven to provide information on the charge state and electrostatic potential of organic molecules [4]. With the aim of gaining a better understanding of the proposed mechanism, we successfully collected X-ray data and electron diffraction data of MqnA crystals of the same packing parameters and produced under the same conditions. We could calculate the Coulomb potential map and determine the MqnA structure to 3 Å resolution.

References:

(1) A. Prasad, C. Breithaupt, D. A. Nguyen, H. Lilie, J. Ziegler, and M. T. Stubbs, "Mechanism of chorismate dehydratase MqnA, the first enzyme of the futalosine pathway, proceeds via substrate-assisted catalysis," *J. Biol. Chem.*, vol. 298, no. 12, p. 102601, Dec. 2022.
(2) M. T. B. Clabbers and H. Xu, "Macromolecular crystallography using microcrystal electron diffraction," *Acta Crystallogr. Sect. D Struct. Biol.*, vol. 77, pp. 313–324, 2021.
(3) A. Shaikhqasem *et al.*, "Structure determination of a protein–peptide complex using microcrystal electron diffraction," *Acta Crystallogr. Sect. A Found. Adv.*, vol. 78, no. a2, pp. e628–e628, Aug. 2022.
(4) K. Takaba *et al.*, "Structural resolution of a small organic molecule by serial X-ray free-electron laser and electron crystallography," *Nat. Chem. 2023 154*, vol. 15, no. 4, pp. 491–497, Mar. 2023.

PP-077

Advancing selective inhibition: Unraveling the distinct mechanisms of DYRK1A and DYRK1B

A. Czarna (Krakow/PL), P. Grygier (Krakow/PL), K. Pustelny (Krakow/PL), G. Dubin (Krakow/PL)

DYRK1A and DYRK1B, integral members of the dual-specificity tyrosine-(Y)-phosphorylation regulated kinase family, exhibit over 85% similarity in their kinase domains but diverge significantly in their biological roles. DYRK1A is implicated in numerous physiological processes, including neuronal development and glucose regulation, with its dysfunction linked to a spectrum of disorders ranging from intellectual disabilities and Down syndrome to metabolic diseases like diabetes (Ackeifi et al., 2019). DYRK1B, in contrast, primarily governs cell cycle progression and division, playing a critical role in the pathogenesis of various cancers, metabolic syndrome, and nonalcoholic fatty liver disease (Alexandrov et al., 2022). The compensatory increase in DYRK1B expression following DYRK1A silencing underscores a complex regulatory mechanism between these kinases, highlighting their potential as therapeutic targets.

In this study, we present a groundbreaking revelation of the DYRK1B crystal structure in complex with its inhibitor, AZ191, a development that marks a significant advancement in the field, given the previous unavailability of the DYRK1B crystal structure (Massey et al., 2021). This is complemented by a comparative analysis with the DYRK1A-AZ191 complex structure, providing a deeper understanding of the molecular interactions. Our approach included a suite of assays: ADP-Glo Kinase Assay and Microscale Thermophoresis for kinetic analysis, Thermal Shift assay for assessing protein-inhibitor stability, and NFAT activity luciferase and translocation assays for evaluating the inhibitor's functional potency. These findings not only elucidate the distinct binding mechanisms of AZ191 at an atomic level but also open avenues for the rational design of selective inhibitors, potentially revolutionizing the therapeutic landscape for diseases associated with DYRK1A and DYRK1B dysregulation.

Poster Session II: Physical crystallography

PP-078

Ferroelastic phase transition in lead bismuth borate, $PbBiBO_4$

P. Becker (Cologne/DE), D. Friesen (Cologne/DE), L. Bohatý (Cologne/DE)

The influence of lone electron pairs in crystal structures on the magnitude of physical properties that benefit from pronounced structural polarity (such as second harmonic generation, pyro- or piezoelectricity) is considered since many years (see, e.g., [1] and references therein). Already fourty years ago, on this account the system PbO-Bi_2O_3-B_2O_3 had been investigated by J. Liebertz, mastering the particular challenge of crystal growth from glass-forming melts of high viscosity [2]. In this context, besides the (nowadays well-known) nonlinear optical crystal BiB_3O_6 also $PbBiBO_4$ had been grown to large single crystals. However, $PbBiBO_4$ turned out to be centrosymmetric and therefore was not further pursued (and not published) by J. Liebertz at that time. More than twenty years later the crystal structure of $PbBiBO_4$ was reported with monoclinic ($P2_1/n$) symmetry [3], but also as an orthorhombic (*Cmca*) structure [4], both structures based on room temperature data.

Using the single crystals grown by J. Liebertz we investigated the temperature-dependent properties of $PbBiBO_4$ by means of heating stage polarization microscopy, (powder) X-ray diffraction and thermal analysis. A single-crystal structure determination at 87 °C reveals an orthorhombic structure similar to that given in [4]. On cooling the crystals undergo a reversible phase transition of second order at 52 °C which leads to the formation of a domain structure that indicates monoclinic symmetry of the low-temperature modification. The phase transition in $PbBiBO_4$ can be classified as proper ferroeleastic of Aizu species mmmF2/m with the occurrence of two different orientation states.

We thank our late colleage J. Liebertz for the donation of the single crystals of $PbBiBO_4$.

References:

(1) D. Li et al., *RSC Adv.* **5** (2015) 79882-79887.
(2) J. Liebertz, *Prog. Crystal Growth Charact.* **6** (1983) 361-369.
(3) X. Chen et al., *J. Solid State Chem.* **179** (2006) 3191-3195.
(4) W. Zhao et al., *Inorg. Chim. Acta* **379** (2011) 130-134.

PP-079

Mechanisms for Multiferroicity in Rare Earch Orthoferrites: An Overview

A. K. Ovsianikov (Aachen/DE), P. Fabrykiewicz (Garching/DE, Jülich/DE), V. Hutanu (Garching/DE), M. Meven (Garching/DE, Jülich/DE), E. Ressouche (Grenoble/FR), U. Christensen (Grenoble/FR), M. Enderle (Grenoble/FR), W. Schmidt (Grenoble/FR), O. V. Usmanov (Gatchina/RU), I. A. Zobkalo (Gatchina/RU), K. A. Shaykhutdinov (Gatchina/RU, Krasnoyarsk/RU)

Magnetic rare-earth ortheferrites of the *R*FeO3 type (*R* = rare earth element, model systems for studies and theoretical considerations on magnetic structures in sixties of the last century [[Whi69, Mar70, Ber68], have regained significant interest in the last decade. Their complex multiferroic and magnetocaloric features make them potential candidates for modern applications, e.g. in the area of spintronics [Tok12, Lee11].

We recently completed an extended project, *Mechanisms for multiferroicity in rare-earth orthoferrites: Role of the Dzyaloshinskii-Moriya interaction*, funded by the DFG (SA-3688/1-1). In this project we used various experimental methods to gain an overview of the exchange parameters of different magnetic exchange interactions, the Heisenberg-exchange, the Dzyaloshinskii-Morya interaction, the single-ion anisotropy and external magnetic fields for different *R*FeO3 compounds. A close quantitative examination and comparisons with results from other groups reveal that the different parameters differ significantly between the different systems [Ovs22a, Ovs22c], . This causes a fragile balance between them and results in very different magnetic phase diagrams e.g. for HoFeO3, TbFeO3 and YbFeO3. [Ovs22a, Art12, Ovs22c], In addition, we also looked at TmFeO3 and DyFeO3 as part of our project and wWe were also able to achieve initial information for them. In our presentation, we provide an overview of the results of the orthoferrites we examined.

References:

(1) [Art12] S. Artyukhin et al.; *Nature Mater.* **11** (2012) 694 – 699.
(2) [Ber68] E.F. Bertaut; *Acta Cryst. A* **24** (1968) 217.
(3) [Mar70] M. Marezio, J.P. Remeika and P. D. Dernier; *Acta Cryst. B* **26** (1970) 2008.
(4) [Ovs20] A.K. Ovsyanikov et al. J. Magn. Magn. Mater. **507** (2020) 166855.
(5) [Ovs22a] A.K. Ovsianikov et al.; JMMM **557** (2022) 169431, ISSN 0304-8853.
(6) [Ovs22c] A.K. Ovsianikov et al.; JMMM **563** (2022) 170025.
(7) [Whi69] R. White; *J. Appl. Phys.* **40** (1969) 1061.

PP-080

Elasticity of dense metal–organic framework compounds

E. Haussühl (Frankfurt a. M./DE), J. Büscher (Frankfurt a. M./DE), L. Pennacchioni (Frankfurt a. M./DE, Potsdam/DE), O. Ivashko (Hamburg/DE), K. Bunk (Frankfurt a. M./DE), V. Milman (Cambridge/GB), A. Bosak (Grenoble/FR), S. Speziale (Potsdam/DE), B. Winkler (Frankfurt a. M./DE)

Metal-organic framework structures (MOFs) consist of transition metals that are connected via organic ligands. Together they form frameworks with cavities, which can contain guest molecules. The incorporation of guest molecules allows to build MOFs with tailored properties by exchanging the transition metals, organic ligands or guest molecules. Metal-guanidinium formates (***M*GuFo**), $[C(NH_2)_3][M^{2+}(HCOO)_3]$, belong to the perovskite-type MOFs with the general formula ABX_3, where B = M^{2+} is a metal cation (here M^{2+}= Cu^{2+}, Zn^{2+}, Mn^{2+}, Co^{2+}) which is octahedrally coordinated by formate ions (X = $HCOO^-$, abbreviated as Fo^-) [1]. The metal and formate ions form *M*−Fo−*M* chains and build up a three-dimensional framework with cuboid cavities, which are occupied by the small organic guanidinium cations (A = $[C(NH_2)_3]^+$). Mn-, Zn- and **CoGuFo** crystallize in the orthorhombic space group *Pnna*, while the Cu-member crystallizes in $Pna2_1$ [1].

In this study, we present for the first time the experimentally derived complete elastic stiffness tensors of orthorhombic metal guanidinium formates, using ultrasound techniques, Brillouin spectroscopy, and thermal diffuse scattering [2]. Density functional theory calculations were also performed to calculate the elastic tensor of orthorhombic ***M*GFos** and also of trigonal ***M*GuFo**s with M^{2+} = Ca^{2+} and Cd^{2+}. All ***M*GuFo**s studied here are very compressible, with bulk moduli ranging from 20 to 30 GPa. They all possess a significant elastic anisotropy. Trigonal CdGF and CaGF in particular, are one order of magnitude more anisotropic than the orthorhombic ones.

References:

(1) Hu K-L et al. Chem. Eur. J. 15, 12050 (2009)
(2) Büscher J, Haussühl E et al. J. Phys. Chem. C 127, 13217−13227 (2023)

E.H. and J.B. acknowledge support by DFG under grant number HA 5137/5.

Poster Session II: Structure-based drug discovery and design

PP-081

Crystallographic compound screening as a tool towards new SARS-CoV-2 inhibitors

L. S. Benz (Berlin/DE), T. Barthel (Berlin/DE), J. Wollenhaupt (Berlin/DE), U. Müller (Berlin/DE), M. S. Weiss (Berlin/DE)

The global impact of the SARS-CoV-2 pandemic has been profound, resulting in over 771 million infections and over 6.9 million fatalities within the last three and a half years[1]. While substantial progress has been made in vaccine development to prevent infection and severe cases, antiviral drugs are crucial for those already infected and at high risk. The recent approval of the first oral treatments like Paxlovid is a positive step, but preparing for future drug resistance remains a substantial challenge.

Finding new compounds with inhibitory potential against SARS-CoV-2 is the aim of the trilateral NECESSITY (New chemical entities for modulating SARS-CoV-2 activity) project, a consortium combining expertise in X-ray crystallography, organic chemistry, and biochemistry. One major target in anti-SARS-CoV-2 drug development is the main protease (M^{pro}), owing to its essential role in viral replication, its low mutation rate, and its druggability, which was already established during the SARS-CoV pandemic[2].

To identify promising starting points, a focused crystallographic compound screening of 330 compounds was conducted against Mpro. The compounds were selected from a library of over 8,000 compounds initially designed as kinase and protease inhibitors provided by our organic chemistry partner, Vladimir Krystof in Olomouc. Sixteen hits could be identified in the initial screen, with eight of them in the active site and one at a known allosteric site. Potential follow-up compounds from the library of our cooperation partner were subjected to virtual docking, and potentially interesting compounds were screened again with crystallography. One hit was identified which will now be analyzed for its inhibitory potential in biochemical and biophysical assays and afterwards further optimized into a lead compound for drug development.

References:

(1) https://covid19.who.int/ accessed 10.10.2023
(2) A. Zumla, et al., Nat. Rev. Drug Discov. (2016), 15, 317

PP-082

Exploring LC3/GABARAP binding pockets for degrader development

A. Kumar (Frankfurt a. M./DE), M. Schwalm (Frankfurt a. M./DE), S. Knapp (Frankfurt a. M./DE), V. Rogov (Frankfurt a. M./DE)

Recent successes in developing small-molecule degraders that act through the ubiquitin system[1] have spurred efforts to extend this technology to other mechanisms, including the autophagosomal-lysosomal pathway. Therefore, reports of autophagosome tethering compounds (ATTECs)[2] – based on the target recruitment to LC3/GABARAP, a family of membrane-bound proteins that tether autophagy receptors to the autophagosome – have received considerable attention from the drug development community. We validated the reported ATTEC ligands and handles by orthogonal biophysical methods. Surprisingly, most available ligands did not show effects on their designated target LC3. Intrigued by the idea of developing ATTECs, we explored the druggability of LC3/GABARAP by large scale crystallographic fragment screening at Xchem. The data revealed that most fragments bound to the HP2, but not the HP1 pocket of the LC3-interacting region (LIR) docking site, suggesting favorable druggability of this binding pocket. Here, we present diverse comprehensively validated ligands for future ATTEC development.

References:

(1) Nemec, V.; Schwalm, M. P.; Muller, S.; Knapp, S. PROTAC degraders as chemical probes for studying target biology and target validation. Chem Soc Rev 2022, 51 (18), 7971-7993
(2) Li, Z.; Wang, C.; Wang, Z.; Zhu, C.; Li, J.; Sha, T.; Ma, L.; Gao, C.; Yang, Y.; Sun, Y.; et al. Allele-selective lowering of mutant HTT protein by HTT-LC3 linker compounds. Nature 2019, 575 (7781), 203-209

PP-083

Fragment-based and computer-aided design of c-di-AMP synthesizing enzyme CdaA inhibitor

P. Kloskowski (Göttingen/DE), P. Neumann (Göttingen/DE), J. L. Heidemann (Göttingen/DE), R. Ficner (Göttingen/DE)

The discovery of a unique essential secondary messenger cyclic di-AMP (c-di-AMP) in 2008 has opened new prospects in the field of antibiotic research. c-di-AMP is a bacterial signalling nucleotide that is involved in regulation of the bacterial cellular processes like DNA integrity scanning, cell wall metabolism, osmolyte and potassium ion homeostasis. Mutation in the genes of the c-di-AMP synthesizing enzymes (the diadenylate cyclases - DACs) is lethal to the bacterial cell. Since its discovery in 2008, several studies have reported the presence of c-di-AMP in a wide range of different bacterial species, mainly in Gram-positive bacteria and archaea. Many of these bacteria are known to be human pathogens e.g. *Listeria monocytogenes*, *Staphylococcus aureus*, and *Streptococcus pneumoniae*. The mentioned pathogens utilize only one class of diadenylate cyclase enzymes (DACs) – namely CdaA, that catalyses the cyclisation of two ATP molecules into c-di-AMP in a metal ion dependent manner. Interestingly, three out of 12 families of bacteria that pose the greatest threat to human health according to WHO (WHO, 2017) utilize CdaA, that is absent in mammalian cells, as the sole enzyme synthesizing c-di-AMP. This renders CdaA a very promising target for the antibiotic research. Crystallographic fragment screening combined with computer-aided lead compound design using OpenEye suite have led to a discovery of a new CdaA inhibitor. Optimisation of the identified compound is a task of ongoing research.

Figure 1. Crystal structure of CdaA complex with the designed lead compound (ball-and-stick). CdaA is coloured by the sequence conservation score.

The authors would like to greatly acknowledge OpenEye Scientific Software, Santa Fe, NM. http://www.eyesopen.com for providing an academic licence of OpenEye suite. We thank the Helmholtz-Zentrum Berlin für Materialien und Energie (BESSY) and EMBL PETRA III in Hamburg for the allocation of synchrotron radiation beam time.

Fig. 1

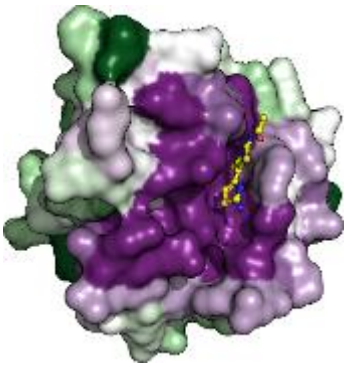

PP-084

Establishing a pipeline for fragment-based drug discovery to tackle the highly pathogenic Influenza A virus H5N1

S. Falke (Hamburg/DE), J. Senst (Hamburg/DE), S. Günther (Hamburg/DE), H. Chapman (Hamburg/DE), C. Wrenger (São Paulo/BR), A. Meents (Hamburg/DE)

Emerging RNA viruses including Orthomyxoviridae like influenza A virus continue to be a major health threat globally. A bird-adapted strain of influenza A virus subtype H5N1 is the causative agent of the highly pathogenic bird-flu. There is a high fatality among infected birds and several hundred infections of humans with a fatality of approx. 60% have been reported with a limited capability of human-to-human transmission. In combination with rapid continuous mutation of the RNA, the virus likely comprises a major risk for a global pandemic with a high fatality rate, which should be addressed with additional drug discovery approaches.

In previous efforts we already performed crystallographic compound screening targeting SARS-CoV-2 proteases as well as cap snatching endonucleases of selected RNA viruses. The established fragment screening pipeline utilizes the PETRAIII beamline P09 (HiPhax). The beamline is designed for automated fragment screening experiments with a special focus on room-temperature fixed target serial crystallography.

Here we present first results of our influenza A virus H5N1 project. The heterotrimeric RNA polymerase and the RNA cap snatching endonuclease are essential for propagation of this virus and were selected for crystallographic experiments and complementary assays. The protein-cap interactions are going to be analyzed and targeted – for example considering the binding of nucleotide-like compounds – in order to develop promising anti-viral lead compounds.

PP-085

Development of Pillarplex SOCs as Viable Platforms for Biomedical Applications

J. Preinl (Garching/DE)

In order to apply pillarplexes as contrast agents, the functionalization of their rim with appropriate tags or peptide vectors is required. The basis for this functionalization has already been laid by J. ZUBER. As part of his master's thesis, he succeeded in brominating the pyrazole units of the pillarplexes in a post-synthetic fashion. My task will be cross-coupling these modified supramolecular entities with adequate tethers. This endeavor however presupposes that the ligand scaffold is available continuously, in sufficient quantities, and excellent purity. Hence, in the early stages of my doctoral thesis, the focus is primarily on optimizing the respective ligand precursors' synthetic procedures and isolation processes. In this context, the crystal structure of compound I will be presented.

PP-086

Structural investigation of bacterial Urease using X-ray structure analysis – basis for the development of new Urease inhibitors

M. Linnert (Halle/DE), F. Gabriel (Halle/DE), M. Wermann (Halle/DE), D. Schlenzig (Halle/DE), C. Schuster (Lutherstadt Wittenberg/DE), U. Radics (Lutherstadt Wittenberg/DE), A. Hucke (Lutherstadt Wittenberg/DE), S. Schilling (Halle/DE, Köthen (Anthalt)/DE)

Plants need nitrogen to grow. This nitrogen usually comes from the inorganic substances ammonium or nitrate. As these compounds are only available in the soil to a limited extent, urea is used as a source of nitrogen (fertilizer) in agriculture worldwide. The plants themselves contain the enzyme Urease, which can break down this urea into dihydrogen carbonate and ammonia and thus make ammonium available to the plant as a source of nitrogen. Soil bacteria such as *Sporosarcina pasteurii* also contain such an enzyme. As a result, the applied urea is broken down faster than the plants can absorb it. The resulting excess of ammonia escapes into the atmosphere. To counteract this problem, inhibitors are added to urea fertilizers to inhibit bacterial Urease. In addition to the already used inhibitors, there is a great need for simple and inexpensive selective inhibitors that are further harmless to the environment. Here we describe the development of a robust bacterial Urease test system, including the development of an enzymatic test and a stable structure solution by X-ray crystallography in an appropriate resolution range. We show this with an already used, but so far not in the enzyme target structural analyzed inhibitor. That should serve as a basis for future developments.

Poster Session II: Structure-property relationships

PP-087

Structural and spectroscopic analysis of mixed valence schafarzikite $PbBi(Fe_{1-x}Mn_x)O_4$.

C. M. Uribe Rincón (Bremen/DE), K. Ghosh (Bremen/DE, Newark, DE/US), M. M. Murshed (Bremen/DE, Bremen/DE), T. M. Gesing (Bremen/DE)

In the mineral schafarzikite ($FeSb_2O_4$) the stereochemically active $5s^2$ lone electron pair (LEP) plays pivotal roles to diverse crystal-physico-chemical properties [1]. Complete substitution of Sb(III) with equivalent amounts of Pb and Bi leads to change the oxidation state of the transition element (e.g., Fe^{3+}) and offers a mixed stereochemical activity of $6s^2$ LEPs of Pb(II) and Bi(III). As such, $PbBiFeO_4$ [2] and $PbBiMnO_4$ are isostructural to $FeSb_2O_4$, and they both belong to the mullite-type family. We report synthesis and characterizations of the solid solution $PbBi(Fe_{1-x}Mn_x)O_4$, synthesized in sealed quartz tubes at 10^{-6} MPa. The crystal structures were analysed by X-ray powder diffraction followed by Rietveld refinements. Substitution of Fe^{3+} with Mn^{3+} leads to a slight expansion of the *a*- and contraction of the *c*-lattice parameter with an overall contraction of the unit cell volume. The deviation of the metric parameters from the Vegard´s law can be related to the microstrain of the crystallites due to co-sharing the *Wyckoff* sites by with different cationic sizes (Pb/Bi and Mn/Fe). The strength of the stereochemical activity of the LEP is measured by the change of the Wang-Liebau eccentricity parameter [3]. The vibrational properties characterized by Raman and FTIR complement the structural features. The optical bandgaps are evaluated from the UV/Vis diffuse reflectance spectra using the RATD methods. Magnetic properties of the end-members are characterized by DC magnetic susceptibility.

References:

(1) B. P. de Laune, et al., *Inorganic chemistry*, 56 (2017), 594.
(2) B. P. de Laune, F. J. Berry, J. F. Marco, S. L. Horswell, C. Greaves, *J. Mater. Chem. C*, 4 (2016), 5320.
(3) M. Curti, T. M. Gesing, M. M. Murshed, T. Bredow, C. B. Mendive, *Z. Kristallogr.*, 228 (2013), 629.

Figure 1: Crystal structure of PbBi(Fe0.5Mn0.5)O4, showing the edge-sharing (Fe/Mn)O6 octahedral chain and trigonal pyramidal (Pb/Bi)O3.

Fig. 1

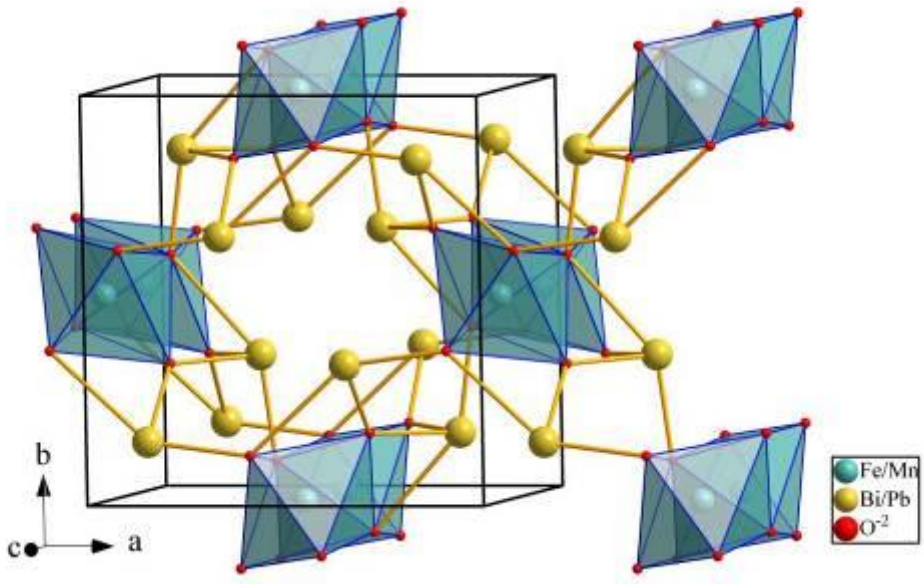

PP-088

Temperature-dependent structural and spectroscopic investigations of mullite-type $SnMBO_4$ compounds with M = V and Cr

S. Wittmann (Bremen/DE), M. M. Murshed (Bremen/DE), A. Koldemir (Münster/DE), R. Pöttgen (Münster/DE), T. M. Gesing (Bremen/DE)

Mullite-type $L_2M_2B_2O_8$, so called O8-phases, have drawn diverse attentions due to the influence of the stereochemical activity of the lone electron pair (LEP) of L-cations. For instance, the $5s^2$ LEP of Sn^{2+} cations play pivotal roles in designing crystal-physico-chemical properties of $SnMBO_4$ [1]. We report two new members of the O8-phases, namely, $SnVBO_4$ and $SnCrBO_4$ synthesized by solid-state method. Both phases crystallize in space group *Pnam*, where MO_6 octahedra build a chain along the crystallographic **c**-axis [2] with interlink by trigonal planar BO_3 groups and distorted LO_4 square pyramids (Fig. 1). Lattice parameters of $SnCrBO_4$ are found to be smaller than those of $SnVBO_4$ due to smaller M^{3+} radii. Temperature-dependent X-ray diffraction investigations (13 - 850 K) allows to model the lattice thermal expansion in the paramagnetic regimes, leading to Debye temperature of 779(74) K and 796(80) K for $SnVBO_4$ and $SnCrBO_4$, resepctively. Each of the axial thermal expansion coefficients (TECs) in $SnVBO_4$ shows a higher value than that of the resepctive paramter in $SnCrBO_4$. Deviations from the Debye behavior at low temperatures point to magnetostrictions presumbly for ferromagnetic coupling in the **a**- and **b**-, and antiferromagnetic coupling in the **c**-direction. Temperature-dependent ^{119}Sn Mössbauer spectra hint for nuclear phase transition as two distinct doublets with isomer shifts at 2.97(1) mm/s and 3.09(2) mm/s are observed at 78 K instead of a single one at 2.93(2) mm/s at 293 K. The nature of transition and band-gap energies of greyish $SnVBO_4$ and greenish $SnCrBO_4$ are determined from UV/Vis diffuse reflectance spectra and analyzed by RATD approach [3].

Fig. 1: Crystal structure with octahedral CrO_6, square pyramidal SnO_4 and trigonal planar BO_3.

References:

(1) S. Wittmann, et al., J. Am. Ceram. Soc., in press. [2] T.M. Gesing, et al., Z. Kristallogr. 228 (2013) 532. [3] T.M. Gesing, et al., J. Mater. Sci. 57 (2022) 19280.

We acknowledge support by DFG (GE1981/14-1).

Fig. 1

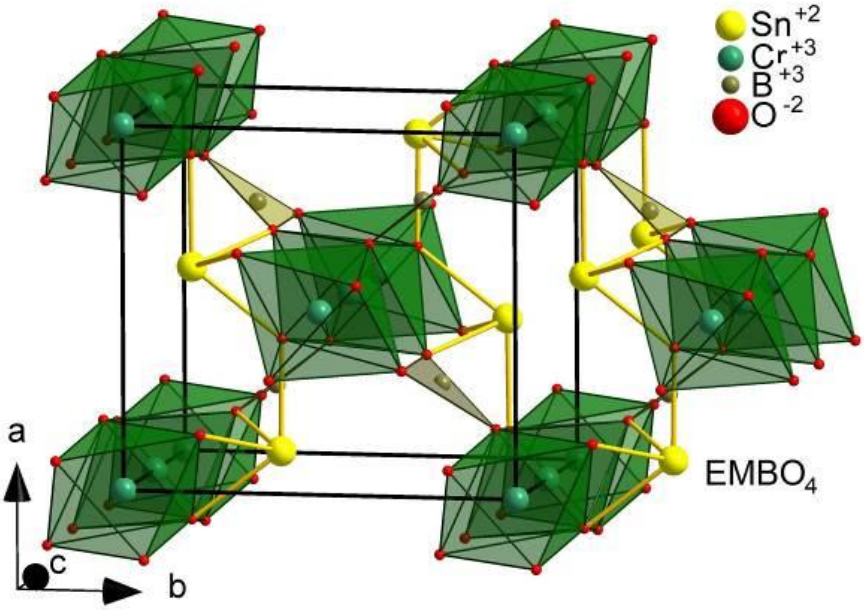

PP-089

Rietveld characterization of Y_2O_3-stabilized zirconia ceramics for dental application

K. Hurle (Erlangen/DE), R. E. Matta (Erlangen/DE), R. Belli (Erlangen/DE)

Question: Due to its outstanding mechanical properties, 3YSZ (yttria stabilized zirconia with 3 mol% Y_2O_3) is applied in dentistry for larger prosthetic reconstructions. 5YSZ - more translucent, but less tough - is used for reduced prosthetic constructs like anterior bridges. YSZ is proposed to contain cubic and tetragonal ZrO_2(Y), while the cubic fraction increases with increasing Y_2O_3 content [1]. Within this study [2], ten dental zirconias with 3-5 mol% nominal Y_2O_3 content were thoroughly characterized to determine the correlation between quantitative phase composition and fracture toughness K_{Ic}.

Methods: XRD measurements were performed using bulk samples of the zirconias. The quantitative phase composition was determined by Rietveld refinement with software TOPAS V5 (Bruker AXS, Karlsruhe). The Y_2O_3 content of tetragonal ZrO_2(Y) was derived from tetragonality c/a according to Miller et al. [3]. K_{Ic} was measured by Chevron Notched Beam method.

Results: For all samples, Rietveld refinement with one tetragonal and one cubic phase did not allow fitting of all observed reflections. However, a good fit was achieved by using two tetragonal ZrO_2(Y) structures differing in their lattice parameters. These tetragonal phases were assigned as Y-lean t with around 2 – 3 mol% Y_2O_3, and as Y-rich t" with 6 – 7 mol% Y_2O_3. The fraction of t" nearly linearly increased with increasing Y_2O_3 bulk content of the sample, accompanied by a decrease in K_{Ic}.

Conclusions: Rietveld results clearly indicate that 3YSZ and 5YSZ materials contain two tetragonal ZrO_2(Y) phases differing in their Y_2O_3 content, revising current literature reports [1]. The reduction of K_{Ic} with increasing t" fraction is ascribed to the non-transformability of t" to monoclinic ZrO_2(Y), reducing the effect of transformation toughening induced by t.

References:

(1) Inokoshi et al. Dental Materials 34 (2018) 508-518.
(2) Belli et al. J Eu Ceram Soc 41 (2021) 7771-7782.
(3) Miller et al. Adv Ceramics 3 (1981) 241-253.

PP-090

Crystal growth and characterization of ruthenium based 12L-perovskites

H. Schilling (Cologne/DE), P. Becker (Cologne/DE)

The synthesis and investigation of novel compounds is an important part of active research in solid state sciences. Here, compounds with perovskite-type structures or structures derived thereof are of ongoing interest. Our present work focuses on the 12L perovskite structure type of composition $Ba_4AM_3O_{12}$ with characteristic [M_3O_{12}] "trimer clusters" of face-sharing [MO_6] octahedra. The occupation of the "trimers" by the 4*d* and 5*d* transition metals Ru and Ir can lead to intriguing physical properties due to competing intra- and inter-cluster spin and orbital interactions and strong spin-orbit coupling.

The aim of this work is single crystal growth of ruthenium compounds $Ba_4ARu_3O_{12}$ with dimensions that allow the measurement of physical properties, including their anisotropy. By occupation of the *A* position by tri-, tetra- or pentavalent cations different oxidation states of ruthenium in the trimers are expected and consequently different total magnetic moment of the [Ru_3O_{12}] trimers. By exploration of suitable crystal growth conditions, we were able to grow single crystals of $Ba_4Ta^{V}Ru_3O_{12}$, and succeeded to grow first single crystals of $Ba_4Ce^{IV}Ru_3O_{12}$ of several mm size. All crystals were grown from melt solution using a $BaCl_2$ flux. The crystals were analyzed concerning the chemical composition, homogeneity and phase stability by means of electron beam microprobe analysis, thermal analysis and X-ray diffraction.

PP-092

Influencing the Bad Metal Behaviour in Polar Amalgams

D. Kraut (Munich/DE), C. Hoch (Munich/DE)

"Bad metal" behaviour is the result of a combination of low free electron concentration with a small free electron path length [1,2]. It results in non-conventional metallic behaviour and has impact on thermoelectric materials, giant magnetoresistance, topologic materials and others.

For many years, amalgams of the less noble metals have been studied as model systems for polar intermetallics with pronounced "bad metal" behaviour. Three key parameters have been identified to determine mean free path and electron concentration: structural complexity, disorder phenomena, and Coulombic polarity [3]. The influence of structural disorder phenomena on the overall properties can be studied on mixed crystals, as the Coulombic polarity mostly follows the Hg content in the amalgams and structural complexity stays largely constant when the crystal structure type is not changed. We have examined the mixed crystal series $A^1_{1-x}A^2_xHg_{11}$ (A^1, A^2: alkali or alkaline earth metal). Two different synthesis strategies can be considered: thermochemical synthesis as well as isothermal electrocrystallisation [4] have proven suitable for the preparation of phase-pure samples of ternary amalgams.

We report synthesis, crystal structures and physical properties of two ternary amalgams belonging to the $BaHg_{11}$ structure type [5]. $K_{1-x}Rb_xHg_{11}$ with x = 0.472(7) and $K_{1-x}Sr_xHg_{11}$ with x = 0.25(10) are both Vegard-type mixed crystals of KHg_{11} and $RbHg_{11}$ or $SrHg_{11}$ (cubic, space group *Pm*-3*m*, No. 221, *a* = 9.69143(3) / 9.6454(6)). The crystal structures were evaluated on the basis of single crystal and Rietveld powder data refinements.

References:

(1) A. F. Ioffe, A. R. Regel, *Prog. Semicond.* **4**, 237 (1960).
(2) O. Gunnnarsson, M. Calandra, J. E. Han, *Rev. Mod. Phys*. **75**, 1085 (2003).
(3) T. Hohl, C. Hoch, *Inorg. Chem.* **62**, 3965 (2023).
(4) F. Tambornino, J. Sappl, F. Pultar, T. M. Cong, S. Hübner, T. Giftthaler, C. Hoch, *Inorg. Chem.* **55**, 11551 (2016).
(5) G. Peyronel, *Gazz. Chim. Ital.* **82**, 679 (1952).

PP-093

Anisotropic platinum-iridium nanoparticles: Synthesis and in-depth characterization

K. Loza (Essen/DE), R. Guo (Essen/DE), M. Heggen (Jülich/DE), M. Epple (Essen/DE)

Nanoparticles of iridium and platinum are of particular interest due to their multiple unique assets, i.e. catalytic activity and chemical inertness. These metals effectively promote the hydrogen evolution reaction, enabling the generation of substantial cathodic current densities at low overpotentials. Blending two metals into one particle offers a new degree of freedom to vary the particle properties. By engineering particle size, composition, surface and internal structure, it is possible to enhance the activity the efficiency. Faceted nanoparticles with well-defined geometrical shapes with multiple facets or crystallographic planes are beneficial for catalysis due to the enhanced surface reactivity, shape-dependent activity, and structural stability.

Here, well-defined anisotropic bimetallic Ir-Pt nanoparticles were synthesized by tailoring the synthesis parameters. Typically, Ir nanoparticles exhibit isotropic or spherical shapes due to the one of the highest surface energies among transition metals. This high surface energy makes it energetically favourable for iridium nanoparticles to minimize their surface area by adopting a spherical shape. In other words, the isotropic shape allows the nanoparticles to reduce their overall energy and achieve a lower thermodynamic state. This limitation can be overcome by using faceted Pt nanocrystals as a seed for the controlled deposition of iridium onto their surface.

Anisotropic Pt-Ir nanoparticles were prepared by wet-chemical syntheses from well-accessible Pt and Ir salt precursors. Variation of the reaction time, temperature, solvent, reducing and capping agents, concentrations resulted in a high-yield of platinum-iridium cubes and cuboctahedra. The nanocrystals were characterized in-depth by colloid-chemical and structural methods as powder X-ray diffraction, spectroscopy and microscopy with electrons.

By a seed-and-growth synthesis approach, it was possible to obtain platinum-iridium cubes and cuboctahedra.

PP-094

Interaction between different TiO_2 polymorphs and their interjunctions for photocatalytic dye degradation.

O. Thueringer (Bremen/DE), A. Wollbrink (Bremen/DE), M. Bäumer (Bremen/DE), T. M. Gesing (Bremen/DE)

Titania (TiO_2) is the most famous material for photocatalytic processes in the UV-light region. Additionally, it is generally used as a reference standard for photocatalytic reactions [1]. Three different polymorphs are known crystallizing in the space groups $P4_2/mnm$ (Rutile), $I4_1/amd$ (Anatase) and Pbca (Brookite). The photocatalytic activity (PA) differs not only due to its band-gap energies of about 3.0 eV, 3.2 eV [2] and 3.1 eV [3], respectively, but also due to its type of transition. Interjunctions between different polymorphs result in noticeable changes in their PA. Ratios of 10/90 of rutile/anatase show in comparison with pure anatase 20 % more degradation of methylene blue [4]. Phase compositions with brookite show the same or better PA degradation for methyl orange (MO) compared to anatase [5]. Therefore, different TiO_2 polymorphs were synthesized, starting from one precursor phase made by a simple sol-gel process, and their interjunctions systematically investigated. Phase compositions are formed by tailored temperature treatment in between 298 K and 1073 K. Samples are characterized by e.g., XRPD, SEM, UV/Vis spectroscopy. Selected samples are tested for their photocatalytic degradation of MO. High PA, higher than for the pure anatase phase, can be determined for interjunctions, synthesized at the temperature of 823 K. A ratio of 30 % of rutile and 70 % of anatase, with an ACS at about 50 nm, is hereby prepared.

We acknowledge support by DFG under grant GE1981/13-1.

References:

(1) Pastrana-Martínez et al. Chem. Eng. J. 224 (2013) 17-23.
(2) Reyes-Coronado et al. Nanotechnology 19 (2008) 145605.
(3) Landmann et al, J. Phys.: Condens. Matter 24 (2012) 195503
(4) Yuangpho et al., Physica E 67 (2015) 18-22.
(5) Allen et al. Polym. Degrad. Stab. 150 (2018) 31-36.

PP-095

Exploring the effect of anion alloying on the structural disorder in Cu_2MnSnX_4 compound semiconductors (X = S, Se)

D. Matzdorff (Berlin/DE), G. Gurieva (Berlin/DE), D. Sheptiakov (Villigen PSI/CH), S. Schorr (Berlin/DE)

The chalcogenides $Cu_2ZnSn(S,Se)_4$ are used as absorber in the only critical raw material free PV technology, reaching efficiencies up to 14.9% [1]. Structural disorder, like Cu-Zn disorder (Cu_{Zn} and Zn_{Cu} anti-sites in fractions up to 50%) occur in these kesterite-type materials [2] which was identified as a limiting factor of solar cell efficiency [3].

We studied $Cu_2MnSn(S,Se)_4$, because replacing Zn by Mn leads to a change of the crystal structure: Cu_2MnSnS_4 as well as $Cu_2MnSnSe_4$ crystallize in the stannite structure [4,5]. From previous studies it is known [4], that in this structure Cu-M^{II} disorder is hindered.

For our study of structural disorder in the $Cu_2MnSn(S_xSe_{1-x})_4$ series we synthesized powders by solid state reaction of the elements in evacuated silica tubes (at 740-800 °C). Chemical composition and homogeneity of the materials were investigated by wavelength dispersive X-ray spectroscopy. To distinguish the electronic similar cations Cu^+ and Mn^{2+} in the structural analysis we used neutron diffraction taking advantage of the distinct neutron scattering lengths of the respective elements. Applying Rietveld analysis and the average neutron scattering length method we determined the cation distribution in the unit cell to deduce on crystal structure and structural disorder.

Like the end members of the studied series all mixed crystals adopt the stannite structure, hindering Cu-Mn disorder. Nevertheless Cu_{Mn} and Mn_{Cu} anti-sites occur in small fractions (< 5%) pointing to the presence of Cu-Mn swapping [5]. Interestingly the Cu-Mn swapping depends on the anion, Cu_2MnSnS_4 shows a higher swapping then $Cu_2MnSnSe_4$. Also Cu-Mn swapping increases in the intermediate range of the solid solution series.

References:

(1) www.nrel.gov/pv/cell-efficiency.html
(2) Schorr et al. (2007) *Europ. J. Mineral.19*,65
(3) Rey et al. (2014) *Appl. Phys. Lett.105*,112106
(4) Matzdorff et al., in prep.
(5) Gurieva et al. (2022) *Faraday Discuss.239*,51
(6) Maca et al. (2019) *J. Magn. Magn. Mat. 474*, 467

PP-096

Lattice strains, stresses and crystal structure defects in $Al_xGa_{1-x}N$ stacks

D. Rafaja (Freiberg/DE)

Gallium aluminum nitride is a direct band gap semiconductor that possesses high electron mobility, high critical electric field, high heat conductivity and a variable energy gap. Its lattice parameters vary between *a* = 3.1130 Å and *c* = 4.9816 Å for AlN, and *a* = 3.1893 Å and *c* = 5.1851 Å for GaN. Stacks made of epitaxially grown $Al_xGa_{1-x}N$ single-crystalline layers with adjusted composition profile and thickness are the central part of high electron mobility transistors. The lattice misfit between the neighboring layers produces local lattice strains that cause piezoelectric polarization, which is needed for formation of a thin channel in the uppermost GaN layer that guides a two-dimensional electron gas. For solely elastic deformation, the lattice strains and stresses in individual layers can be calculated from the lattice misfits and thicknesses of individual layers using a micromechanical model [1] that assumes a constant strain energy through the whole $Al_xGa_{1-x}N$ stack. In real $Al_xGa_{1-x}N$ stacks, however, the lattice strains are frequently compensated by crystal structure defects like threading dislocations and V pits.

In this contribution, it will be shown how the lattice strains, the residual stresses and the dislocation densities can be determined from the positions and from the shape of the reciprocal lattice points measured via reciprocal space mapping using X-ray or synchrotron diffraction. Furthermore, the capabilities of the combination of the theoretical prediction of the lattice strains with the experimental results will be discussed. It will be demonstrated, how the combination of the stress profile prediction with the experimentally determined residual stresses and threading dislocation densities obtained from the XRD analyses can be applied to identify the mechanisms of the lattice strain reduction, and how these results can be applied for systematic "defect design" and "defect engineering".

References:

(1) D. Rafaja et al., Thin Solid Films 732 (2021) 138777.

PP-097

Hydrocarbons under high pressure: Full-color luminescence by altering molecular packing

T. Nakagawa (Beijing/CN), Y. Ding (Beijing/CN)

Recently, the use of high pressure has proven to be an effective approach to uncover the relationship between the crystal structure and material properties.[1] Pressurization can effectively alter the molecular packing of organic materials and by combining various spectroscopic technique, we can investigate pressure-induced changes in the optical properties, intermolecular interaction, molecular conformation, phase transformation, and more. Here, we introduce recent investigation results on optical properties of a large Polycyclic Aromatic Hydrocarbons (PAHs), where we employed high pressure to obtain deeper insight of the structure-optical property relationships.

PAHs are known as both carbon-rich and hydrogen-rich organic molecules and their outstanding tuneability of crystal structure and molecular packing have been attracting continuous research interest for their possibilities for technological application, such as organic optoelectronic and photovoltaic devices, semiconductors, and nanoelectronics. In this work, we prepared coronene (C24H12) nano-rod single-crystal that exhibits blue fluorescence at ambient conditions, which, via high pressure compression, realized full-color piezochromic emission under UV-light.[2] During compression, we discovered that the tuneable piezochromic luminescence of coronene is strictly related to the molecular packing, that is, crystal structure transitions observed are associated with each emission color changes from blue to green, and to red. We combined in-situ photoluminescence, UV-visible absorption, Raman, infrared spectroscopy, and synchrotron powder XRD measurements to demonstrate their outstanding tuneability and high stability of coronene crystal structure allows significant modifications of chromaticity of their emission.

Fig1: Piezochromic behavior of coronene

References:

(1) T. Nakagawa, et al. Carbon, 197, 563-569, 2022.
(2) T. Nakagawa, et al. Adv. Opt. Mater, 11(20), 2300586, 2023

Fig. 1

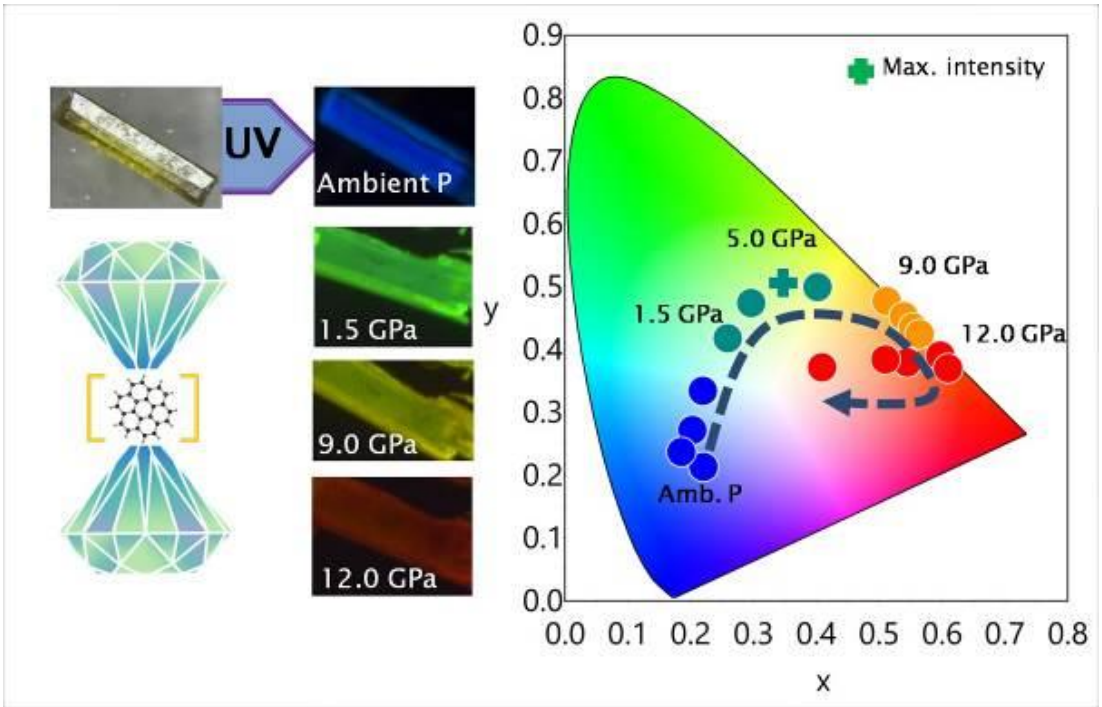

PP-098

The impact of phase composition on temperature-dependent structure-property relations in continuous mullite-based ceramic fibers

L. Reinders (Denkendorf/DE), J. Birkenstock (Bremen/DE), S. Pfeifer (Denkendorf/DE), B. Clauß (Denkendorf/DE)

Mullite ceramic fibers are promising candidates for reinforcement fibers in ceramic matrix composites. We studied continuously produced mullite and novel zirconia-toughened mullite (ZTM) ceramic fibers [1] (ZTM15 – 15 wt% ZrO_2) after annealing in air at temperatures between 1000 and 1500°C (25 h each) and characterized them ex-situ by mechanical testing (Weibull strength), SEM and detailed phase analyses using the Rietveld method.

The Weibull strength σ_0 of mullite fibers remains almost constant at 1200°C and failed above, for ZTM fibers it remains constant up to 1000°C and then experiences a significant decrease, retaining 66-76 % (1200-1310 MPa) at 1300°C.

Next to mullite and tetragonal zirconia in ZTM, the initial samples contain amorphous silica and meta-stable γ-Al_2O_3, the fractions of which are the larger the faster the throughput speed was. Surprisingly, in all types the composition of initial mullite is close to 2/1 ($2\ Al_2O_3 \cdot SiO_2$). With increasing annealing temperature, the Al_2O_3 content in mullite continuously decreases to 61 mol%, closely approaching the expected 3/2 composition above 1300°C. Above 1200°C significant grain growth of mullite and tetragonal zirconia occurs. For all fibers, the fraction of mullite increases to its maximum at 1200°C (e.g., 98 wt% for mullite fibers) and then decreases again, releasing increasing amounts of α-Al_2O_3 up to ca. 15 wt% (ZTM15 fibers) or ca. 8 wt% (mullite fibers) at 1500°C.

The above phase changes, notably the advent of α-Al_2O_3, together with grain growth above 1200°C may have led to the observed decrease of σ_0. At 1400°C and above, the tetragonal zirconia is increasingly transformed into stable nano-crystalline monoclinic zirconia, the impact of which needs to be studied in future work.

References:

(1) L. Reinders, S. Pfeifer, S. Kröner, H. Stolpmann, A. Renfftlen, L. C. Greiler, B. Clauß, M. R. Buchmeiser (2021), J. Eur. Ceram. Soc. 2021, 41 (6), 3570-3580.

PP-099

New Dion-Jacobsen-phases within the $A_2AgBiBr_8$ family

C. F. Schweinle (Freiburg i. Br./DE), H. Hillebrecht (Freiburg i. Br./DE)

Due to their high stability and low ion migration, two-dimensional organic-inorganic halide perovskite (HOIP) have become the focus of attention of promising optoelectronic materials.[1,2] The variety of organic cations can influence properties such as band gap, carrier lifetime or device efficiency[3]. Using linear cations new DJ-phases in the system $A_2AgBiBr_8$ could be prepared.

Yellow plates are obtained using terminal 1,n-diamines (n = 3-5) which can be classified as $(1,3\text{-PDA})_2AgBiBr_8$, $(1,4\text{-PDA})_2AgBiBr_8$ and $(1,5\text{-PDA})_2AgBiBr_8$. All the structures can be described as alternating layers, constructed from corner-sharing $AgBr_6$ and $BiBr_6$ octahedra, separated by organic spacer cations which are protonated and building up hydrogen bonds. Expect in $(1,3\text{-PDA})_2AgBiBr_8$, no distortion of the spacer cation can be observed.

The $AgBr_6$ octahedron shows a 2+4 coordination (compressed octahedron). This can been calculated by the octahedral elongation factors (OEL), and also seen in the Raman-spectrum by a shift to lower wavelenght compared to the original 3D compound $Cs_2AgBiBr_6$, which was also examined by Martín-García et al.[4] for low-Dimensional Layered Double Perovskites.

A slight distortion can also be observed for the $BiBr_6$ ochtahedron, but the OEL is at least one dimension lower than the one for the $AgBr_6$ octahedron.

All the products have been crystallized from a hot hydrobromic acid solution, with a stoichiometric amount of AgBr, Bi_2O_3, and the corresponding amine.

References:

(1) L. Mao, S. M. L. Teicher, C. C. Stoumpos, R. M. Kennard, R. A. DeCrescent, G. Wu, J. A. Schuller, M. L. Chabinyc, A. K. Cheetham, R. Seshadri, *JACS* **2019**, *141*, 19099.
(2) W. Guo, Z. Yang, J. Dang, M. Wang, *Nano Energy* **2021**, *86*, 106129.
(3) X. Li, J. M. Hoffman, M. G. Kanatzidis, *Chem. Rev.* **2021**, *121*, 2230.
(4) B. Martín-García et al., *J Phys Chem Lett* **2021**, *12*, 280.

PP-100

Pre-degeneration, pre-phase transition effects under illumination in the tetragonal room temperature crystal structure of $MAPbI_3$

G. Schuck (Berlin/DE), D. M. Többens (Berlin/DE), I. Zizak (Berlin/DE), J. Breternitz (Münster/DE), S. Schorr (Berlin/DE)

The fact that hybrid perovskites, such as methylammonium lead iodide ($MAPbI_3$), are already in practical usage as active light-harvesting layers in photovoltaic devices, but that many fundamental properties are still unclear, makes it obvious that this class of materials still is attracting considerable research interest. Surprisingly, for example, the question of whether and, if so, how illumination directly affects the tetragonal perovskite-type crystal structure of $MAPbI_3$ at room temperature has hardly been explored to date. The question is not whether $MAPbI_3$ degenerates under the influence of light, which has been known for a long time [1] and takes place over hours to days, but whether structural reactions of the tetragonal structure under illumination can be observed in the range of seconds. This question also implies that only effects that occur before the phase transformation into the cubic perovskite structure should be discussed here (which would occur by thermal stressing at 330 K). The present work is mostly limited to thin film samples,[2] so that usually no crystal structure refinements are possible and/or the thermal effect generated by the illumination is too large,[2,3] so that the phase transformation into the cubic structure already takes place. Illumination-dependent synchrotron powder X-ray diffraction (PXRD) measurements in transmission geometry were carried out at the BESSY II Beamline mySpot.[4] A specially adapted illumination device based on a white LED enabled illumination cycles with low thermal heating. The analysis of the illumination-dependent synchrotron PXRD data is performed by Rietveld analysis with FullProf and is based on our published results [5] of temperature dependent structural studies on $MAPbI_3$.

References:

(1) J.S. Manser et al., Acc. Chem. Res. 2016, 49, 330
(2) N. Phung et al., Jule 2022, 6, 2152
(3) A. Leonard et al., ACS Nano 2023, 17, 5306
(4) I. Zizak, J. large-scale res. fac. JLSRF 2016, 2, 101
(5) G. Schuck et al., J. Phys. Chem. C 2022, 126, 5388

PP-101

Polymorphism and its Effect on the Luminescence Properties of $Li_3SiNO_2:Eu^{2+}$

K. M. Rießbeck (Innsbruck/AT), D. S. Wimmer (Innsbruck/AT), K. Wurst (Innsbruck/AT), G. Heymann (Innsbruck/AT), H. Huppertz (Innsbruck/AT)

With the aim to find new luminescence materials for application in pc-LEDs and for a deeper understanding of the structure-property relationships in rare-earth activated compounds, our attention was drawn to the substance class of oxonitridolithosilicates. The lithium oxonitridolithosilicate Li_3SiNO_2 has been synthesized using high-temperature solid-state reactions in sealed tantalum tubes. Single-crystal X-ray diffraction revealed the existence of two polymorphs both showing previously unknown structure types. The monoclinic α-phase crystallizes with the lattice parameters a = 10.4901(3), b = 11.0342(3), c = 5.1186(2) Å, β = 116.14(1)°, and a volume of V = 531.87(2) Å^3 in space group $C2/c$ (no. 15) and the orthorhombic β-phase with lattice parameters of a = 18.736(2), b = 11.1267(5), c = 5.0897(3) Å, and a cell volume of V = 1057.2(1) Å^3 in space group *Pbca* (no. 61). By synthesis optimization it was possible to obtain high purity samples containing almost exclusively one or the other polymorph, depending solely on the cooling rate. While the monoclinic phase can be described by two alternating layers, orthorhombic Li_3SiNO_2 additionally contains a third layer and shows a layer-sequence of the type *ABCB*. With Eu(II) as activator, the two polymorphs exhibit different emissions (α: λ_{max} = 606 nm, *fwhm* = 100 nm, β: λ_{max} = 589 nm, *fwhm* = 97 nm) when irradiated with UV to blue light. The structural differences of the two polymorphs therefore cause a significant luminescence shift of 17 nm.[1,2]

Figure 1: Visualization of the crystal structure of the Li_3SiNO_2 polymorphs and their optical appearance under white and UV-Light.

References:

(1) D. S. Wimmer, K. M. Rießbeck, M. Seibald, D. Baumann, K. Wurst, G. Heymann and H. Huppertz, *Dalton Trans.* 2022, 51, 16465–16478.
(2) K. M. Rießbeck, D. S. Wimmer, M. Seibald, D. Baumann, K. Wurst, G. Heymann and H. Huppertz, *Dalton Trans.* 2023, 52, 4900-4910.

Fig. 1

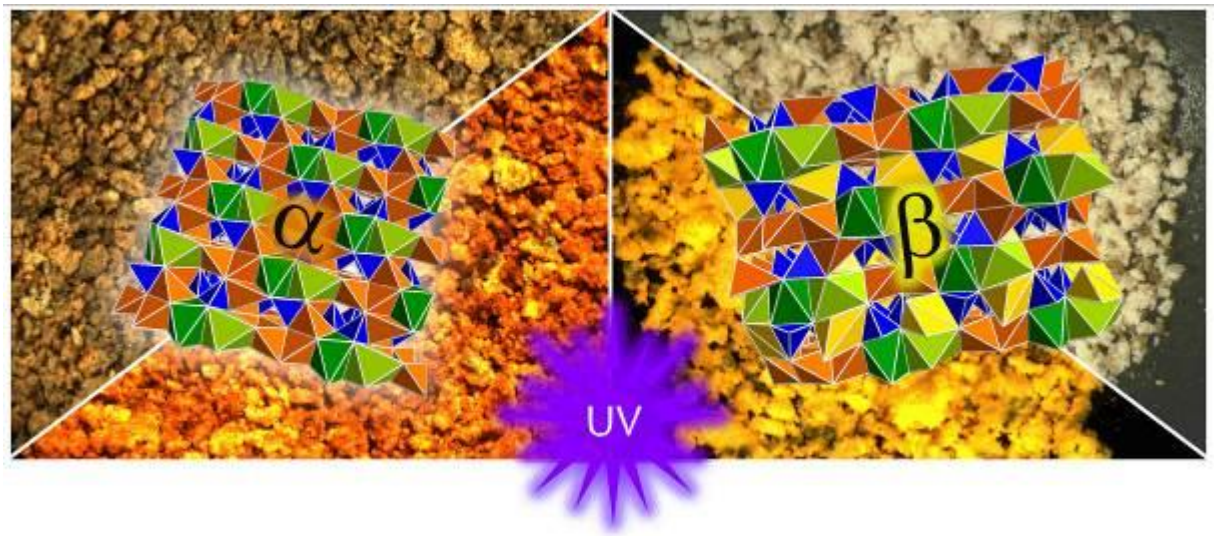

PP-102

Structure and composition of bimetallic nanoparticles and quantum dots as analysed by Anomalous SAXS

A. Hoell (Berlin/DE), M. Heilmann (Berlin/DE), K. D. Wegner (Berlin/DE), S. Haas (Hamburg/DE), F. Emmerling (Berlin/DE), S. Schorr (Berlin/DE)

Tailor-made nanoparticles are of increasing interest in e.g. catalysis, as sensor materials, analytical assays, or can have superior photophysical properties. A major issue concerning the preparation of high-quality and functional nanoparticles is a good control of particle size, shape, polydispersity, and composition.

Anomalous SAXS (ASAXS) exploits the anomalous dispersion of the scattering amplitude near the X-ray absorption edges of an element contained in the sample. These element-sensitive contrast variations can be used to analyse average composition fluctuations and to determine averaged structural parameters on the nm scale [1].

A facile and efficient methodology is developed for the thermal synthesis of size-tunable, stable, and uniform bimetallic NiCu core–shell nanoparticles (NPs) for various applications in catalysis [2]. Their diameter can be tuned in a range from 6 nm to 30 nm and the Ni:Cu ratio is adjustable in a wide range from 1:1 to 30:1. The NPs are structurally characterized by a method combination of TEM, ASAXS, XAF, and XPS. Here, we focus on ASAXS and its ability to analyze nanostructure parts and their compositions at once. As a result, a NiCu alloyed core surrounded by a Ni-enriched shell and an outer NiO shell was found.

Semiconductor nanocrystals (QDs) are well known for their superior photophysical properties. To achieve high photoluminescence quantum yields (PLQY) and enhanced photostability the QD core needs to be passivated by a second semiconductor, which possesses a larger band gap to confine the charges within the QD core. An important parameter is thereby the lattice mismatch between the core and shell [3]. ASAXS was used to better understand the structure of InP/ZnSe/ZnS QDs to enable a correlation between their structural and photophysical properties.

References:

(1) Hoell, A., et al, J. Appl. Cryst. **2009**, 42, 323
(2) Heilmann, M., et al, Adv. Eng. Mater. **2022**, 2101308, 1
(3) Wegner, K. D., et al, Front. Chem. **2019**, 7, 466, 1

PP-103

Swift heavy ion irradiation induces structural changes in lanthanide-bearing monazite

J. Marquardt (Frankfurt a. M./DE), T. Lender (Aachen/DE), D. Spahr (Frankfurt a. M./DE), L. Bayarjargal (Frankfurt a. M./DE), E. Haussühl (Frankfurt a. M./DE), C. Trautmann (Darmstadt/DE), L. Peters (Aachen/DE), B. Winkler (Frankfurt a. M./DE)

A major concern affecting future generations and requiring immediate action is the proper disposal of nuclear waste. A possible technique for effectively immobilize radionuclides is through their incorporation into crystalline solid phases in future radioactive waste repositories. This approach shows potential, particularly for waste streams that have minor actinides (Np, Am, Cm) or plutonium, because crystalline solid phases have advantages over glass matrices that could be more susceptible to leaching and disintegration [1-3]. Monazite-type compounds, notable for their ability to endure radiation, as well as their chemical and structural flexibility, are recommended for this purpose [4].

Experiments were carried out to enhance comprehension of the structural alterations resulting from radiation damage. Synthetic single crystals and ceramics of monazite with different chemical compositions (La, Nd, Pm, Sm)PO4 were exposed to irradiation at the UNILAC beamline of GSI Helmholtzzentrum Darmstadt. During the irradiation, 1.7 GeV Au ions were utilized at fluences of up to 1e13 ions/cm2. After irradiation, the samples underwent detailed analysis using Raman spectroscopy, SEM and X-ray diffraction.

The irradiation of monazite with 1.7 GeV Au ions results in an amorphization of the surface layer of ~48 µm thickness, which is in agreement with SRIM-2013 [5] calculations. It also results in a significant broadening of the Raman modes and further changes in the lattice dynamics. The differences in irradiation-induced damage between single crystals and ceramics are also presented in this study.

References:

(1) Donald et al. (1997) J. Mater. Sci. 32
(2) Ewing (1999) PNAS, 96
(3) Lumpkin et al. (2006) Elements, 2
(4) Schlenz et al. (2013) Z. Kristallogr. Cryst. Mater. 228
(5) Ziegler et al. (2010) Nucl. Instrum. Methods Phys. Res. B 268

The authors acknowledge the German Federal Ministry of Education and Research (BMBF) for financial support in the project No. 02NUK060.

PP-104

Synthesis of two new cadmium carbonates at extreme conditions

Y. Wang (Frankfurt a. M./DE), L. Bayarjargal (Frankfurt a. M./DE), E. Bykova (Frankfurt a. M./DE), D. Spahr (Frankfurt a. M./DE), M. Bykov (Frankfurt a. M./DE), V. Milman (Cambridge/GB), N. Giordano (Hamburg/DE), T. Fedotenko (Hamburg/DE), B. Winkler (Frankfurt a. M./DE)

Understanding the thermodynamic properties and *p-T* phase diagrams of carbonates ($CaCO_3$, $MgCO_3$ and $(Ca,Mg)CO_3$) is important, as carbonates play a key role in the recycling and transportation of carbon in the Earth[3]. Their phase diagrams are complex, as, for example, at least thirteen polymorphs of $CaCO_3$ have been identified [1]. The complexity of the phase diagrams increases substantially if variations of the composition, such as Ca_2CO_4 or CaC_2O_5, are included [2, 4].

Investigations of $CdCO_3$ ideally complement studies of $CaCO_3$, as the metal cations have similar ionic radii (Ca^{2+} ~ 1.0 Å, Cd^{2+} ~ 0.95 Å), but the former has fully filled 4d orbitals. This allows to investigate the role of cation-carbonate interactions by comparison. Only a few studies of the high-pressure behavior of $CdCO_3$ have been published, and the structure of a high pressure phase identified above 20 GPa is currently unknown [5, 6].

We carried out high-*p,T* experiments where $CdCO_3$ was loaded together with CO_2 in Diamond Anvil Cells (DACs). We successfully synthesized and characterized the new cadmium carbonate CdC_2O_5 -*Fdm,* containing *sp*3-carbon forming $[C_4O_{10}]^{4-}$ -groups. We also solved the structure of a new high-pressure phase, monoclinic $CdCO_3$ – *P21/c*, containing isolated $[CO_3]^{2-}$ groups. Raman spectroscopy reveals that both the new phases can exist, presumably metastable, down to at least 8 GPa.

References:

(1) Bayarjargal, L. et al. 2018. $CaCO_3$ phase diagram studied with raman spectroscopy at pressures up to 50 GPa and high temperatures and DFT modeling. *Physics of the Earth and Planetary Interiors*. 281, (2018), 31.
(2) Binck, J. et al. 2022. Synthesis of calcium orthocarbonate, Ca_2CO_4 - *Pnma* at *P-T* conditions of Earth"s transition zone and lower mantle. *American Mineralogist*. 107, 3 (Mar. 2022), 336–342.
(3) Gao, J. et al. 2022. Fate of carbonates in the Earth"s mantle (10-136 GPa). *Frontiers in Earth Science*. 10, (Mar. 2022), 837775.
(4) König, J. et al. 2022. Novel calcium *sp3* carbonate CaC_2O_5-$I\bar{4}2d$ may be a carbon host in Earth"s lower mantle. *ACS Earth and Space Chemistry*. 6, 1 (Jan. 2022), 73–80.
(5) Liu, L. and Lin, C.-C. 1997. A calcite –> aragonite-type phase transition in $CdCO_3$. *American Mineralogist*. 82, 5–6 (Jun. 1997), 643–646.
(6) Minch, R. et al. 2010. High-pressure behavior of otavite ($CdCO_3$). *Journal of Alloys and Compounds*. 508, 2 (2010), 251–257.

The authors acknowledge the funding from the DFG (projects WI1232 and BA4020) and the

DFG-Research Unit FOR2125/CarboPaT.

PP-105

Comparative study on structure-property relationships of mullite-type compounds $Bi_2M_4O_9$ (M = Al^{3+}, Fe^{3+}, Ga^{3+})

S. Schuh (Bremen/DE), A. Wollbrink (Bremen/DE), T. M. Gesing (Bremen/DE)

At present, environmental pollution of water is still one of the most important issues in the world. Therefore, oxidic semiconductors materials with tailored photocatalytic activity in the visible light range are the most promising tool for the decomposition of persistent organic pollutants (POPs) [1]. Mullite-type compounds $Bi_2M_4O_9$ are possible photocatalytic materials with a narrow bandgap energy (Eg) in the visible light range from 2.05 - 2.86 eV [2,3]. The E_g can be tailored by substitution of the M-cationas well as by the average crystallite size (ACS).

In this work, the structure-property relationship between E_g, M-cation substitution and ACS is investigated for selected M = Al^{3+}, Fe^{3+}, Ga^{3+} by XRPD, UV/Vis and FTIR spectroscopy.

The M-cation substitution results in lattice parameters, cell volume, vibration modes and E_g that are in accordance with respective compositions. With the decrease of ACS the E_g and strain (ε_0) is changed while the average crystal structure remains.

With the decrease of ACS the E_g increases for Fe-mullites from 2.17 – 2.25 eV whereas for Al- and Ga-mullites E_g decreases from 3.04 – 2.99 eV and 3.10 – 2.88 eV, respectively. The ratio of the calculated ε_0 for Fe-, Ga- and Al-mullites is approximately 1 : 2 : 3, respectively. Additionally, ε_0 generally increases with decreasing ACS for all compositions.

For the respective Al-Fe and Ga-Fe solid solutions a linear correlation of E_g is observed between the relative endmembers. In contrast to that, for the Ga-Fe samples mostly rather low and comparable ε_0 values could be determined while the ε_0 of Al-Fe first increases with the decrease of Fe-content (100 to 40 %) and decreases for Fe-contents from 30 - 0 %. This effect increases with decreasing ACS for Al-Fe solid solutions.

References:

(1) M. R. Hoffmann et al. *Chem. Rev. 95* (1995) 69-96.
(2) Y. Wang et al. *J. Mater. Chem. A7* (2019) 9537–9541.
(3) E. Zahedi et al. *Inorg. Chem.55, 10* (2016) 4824–4835.

We acknowledge support by DFG under grant number GE1981/13-1.

Poster Session II: Teaching of crystallography

PP-106

Visualising Symmetry

C. Wölper (Essen/DE)

When teaching crystallography lecturers are faced with widely variing spacial sense of students and their ability to imagine what symmetry operations do and how symmetry elements are oriented in a Bravais lattice. Tools as simple as a sheet of paper, a set of flip-flops or unit cell models with holes drilled along their special directions can be very helpful. Though the teaching success was not scientifically inverstigated positive experience and student feedback prompted me to present them to a wider public.